2013

Cyclic Peptides: Design, Characterization, Self-Assembly, and Applications as Nano Drug Delivery Systems

Amir Nasrolahi Shirazi
University of Rhode Island, ashirazi@mail.uri.edu

CYCLIC PEPTIDES: DESIGN, CHARACTERIZATION, SELF-ASSEMBLY, AND APPLICATIONS AS NANO DRUG DELIVERY SYSTEMS

BY

AMIR NASROLAHI SHIRAZI

A DISSERTATION SUBMITTED IN PARTIAL FULFILLMENT OF THE REQUIREMENTS FOR THE DEGREE OF DOCTOR OF PHILOSOPHY IN PHARMACEUTICAL SCIENCES

UNIVERSITY OF RHODE ISLAND

2013

DOCTOR OF PHILOSOPHY DISSERTATION

OF

AMIR NASROLAHI SHIRAZI

APPROVED:

Dissertation Committee:

Keykavous Parang (Major Professor)

Navindra Seeram

Mindy Levine

Nasser H. Zawia

Keith T. Killingbeck
ASSOCIATE DEAN OF THE GRADUATE SCHOOL

UNIVERSITY OF RHODE ISLAND
2013

ABSTRACT

Over the past two decades, drug delivery systems have become a subject of major interest in the pharmaceutical industry for the treatment of different diseases, such as cancer, viral infections, and genetic disorders. A wide range of compounds show high binding affinity and great potential in *in vitro* non-cellular assays through direct interacting with molecular targets. However, many compounds show low potency in cell-based assays due to their limited delivery across the cell membrane. The physicochemical properties of several compounds, such as size, poor water solubility, hydrophobic nature, and negative charge, limit their cellular uptake significantly. Thus, there is an urgent need in design and synthesis of novel molecular transporters for efficient delivery of effective compounds to cellular targets.

The recent growth of nanotechnology products will expand the current resources of therapeutics for the pharmaceutical industry in the next few years. The use of nanotechnology in drug delivery is widely expected to change the future of the pharmaceutical and biotechnology industries. The application of nanotechnology in drug delivery has led to the discovery of nano Drug Delivery Systems (nano-DDS).

Nanocarriers exhibit unique properties and take advantage of specific physiochemical behavior of nanoparticles. Properties such as, magnetism, conductivity, melting and boiling points, and chemical and biological reactivity become different at nano scale due to the quantum mechanical behavior of extremely small structures at molecular dimensions. Furthermore, nanoparticles behave

differently since they take advantage of extraordinary high surface area to mass ratio, leading to increased surface interactions and distinct biological performance. Nanoparticles have the potential to be manipulated through changing their size, electronic, and hydrophobic nature. Employing nanosized carriers offer several advantages, including enhanced intracellular delivery of poorly water-soluble drugs, targeted delivery, transporting relatively large biologically important molecules across the cell membrane, delivery of a combination of drugs to overcome drug resistance, and transporting drugs through challenging epithelial and endothelial barriers.

Thus, design and development of nano-sized pharmaceutical carriers has become attractive for chemists, biologists, and physicists. Functionalized Nano-DDS are designed to deliver and release cargo drugs intracellularly more efficiently than the currently available systems, leading to the enhanced drug tissue bioavailability and eventually therapeutics efficacy.

Among all nano-DDS, Cell-Penetrating Peptide (CPP)-mediated intracellular DDS has been widely used for the enhanced delivery of water insoluble drugs, negatively charged molecules (e.g., DNA, siRNA, phosphopeptides), and proteins. However, the application of (CPP)-mediated intracellular DDS in *in vivo* models has been challenging due to their inherent toxicity to normal cells and organs. Several studies have been performed to facilitate the intracellular delivery of a wide range of low-molecular weight and macromolecular drugs using carriers through the cell cytoplasm bypassing the endocytic pathway to avoid lysosomal degradation. In this process, although the drug is delivered into cytoplasm protected, it still needs to be transported to a certain organelles, such as mitochondria or nuclei, where therapeutic

function occurs. Several CPPs promote the delivery of drugs through receptor-mediated endocytosis. However, this mechanism requires high affinity between the drug-carrier complex and the target in the cell membrane for endocytosis. This process will be followed by energy-dependant formation of endosomes. However, this method suffers from entrapment and release challenges. After delivery of the molecular cargo into cells through endocytic pathway, and its entrapment in endosome, the cargo molecules or drug may end up in lysosome and degraded by the lysosomal enzymes. Thus, a limited amount of the drug can reach the cytoplasm because of inadequate endosomal escape and lysosomal degradation. As a result, although numerous CPPs exhibit promising results in *in vitro* assays, they fail *in vivo* because of the poor bioavailability.

Furthermore, the nuclear delivery of cargo drugs with known CPPs has been unsuccessful. The nucleus of a cell is an important target for drug delivery systems, due to presence of the genetic information and transcription machinery. An efficient cellular uptake of the drug is highly desired in nucleus where it can interact with nucleic acids. The nuclear targeting delivery is challenging. The designed drug-CPP complex must meet several requirements for nuclear delivery including efficient cell internalization by receptor-mediated endocytosis (RME), escaping endosomal/lysosomal pathways, acquiring a nuclear localization signal to communicate with nuclear pore complexes, and eventually, being sufficiently small to enter the nuclear membrane. Not many CPPs have been found efficient for the nuclear delivery applications.

CPPs can be classified into two major classes, linear and cyclic CPPs. Most reported CPPs are linear peptides that are flexible in solution and contain up to 10 amino acids. However, cyclization of peptides has been employed as a strategy to generate constrained structures. The rigidity imposed by cyclization reduces the flexibility and causes the system to adopt a restricted numbers of molecular conformations. Peptide cyclization has become a unique approach to generate conformations not available to linear peptides. Cyclic and linear peptides containing an equal number of similar amino acids create different geometries leading to different affinities for similar targets. Furthermore, cyclic CPPs containing specific amino acids have shown to have a different cellular uptake mechanism compared to linear CPPs. While most of the linear CPPs undergo endocytosis pathways in cellular uptake, some of the cyclic CPPs have endocytosis-independent uptake and target nucleus. Thus, cyclic peptides can be designed to be used as nuclear delivery vehicles of anticancer compounds targeting DNA. Functionalizing cyclic peptides with tumor targeting moieties can be used as a strategy for selective cancer cell targeting and improving nuclear targeting of anticancer drugs.

Cyclic CPPs can be also covalently conjugated to active drug cargos to generate prodrugs. Prodrugs are chemically modified analogs of an active metabolite that can improve pharmacokinetics and pharmacodynamics (PK/PD) properties of the drug. Prodrug strategy could offer several advantageous, such as enhancing water solubility, drug delivery, and chemical stability, and reducing toxicity. However, chemical transformation to the active drug is required in the presence of different intracellular enzymes to convert prodrugs to their corresponding pharmacologically

potent moieties in *in vivo* systems. Cyclic peptide-drug conjugates can be used as alternative prodrug approach for improving delivery of compounds with limited cellular uptake.

This dissertation focuses on a class of cyclic peptides as intracellular molecular transporters that can be used as prodrugs or peptide-capped gold nanoparticles. We **hypothesized** that the combination of alternate hydrophobic tryptophan and positively charged arginine or lysine residues in the sequence of the cell-penetrating cyclic peptide was critical for improving the cell-penetrating properties of the system. Furthermore, the presence of arginine and tryptophan facilitated the formation of gold nanoparticles. The molecular transporting efficiency of the peptide alone and peptide-capped gold nanoparticles was evaluated for a broad range of molecular cargos including anti-HIV drugs, anticancer agents, and negatively charged phosphopeptides.

The cyclic peptides containing alternate tryptophan and arginine residues and their corresponding peptide-capped gold nanoparticles enhanced the delivery of water insoluble drugs and negatively charged biologically important molecules. A broad range of parameters including concentration, toxicity, time, and different sequences of amino acids were explored to optimize the cellular uptake. Several characterization methods were used to determine the interaction between drugs and carrier through the formation of the complex. Different methods were also used to investigate the mechanism of the cellular uptake.

This work presents examples where prodrugs containing linear peptides are compared with their corresponding cyclic peptides in terms of biological properties

and in delivery of different drugs. For example, cyclic peptides containing certain amino acids generated gold nanoparticles more efficiently compared to their corresponding linear peptides. Moreover, cyclic peptide capped gold nanoparticles exhibited higher molecular transporting potency when compared with the linear counterparts. This dissertation will be discussed in four manuscripts:

The objective of **Manuscript I** (*published in Molecular Pharmaceutics 2013, 10(5), 2008-2020*) was to evaluate a cyclic octapeptide containing arginine and tryptophan for their ability to transport negatively charged phosphopeptides. Phosphopeptides are important compounds for studying protein-protein interactions. Phosphopeptides suffer from their limited cellular uptake due to the presence of negatively charged phosphate group in their structure. The **hypothesis** of this manuscript is that cyclic peptide $[WR]_4$ containing positively charged arginine can interact with negatively charged cell-impermeable phosphopeptides and improve their cellular uptake. Furthermore, the positively charged arginine and hydrophobic tryptophan can interact with negatively charged and hydrophobic residues in the cell membrane phospholipids and improve cell permeability of phosphopeptides. The cellular uptake of several biologically important phosphopeptides such as GpYLPQTV, NEpYTARQ, AEEEIY GEFEAKKKK, PEpYLGLD, $pYVNVQNNH_2$, and GpYEEI was evaluated in the presence and absence of $[WR]_4$. The cyclic peptide enhanced the cellular uptake of all phosphopeptides significantly in human leukemia cells (CCRF-CEM) after 2 h incubation. Confocal microscopy studies in live cells confirmed that the mixture of F′-PEpYLGLD and $[WR]_4$ was localized in cells and showed higher cellular uptake than the phosphopeptides alone. Several tools including

Transmission Electron Microscopy (TEM) and Isothermal Calorimetry (ITC) were used to understand the interaction between the drug and carrier. TEM results showed that the phosphopeptide-drug complex (PEpYLGLD-$[WR]_4$) formed specific nano-sized structures with the 125 × 60 nm dimensions. The ITC investigation proved an exothermic interaction driven by entropy. The result of this paper showed that the presence of the cyclic peptide enhanced the cellular uptake of phosphopeptides significantly. To this end, it was discovered that $[WR]_4$ can be employed as a cellular delivery tool of negatively charged phosphopeptides through non-covalent interaction. However, the evaluation of the covalent conjugation between the drug and cyclic peptide remained unexplored.

Manuscript II (*published in Molecular Pharmaceutics 2013, 10(2), 488-499*) embarked on taking advantage of both the cell-penetrating properties of the peptide and prodrug strategy. The **hypothesis** underlying this project is that cyclic CPP-drug conjugates can be used as potential prodrug to improve the cellular delivery of anticancer compounds. Doxorubicin (Dox), a potent anticancer drug, was covalently linked with the cyclic peptide containing alternate tryptophan and arginine ($[W(RW)_4]$) to afford their corresponding prodrug cyclic $[W(RW)_4]$−Dox. To study the effect of the cyclic nature of the peptide, linear peptide attached to Dox (linear $(RW)_4$−Dox) was also synthesized for comparative studies. The biological activities of cyclic $[W(RW)_4]$−Dox and linear $(RW)_4$−Dox prodrugs including their cellular uptake and anticancer potency were compared in cell-based assays. Comparative antiproliferative assays between covalent (cyclic $[W(RW)_4]$−Dox and linear $(RW)_4$−Dox) and the corresponding noncovalent physical mixtures of the peptides and

Dox were performed. Cyclic $[W(RW)_4]$−Dox inhibited the CCRF-CEM (62−73%), ovarian adenocarcinoma (SK-OV-3) (51−74%), colorectal carcinoma (HCT-116) (50−67%), and breast carcinoma (MDA-MB-468) (60−79%) cells at a concentration of 1 μM after 72−120 h of incubation. Cyclic $[W(RW)_4]$−Dox exhibited higher antiproliferative activity than linear $(RW)_4$−Dox in all cancer cells after 72 h.. Furthermore, the cellular uptake of $[W(RW)_4]$−Dox was observed to be higher than that of the linear prodrug after 24 h incubation in SK-OV-3 cells, suggesting that the cyclic nature offers major advantageous when compared with the corresponding linear ones. The result of this manuscript revealed that cyclic prodrug (cyclic $[W(RW)_4]$−Dox) can be used as a potential prodrug candidate for enhancing the cellular retention of the drug in the treatment of ovarian cancer.

In **Manuscript III** (*published in Molecular Pharmaceutics, 2013, 10(2), 500-511*), we investigated the application of cyclic peptides in generating gold nanoparticles. We **hypothesize** that cyclic peptides containing specific amino acids can be used as reducing agents and generate peptide-capped gold nanoparticles (CP-AuNPs) from gold ion (Au^{3+}). Several cyclic peptides including $[WR]_4$, $[FK]_4$, $[AK]_4$, $[EL]_4$, $[RFEF]_2$, $[EK]_4$, and $[FR]_4$ containing hydrophobic residues (W, F, L) and charged residues (K, R, E) where A = alanine, E = glutamic acid, F = phenylalanine, K = lysine, L = leucine, R = arginine, W= tryptophan were investigated for their ability to generate gold nanoparticles. Among all of them, only $[WR]_4$ was discovered to be appropriate for the synthesis of CP-AuNPs. Flow cytometry studies showed that the cellular uptake of fluorescence-labeled anti-HIV drugs such as lamivudine,

emtricitabine, and stavudine was significantly enhanced in human ovarian adenocarcinoma (SK-OV-3) cells in the presence of $[WR]_4$-AuNPs. For instance, the cellular uptake of fluorescence labeled lamivudine-loaded $[WR]_4$-AuNPs showed 12-fold higher cellular uptake compared to fluorescence labeled lamivudine alone in CCRF-CEM cells after 2 h incubation. The morphology and size of nanoparticles were characterized using TEM.. TEM results showed $[WR]_4$-AuNPs form nano-sized structures with approximate size 5-50 nm. $[WR]_4$-AuNPs (100 μM) did not show significant toxicity in CCRF-CEM, SK-OV-3, and normal human colon myofibroblast (CCD-18Co) cells after 24-72 h incubation. To this point, we understand that the cell-penetrating peptide-capped gold nanoparticles have potential to be used as prodrugs for delivery of antiviral and anticancer drugs through noncovalent conjugation. However, this strategy was required to be evaluated for non-cell penetrating peptides. Thus, we used a sequence of amino acids for designing a non-cell-penetrating peptide that generated peptide-capped gold nanoparticles with molecular transporting property.

In **Manuscript IV**, (*published in Molecular Pharmaceutics*, ***DOI:*** *10.1021/mp400199e*), a green method for the synthesis of non-cell penetrating peptide-capped gold nanoparticles was reported. We **hypothesize** that a non-cell penetrating peptide containing lysine and tryptophan namely linear $(KW)_5$ and cyclic $[KW]_5$ can be converted to a cell-penetrating molecular transporter upon generation of cyclic peptide-capped gold nanoparticles (linear $(KW)_5$-AuNPs and cyclic $[KW]_5$-AuNPs). A comparative flow cytometry results revealed that the cellular uptake of fluorescence-labeled anti-HIV drugs (emtricitabine (FTC) and lamivudine (3TC)) in

CCRF-CEM cells, and a negatively charged cell-impermeable phosphopeptide (GpYEEI) in SK-OV-3 cells was significantly higher in the presence of cyclic $[KW]_5$-AuNPs than that of linear $(KW)_5$-AuNPs, parent cyclic $[KW]_5$, and linear $(KW)_5$ peptides. For example, the cellular uptake of F′-GpYEEI was enhanced 12.8-fold by cyclic$[KW]_5$-AuNPs when compared with F′-GpYEEI alone. Microscopy results showed that fluorescence-labeled-3TC-loaded cyclic$[KW]_5$-AuNPs were localized in nucleus in SK-OV-3 cells after 1 h incubation. However, linear$(KW)_5$-AuNPs delivered the majority of fluorescence-labeled-3TC into cell cytoplasm. The results from this work suggest that non-cell penetrating peptides can be converted to efficient drug carriers by forming peptide-capped gold nanoparticles.

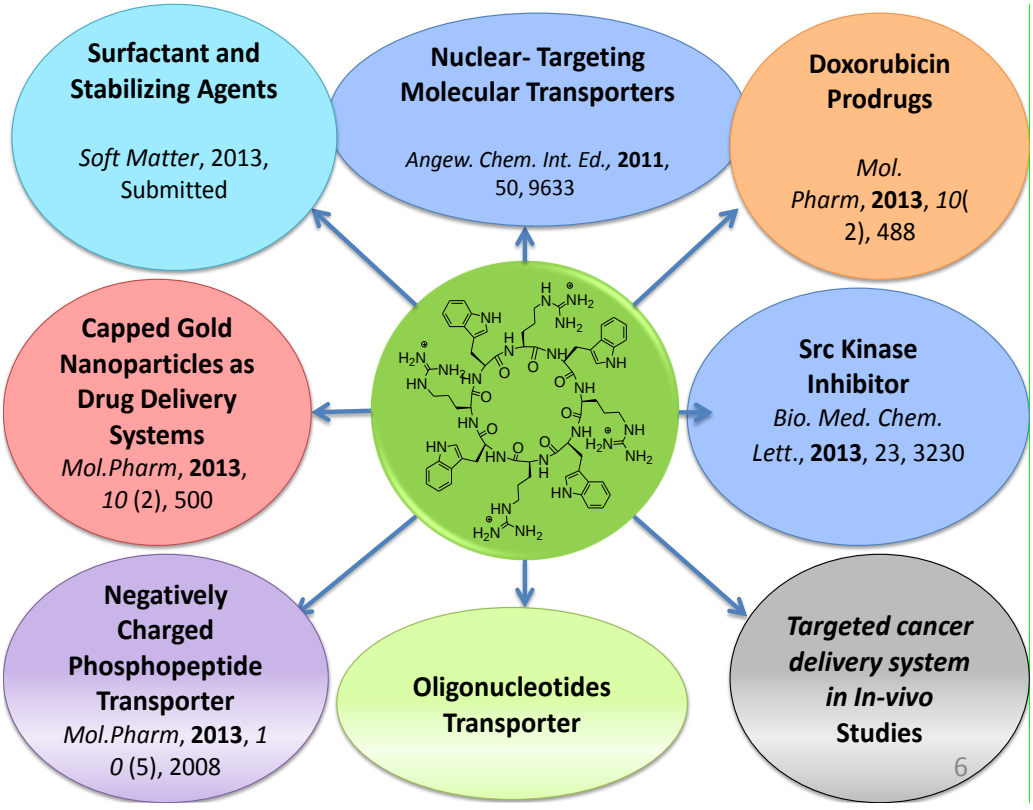

Figure 1. General Application of $[WR]_4$.

In summary, the studies described in this dissertation provided insights about the application of a new generation of cyclic peptides for the delivery of a broad range of drugs and biomolecules. The cyclic peptide containing alternate tryptophan and arginine residues was found to be efficient molecular transporters and nuclear delivery agents (Figure 1). In addition, we have demonstrated that a non-cell penetrating cyclic peptide can be converted to an efficient intracellular drug transporter through generation and capping of the gold nanoparticles. A detailed investigation on the cyclic nature of the peptide compared to the linear one in terms of their chemical behavior and biological activity was provided. Overall, a concrete strategy has been established by developing non-toxic cyclic peptide molecular transporters that can be used in prodrug strategy or gold nanoparticle formation. The scientific knowledge was advanced in the area of application of cell-penetration peptides in prodrug strategy and designing nanocarriers.

ACKNOWLEDGEMENTS

The completion of this doctoral dissertation would not have been possible without the assistance of many people. First of all, I appreciate the support and encouragement of my major professor, **Dr. Keykavous Parang**, for providing me a chance to work with him as a graduate student. His leadership, patience, and personality thought me how to improve the way of thinking and more importantly, to be a better human being. I am thoroughly grateful to learn many things from him in both academic and personal aspects. I believe that I have spent some of the best years of my life under his supervision and look forward to working with him by any title and position in future.

I would like to thank my collaborators and coauthors for their great ideas and advices. I also acknowledge my doctoral dissertation committee members, Dr. Nasser H. Zawia, Dr. Navindra Seeram, Dr. Mindy Levine, Dr. Mohammad Faghri, and Dr. Hany Alashwal for their time and scientific inputs. I appreciate the generosity of the INBRE core facility and the College of Pharmacy, University of Rhode Island. Dr. Aftab Ahmed was always helpful in providing ideas and maintaining the core facility. I also thank all my coworkers for making a scientific and peaceful environment in laboratory.

Finally, I need to mention that my family never stopped supporting me in all the ways they could. My Mother is the main reason that keeps me going endlessly. Her encouragement and passion makes me work consistently and efficiently. I am also, indebted to my father, brother, and sister for their support.

PREFACE

This dissertation is written based on the University of Rhode Island "Guidelines for the Format of Theses and Dissertations" standards for Manuscript format. This dissertation is composed of four manuscripts that have been combined to satisfy the requirements of the department of Biomedical and Pharmaceutical Sciences, College of Pharmacy, University of Rhode Island.

MANUSCRIPT I: Efficient delivery of cell impermeable phosphopeptides by a cyclic peptide amphiphile containing tryptophan and arginine

This manuscript was published in "Molecular Pharmaceutics", May 2013(10(5), 2008-2020)

MANUSCRIPT II: Design and biological evaluation of cell-penetrating peptide–doxorubicin conjugates as prodrugs

This manuscript was published in "Molecular Pharmaceutics", January 2013 (10(2), 488-499)

MANUSCRIPT III: Cyclic peptide-capped gold nanoparticles as drug delivery systems

This manuscript was published in "Molecular Pharmaceutics", January 2013 (10(2), 500-511)

MANUSCRIPT IV: Surface decorated gold nanoparticles by linear and cyclic peptides as molecular transporters

This manuscript was published in "Molecular Pharmaceutics", July 2013, ***DOI:*** *10.1021/mp400199e*

TABLE OF CONTENTS

LIST OF FIGURES

MANUSCRIPT I

MANUSCRIPT II

LIST OF SUPPORTING FIGURES AND SCHEMES

LIST OF ABBREVIATIONS

BT-20, human breast carcinoma cell line; CCRF-CEM, human leukemia carcinoma cell line; CD, circular dichroism; CCD-18Co, normal human colon myofibroblast; CPPs, cell-penetrating peptides; DCM, dichloromethane; DIPEA, *N*,*N*-diisopropylethylamine; DMF, *N*,*N*-dimethylformamide; EIA, 5-(*N*-ethyl-*N*-isopropyl)amiloride; F′, fluorescein; FACS, fluorescence activated cell sorter; FBS, fetal bovine serum; EDT, ethandithiol; HBTU, 2-(1H-benzotriazole-1-yl)-1,1,3,3-tetramethyluronium hexfluoro phosphate; HCT-116, human colorectal carcinoma; HOBt, hydroxybenzotriazole; HOAt, 1-hydroxy-7 azabenzotriazole; ITC, isothermal calorimetry; NMM, *N*-methylmorpholine; PAs, peptide amphiphiles; PTB, phosphotyrosine binding; PyAOP, 7-azabenzotriazol- 1-yloxy tri pyrrolidin ophosphonium hexafluorophosphate); SH2, Src homology 2; TFA, trifluoroacetic acid; TEM, transmission electron microscopy. Dox, doxorubicin; HBTU, DDS, drug delivery systems; HCT-116, human colorectal carcinoma; HOBt, hydroxybenzotriazole; HBTU, 1,1,3,3-tetramethyluronium hexafluorophosphate; MDA-MB-468, human breast adenocarcinoma; MRPs, multidrug resistance proteins; NMM (*N*-methylmorpholine); P-gp, P-glycoprotein; PBS, phosphate buffered saline solution; PyBOP, benzotriazol-1-yloxytripyrrolidinophosphonium hexafluoro phosphate; SK-OV-3, human ovarian adenocarcinoma, 1,1,3,3-tetramethyluronium hexafluorophosphate; TOPO II, topoisomerase II

LIST OF TABLES

There are no Tables in the manuscripts.

LIST OF SCHEMES

MANUSCRIPT I

MANUSCRIPT II

MANUSCRIPT ІII

There are no Schemes in Manuscript ІII

MANUSCRIPT IV

There are no Schemes in Manuscript IV

Manuscript I

Published in ***Molecular Pharmaceutics***, 2013, 10, 2008-2020

Efficient delivery of cell impermeable phosphopeptides by a cyclic peptide amphiphile containing tryptophan and arginine

Amir Nasrolahi Shirazi,[†] Rakesh Kumar Tiwari,[†] Donghoon Oh,[†] Antara Banerjee,[‡] Arpita Yadav,[‡] and Keykavous Parang*,[†]

[†]Department of Biomedical and Pharmaceutical Sciences, College of Pharmacy, University of Rhode Island, Kingston, Rhode Island 02881, United States

[‡]Department of Chemistry, University Institute of Engineering and Technology, Chhatrapati Shahuji Maharaj University, Kanpur 208024, India

Corresponding Author

*7 Greenhouse Road, Department of Biomedical and Pharmaceutical Sciences, College of Pharmacy, University of Rhode Island, Kingston, Rhode Island 02881, United States. Tel: +1-401-874-4471. Fax: +1-401-874-5787. E-mail: kparang@uri.ed

Abstract

Phosphopeptides are valuable reagent probes for studying protein−protein and protein−ligand interactions. The cellular delivery of phosphopeptides is challenging because of the presence of the negatively charged phosphate group. The cellular uptake of a number of fluorescent-labeled phosphopeptides, including F′-GpYLPQTV, F′-NEpYTARQ, F′-AEEEIYGEFEAKKKK, F′-PEpYLGLD, F′-pYVNVQNNH$_2$, and F′-GpYEEI (F′ = fluorescein), was evaluated in the presence or absence of a [WR]$_4$, a cyclic peptide containing alternative arginine (R) and tryptophan (W) residues, in human leukemia cells (CCRF-CEM) after 2 h incubation using flow cytometry. [WR]$_4$ improved significantly the cellular uptake of all phosphopeptides. PEpYLGLD is a sequence that mimics the pTyr^{1246} of ErbB2 that is responsible for binding to the Chk SH2 domain. The cellular uptake of F′-PEpYLGLD was enhanced dramatically by 27-fold in the presence of [WR]$_4$ and was found to be time-dependent. Confocal microscopy of a mixture of F′-PEpYLGLD and [WR]$_4$ in live cells exhibited intracellular localization and significantly higher cellular uptake compared to that of F′-PEpYLGLD alone. Transmission electron microscopy (TEM) and isothermal calorimetry (ITC) were used to study the interaction of PEpYLGLD and [WR]$_4$. TEM results showed that the mixture of PEpYLGLD and [WR]$_4$ formed noncircular nanosized structures with width and height of 125 and 60 nm, respectively. ITC binding studies confirmed the interaction between [WR]$_4$ and PEpYLGLD. The binding isotherm curves, derived from sequential binding models, showed an exothermic interaction driven by entropy. These studies suggest that amphiphilic

peptide $[WR]_4$ can be used as a cellular delivery tool of cell-impermeable negatively charged phosphopeptides.

KEYWORDS: cellular uptake, cyclic peptides, nanoparticles, phosphopeptides, SH2 domain

Introduction

Peptide amphiphiles (PAs) are composed of a combination of amino acids carrying hydrophobic/hydrophilic and positively/ negatively charged residues.[1] PAs have been found to be promising tools in drug and gene delivery due to their biocompatibility and bioactivity.[2−4] These compounds are not toxic to cells at their experimental concentration and are able to cross the cell membrane because of their unique structural properties.

Hydrophobic unit of PAs can contain long chain fatty acids or amino acids with hydrophobic side chain residues. This unit generates a pocket that could be responsible for the entrapment of drugs and facilitates the internalization into the cell membrane.[5] At the same time, the presence of positively charged arginine facilitates the interaction between the peptide and the negatively charged phospholipids on the cell membrane. The application of positively charged linear cell-penetrating peptides (CPPs) as drug carriers for biologically active cargos has been reported previously.[6−9] Polyarginines, TAT (trans-acting activator of transcription), and Penetratin have been found to enhance the cellular uptake of a diverse range of drugs.[10−12] Thus, the appropriate combination of amino acids in the structure of peptide determines the efficiency and function of the delivery system.

Phosphopeptides are valuable reagent probes mimicking phosphoproteins for studying protein−protein and protein−ligand interactions [13,14] and determination of substrate specificity of the Src homology 2 (SH2) domain,[15] phosphatases,[16,17] and phosphotyrosine binding (PTB) domains.[18,19] The use of phosphopeptides has been

challenging due to the fact that they have limited cellular uptake because of the presence of the negatively charged phosphate group. Several chemical modifications have been used to enhance the intracellular delivery of phosphopetides through covalent conjugation to other transporter peptides.[20−22] These strategies suffer from several disadvantages including multistep synthesis of the fusion conjugates, low loading yields, and the requirement of cleavage through chemical or enzymatic reactions to release phosphopeptides.[23]

Peptidomimetic prodrugs have been reported for intracellular delivery of aryl phosphoramidates[24] and difluoromethyl phosphonates.[25] Arrendale and co-workers developed a (difluoromethylene)phosphoserine prodrug to deliver negatively charged phosphoserine peptidomimetic intracellularly. FOXO3a is a transcription factor that is phosphorylated by Akt1 and binds to 14-3-3-adaptor protein. The released modified phosphopeptide was able to release FOXO3a from 14-3-3 protein, leading to cell death in leukemia cells.[26,27] Other phosphoserine and phosphothreonine masked phosphopeptides have been evaluated in studying kinase regulation.[28,29]

Considering the critical roles of the phosphopeptides in cellular signaling pathways, we have previously reported amphiphilic linear peptide analogs to improve the intracellular uptake of negatively charged phosphopeptides through noncovalent conjugation.[30] The linear positively charged peptides were designed based on the Src SH2 domain phosphotyrosine (pTyr) binding pocket.

We introduced a new class of homochiral cyclic peptides containing arginine (R) and tryptophan (W) such as $[WR]_4$ that were appropriate carriers for a wide range

of drugs.[31] This system showed that the optimized balance between positive charge and hydrophobicity was critical for the peptide to enhance the intracellular delivery of drugs through interaction with the cell membrane and penetration into the lipid bilayer. Cyclic $[WR]_4$ provided major advantages compared to their linear counterparts, including higher enzymatic stability, bypassing endosomal uptake, improved cell permeability, and nuclear targeting.[31]

In continuation of our efforts to introduce new applications of $[WR]_4$ for the delivery of biomolecules, we report here using $[WR]_4$ for improving the cellular delivery of negatively charge phosphopeptides. Addition of negatively charged phosphopeptides to the positively charged $[WR]_4$ led to the formation of nanostructures through intermolecular interactions. To the best of our knowledge, this is the first report of using a cell-penetrating cyclic peptide for cellular delivery of impermeable phosphopeptides.

EXPERIMENTAL SECTION

General. All amino acids were purchased from Chem-Impex International, Inc. HBTU was purchased from Oakwood products, Inc. All other chemicals and reagents were purchased from Sigma-Aldrich Chemical Co. (Milwaukee, WI). The chemical structures of final products were confirmed by high resolution MALDI AXIMA performance TOF/TOF mass spectrometer (Shimadzu Biotech). Details of procedures and spectroscopic data of the respective compounds are presented below. Final compounds were purified on a Phenomenex Prodigy 10 μm ODS reversed-phase

column (2.1 cm × 25 cm) with a Hitachi HPLC system using a gradient system of acetonitrile (CH_3CN) or methanol and water (CH_3OH/H_2O) (0−100%, pH 7.0, 60 min). The purity of final products (≥95%) was confirmed by analytical HPLC. The analytical HPLC was performed on a Hitachi analytical HPLC system using a C18 Shimadzu Premier 3 μm column (150 cm × 4.6 mm) and a gradient system (water/CH_3CN), and a flow rate of 1 mL/min with detection at 220 nm. Cyclic peptide $[WR]_4$ was synthesized according to our previously reported procedure.[31] As representative examples, the synthesis of Ac-PEpYLGLD and F′-PEpYLGLD is outlined here.

Synthesis of Ac-PE(pY)LGLD and F'-PE(pY)LGLD. Side chain protected peptide PE(pY)LGLD was assembled on Fmoc-Asp(OtBu)-Wang resin (740 mg, 0.54 mmol/g, 0.4 mmol) by solid-phase peptide synthesis strategy using Fmoc-protected amino acids [Fmoc-Leu-OH, Fmoc-Gly-OH, Fmoc-Leu-OH, Fmoc-Tyr(PO_3tBu_2)-OH, Fmoc-Glu(OtBu)-OH, and Fmoc- Pro-OH] on a PS3 automated peptide synthesizer at room temperature using 2-(1H-benzotriazole-1-yl)-1,1,3,3-tetramethyluronium hexafluorophosphate (HBTU) and *N*-methylmorpholine (NMM, 0.4 M) in *N*,*N*-dimethylformamide (DMF) as coupling and activating agents, respectively (Scheme 1). After the assembly of the side chain protected peptide sequence, the Fmoc protecting group at the *N*-terminal proline was removed using piperidine in DMF (20% v/v). The resin was washed with DCM (3 × 15 mL) and MeOH (3 × 15 mL) for further modification using either capping reagent (acetic anhydride) or fluorescein labeling reagent (5(6)-carboxyfluorescein isobutyrate). The resin was dried overnight under vacuum and divided into two parts. The capping reaction was carried out on the

first portion using acetic anhydride ($(CH_3CO)_2O$) (953 μL) and *N*,*N*-diisopropylethylamine (DIPEA) (1,742 μL) (50/50 equiv) in DMF (10 mL). The mixture containing peptide-attached resin and reagents was shaken for 30 min, followed by washing with DMF (5 × 15 mL), DCM (5 × 15 mL), and MeOH (3 × 15 mL), respectively. The resin was dried under vacuum at room temperature for 24 h. The second portion of the resin was swelled in DMF (2 × 20 mL) for 2 h. The preactivation reaction was performed on the fluorescein reagent using a mixture of 5(6)-carboxyfluorescein isobutyrate (5 equiv), 1-hydroxy-7-azabenzotriazole (HOAt, 5 equiv)/7- azabenzotriazol-1-yloxy tripyrrolidinophosphonium hexafluorophosphate) (PyAOP, 5 equiv)/DIPEA, 10 equiv) in DMF:DCM (5:1 v/v, 12 mL) for 10 min. The activated fluorescein reagent was added to the peptide-attached resin and stirred at room temperature for 3 h. After the completion of the reaction, the resin was washed by DMF (5 × 15 mL), DCM (3× 15 mL), and MeOH (5 × 15 mL), respectively. The protecting group (isobutyrate) was removed from the carboxyfluorescein by treating the peptide-attached resin with 20% piperidine in DMF (5 × 15 mL, 25 min each). Finally, the resin was washed with DMF (5 × 15 mL), DCM (5 × 15 mL), and MeOH (5 × 15 mL), respectively, followed by drying under a high vacuum at room temperature for 24 h. The cleavage reagent R cocktail containing trifluoroacetic acid (TFA)/thioanisole/ethandithiol (EDT)/anisole (90:5:3:2 v/v/v/v, 12 mL) was added to both portions of the resin, and the mixtures were stirred at room temperature for 2 h. The resins were filtered and washed with Reagent R (2 mL) again. The filtrates were evaporated to reduce the volume under dry nitrogen. The crude peptides were precipitated by adding cold diethyl ether (200 mL, Et_2O) and centrifuged at 4000 rpm

for 5 min, followed by decantation to obtain the solid precipitates. The solid materials were further washed with cold ether (2 × 100 mL) for 2 times. The peptides were lyophilized and purified by reversed-phase Hitachi HPLC (L-2455) on a Phenomenex Prodigy 10 μm ODS reversed-phase column (2.1 cm × 25 cm) using a gradient system to yield the linear capped Ac-PE(pY)LGLD and fluorescein-labeled F′-PE(pY)LGLD peptides, respectively. Similarly, other fluorescein-labeled peptides were synthesized according to this procedure.

Ac-PE(pY)LGLD (Shown Here as PE(pY)LGLD). MALDITOF (*m/z*) [$C_{39}H_{58}N_7NaO_{17}P$]: calcd [M + Na]$^+$, 950.3524; found, 950.3524.

F′-PE(pY)LGLD. MALDI-TOF (*m/z*) [$C_{58}H_{67}N_7O_{22}P$]: calcd [M + H]$^+$, 1244.4077; found, 1244.4080. [$C_{58}H_{66}N_7NaO_{22}P$]: calcd [M + Na]$^+$, 1266.3896; found, 1266.3899.

F′-G(pY)LPQTV. MALDI-TOF (*m/z*) [$C_{57}H_{67}N_8NaO_{20}P$]: calcd [M + Na]$^+$, 1237.4107; found, 1237.4108. [$C_{57}H_{67}KN_8O_{20}P$]: calcd [M + K]$^+$, 1253.3846; found, 1253.3846.

F′-NE(pY)TARQ. MALDI-TOF (*m/z*) [$C_{57}H_{68}N_{12}O_{23}P$]: calcd [M + H]$^+$, 1319.4258; found, 1319.4258.

F ′-AEEEI(pY)GEFEAKKKK. MALDI-TOF (*m/z*) [$C_{102}H_{139}N_{19}O_{36}P$]: calcd [M + H]$^+$, 2236.9368; found, 2236.9370.

F′-PS(pY)VNVQN-NH$_2$. MALDI-TOF (*m/z*) [$C_{61}H_{74}N_{12}O_{22}P$]: calcd [M + H]$^+$, 1357.4778 ; found, 1357.4781.

F′-G(pY)EEI. MALDI-TOF (*m/z*) [$C_{48}H_{51}N_5O_{20}P$]: calcd [M+ H]$^+$, 1048.2865; found, 1048.2872.

Cell Culture and Cytotoxicity Assay.

Cell Culture. Human leukemia carcinoma cell line CCRF-CEM (ATCC No. CCL-119), ovarian adenocarcinoma SK-OV-3 (ATCC No. HTB-77), colorectal carcinoma HCT-116 (ATCC No. CCL-247), and normal human colon myofibroblast (CCD-18Co, ATCC No. CRL-1459) were obtained from American Type Culture Collection. Cells were grown in 75 cm^2 cell culture flasks with EMEM (Eagle's minimum essential medium), supplemented with 10% fetal bovine serum, and 1% penicillin/streptomycin solution (10,000 units of penicillin and 10 mg of streptomycin in 0.9% NaCl) in a humidified atmosphere of 5% CO_2, 95% air at 37 °C.

Flow Cytometry Studies. Human leukemia adenocarcinoma (CCRF-CEM, 1×10^7 cells) or human ovarian adenocarcinoma cells (SK-OV-3, 3×10^5 cells) were taken in 6-well plates in opti-MEM or serum-free RPMI medium. Then the fluorescence-labeled phosphopeptides (F′-PE(pY)LGLD, F′-G(pY)-LPQTV, F′-NE(pY)TARQ, F′-PS(pY)VNVQN-NH_2, F′-AEEEI(pY)G EFEAKKKK, or F′-G(pY)EEI) (5−10 μM) were added to the different wells containing $[WR]_4$ (25−50 μM) in media. The plates were incubated for 1−2 h at 37 °C. Cells and fluorescence-labeled phosphopeptides alone were used as negative controls. After 1−2 h incubation, the medium containing the peptide was removed. The cells were digested with 0.25% trypsin/EDTA (0.53 mM) for 5 min to remove any artificial surface binding. Then the cells were washed

twice with PBS. Finally, the cells were resuspended in flow cytometry buffer and analyzed by flow cytometry (FACSCalibur: Becton Dickinson) using FITC channel and CellQuest software. The data presented were based on the mean fluorescence signal for 10,000 cells collected. All assays were performed in triplicate. A similar procedure was used for linear $(WR)_4$ and linear tripodal peptide LPA4 FACS studies.

Cell Cytotoxicity Assay of $[WR]_4$ + *PEpYLGLD Mixture*. SK-OV-3 (5,000 cells), CCRF-CEM (40,000 cells), HCT-116 (4,000), and CCD-18Co (3,000 cells) were seeded in 0.1 mL per well in 96-well plates 24 h prior to the experiment. The old medium (EMEM containing fetal bovine serum (FBS) (10%) for SK-OV-3, HCT-116, and CCD-18Co was removed. The stock solutions were prepared at high concentrations to generate maximum intermolecular interactions and then were diluted to desired concentrations for cellular studies. $[WR]_4$ (25 μM) + PEpYLGLD (5 μM) or $[WR]_4$ (50 μM) + PEpYLGLD (10 μM) in serum containing medium was added, and the cells were incubated for 24 h at 37 °C in a humidified atmosphere of 5% CO_2. In the case of CCRF-CEM (nonadherent cells), the final concentration was calculated after addition of the compounds. Cell viability was then determined by measuring the fluorescence intensity of the formazan product at 490 nm using a SpectraMax M2 microplate spectrophotometer. The percentage of cell survival was calculated as [(OD value of cells treated with the test mixture of compounds) − (OD value of culture medium)]/[(OD value of control cells) − (OD value of culture medium)] × 100%.

Cellular Uptake Studies in the Presence of Inhibitors. Human ovarian adenocarcinoma cells (SK OV-3) were seeded in 6-well plates (3×10^5 cells/well) in opti-MEM. The cells were preincubated by various inhibitors including nystatin (50 μg/mL),

chloroquine (100 μM), chlorpromazine (30 μM), methyl-β-cyclodextrin (2.5 mM), and 5-(*N*-ethyl-*N*-isopropyl) amiloride (EIA, 50 μM) for 30 min. The treatment was removed, and the cells were incubated with $[WR]_4$ (25 μM), F′-PE(pY)LGLD (5 μM), and a similar concentration of inhibitors for 1 h. To induce ATP depletion, the cells were preicubated with 0.5% of 150 mM sodium azide in opti MEM prior to the addition of the compound followed by 1 h incubation. Consequently, a similar FACS protocol was performed as described above.

Confocal Microscopy on Live Cells. Adherent SK-OV-3 cells were seeded with EMEM media overnight on coverslips in 6-well plates. Then the media were removed and washed with opti-MEM. The cells were treated with F′-PEpYLGLD (5 μM) in the presence or absence of $[WR]_4$ (25 μM) for 1 h at 37 °C. The stock solutions were prepared at high concentrations to generate maximum intermolecular interactions and then were diluted to desired concentrations for cellular studies. After 1 h incubation, the media containing the treatments were removed followed by washing with PBS three times. Then the coverslips were mounted on a microscope slide with mounting media with the cell-attached side facing down. Laser scanning confocal microscopy was carried out using Carl Zeiss LSM 510 system. The cells were imaged using FITC and phase contrast channels.

Transmission Electron Microscopy (TEM). TEM samples were prepared by drop casting of PEpYLGLD (1 mM in H_2O), $[WR]_4$ (1 mM in H_2O), or mixture of PEpYLGLD and $[WR]_4$ (1 mM in H_2O) solution (incubated for one day) (10 μL) onto the Formvar coated carbon grid of mesh size 300, which was allowed to sit for 2 min. Excess solvent was carefully removed by capillary action (filter paper). Grids were

allowed to dry at room temperature overnight. All images were taken using a JEOL transmission electron microscope (Tokyo, Japan) maintained at 80 kV. After drop casting of peptide solutions, grids were then stained with uranyl acetate (20 μL) for 2 min. Excess stain was removed, and the grids were allowed to dry overnight. *Isothermal Titration Calorimetry (ITC).* ITC was performed on a Microcal VP-ITC microcalorimeter (Microcal, Northampton, MA). Data acquisition and instrument control were carried out using a dedicated Origin software package. All the experiments were performed at 30 °C using cyclic peptide $[WR]_4$ (500 μM) and PEpYLGLD (6 mM). Both PEpYLGLD and $[WR]_4$ were dissolved in water. A solution containing $[WR]_4$ (1.42 mL) was transferred into the sample cell. A solution of PEpYLGLD (6 mM, 10 μL) was injected from the syringe (280 μL) into the stirred sample cell (stirring speed 307 rpm). The reference cell was filled with deionized water. A 180 s time interval between injections was applied in order to allow the system to reach thermal equilibrium after each addition. Corrections were made for the dilution heat of the phosphopeptide, which was determined in control experiments under similar conditions. Analysis of the integrated heat data was performed using the Origin 7 package provided with the ITC instrument. Experimental data was fitted using a nonlinear least-squares minimization algorithm to a theoretical titration curve. Different binding models were assumed, involving a single set of identical sites, two sets of independent sites, or sequential binding events. The equations were included in the commercial ITC Data analysis software package of Origin 7.0. The chi-square parameter $\chi 2$ was used to establish the best fit.

Circular Dichroism. CD spectra were recorded on a JASCO J-810 spectropolarimeter using 1 mm path length cuvettes. The scan speed was 100 nm/min, and spectra were averaged over 8 scans. All experiments on the samples including $[WR]_4$ (25 μM, H_2O) and PEpYLGLD (25 μM, H_2O) were tested at room temperature. The CD for background reference (water) was measured and subtracted from the sample.

Molecular Modeling. Initial coordinates for $[WR]_5$ were obtained using GAUSSVIEW.[32] Ab initio Hartree−Fock molecular orbital calculations with complete geometry optimizations were performed with 6-31G33 basis set on monomer $[WR]_5$ utilizing GAUSSIAN'03 software. Geometry of monomers was completely optimized. All bond lengths, bond angles, and dihedral angles were allowed to relax without any constraint.

RESULTS AND DISCUSSION

Chemistry. A number of fluorescence labeled phosphopeptides, F′-GpYLPQTV, F′ NEpYTARQ, F′-AEEEIYGEFEAKKKK, F′-PEpYLGLD, F′-pYVNVQN-NH_2, and F′-GpYEEI, where F′ is fluorescein (Figure 1), were synthesized according to the previously reported procedure.[34] These phosphopeptides were selected based on the sequence of phosphoprotein binding motif of protein tyrosine kinases that binds to the SH2 domain of other protein tyrosine kinases and leads to enzyme activation.[35]

As representative examples, the synthesis of Ac-PEpYLGLD (mentioned here as PEpYLGLD) and F′-PEpYLGLD is outlined here (Scheme 1). In general, the peptides were assembled on Wang resin using Fmoc solid-phase synthesis. Fmoc

protection group at the *N*-terminal was removed. Subsequent capping reaction by acetic anhydride or conjugation reaction with 5(6)-carboxyfluorescein isobutyrate was performed in the presence of HOAt, PyAOP, and *N*,*N*-diisopropylethylamine (DIPEA) in DMF:DCM (5:1 v/v) followed by deprotection, and cleavage from the resin in the presence of reagent R containing TFA/thioanisole/EDT/ anisole (90:5:3:2 v/v/v/v) afforded crude products, which were purified by preparative reversed-phase HPLC. The structures of the compounds were confirmed by high-resolution MALDI TOF/TOF and/or high-resolution electrospray mass spectrometry. We have previously reported the synthesis of $[WR]_4$.[31] A similar procedure was employed for the synthesis of other phosphopeptides by using appropriate resins and side chain protected amino acids.

Cellular Uptake Studies. The cellular uptake of synthesized fluorescence-labeled phosphopeptides (10 μM) was examined in the presence and absence of $[WR]_4$ (50 μM) in human leukemia carcinoma (CCRF-CEM) cells after 2 h incubation at 37 °C using flow cytometry. After the incubation, cells were treated with trypsin to remove the cell surface-bound compound. $[WR]_4$ enhanced the cellular uptake of all phosphopeptides, including F′-GpYLPQTV, F′-NEpYTARQ, F′-AEEEIYGEFEAKKKK, F′-pYVNVQN-NH_2, and F′-GpYEEI by 7-, 5-, 10-, 4-, and 19-fold, respectively. Fluorescence activated cell sorting (FACS) analysis showed that the cellular uptake of F′-PEpYLGLD in the presence of $[WR]_4$ was increased dramatically by 27-fold when compared to F′-PEpYLGLD alone (Figure 2). These data indicate that the cellular uptake of the phosphopeptides was improved in the

presence of $[WR]_4$ in a sequence dependent manner possibly due to different binding affinity between the phosphopeptides and $[WR]_4$.

Because of dramatic effect of $[WR]_4$ on improving the cellular delivery of F′-PEpYLGLD, this phosphopeptide was selected for further studies. PEpYLGLD is a sequence that mimics the pTyr1246 of ErbB2 that is responsible binding to the Chk SH2 domain.[14] The cellular uptake of F′-PEpYLGLD (10 μM) was also evaluated in the presence of the linear $(WR)_4$ (50 μM) using FACS under similar conditions and compared with that of cyclic $[WR]_4$ (Figure 3). The results showed that the linear $(WR)_4$ enhanced the cellular uptake of F′-PEpYLGLD by 17-fold in CCRF-CEM cells after 1 h incubation. However, the cyclic $[WR]_4$ was found to enhance the cellular uptake of F′-PEpYLGLD approximately 24-fold after 1 h incubation under similar conditions, suggesting the cyclic nature of the peptide is important for improving the cellular delivery of the phosphopeptide.

We have previously reported that Lys-$(CH_2)_{11}$-Arg-$(CH_2)_{11}$-Arg, a linear tripodal amphipathic peptide containing two arginine and one lysine residues (LPA4), enhanced the cellular delivery of a phosphopeptide (F′-GpYEEI) in the human breast carcinoma cells BT-20 (ATCC No. HTB-19) cells by 10-fold.[30] A comparative FACS study exhibited that the cellular uptake of F′-PEpYLGLD (10 μM) enhanced approximately 6 times in the presence of LP4 (50 μM) in CCRF-CEM cells after 1 h incubation. Thus, the transporting efficiency of LPA4 for F′-PEpYLGLD was significantly less than that of the cyclic $[WR]_4$ that showed 24-fold higher cellular delivery of the same phosphopeptide after 1 h incubation (Figure 3).

To evaluate the cytotoxicity of PEpYLGLD and $[WR]_4$, cell viability assay was employed in three different cancer cell lines, including CCRF-CEM, SK-OV-3, HCT-116 cells, and CCD-18Co cells at the experimental concentration of PEpYLGLD (5 μM) and $[WR]_4$ (25 μM). We have previously shown that cyclic $[WR]_4$ is not cytotoxic in HCT-116, CCRF-CEM, and SK-OV-3 cells at similar concentrations.[31] The mixture of $[WR]_4$ (25 μM) and PEpYLGLD (5 μM) or $[WR]_4$ (50 μM) and PEpYLGLD (10 μM) did not show any significant toxicity in normal cells and HCT-116 carcinoma cells after 24 h incubation at 37 °C (Figure 4). While $[WR]_4$ (25 μM) and PEpYLGLD (5 μM) did not exhibit any cytotoxicity in SK-OV-3 and CCRF-CEM cells, the mixture showed 10−12% toxicity when higher concentrations of phosphopeptide (10 μM) and $[WR]_4$ (50 μM) were used. Thus, a concentration of PEpYLGLD (5 μM) and $[WR]_4$ (25 μM) was used in SKOV-3 and CCRF-CEM cells in all cellular uptake and confocal microscopy studies.

To investigate whether the performance of $[WR]_4$ is cell-type dependent, the intracellular uptake of a lower concentration of F′-PEpYLGLD (5 μM) was examined in human ovarian adenocarcinoma (SK-OV-3) cells in the presence or absence of $[WR]_4$ (25 μM). After 1 h incubation at 37 °C, FACS showed 22-fold higher fluorescence signals in the cells treated with F′-PEpYLGLD-loaded $[WR]_4$ compared to those treated with F′-PEpYLGLD alone, suggesting that the uptake of F′-PEpYLGLD is also enhanced by $[WR]_4$ in SK-OV-3 cells (Figure 5a).

The cellular uptake and internalization of many CPPs along with the conjugated cargo occurs predominantly via an endocytic pathway that involves macropinocytosis, caveolae pathway, clathrin-mediated endocytosis, or lipid-raft

dependent endocytosis. The nature of the cell lines and the presence and type of the cargo could affect the specific mechanism employed by the CPP.[36] We have previously shown that the cellular uptake of $[WR]_4$ was independent of endocytosis.[31a] Thus, the mechanism of the cellular uptake of the complex mixture of $[WR]_4$ and F′-PEpYLGLD was evaluated in the presence of different inhibitors to determine whether the cargo changes the uptake mechanism

To perform the ATP depletion, sodium azide was incubated with cells for 30 min prior to the incubation with the complex followed by 1 h incubation. Significant intracellular uptake of F′-PEpYLGLD in the presence of $[WR]_4$ in SK-OV-3 cells (Figure 5a) was still observed in the presence of sodium azide, suggesting that the cellular uptake is not significantly reduced by inducing ATP depletion.

Furthermore, $[WR]_4$ was still able to improve the cellular uptake of F′-PEpYLGLD in SK-OV-3 cells in the presence of different endocytic inhibitors, such as nystatin, EIA, chlorpromazine, chloroquine, and methyl β-cyclodextrin, ruling out clathrin-mediated or caveolae-mediated endocytosis, and macropinocytosis as the major mechanism of uptake after 1 h incubation (Figure 5a). The cellular delivery of the phosphopeptide in the presence of $[WR]_4$ and inhibitors was still higher than F′-PEpYLGLD alone, suggesting the mechanism of cellular uptake is not exclusively endocytosis. This is a key advantage of $[WR]_4$ compared to known CPPs, which are dependent on endocytotic entry. Another proposed mechanism for cellular uptake of CPPs is direct membrane transduction. The amphipathic nature of $[WR]_4$ and interactions of arginine and tryptophan residues in $[WR]_4$ with the corresponding negatively charged phospholipids and hydrophobic residues in lipid bilayer may have

contributed to the initial entry into the cell membrane. Hydrophobic interactions between tryptophan residues and the lipids could lead to possible distortion of the outer phospholipid monolayer, followed by peptide internalization and enhanced cellular uptake of the cargo. Model studies have suggested that the direct transduction occurs through carpet-like perturbations, pore formation, or inverted micelles formed in the bilayer membrane.[36] Further mechanistic studies will provide insights for designing the next generation of cyclic peptides as molecular transporters of phosphopeptides.

The cellular uptake of F′-PEpYLGLD was found to be rapid and time-dependent. F′-PEpYLGLD (5 μM) was incubated with $[WR]_4$ (25 μM) at different incubation times including 10 min, 30 min, and 1 h. FACS results showed that the cellular uptake of F′-PEpYLGLD was increased in a time-dependent pattern (Figure 5b). On the other hand, the cellular uptake of F′-PEpYLGLD was not changed significantly in the absence of $[WR]_4$.

Confocal microscopy in live cells was used to monitor the cellular uptake of F′-PEpYLGLD in the presence and absence of the peptide. Incubation of a mixture of F′-PEpYLGLD $[WR]_4$ showed significantly higher cellular uptake when compared to that of F′-PEpYLGLD alone as shown by intracellular fluorescence. Comparison of the intracellular localization of F′-PEpYLGLD-loaded $[WR]_4$ to F′-PEpYLGLD alone after 1 h incubation at 37 °C confirmed that the presence of the cyclic peptide is critical for the enhanced cellular permeability (Figure 6).

Circular dichroism (CD), transmission electron microscopy (TEM), and isothermal titration calorimetry (ITC) were used to gain a better insight about the interaction of $[WR]_4$ and PEpYLGLD. CD was used to get a better understanding of the secondary structure change in $[WR]_4$ and PEpYLGLD upon mixing and intermolecular interactions. All spectra were corrected for background by subtraction of the blank. CD results showed that PEpYLGLD (25 μM) loaded with $[WR]_4$ (25 μM) showed a different CD pattern compared to those of parent analogs, $[WR]_4$ (25 μM) and PEpYLGLD (25 μM). While PEpYLGLD did not show any specific structure, both PEpYLGLD loaded $[WR]_4$ and $[WR]_4$ exhibited a maximum at 230 nm and a minimum at 203−205 nm, suggesting that $[WR]_4$ maintain the secondary structure partially upon binding with in PEpYLGLD. These secondary structures are distinct from known α and β structures. However, the pattern of the spectra shows some major differences between PEpYLGLD loaded $[WR]_4$ and $[WR]_4$ at <190 nm and in intensity of ellipticity in maximum and minimum peaks (Figure 7).

The interaction between PEpYLGLD and $[WR]_4$ was visualized by using TEM. The stable mixture of $[WR]_4$ and PEpYLGLD was prepared at a high concentration to achieve the maximum interaction. An optimized balance between the hydrophobic and electrostatic interactions generated by the drug and the carrier led to the formation of nanosized particles. $[WR]_4$ generated self-assembled nanostructures after one day incubation at room temperature. Initial TEM imaging of negatively stained $[WR]_4$ (1 mM aqueous solution) showed circular vesicle-like structures with approximate size of 25−60 nm. TEM images of PEpYLGLD (Figure 8a) exhibited amorphous structures with approximate size of 40 nm. When PEpYLGLD was added

to $[WR]_4$ in solution, PEpYLGLD-loaded $[WR]_4$ formed some larger noncircular nanosized structures with approximate width and height of 125 and 60 nm, respectively, possibly through electrostatic and/or hydrophobic intermolecular interactions between the positively charged cyclic peptide and negatively charged phosphopeptides (Figure 8b). TEM images further confirm that the structures of $[WR]_4$ modify upon binding with PEpYLGLD, generating new nanostructures.

ITC was used to measure the binding constants between PEpYLGLD and $[WR]_4$ in complex formation. The ITC measurements were carried out at 30 °C by adding an aqueous solution PEpYLGLD (6 mM) to $[WR]_4$ (500 μM) solution in water. The equation for three sequential binding events was found to be the best fit for the data as shown by the Origin software. The chi squared $\chi 2$ value was found to be 1.6×10^2 produced by three sequential models. The binding constant values for three sequential events were determined as $K_1 = 7.1 \times 103\ M^{-1}$, $K_2 = 4.9 \times 103\ M^{-1}$, and $K_3 = 1.1 \times 104\ M^{-1}$ (Figure 9). The enthalpies (ΔH) for the binding were −0.17, 0.30, and −0.23 kcal/mol, and the entropies (TΔS) were 5.2, 5.4, and 5.3 kcal/mol, respectively. Therefore, the Gibbs free energies (ΔG) calculated from ΔH and TΔS were −5.4, −5.1, and −5.6 kcal/mol for each binding site. ITC data suggest that PEpYLGLD and $[WR]_4$ form a complex through multistep intermolecular interactions including hydrophobic interactions driven by entropy as shown previously.[37] These data indicate that, in addition to the electrostatic interactions between positively charged cyclic peptide and negatively charged phosphopeptide, hydrophobic forces also contribute to the complex formation possibly due to the interactions of the hydrophobic tryptophan and leucine residues in $[WR]_4$ and PEpYLGLD, respectively. ITC and TEM results are relevant to

cellular studies since the stock solutions were prepared at high concentrations to generate maximum intermolecular interactions and then were diluted further to obtain desired concentration for cell-based assays.

Molecular modeling studies of $[WR]_5$, a similar model cyclic peptide, were used to gain better insights of three-dimensional structure of this class of peptides. Initial coordinates for $[WR]_5$ were obtained followed by ab initio Hartree−Fock molecular orbital calculations with complete geometry optimizations utilizing GAUSSIAN'03 software.[32] Two different conformations were obtained (Figure 10). The lowest energy conformation did not allow any intramolecular H-bonding. Higher energy conformation (25 kcal/mol) showed intramolecular H-bonding between cationic and neutral side chains. Side chains have to reorganize for efficient intramolecular hydrogen bonding resulting in higher energy conformation. In the lowest energy conformation tryptophan side chains are disposed perpendicular to backbone. Higher energy conformation being more planar seems more suited for stacking.

Conclusions

In summary, a new carrier system for the delivery of cell impermeable phosphopeptides was discovered using cyclic octapeptide $[WR]_4$ containing alternative tryptophan and arginine residues. The cellular uptake of F′-PEpYLGLD was enhanced by 27-fold in the presence of $[WR]_4$, and was found to be time-dependent. Positively charged cyclic peptide formed nanostructures in the presence of

negatively charged PEpYLGLD as shown by TEM. Binding affinity between $[WR]_4$ and PEpYLGLD was further confirmed by ITC studies. To the best of our knowledge, this is the first report of using cyclic peptides for noncovalent cellular delivery of cell impermeable phosphopeptides. These data provide insights about using cell-penetrating cyclic peptides as PAs for delivery of negatively charged cell impermeable phophopeptides.

ASSOCIATED CONTENT

Supporting Information

Analytical HPLC data, high resolution mass spectra, and additional supporting data. This material is available free of charge via the Internet at *http://pubs.acs.org*.

Notes

The authors declare no competing financial interest.

ACKNOWLEDGMENTS

We acknowledge the financial support from National Science Foundation, Grant No. CHE 0748555. We thank the National Institute of General Medical Sciences of the National Institutes of Health under Grant No. 8 P20 GM103430-12 for sponsoring the core facility.

ABBREVIATIONS USED

BT-20, human breast carcinoma cell line; CCRF-CEM, human leukemia carcinoma cell line; CD, circular dichroism; CCD-18Co, normal human colon myofibroblast; CPPs, cell-penetrating peptides; DCM, dichloromethane; DIPEA, *N*,*N*-diisopropylethylamine; DMF, *N*,*N*-dimethylformamide; EIA, 5-(*N*-ethyl-*N*-isopropyl)amiloride; F′, fluorescein; FACS, fluorescence activated cell sorter; FBS, fetal bovine serum; DCM, dichloromethane; EDT, ethandithiol; HBTU, 2-(1H-benzotriazole-1-yl)-1,1,3,3-tetramethyluronium hexfluoro phosphate; HCT-116, human colorectal carcinoma; HOBt, hydroxybenzotriazole; HOAt, 1-hydroxy-7 azabenzotriazole; ITC, isothermal calorimetry; NMM, *N*-methylmorpholine; PAs, peptide amphiphiles; PTB, phosphotyrosine binding; PyAOP, 7-azabenzotriazol- 1-yloxy tripyrrolidinophosphonium hexafluorophosphate); SH2, Src homology 2; SK-OV-3, human ovarian adenocarcinoma; TFA, trifluoroacetic acid; TEM, transmission electron microscopy.

REFERENCES

(1) Bulut, S.; Erkal, T. S.; Toksoz, S.; Tekinay, A. B.; Tekinay, T.; Guler, M. O. Slow release and delivery of antisense oligonucleotide drug by self-assembled peptide amphiphile nanofibers. Biomacromolecules 2011, 12, 3007−3014.

(2) Kim, J. K.; Anderson, J.; Jun, H. W.; Repka, M. A.; Jo, S. Self-assembling peptide amphiphile-based nanofiber gel for bioresponsive cisplatin delivery. Mol. Pharmaceutics 2009, 6, 978−85.

(3) Dheur, S.; Dias, N.; Van Aerschot, A.; Herdewijn, P.; Bettinger, T.; Rémy, J. S.; Hélène, C.; Saison-Behmoaras, E. T. Polyethylenimine but not cationic lipid improves antisense activity of 3′-capped phosphodiester oligonucleotides. Antisense Nucleic Acid Drug Dev. 1999, 9, 515−25.

(4) Jeong, J. H.; Kim, S. H.; Kim, S. W.; Park, T. G. Intracellular delivery of poly(ethylene glycol) conjugated antisense oligonucleotide using cationic lipids by formation of self-assembled polyelectrolyte complex micelles. J. Nanosci. Nanotechnol. 2006, 6, 2790−2795.

(5) Crombez, L.; Aldrian-Herrada, G.; Konate, K.; Nguyen, G. N.; McMaster, G. K; Brasseur, R.; Heitz, G. K.; Divita, G. A new potent secondary amphipathic cell-penetrating peptide for siRNA delivery into mammalian cells. Mol. Ther. 2008, 17, 95−103.

(6) El-Andaloussi, S.; Holm, T.; Langel, U. Cell-penetrating peptides: mechanisms and applications. Curr. Pharm. Des. 2005, 11, 3597−3611.

(7) Fotin-Mleczek, M.; Fischer, R.; Brock, R. Endocytosis and cationic cell-penetrating peptides–a merger of concepts and methods. Curr. Pharm. Des. 2005, 11, 3613−3628.

(8) Fernandez-Carneado, J.; Kogan, M. J.; Pujals, S.; Giralt, E. Amphipathic peptides and drug delivery. Biopolymers 2004, 76, 196−203.

(9) Deshayes, S.; Morris, M. C.; Divita, G.; Heitz, F. Cell-penetrating peptides: tools for intracellular delivery of therapeutics. Cell. Mol. Life. Sci. 2005, 62, 1839−1849.

(10) Torchilin, V. P.; Rammohan, R.; Weissig, V.; Levchenko, T. S. TAT peptide on the surface of liposomes affords their efficient intracellular delivery even at low temperature and in the presence of metabolic inhibitors. Proc. Natl. Acad. Sci. U.S.A. 2001, 98, 8786−8791.

(11) Silhol, M.; Tyagi, M.; Giacca, M.; Lebleu, B.; Vives, E. Different mechanisms for cellular internalization of the HIV-1 Tat-derived cell penetrating peptide and recombinant proteins fused to Tat. Eur. J. Biochem. 2002, 269, 494−501.

(12) Thorén, P. E.; Persson, D.; Isakson, P.; Goksör, M.; Onfelt, A.; Nordén, B. Uptake of analogs of penetratin, Tat(48−60) and oligoarginine in live cells. Biochem. Biophys. Res. Commun. 2003, 307, 100−107.

(13) Zhou, Y.; Abagyan, R. How and why phosphotyrosine-containing peptides bind to the SH2 and PTB domains. Folding Des. 1998, 3, 513−522.

(14) Machida, K.; Mayer, B. J. The SH2 domain: versatile signaling module and pharmaceutical target. Biochim. Biophys. Acta 2005, 1747, 1−25.

(15) Songyang, Z.; Shoelson, S. E.; Chaudhuri, M.; Gish, G.; Pawson, T.; Haser, W. G.; King, F.; Roberts, T.; Ratnofsky, S.; Lechleider, R. J.; Neel, B. G.; Birge, R. B.; Fajardo, J. E.; Chou, M. M.; Hanafusa, H.; Schaffhausen, B.; Cantley, L. C. SH2 domains recognize specific phosphopeptide sequences. Cell 1993, 72, 767−778.

(16) Pinna, L. A.; Donella-Deana, A. Phosphorylated synthetic peptides as tools for studying protein phosphatases. Biochim. Biophys. Acta 1994, 1222, 415−431.

(17) Ottinger, E. A.; Shekels, L. L.; Bernlohr, D. A.; Barany, G. Synthesis of phosphotyrosine-containing peptides and their use as substrates for protein tyrosine phosphatases. Biochemistry 1993, 32, 4354−4361.

(18) Burke, T. R.; Yao, Z. J.; Liu, D. G.; Voigt, J.; Gao, Y. Phosphoryltyrosyl mimetics in the design of peptide-based signal transduction inhibitors. Biopolymers 2001, 60, 32−44.

(19) Eck, M. J. A new flavor in phosphotyrosine recognition. Structure 1995, 3, 421−424.

(20) Dunican, D. J.; Doherty, P. Designing cell-permeant phosphopeptides to modulate intracellular signaling pathways. Biopolymers 2001, 60, 45−60.

(21) Williams, E. J.; Dunican, D. J.; Green, P. J.; Howell, F. V.; Derossi, D.; Walsh, F. S.; Doherty, P. Selective inhibition of growth factor-stimulated mitogenesis by a cell-permeable Grb2-binding peptide. J. Biol. Chem. 1997, 272, 22349−22354.

(22) Derossi, D.; Williams, E. J.; Green, P. J.; Dunican, D. J.; Doherty, P. Stimulation of mitogenesis by a cell-permeable PI 3-kinase binding peptide. Biochem. Biophys. Res. Commun. 1998, 251, 148−152.

(23) Theodore, L.; Derossi, D.; Chassaing, G.; Llirbat, B.; Kubes, M.; Jordan, P.; Chneiweiss, H.; Godement, P.; Prochiantz, A. Intraneuronal delivery of protein kinase C pseudosubstrate leads to growth cone collapse. J. Neurosci. 1995, 15, 7158−7167.

(24) Garrido-Hernandez, H.; Moon, K. D.; Geahlen, R. L.; Borch, R. F. Design and synthesis of phosphotyrosine peptidomimetic prodrugs. J. Med. Chem. 2006, 49, 3368−3376.

(25) Boutselis, I. G.; Yu, X.; Zhang, Z. Y.; Borch, R. F. Synthesis and cell-based activity of a potent and selective protein tyrosine phosphatase 1B inhibitor prodrug. J. Med. Chem. 2007, 50, 856−864.

(26) Arrendale, A.; Kim, K.; Choi, J. Y.; Li, W.; Geahlen, R. L.; Borch, R. F. Synthesis of a phosphoserine mimetic prodrug with potent 14−3-3 protein inhibitory activity. Chem. Biol. 2012, 19, 764−771.

(27) Panigrahi, K.; Nelson, D. L.; Berkowitz, D. B. Unleashing a “true” pSer-mimic in the cell. Chem. Biol. 2012, 19, 666−667.

(28) Tarrant, M. K.; Rho, H. S.; Xie, Z.; Jiang, Y. L.; Gross, C.; Culhane, J. C.; Yan, G.; Qian, J.; Ichikawa, Y.; Matsuoka, T.; Zachara, N.; Etzkorn, F. A.; Hart, G. W.; Jeong, J. S.; Blackshaw, S.; Zhu, H.; Cole, P. A. Regulation of CK2 by phosphorylation and OGlcNAcylation revealed by semisynthesis. Nat. Chem. Biol. 2012, 8, 262−269.

(29) Goguen, B. N.; Hoffman, B. D.; Sellers, J. R.; Schwartz, M. A.; Imperiali, B. Light-triggered myosin activation for probing dynamic cellular processes. Angew. Chem., Int. Ed. 2011, 50, 5667−5670.

(30) Ye, G.; Nam, N. H.; Kumar, A.; Saleh, A.; Shenoy, D. B.; Amiji, M. M.; Lin, X.; Sun, G.; Parang, K. Synthesis and evaluation of tripodal peptide analogs for cellular delivery of phosphopeptides. J. Med. Chem. 2007, 50, 3604−3617.

(31) (a) Mandal, D.; Nasrolahi Shirazi, A.; Parang, K. Cellpenetrating homochiral cyclic peptides as nuclear-targeting molecular transporters. Angew. Chem., Int. Ed. 2011, 50, 9633−9637. (b) Nasrolahi Shirazi, A.; Tiwari, R. K.; Chhikara, B. S.; Mandal, D.; Parang, K. Design and evaluation of cell-penetrating peptidedoxorubicin conjugates as prodrugs. Mol. Pharmaceutics 2013, 10, 488−499.

(32) Dennington, R., II; Keith, T.; Millan, J.; Eppinnett, K.; Hovell, W. L.; Gilliand, R.; Gaussview, Version 3.09; Semichem Inc.: S. Mission, KS, 2003.

(33) Ditchfield, R.; Hehre, W. J.; Pople, J. A. An Extended Gaussian- Type Basis for Molecular-Orbital Studies of Organic Molecules. J. Chem. Phys. 1971, 54, 724−728.

(34) Nam, N. H.; Ye, G.; Sun, G.; Parang, K. Conformationally constrained peptide analogs of pTyr-Glu-Glu-Ile as inhibitors of the Src SH2 domain binding. J. Med. Chem. 2004, 47, 3131−3141.

(35) (a) Sawyer, T. K. Src homology-2 domains: structure, mechanisms, and drug discovery. Biopolymers 1998, 47, 243−261. (b) Vu, C. B.; Corpuz, E. G.; Pradeepan, S. G.; Violette, S.; Bartlett, C.; Sawyer, T. K. Nonpeptidic SH2 inhibitors of the tyrosine kinase ZAP-70. Bioorg. Med. Chem. Lett. 1999, 9, 3009−3014. (c) Vu, C. B. Recent advances in the design and synthesis of SH2 inhibitors of Src, Grb2 and ZAP-70. Curr. Med. Chem. 2000, 7, 1081−100. (d) Muller, G. Peptidomimetics SH2 domain antagonists for targeting signal transduction. Top. Curr. Chem. 2000, 211,

17−59. (e) Vu, C. B.; Corpuz, E. G.; Merry, T. J.; Pradeepan, S. G.; Bartlett, C.; Bohacek, R. S.; Botfield, M. C.; Eyermann, C. J.; Lynch, B. A.; MacNeil, I. A.; Ram, M. K.; van Schravendijk, M. R.; Violette, S.; Sawyer, T. K. Discovery of potent and selective SH2 inhibitors of the tyrosine kinase ZAP-70. J. Med. Chem. 1999, 42, 4088−98. (f) Cody, W. L.; Lin, Z.; Panek, R. L.; Rose, D. W.; Rubin, J. R. Progress in the development of inhibitors of SH2 domains. Curr. Pharm. Des. 2000, 6, 59−98.

(36) Madani, F.; Lindberg, S.; Langel, U.; Futaki, S.; Gräslund, A. Mechanisms of cellular uptake of cell-penetrating peptides. J. Biophys. 2011, 2011, 414729.

(37) (a) Ball, V.; Maechling, C. Isothermal microcalorimetry to investigate non specific interactions in biophysical chemistry. Int. J. Mol. Sci. 2009, 10, 3283−3315. (b) Bouchemal, K. New challenges for pharmaceutical formulations and drug delivery systems characterization using isothermal titration calorimetry. Drug Discovery Today 2008, 13, 960−972.

Figure Legends:

Figure 1: Chemical structure of $[WR]_4$ and phosphopeptides synthesized by Fmoc-based peptide chemistry

Figure 2: Comparative cellular uptake of F′-phosphopeptides (10 μM) in the presence of $[WR]_4$ (50 μM) in CCRF-CEM cells after 2 h

Figure 3: Cellular uptake of F′-PEpYLGLD (10 μM) in the presence of cyclic $[WR]_4$ (50 μM), linear $(WR)_4$ (50 μM), or a tripodal linear peptide (LP_4) (50 μM) in CCRF-CEM cells after 1 h incubation

Figure 4: Cytotoxicity assay of the mixture of PEpYLGLD (5 and 10 μM) and $[WR]_4$ (25 and 50 μM) in CCRF-CEM, HCT-116, SK-OV-3, and CCD-18Co cells after 24 h.

Figure 5: (a) Cellular uptake of F′-PEpYLGLD (5 μM) + $[WR]_4$ (25 μM) in the absence or presence of different endocytic inhibitors and sodium azide in SK-OV-3 cells after 1 h. (b) FACS analysis of cellular uptake assays of F′-PEpYLGLD (5 μM)-loaded $[WR]_4$ (25 μM) compared to F′-PEpYLGLD (5 μM) alone in CCRF-CEM

Figure 6: Confocal microscope images of F′-PEpYLGLD (5 μM) uptake by SK-OV-3 cells in the presence of $[WR]_4$ (25 μM)

Figure 7: CD pattern of PEpYLGLD and $[WR]_4$ compared to the PEpYLGLD-loaded $[WR]_4$

Figure 8: (a) Negatively stained TEM images of $[WR]_4$ (1 mM), PEpYLGLD (1 mM), and PEpYLGLD-loaded $[WR]_4$ (1 mM) in water after one day. (b) Proposed mechanism of interactions between PEpYLGLD and $[WR]_4$

Figure 9: The binding isotherm obtained from titration of PEpYLGLD (6 mM) with $[WR]_4$ (500 μM) using a three sequential-binding sites model

Figure 10: Two different conformers of $[WR]_5$

Scheme Legends:

Scheme 1: Solid-Phase synthesis of Ac-PE(pY)LGLD and F′-PE(pY)LGLD

Figure 1

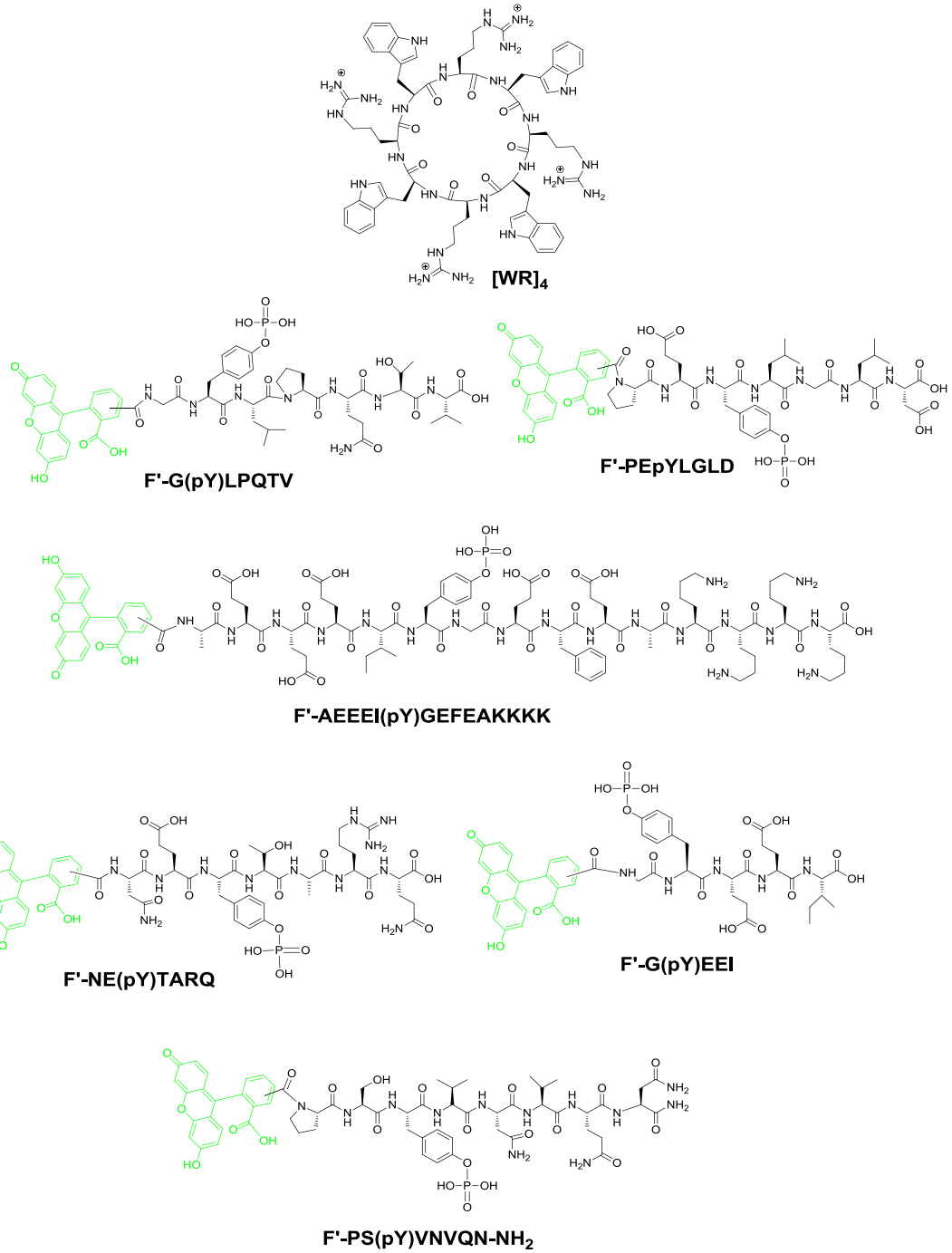
[WR]4
F'-G(pY)LPQTV
F'-PEpYLGLD
F'-AEEEI(pY)GEFEAKKKK
F'-NE(pY)TARQ
F'-G(pY)EEI
F'-PS(pY)VNVQN-NH2

Figure 2

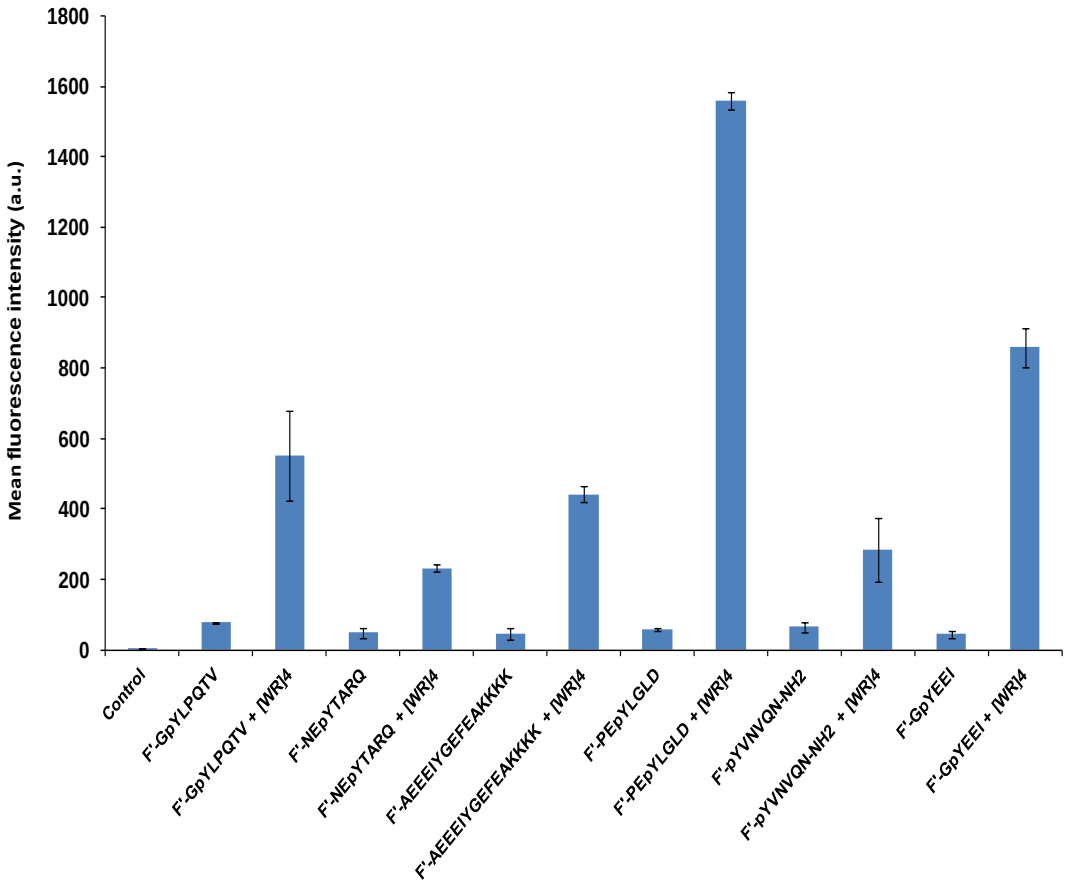
Mean fluorescence intensity (a.u.)
1800
1600
1400
1200
1000
800
600
400
200
0
Control
F'-GpYLPQTV
F'-GpYLPQTV + [WR]4
F'-NEpYTARQ
F'-NEpYTARQ + [WR]4
F'-AEEEIYGEFEAKKK
F'-AEEEIYGEFEAKKK + [WR]4
F'-PEpYLGLD
F'-PEpYLGLD + [WR]4
F'-pYVNVQN-NH2
F'-pYVNVQN-NH2 + [WR]4
F'-GpYEEI
F'-GpYEEI + [WR]4

Figure 3

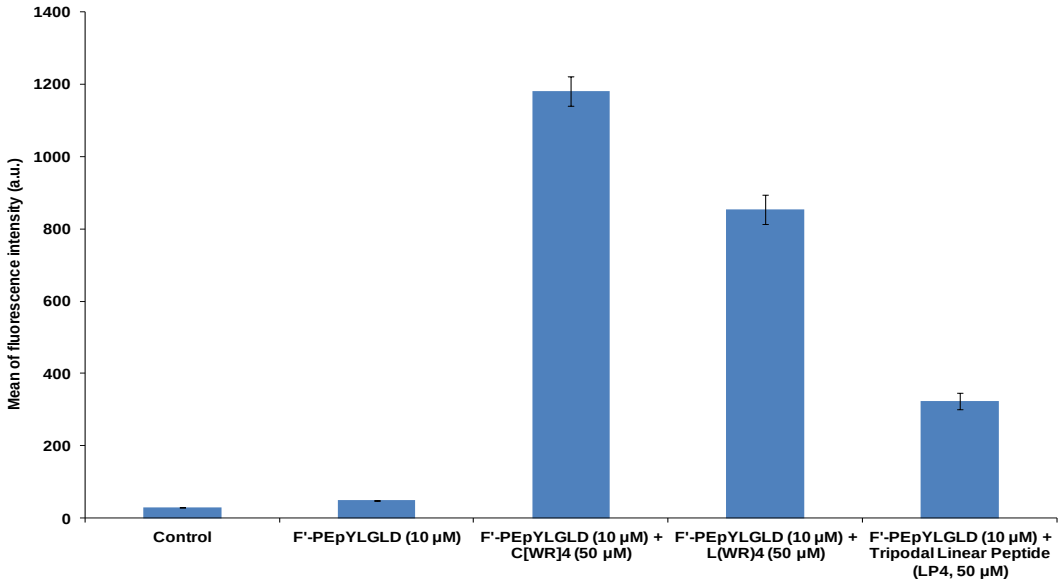

Figure 4

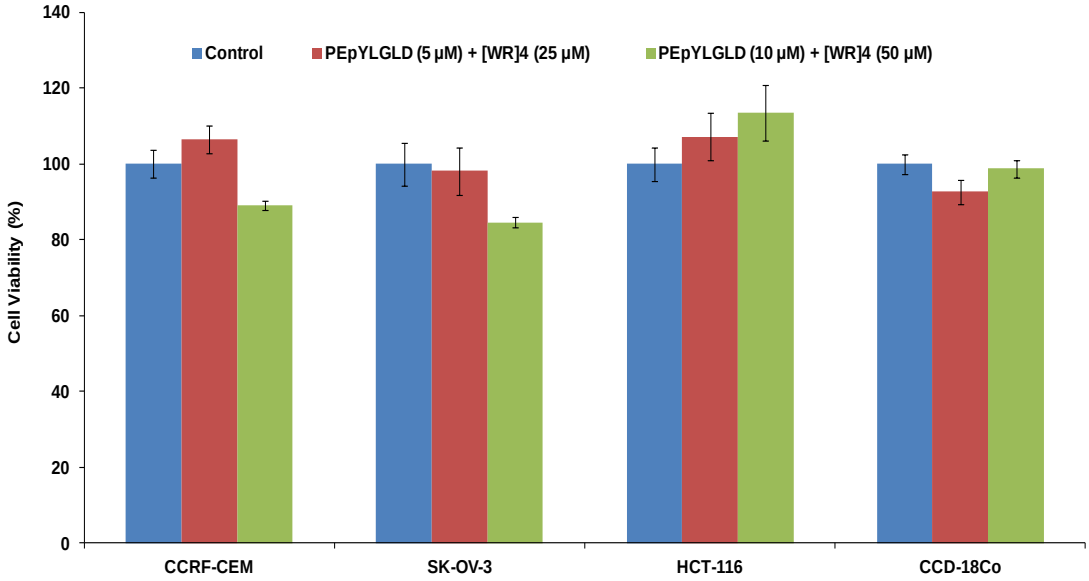

Figure 5

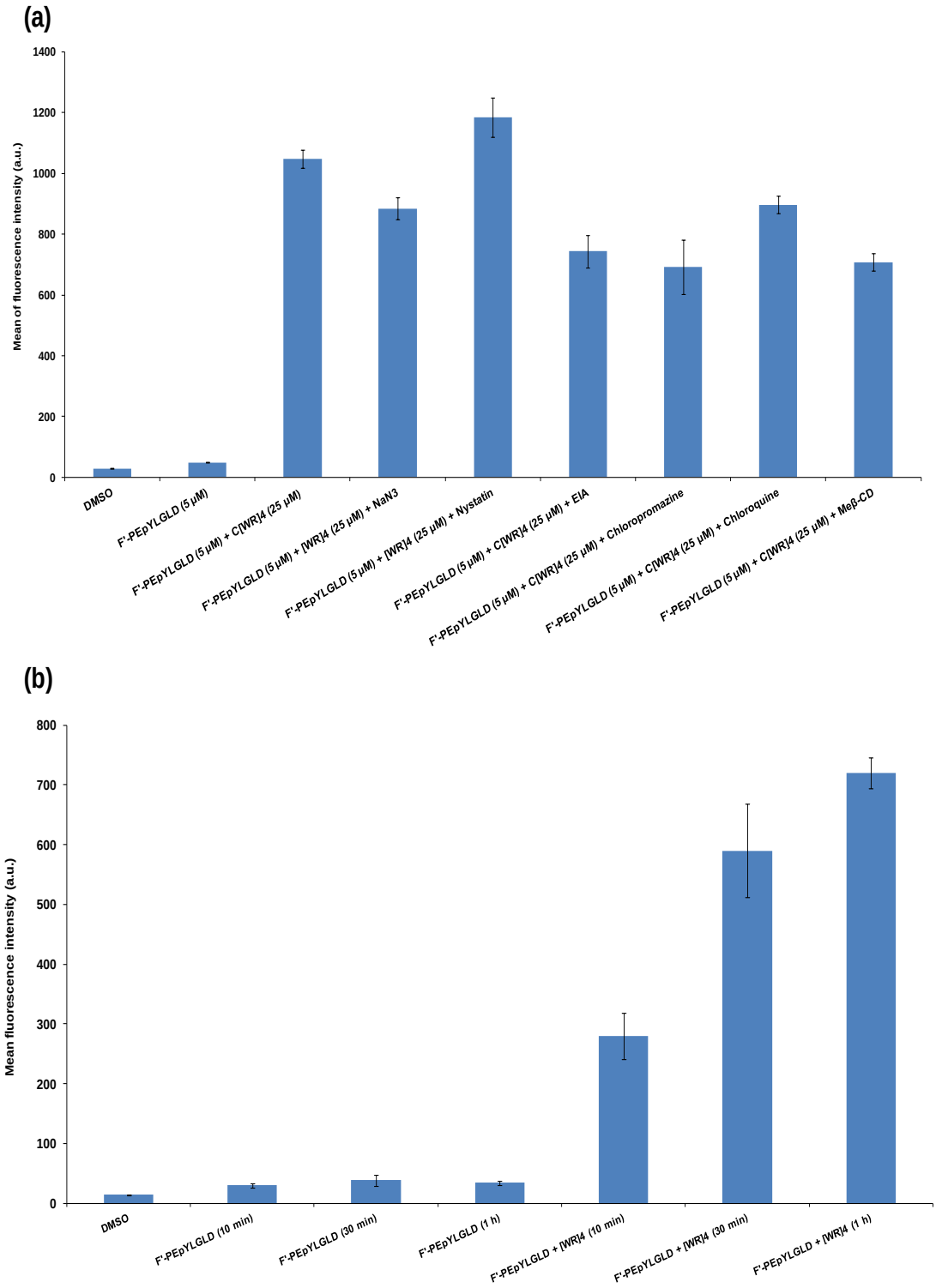
(a)
Mean of fluorescence intensity (a.u.)
1400
1200
1000
800
600
400
200
0
DMSO
F'-PEpYLGLD (5 μM)
F'-PEpYLGLD (5 μM) + C[WR]4 (25 μM)
F'-PEpYLGLD (5 μM) + [WR]4 (25 μM) + NaN3
F'-PEpYLGLD (5 μM) + [WR]4 (25 μM) + Nystatin
F'-PEpYLGLD (5 μM) + C[WR]4 (25 μM) + EIA
F'-PEpYLGLD (5 μM) + C[WR]4 (25 μM) + Chloropromazine
F'-PEpYLGLD (5 μM) + C[WR]4 (25 μM) + Chloroquine
F'-PEpYLGLD (5 μM) + C[WR]4 (25 μM) + Meβ-CD
(b)
Mean fluorescence intensity (a.u.)
800
700
600
500
400
300
200
100
0
DMSO
F'-PEpYLGLD (10 min)
F'-PEpYLGLD (30 min)
F'-PEpYLGLD (1 h)
F'-PEpYLGLD + [WR]4 (10 min)
F'-PEpYLGLD + [WR]4 (30 min)
F'-PEpYLGLD + [WR]4 (1 h)

Figure 6

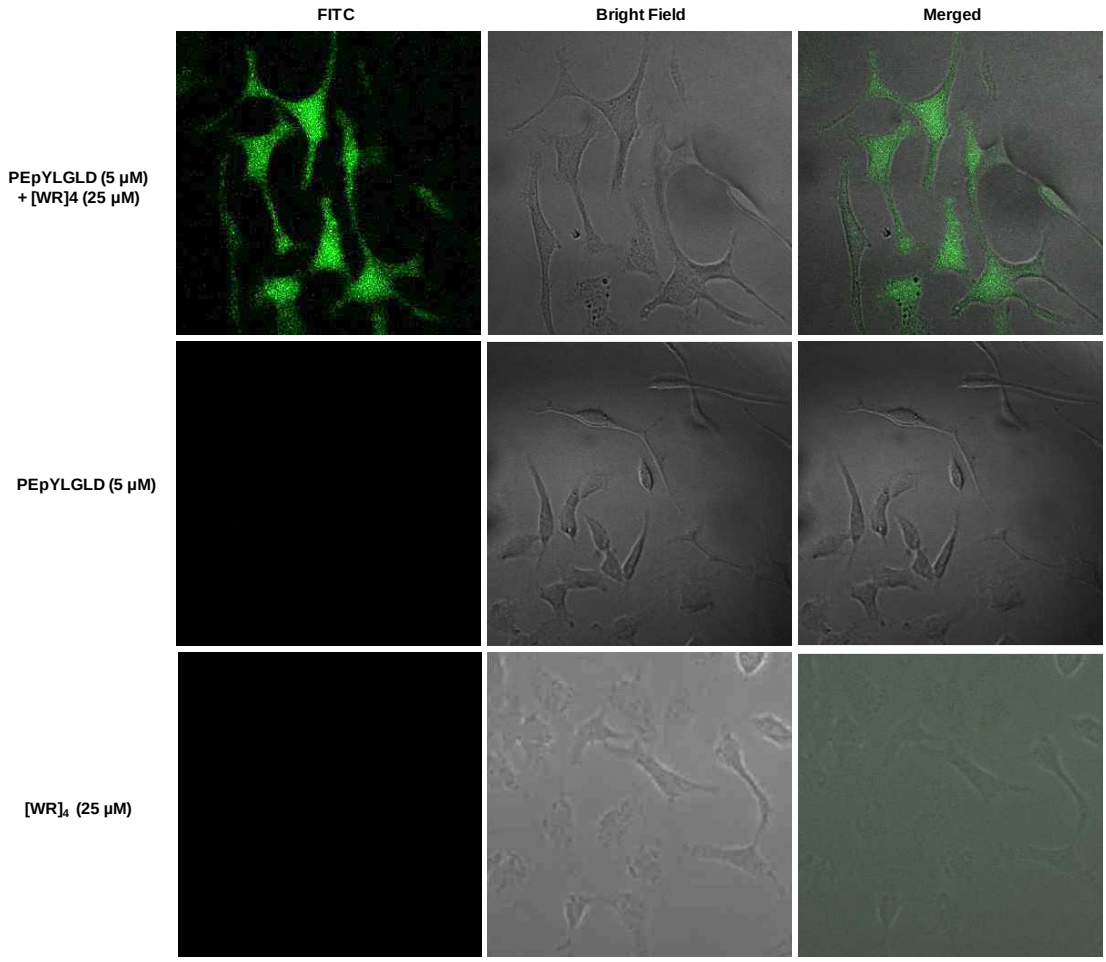
FITC
Bright Field
Merged
PEpYLGLD (5 µM) + [WR]4 (25 µM)
PEpYLGLD (5 µM)
[WR]4 (25 µM)

Figure 7

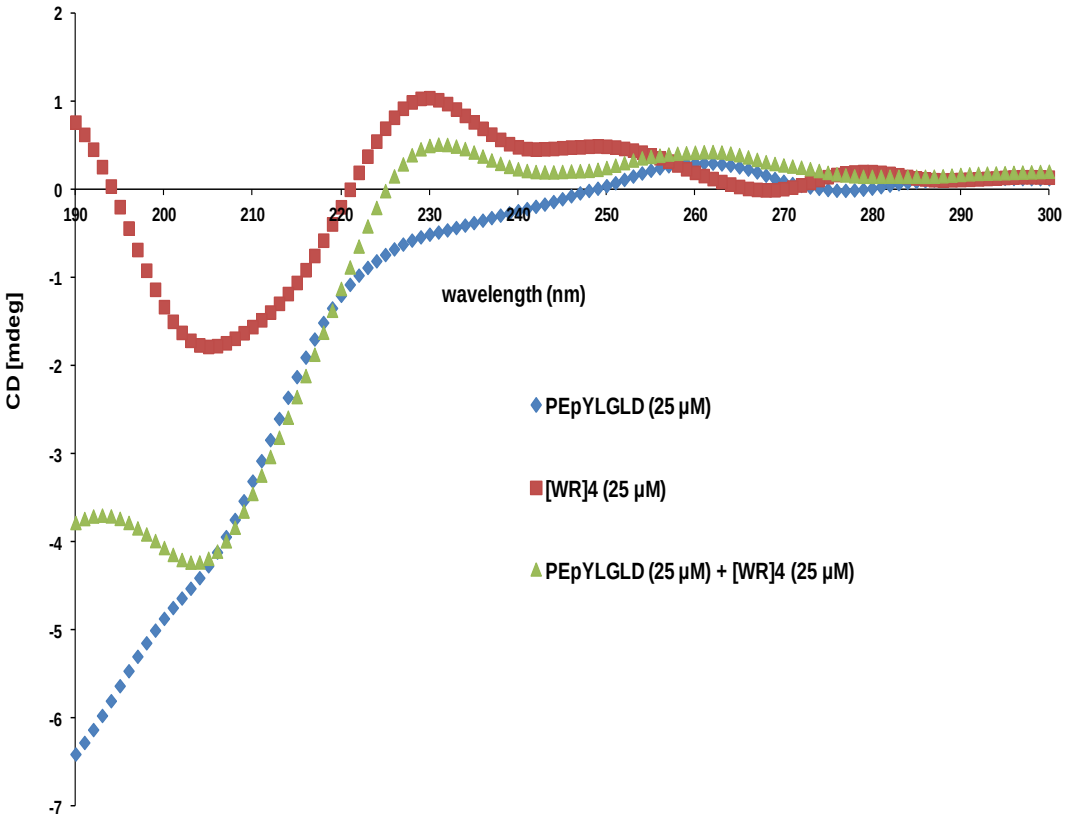
2
1
0
-1
-2
-3
-4
-5
-6
-7
190
200
210
220
230
240
250
260
270
280
290
300
CD [mdeg]
wavelength (nm)
PEpYLGLD (25 µM)
[WR]4 (25 µM)
PEpYLGLD (25 µM) + [WR]4 (25 µM)

Figure 8

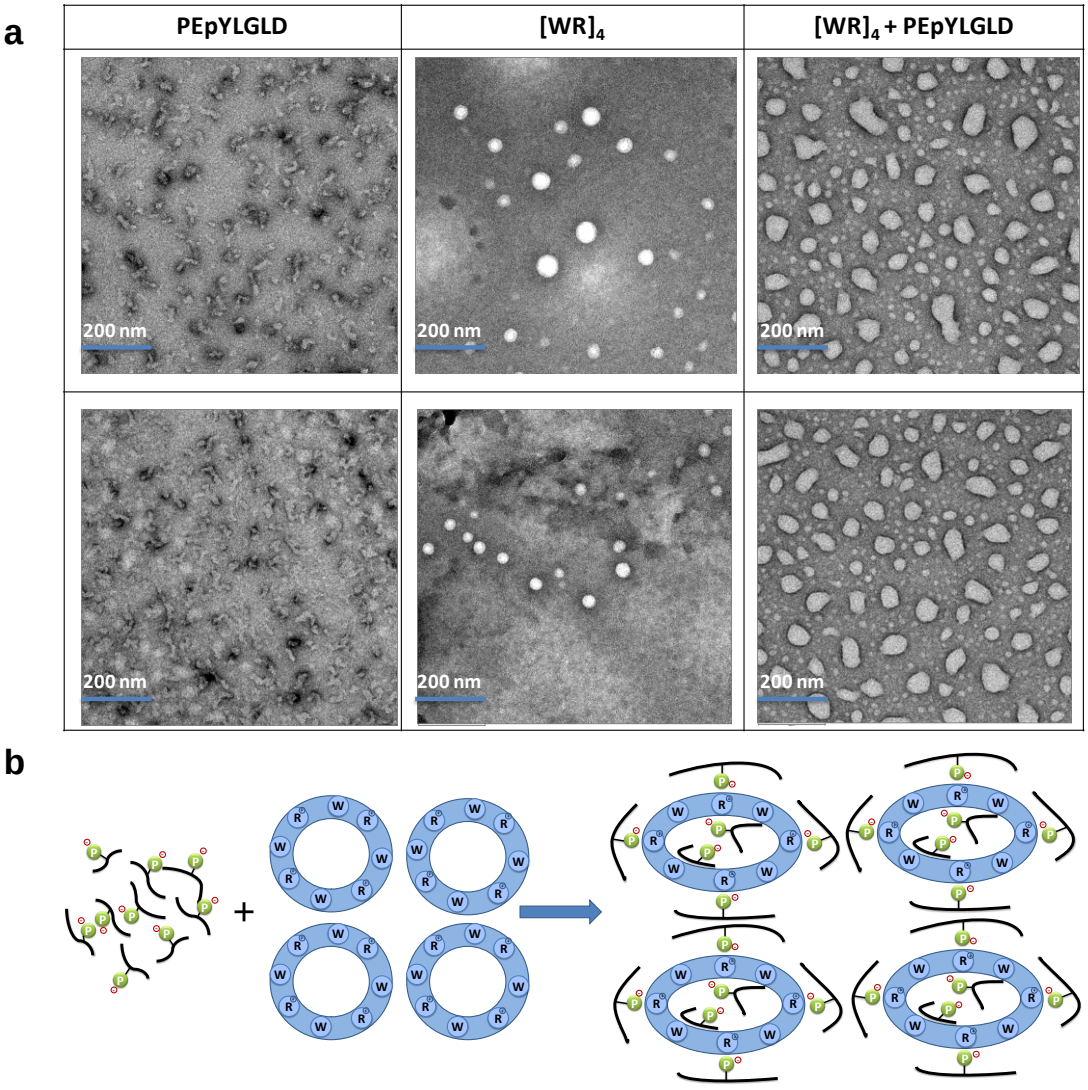
a
PEpYLGLD
[WR]4
[WR]4 + PEpYLGLD
200 nm
200 nm
200 nm
200 nm
200 nm
200 nm
b
P
R
W

Figure 9

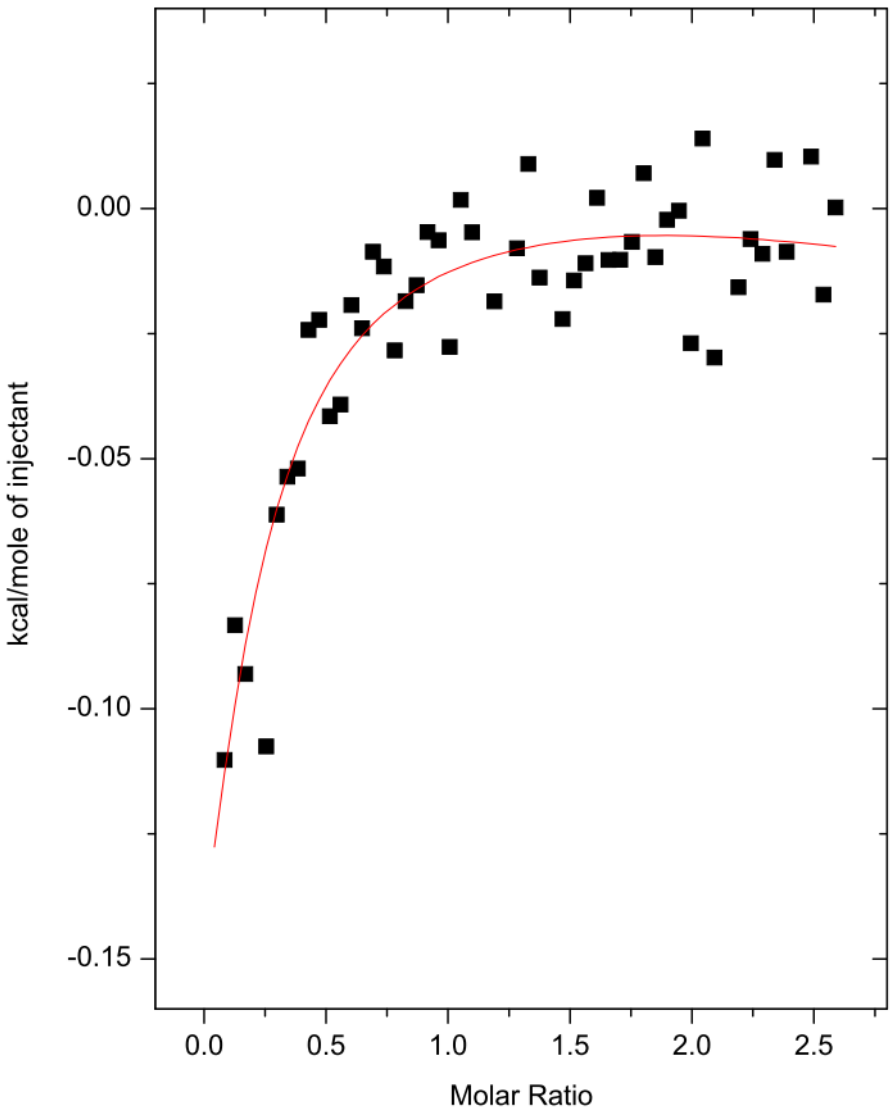
0.00
-0.05
-0.10
-0.15
kcal/mole of injectant
0.0
0.5
1.0
1.5
2.0
2.5
Molar Ratio

Figure 10

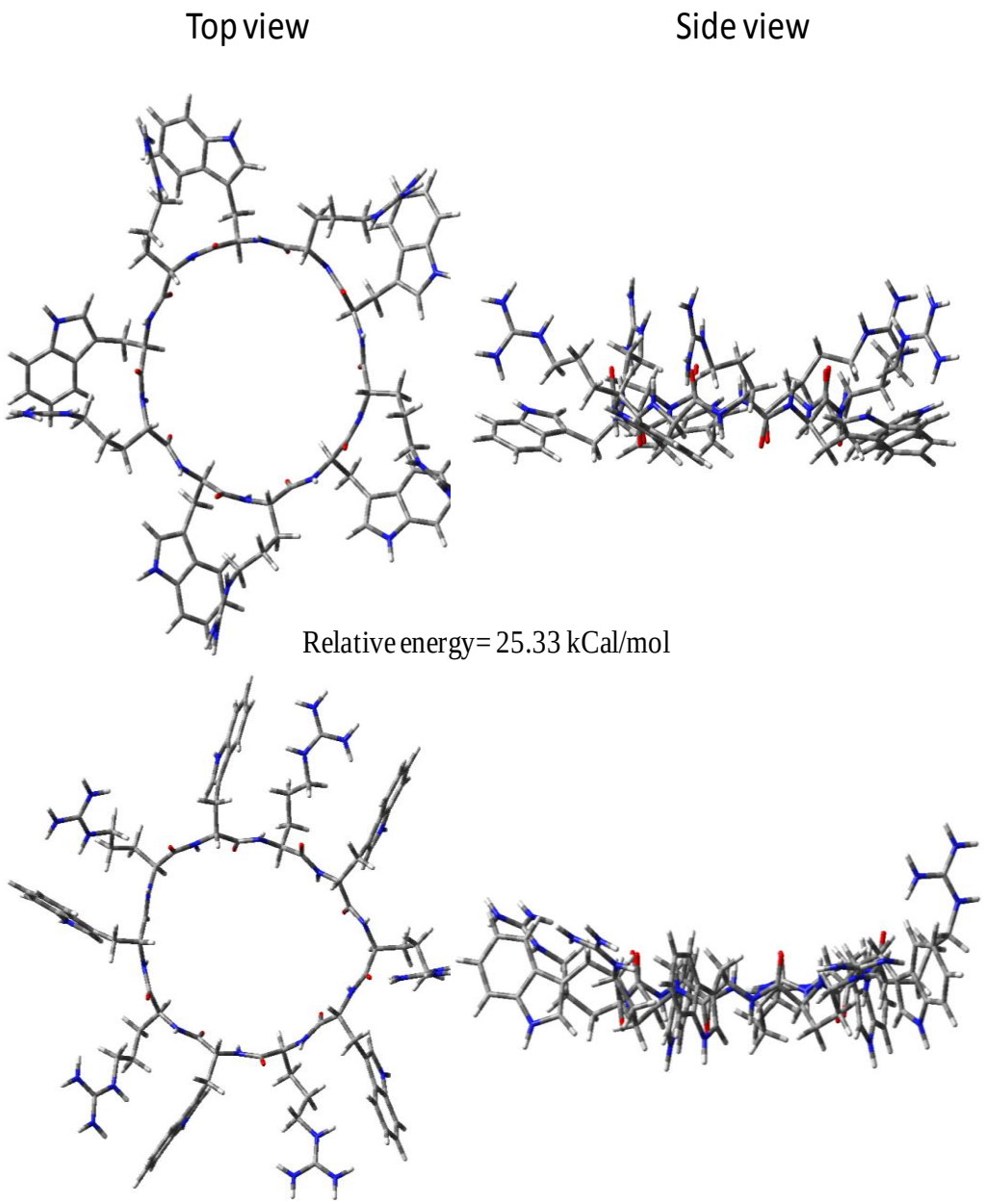
Top view
Side view
Relative energy= 25.33 kCal/mol
Relative energy= 0.0 kCal/mol

Scheme 1

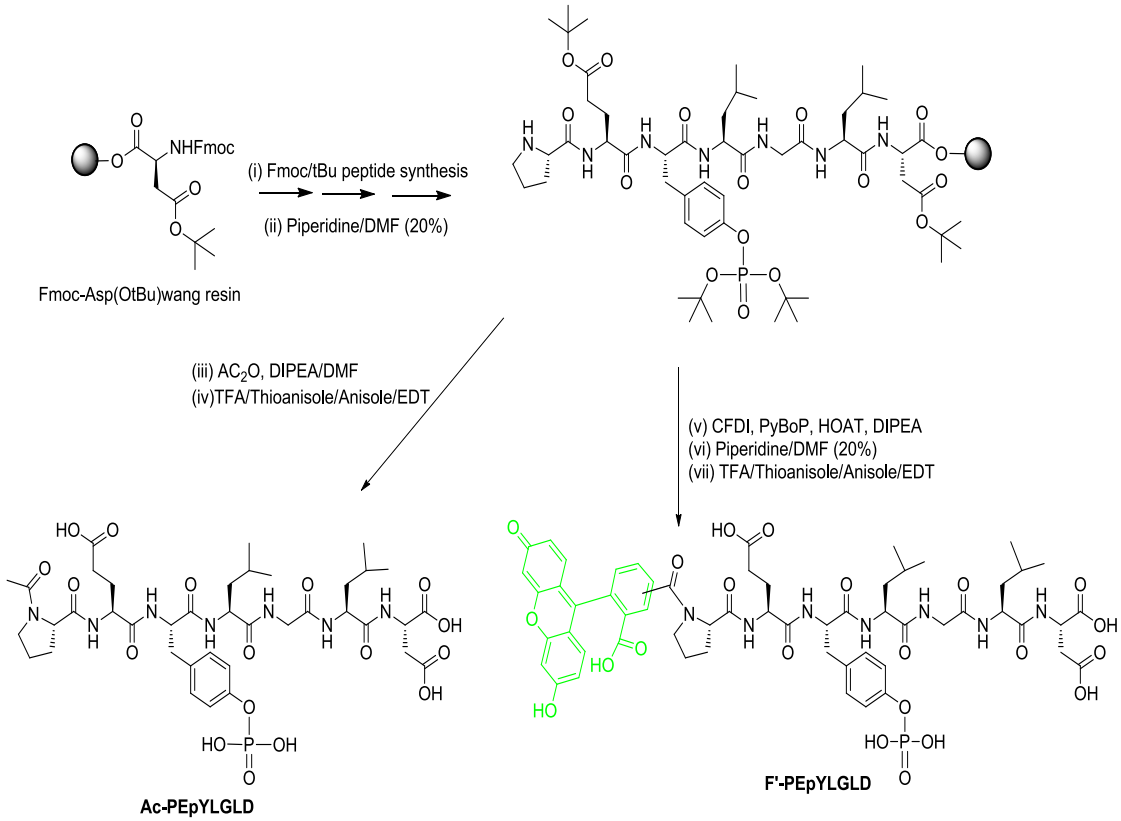
NHFmoc
(i) Fmoc/tBu peptide synthesis
(ii) Piperidine/DMF (20%)
Fmoc-Asp(OtBu)wang resin
(iii) AC2O, DIPEA/DMF
(iv)TFA/Thioanisole/Anisole/EDT
(v) CFDI, PyBoP, HOAT, DIPEA
(vi) Piperidine/DMF (20%)
(vii) TFA/Thioanisole/Anisole/EDT
Ac-PEpYLGLD
F'-PEpYLGLD

Manuscript II

Published in ***Molecular Pharmaceutics***, 2013, 10, 488-499

Design and biological evaluation of cell-penetrating peptide−doxorubicin conjugates as prodrugs

Amir Nasrolahi Shirazi, Rakesh Tiwari, Bhupender S. Chhikara, Dindyal Mandal, and Keykavous Parang*

Department of Biomedical and Pharmaceutical Sciences, College of Pharmacy, University of Rhode Island, Kingston, Rhode Island 02881, United States

Corresponding Author

*7 Greenhouse Road, Department of Biomedical and Pharmaceutical Sciences, College of Pharmacy, University of Rhode Island, Kingston, Rhode Island 02881, United States. Tel: +1-401-874-4471. Fax: +1-401-874-5787. E-mail: kparang@uri.edu.

Abstract

Doxorubicin (Dox) is a hydrophilic anticancer drug that has short retention time due to the efficient efflux in some cancer cells (e.g., ovarian adenocarcinoma SK-OV-3). Cyclic [W$(RW)_4$] and the corresponding linear peptide $(RW)_4$ were conjugated with Dox through an appropriate linker to afford cyclic [W$(RW)_4$]−Dox and linear $(RW)_4$−Dox conjugates to enhance the cellular uptake and cellular retention of the parent drug for sustained anticancer activity. Comparative antiproliferative assays between covalent (cyclic[W$(RW)_4$]−Dox and linear $(RW)_4$−Dox) and the corresponding noncovalent physical mixtures of the peptides and Dox were performed. Cyclic [W$(RW)_4$]−Dox inhibited the cell proliferation of human leukemia (CCRF-CEM) (62−73%), ovarian adenocarcinoma (SK-OV-3) (51−74%), colorectal carcinoma (HCT-116) (50−67%), and breast carcinoma (MDA-MB-468) (60−79%) cells at a concentration of 1 μM after 72−120 h of incubation. Cyclic [W$(RW)_4$]−Dox exhibited higher antiproliferative activity than linear $(RW)_4$−Dox in all cancer cells with the highest activity observed after 72 h. Flow cytometry analysis showed 3.6-fold higher cellular uptake of cyclic [W$(RW)_4$]−Dox than Dox alone in SK-OV-3 cells after 24 h incubation. The cellular hydrolysis study showed that 99% of cyclic [W$(RW)_4$]−Dox was hydrolyzed intracellularly within 72 h and released Dox. These data suggest that cyclic [W$(RW)_4$]−Dox can be used as a potential prodrug for improving the cellular delivery and retention of Dox.

KEYWORDS: anticancer, cellular uptake, doxorubicin, cyclic peptides, cell-penetrating peptides

INTRODUCTION

Doxorubicin (Dox) is a well-known anthracycline and widely used anticancer agent for the treatment of a wide variety of cancers, such as breast carcinoma, leukemia, and other solid tumors.[1] The major mechanism of Dox activity is the inhibition of topoisomerase II (TOPO II)−DNA complex, causing DNA damage through intercalating with the DNA double helix.[2]

One of the major limitations of cancer chemotherapy treatment is the development of resistance to a certain dose of anticancer drugs, such as Dox. Several mechanisms of drug resistance have been introduced at different levels, including alteration of the target protein, decreased membrane permeability and drug metabolism, and/or efflux pumping.[3−5] Dox is not being used widely for treating other tumors like ovarian carcinoma, liver cancer, and stomach cancer in the clinic,[6,7] due to the development of resistance associated with Dox. Furthermore, the use of Dox for clinical application revealed undesired pharmacokinetics properties, such as rapid distribution, excretion, and low bioavailability of the drug, due to the hydrophilic nature, high volume of distribution, and short half-life.[8−10] Thus, a high cumulative dose of Dox is required in cancer chemotherapy to achieve a sufficient therapeutic effect, which leads to dose-dependent side effects, such as such as cumulative cardiotoxicity, nephrotoxicity, and extravasation.[11,12]

Moreover, intracellular Dox accumulation is dependent on a number of factors including cellular uptake, retention, relocalization, and efflux from the cell. Among

these factors, intracellular uptake of Dox suffers from efflux pumping in some cancer cells, such as ovarian carcinoma cells, leading to decreased intracellular Dox levels that could be related to the overexpression of energy-dependent drug efflux pump proteins such as P-glycoprotein (P-gp). This integral membrane protein removes drugs and thus reduces intracellular anticancer drug concentrations.[13]

Efficacy and toxicity of an anticancer drug can be modified through using drug delivery systems and altering the physicochemical properties, such as lipophilicity, cellular uptake, and prolonging activity through chemical conjugation with various chemical moieties. One of the main applications of drug delivery systems is to avoid the P-gp and multidrug resistance proteins (MRPs) that are involved in drug efflux to overcome the resistance problem and P-gp-mediated drug efflux.[14−16]

Prodrug strategy as one of the drug delivery systems through chemical conjugation with a parent drug[17,18] has been widely used in Dox delivery.[6,19] Several conjugation methods have been used to improve Dox delivery, including using gold nanoparticles,[20] gold nanospheres,[21] liposomes,[22] peptides, [23−27] and dendrimers.[28] Conjugation of Dox with cellpenetrating peptides (CPPs) has been employed as one of the privileged methods to translocate a wide variety of cargo molecules into various cell lines.[16] For instance, Dox has been conjugated with different linear CPPs including penetratin,[24] tat,[29] and polyarginine,[30] and maurocalcine.[31]

However, development of efficient and safe prodrug carriers to enhance delivery and retention of Dox into drug-resistant tumor cells and to reduce efflux remains less explored. We previously reported the application of a number of cyclic

peptides as noncovalent nuclear targeting molecular transporters[32] of Dox. Cyclic peptides containing arginine and tryptophan $[WR]_n$ (n = 3−5) were found to be appropriate noncovalent carriers for Dox, however, the drug intracellular retention and toxicity behavior for cyclic peptide−Dox covalent conjugates remain unexplored. Herein, we report the synthesis of linear and cyclic peptides through the covalent conjugation with a 3-carbon chain linker at the 14-hydroxyl group, evaluation of their in vitro anticancer activities in multiple cancer cell lines, and cellular uptake and retention. The prodrug conjugates were designed to improve cellular uptake, to prolong biological activity, and to reduce intrinsic cellular efflux of Dox.

EXPERIMENTAL SECTION

Synthesis of Linear $(RW)_4$ **Peptide.** The linear peptide was assembled on Fmoc-Rink amide resin (0.56 g, 0.54 mmol/ g, 0.3 mmol) by solid-phase peptide synthesis strategy using Fmoc-protected amino acids [Fmoc-Trp(Boc)-OH and Fmoc- Arg(Pbf)-OH] on a PS3 automated peptide synthesizer at room temperature (Scheme 1). Linear peptide sequence was assembled on the resin after removing the Fmoc group at the end of the sequence (NH_2-RWRWRWRW) $(RW)_4$, using 20% piperidine in DMF. The resin was washed with DCM (3 × 15 mL) and MeOH (3 × 15 mL) for complete cleavage of peptide from the resin and side chain protecting groups. The resin was dried in vacuum for 24 h. A cleavage cocktail, namely, reagent R containing TFA/thioanisole/EDT/anisole (90:5:3:2 v/v/v/v, 12 mL), was added to the resin. The mixture was shaken at room temperature for 2 h. The resin was collected by filtration

and consequently washed with 2 mL of reagent R again. Collected filtrates were evaporated to reduce the volume under dry nitrogen. The crude peptide was precipitated by adding cold diethyl ether (200 mL, Et_2O) and centrifuged at 4000 rpm for 5 min followed by decantation to obtain the solid precipitate. The solid material was further washed with cold ether (2 × 100 mL) for 2 times. The peptide was lyophilized and purified by reversed-phase Hitachi HPLC using a gradient system as described in the Supporting Information to yield linear $(RW)_4$ peptide.

$(RW)_4$. MALDI-TOF (*m/z*) $[C_{68}H_{91}N_{25}O_8]$: calcd, 1385.7482; found, 1386.8219 $[M + H]^+$.

Synthesis of Cyclic Peptide [W$(RW)_4$**K]β-Ala**. The linear-protected peptides sequence was assembled using a PS3 automated peptide synthesizer. The linear protected peptide (Dde-K(Boc-β-Ala)(WRWRWRWRW) was assembled on the H-Trp(Boc)-2-chlorotrityl chloride resin (513 mg, 0.78 mmol/g, 0.40 mmol) in 0.40 mmol scale (Scheme 2). After the final coupling with Boc-β-Ala-OH, the resin was washed with DMF (3 × 25 mL, each time 5 min). Then the Dde group at the lysine *N*-terminal was deprotected by using hydrazine monohydrate (2% v/v) solution in DMF (3 × 25 mL, each time 5 min). The resin was washed with DMF (5 × 50 mL) followed by washing with DCM (3 × 50 mL). The side chain protected peptide was cleaved from trityl resin by using cleavage cocktail reagent, acetic acid/TFE/DCM (1:2:7 v/v/v, 50 mL), by shaking for 1 h at room temperature to yield the side chain protected linear peptide. The resin was collected by filtration and washed with TFE/DCM (2:8 v/v, 2 × 10 mL). The combined filtrates were evaporated under reduced pressure. Hexane (2 × 25 mL) and DCM (1 × 25 mL) were added to the residue to remove the

acetic acid from the cleaved crude peptide. The crude peptide was obtained as a white solid and was dried in vacuum overnight. The compound was directly used for the next cyclization reaction. The linear peptide was dissolved in DMF/DCM (5:1 v/v, 250 mL). 1-Hydroxy-7-azabenzotriazole (HOAt, 223 mg, 1.64 mmol, 4 equiv) and 1,3-diisopropylcarbodiimide (DIC, 290 μL, 1.86 mmol, 4.5 equiv) were added to the mixture, and the solution was stirred at room temperature for 6 h. The completion of the cyclization was checked by MALDI-TOF. After the reaction was completed, the solvents were removed under reduced pressure by using a rotary evaporator. The crude product was dried overnight in vacuum before the final cleavage reaction. The cleavage reaction was performed by using reagent R as previously described. The crude peptides were lyophilized and purified by reversed-phase Hitachi HPLC (L-2455) as described in the Supporting Information to yield cyclic peptide [W(RW)$_4$K(β-Ala)].

MALDI-TOF (*m/z*) [$C_{88}H_{115}N_{29}O_{11}$]: calcd, 1753.9331; found, 1756.6570 $[M + 3H]^+$.

Synthesis of *N*-Fmoc-Dox-14-O-hemiglutarate. The synthesis of this *N*-Fmoc Dox derivative was carried out according to the previously reported procedure.33 In brief; Dox hydrochloride (100 mg, 0.17 mmol) was dissolved in anhydrous DMF (4 mL) in a round-bottom flask and stirred at room temperature under nitrogen atmosphere. Fmoc-OSu (60 mg, 0.18 mmol) was added to the reaction mixture followed by dropwise addition of anhydrous *N*,*N*-diisopropylethylamine (DIPEA, 60 μL, 0.34 mmol). Aluminum foil was used to cover the reaction vessel from light, and stirring of the reaction mixture was continued at room temperature. The reaction was stopped, and the solvent was removed after 4 h. The remaining oily liquid was triturated with

0.1% TFA solution in water (v/v) to afford crystalline solid compound. The crystalline solid was collected through filtration and washed with cold diethyl ether to remove traces of excess of Fmoc-OSu. HPLC analysis showed that the crude product was pure (95%). The Fmoc-*N*-Dox (110 mg, 0.14 mmol) was reacted with glutaric anhydride (19.7 mg, 0.17 mmol) in the presence of anhydrous DIPEA (46 μL, 0.26 mmol) in anhydrous DMF (5 mL) for 16 h under nitrogen atmosphere. Analytical HPLC analysis showed that the reaction was completed after 16 h. The solvent was removed under reduced pressure, and the oily liquid was triturated with 0.1% TFA solution in water (v/v) to precipitate the crude solid material. The crude solid material was filtered and dried in high vacuum. The material was purified by HPLC to afford pure *N*-Fmoc-Dox-14-O-hemiglutarate (95%).

General Procedure for Coupling of the Peptides to Dox. *N*-Fmoc-Dox-14-O-hemiglutarate (1 equiv), cyclic or linear peptide (1 equiv), benzotriazol-1-yloxytripyrrolidinophosphonium hexafluorophosphate (PyBOP, 1.35 equiv), and hydroxybenzotriazole (HOBt, 2.70 equiv) were added to the glass vial under nitrogen atmosphere (Scheme 3). Anhydrous DMF (1−2 mL) was used as a solvent, and the reaction mixture was stirred to dissolve the compounds followed by the addition of DIPEA (8 equiv). Then, the reaction mixture was stirred for 1.5 h in the absence of light. The solvent was removed under reduced pressure, and cold diethyl ether was added to the residue. The crude peptide was precipitated and centrifuged to obtain the crude solid peptide conjugate. The peptide was dried under nitrogen gas. To remove the Fmoc group, a solution of piperidine in DMF was used (20% v/v, 2 mL for 5 min). The solution color turned to blue, and the reaction was terminated by adding drops of

TFA solution in DMF (20% v/v) until the solution color turned to light red. The solvent was removed under reduced pressure, and oily liquid was dissolved in acetonitrile/water (50% v/v). The HPLC purification afforded the final linear peptide or cyclic peptide−Dox conjugates.

Cyclic [W(RW)$_4$]−Dox **Peptide.** ^{1}H NMR (DMSO-d$_6$, 500 MHz, δ ppm): 0.80−0.97 (m, 8H, $CH_2CH_2CH_2NH$, Arg), 1.10−1.25 (m, 13H, $CH_2CH_2CH_2NH$, Arg, Lys, 6′-CH3), 1.89−2.25 (m, 4H, H-8 and H-2′), 2.40−2.67 (m, 14H, CH_2CO and $CH_2CH_2CH_2NH$), 2.90−3.20 (m, 12H, CH_2, Trp, H-10), 3.55−3.52 (m, H-3′, H-4′ overlapped with DMSO peaks), 3.99 (s, 3H, OCH_3), 4.20−4.40 (m, 6H, αCH, Arg, Lys, H-5′), 4.85−4.98 (m, 5H, αCH, Trp), 5.10−5.48 (m, 3H, H-7, OCH_2CO), 5.61−5.65 (m, 1H, H-1′), 6.27 (br s, 12 H, NH), 6.85−7.70 (m, aromatic, 25 H, Trp, aromatic CH), 7.75−8.00 (m, 4H, aromatic CH), 10.74 (br s, 5H, NH, Trp), 13.27 (s, 2H, PhOH). MALDI-TOF (*m/z*) [$C_{120}H_{148}N_{30}O_{24}$]: calcd, 2393.1283; found, 2393.5332 $[M]^+$.

Linear (RW)$_4$−Dox. MALDI-TOF (*m/z*) [$C_{100}H_{124}N_{26}O_{21}$]: calcd, 2024.9434; found, 2024.6139 $[M]^+$.

Cell Culture. Human leukemia carcinoma cell line CCRFCEM (ATCC no. CCL-119), breast adenocarcinoma MDAMB-468 (ATCC no. HTB-132), ovarian adenocarcinoma SKOV-3 (ATCC no. HTB-77), and colorectal carcinoma HCT-116 (ATCC no. CCL-247) were obtained from American Type Culture Collection. The cells were grown on 75 cm^2 cell culture flasks with RPMI-16 medium for leukemia and EMEM medium for other cell lines and supplemented with 10% fetal bovine

serum (FBS) and 1% penicillin−streptomycin solution (10,000 units of penicillin and 10 mg of streptomycin in 0.9% NaCl) in a humidified atmosphere of 5% CO_2, 95% air at 37 °C.

Antiproliferation Assay. Antiproliferative activities of covalently synthesized cyclic $[W(RW)_4]$−Dox, linear $(RW)_4$−Dox derivatives, and noncovalent mixtures of cyclic $[RW]_4$ + Dox and linear $(RW)_4$ + Dox were evaluated in MDA-MB-468, CCRF-CEM, SK-OV-3, and HCT-116 cells, and the results were compared with that of Dox alone. The assay was carried out using CellTiter 96 AQueous One Solution Cell Proliferation Assay Kit (Promega, USA). As a representative example, SK-OV-3 cells were suspended in 5×10^3/mL (CCRF-CEM, 4×10^4/mL), and 100 μL of the cell suspension was placed in each well of the 96 well culture plates. The cells were incubated with Dox (1 μM), cyclic $[W(RW)_4]$−Dox (1 μM), linear $(RW)_4$−Dox (1 μM), cyclic $[RW]_4$ (1 μM) + Dox (1 μM), and linear $(RW)_4$ (1 μM) + Dox (1 μM) in 2% DMSO and tested in triplicate. For the physical mixtures, an appropriate volume of Dox stock solution was mixed with an appropriate volume of an aqueous solution of cyclic and linear peptides physically to obtain a final concentration of Dox (1 μM) and the peptide (1 μM). The mixture was vigorously mixed and vortexed until the solution became homogeneous/ clear red color. Subsequently, the mixture was incubated for 30 min at 37 °C before addition to the cells. Incubation was carried out at 37 °C in an incubator supplied with 5% CO_2 for 24−120 h. At the end of the sample exposure period (24−120 h), 20 μL of CellTiter 96 aqueous solution was added. The plate was returned to the incubator for 1 h in a humidified atmosphere at 37 °C. The absorbance of the formazan product was measured at 490 nm using a microplate

reader. The percentage of cell survival was calculated as [(OD value of cells treated with the test compound) − (OD value of culture medium)]/[(OD value of control cells) − (OD value of culture medium)] × 100%.

Cell Cytotoxicity Assay. The cytotoxicity of Dox and cyclic [$W(RW)_4$]−Dox against MDA-MB-468, HCT-116, CCRF-CEM, and SK-OV-3 was determined by MTS assay using CellTiter 96 AQueous One Solution Cell Proliferation Assay Kit (Promega, USA). All cells were plated overnight in 96 well plates with a density of 5000 cells per well in 0.1 mL of appropriate growth medium at 37 °C. Different concentrations of Dox or cyclic [$W(RW)_4$]−Dox (up to a maximum of 10 μM) were incubated with the cells for 2 h. Compounds were removed from medium by replacing with fresh medium, and the cells were kept in an incubator for another 72 h. The cells without compounds were included in each experiment as controls. After 72 h of incubation, 20 μL of MTS was added and incubated for 2 h. The absorbance of the formazan product was measured at 490 nm using microplate reader. The percentage of cytotoxicity was calculated as [(OD value of untreated cells) − (OD value of treated cells)]/(OD value of untreated cells) × 100%.

Confocal Microscopy. SK-OV-3 cells were seeded with EMEM media overnight on coverslips in six well plates. Then the medium was removed and washed with opti-MEM. The cells were treated with Dox or cyclic [$W(RW)_4$]−Dox (5 μM) in opti-MEM for 1 h at 37 °C. After 1 h incubation, the media containing the compound were removed followed by washing with PBS three times. Then coverslips were placed on a drop of mounting medium on a microscope slide with cell-attached side facing down. Laser scanning confocal microscopy was carried out using a Carl Zeiss LSM 510

system. The cells were imaged using rhodamine and phase contrast channels. In the case of drug efflux studies, after a 1 h incubation period, the medium containing drugs was removed and washed with opti-MEM. Then fresh medium with serum was added into the cells. After 24 h, the medium was removed and washed with PBS three times, and then the cells were visualized under confocal microscopy.

Fluorescence Activated Cell Sorter (FACS) Analysis of Cellular Uptake Experiment. Ovarian carcinoma cells were plated overnight in six well plates (2×10^5 cells/well) in EMEM media. Then Dox (5 μM), cyclic $[W(RW)_4]$−Dox (5 μM), linear $(RW)_4$−Dox (5 μM), cyclic $[RW]_4$ (5 μM) + Dox (5 μM), and $(RW)_4$ (5 μM) + Dox (5 μM) were added in serum-free RPMI to the cells. For the physical mixtures, an appropriate volume of Dox stock solution was mixed with an appropriate volume of an aqueous solution of cyclic and linear peptides physically to obtain a final concentration of Dox (5 μM) and CPPs (5 μM). The mixture was vigorously mixed and vortexed until the solution became homogeneous/clear red color. Subsequently, the mixture was incubated for 30 min at 37 °C before addition to the cells. The plates were incubated for 1 h at 37 °C. After 1 h incubation, the media containing drugs were removed. The cells were digested with 0.25% trypsin/0.53 mM EDTA for 5 min to detach from the plate. Then the cells were centrifuged and washed twice with PBS. Finally, the cells were resuspended in flow cytometry buffer and analyzed by flow cytometry (FACSCalibur: Becton Dickinson) using FL2 channel and CellQuest software. The data presented are based on the mean fluorescence signal for 10,000 cells collected. All assays were performed in triplicate.

Fluorescence Activated Cell Sorter (FACS) Analysis of Cell Cycle Arrest. Colorectal carcinoma cells (2×10^5 per well) were treated with cyclic $[W(RW)_4]$−Dox at 1 μM for 1 h followed by 24 h incubation in drug-free medium. Cells were fixed in ice-cold ethanol:PBS (70:30, v/v) for 30 min at 4 °C, further resuspended in PBS with 100 μg/mL RNase and 40 μg/ mL propidium iodide, and incubated at 37 °C for 30 min. The DNA content (for 10,000 cells) was analyzed using a FACSCalibur instrument equipped with FACStation with FACSCalibur software (BD Biosciences, San Diego, CA, USA). The analyses of cell cycle distribution were performed in triplicate (n = 2 plates per experiment) for the sample treatment. The coefficient of variation, according to the ModFit LT Version 2 acquisition software package (Verity Software House, Topsham, ME, USA), was always less than 5%.

Topo II Decatenation Assay. The topoisomearase II assay kit (Catalog No. 1001-1) was purchased from TopoGEN, Inc. (Port Orange, FL). Eukaryotic Topo II was assayed by decatenation of kDNA and monitoring the appearance of a smaller DNA (decatenated DNA circles). Reaction mixtures containing kDNA (0.1 μg) in a final volume of 20 μL and 1× reaction buffer containing Tris-HCl (50 mM, pH 8.0), NaCl (150 mM), $MgCl_2$ (10 mM), dithiothreitol (0.5 mM), and ATP (2 mM) were incubated for 30 min at 37 °C without and with Dox, and cyclic $[W(RW)_4]$−Dox at 10, 20, 30, 40, and 50 μM final concentration. Reactions were terminated with the addition of 0.4 volume of stop buffer (5% sarkosyl, 0.125% bromophenol blue, and 25% glycerol). One unit of Topo II is defined as the amount of enzyme required to fully decatenate 0.1 μg of kDNA in 30 min at 37 °C. The decatenation products were analyzed on 1% agarose gels having 0.5 μg of ethidium bromide/mL. Eukaryotic Topo II products

were separated at 108 V, which allowed rapid resolution of catenated networks from the minicircles. Gels were photographed by ethidium bromide fluorescence on Typhoon Imager.

Stability Studies. The stability of cyclic [W(RW)$_4$]−Dox was evaluated using phosphate-buffered saline (PBS) and fetal bovine serum (FBS). PBS and FBS were purchased from Invitrogen and ATCC (Manassas, VA). FBS (1 mL, 100%) and PBS (1 mL, pH 7.0) were incubated with cyclic [W(RW)$_4$]−Dox (75 μL, 1 mM in water) at 37 °C followed by intermediate mixing. An aliquot of 75 μL of the mixture was taken out at different time intervals (10 min to 96 h) and diluted with water (75 μL). The mixture was analyzed by using analytical HPLC detecting the wavelength of 490 nm. The area under the curve (AUC) was calculated and used to find out the percentage of released Dox and remaining prodrug at a given time. Figure S1 (Supporting Information) was plotted between relative percentage of released Dox and cyclic [W(RW)$_4$]−Dox based on HPLC analysis.

Cellular Hydrolysis. Intracellular hydrolysis of cyclic [W(RW)$_4$]−Dox and accumulation of Dox and the peptide−Dox conjugate were determined in CCRF-CEM cells by HPLC analysis. CCRF-CEM cells were grown in 75 cm^2 culture flasks with serum-free RPMI medium to ∼70−80% confluence (1.37×10^7 cells/mL). The medium was replaced with fresh RPMI medium having cyclic [W(RW)$_4$]−Dox (1 μM), and the cells were incubated at 37 °C for 4 h. The medium containing cyclic [W(RW)$_4$]−Dox was carefully removed by using centrifugation and replaced with fresh RPMI serum-free medium. The cells were partitioned/transferred to culture plates (six well) having 1.37×10^7 cells per well in 5 mL of medium and incubated for

the indicated time. After incubation, the cells were collected by centrifugation. The medium was removed carefully by decantation, and cell pellets were washed with ice-cold PBS to remove any medium. The cell pellets were thoroughly extracted with an equal volume of methanol, chloroform, and isopropanol mixture (4:3:1 v/v/v) and filtered through 0.2 μm filters. The relative Dox and cyclic $[W(RW)_4]$−Dox concentrations in cell lysates were quantified by analytical HPLC analysis as described in the Supporting Information at 490 nm using the water/acetonitrile solvent method.

RESULTS AND DISCUSSION

Chemistry. Linear and cyclic peptides were synthesized by Fmoc/tBu solid-phase peptide synthesis. Scheme 1 depicts the synthesis of linear peptide $(RW)_4$ on the Rink amide resin. The linear peptide sequence was assembled using a PS3 peptide synthesizer. The last Fmoc group on the *N*-terminal was deprotected by piperidine (20% v/v, DMF). The resin was dried, washed, and cleaved by cleavage cocktail (reagent R) to afford the linear $(RW)_4$, which was purified by reversed-phase Hitachi HPLC. For the synthesis of the cyclic peptide, first the linear protected peptide (Dde-K(Boc-β-Ala)(WRWRWRWRW) was assembled on the H-Trp(Boc)-2-chlorotrityl chloride resin. The Dde group of *N*-terminal lysine was removed in the presence of hydrazine (2% in DMF). The side chain protected peptide was cleaved from the resin using AcOH/TFE/DCM (1:2:7 v/v/v) cocktail. The cyclization of the side chain protected peptide was performed under pseudodilute conditions in the presence of HOAt and DIC (Scheme 2). The cyclic peptide was cleaved in the presence of reagent

R, purified using reversed-phase HPLC, and used for the conjugation with Dox. *N*-Fmoc-Dox-14-O-hemiglutrate was prepared as described previously.[33] In brief, the reaction of glutaric anhydride with Fmoc-protected Dox was carried out to produce the Dox hemiglutarate ester with a free COOH, which after HPLC purification and lyophilization was used for coupling with linear and cyclic peptides. The conjugation of the peptides with *N*-Fmoc-Dox-14-O-hemiglutrate was achieved in a similar pattern (Scheme 3). The equimolar amount of the peptide and Dox was coupled through formation of an amide bond between the amino group of peptides and carboxylic acid in the Fmoc-protected Dox. The carboxylic group in Fmoc-protected Dox was preactivated in the presence of HOAt/PyBOP/DIPEA in DMF for 15 min before reacting with the peptides. After conjugation, the Fmoc protecting group was removed using piperidine and was then acidified. The coupled peptide was purified using HPLC and lyophilized. The structures of all the final compounds were confirmed by a high-resolution MALDI TOF/TOF mass spectrometer. The purity of the final product (≥95%) was confirmed by reversed-phase analytical HPLC using a gradient system with water (0.1% TFA) and acetonitrile as eluting solvents.

Biological Activities. Cytotoxicity and Antiproliferative Activity of Peptide−Dox Derivatives. Cyclic $[WR]_4$ and cyclic $[W(RW)_4K]$(β-Ala) did not show any significant toxicity in MDA-MB-468, HCT-116, CCRF-CEM, and SK-OV-3 cells at a concentration of 10 μM (Figure 1) after different incubation times including 24 h, 72 h, and 120 h. These data are consistent with previously reported data of cyclic $[WR]_4$.[32] Thus, a noncytotoxic concentration of 1 μM was selected for cell-based

studies of cyclic peptide conjugate cyclic [W(RW)$_4$]−Dox and the physical mixture cyclic [RW]$_4$ + Dox.

We recently compared the toxicity of [WR]$_4$ versus commonly used cellpenetrating peptides and transporters including polyArg CR7, TAT (YGRKKRRQRRRC) (100 μM), and oligofectamine 2000 (Invitrogen, a cationic lipid formulation).34 [WR]$_4$ did not show any significant toxicity in human ovarian adenocarcinoma (SK-OV-3) and human leukemia (CCRFCEM) cancer cells and normal human colon myofibroblast (CCD-18Co) cells, while other cell-penetrating peptides polyArg CR7, TAT (YGRKKRRQRRRC), and oligofectamine 2000 (Invitrogen, a cationic lipid formulation) reduced the viability by 21−55%. The activity of compounds on the cell proliferation of different cancer cells, CCRF-CEM, SK-OV-3, HCT-116, and MDA-MB-468, was investigated for up to 120 h at the concentration of 1 μM. The activity of synthesized compounds, linear (RW)$_4$−Dox and cyclic [W(RW) 4]−Dox, was evaluated in a comparative study with the noncovalent physical mixtures of linear (RW)$_4$ + Dox and cyclic [RW]$_4$ + Dox, and Dox alone (Figure 2). Cyclic [W(RW)$_4$]−Dox exhibited higher antiproliferative activity than linear (RW)$_4$−Dox in all cancer cells, with the highest activity observed after 72 h.

The effect of compounds was found to be time dependent. The cell proliferation inhibitory activity of compounds was enhanced at longer incubation period of compounds with cells presumably because of the hydrolysis of the conjugate to Dox. Cyclic [W(RW)$_4$]−Dox inhibited the cell proliferation of CCRF-CEM (62−73%), SK-OV-3 (51−74%), HTC-116 (50−67%), and MDA-MB-468 (60−79%) cells at a concentration of 1 μM after 72−120 h of incubation, while linear (RW)$_4$−Dox

exhibited antiproliferative activity against CCRF-CEM (46−69%), SK-OV-3 (28−34%), HTC-116 (21−61%), and MDA-MB-468 (60−74%) under similar conditions.

These data suggest that cyclization of peptide provided a more effective transporter for Dox. The antiproliferative activity of cyclic [W(RW)$_4$]−Dox was in the order MDA-MB-468 > CCRF-CEM > SK-OV-3 > HTC-116. In general, the physical mixture of linear (RW)$_4$ and cyclic [RW]$_4$ with Dox derivative showed less antiproliferative activity in comparison to cyclic [W(RW)$_4$]−Dox conjugate after 72−120 h against CCRF-CEM (52−68%), SK-OV-3 (47−67%), and HTC-116 (38−62%), and showed slightly better or comparable activity against MDA-MB-468 (71−78%). Dox exhibited also similar antiproliferative activity in comparison to the physical mixture against CCRF-CEM (59−71%), SK-OV-3 (48−59%), HTC-116 (37−64%), and MDA-MB-468 (71− 77%) after 72−120 h of incubation, indicating that conjugation of the cyclic peptide with Dox in cyclic [W(RW)$_4$]−Dox improved the antiproliferative activity of Dox in some of the tested cancer cells. The cyclic peptide−Dox conjugate showed comparable antiproliferative activity against CCRF-CEM and MDA-MB-468 when compared to Dox after 96 and 120 h incubation. However, the antiproliferative activities of cyclic [W(RW)$_4$]−Dox conjugate in SK-OV-3 and HCT-116 cells were higher than those of Dox at a concentration of 1 μM after 96 and 120 h incubation. For example, cyclic [W(RW)$_4$]−Dox inhibited the cell proliferation of SK-OV-3 (67−74%) and HTC-116 (65−67%) cells at a concentration of 1 μM after 96−120 h of incubation, while Dox exhibited antiproliferative activity

against SK-OV-3 (57−59%) and HTC-116 (57−64%) under similar conditions. Cyclic [W(RW)$_4$]−Dox showed higher cellular retention Than Dox and Linear (RW)$_4$−Dox.

Dox is easy to track by using fluorescence-based techniques, due to the inherent red fluorescence. Because of the higher antiproliferative activity of cyclic [W(RW)$_4$]−Dox after 72 h compared to linear (RW)$_4$−Dox and Dox, this compound was selected for further cellular uptake studies in comparison to other compounds to determine whether the higher activity of this compound is consistent with enhanced uptake of the compound. The cellular uptake of all derivatives was examined in Dox-resistant SK-OV-3 cells using fluorescence-activated cell sorter (FACS) analysis (Figure 3). To obtain the primary influx, cells were allowed to be incubated with covalent cyclic [W(RW)$_4$]−Dox and linear (RW)$_4$−Dox peptides, noncovalent physical mixtures, cyclic [W(RW)$_4$] + Dox and linear (RW)$_4$ + Dox, and Dox for 1 h. This process was followed by 24 h incubation with media to allow the cells to start the efflux process through pumping the compounds out. Then the amounts of Dox in cells were evaluated by using FACS in Dox-resistant SK-OV-3 cells. The data showed 3.3−3.6-fold more cellular uptake of cyclic [W(RW)$_4$]−Dox compared to Dox alone and noncovalent physical mixtures, cyclic [W(RW)$_4$] + Dox and linear (RW)$_4$ + Dox, in SK-OV-3 (Figure 3). Between linear and cyclic peptide−Dox covalent conjugates, the retention of cyclic [W(RW)$_4$]−Dox was found to be 2.6-fold higher compared to that of linear (RW)$_4$−Dox. These data suggest that cyclic peptide−Dox, cyclic [W(RW)$_4$]−Dox, enhanced the cellular uptake of the compound. The cyclic nature of the peptide was found to contribute in inhibition of the efflux. These data are consistent with higher antiproliferative activity of cyclic [W(RW)$_4$]−Dox versus linear

$(RW)_4$−Dox and Dox, suggesting that the presence of cyclic peptide in the conjugate reduces efflux, increases cellular uptake and retention of Dox, and enhances antiproliferative activity.

Cyclic [W$(RW)_4$]−Dox **Nuclear Localization in SK-OV-3 Cells**. The cellular localization of free Dox and conjugate cyclic [W$(RW)_4$]−Dox was compared in SK-OV-3 cells after 1 and 24 h incubation at 37 °C. A noncytotoxic concentration of 5 μM was chosen to ensure Dox fluorescence detection by confocal microscopy. Confocal microscopy images of SK-OV-3 cells are shown after 1 h incubation. Free Dox and cyclic [W$(RW)_4$]−Dox were localized mainly in the nucleus (Figure 4a). The results showed that the covalent conjugation of Dox with cyclic [W$(RW)_4$] did not prevent the nuclear accumulation of the drug. To compare the retention ability of cyclic [W$(RW)_4$]−Dox versus Dox alone against efflux effects, SKOV-3 cells were incubated with both compounds for 1 h followed by incubation in drug-free media for 24 h at 37 °C. The fluorescence intensity of Dox in cells treated with cyclic [W$(RW)_4$]−Dox was found to be significantly higher than that in cells treated with Dox alone (Figure 4b), indicating that cyclic [W$(RW)_4$]−Dox was retained in cells much longer than free Dox. Thus, this conjugate has a potential to be used as a tool for enhancing the nuclear retention of Dox.

Stability of Cyclic [W$(RW)_4$**]−Dox**. Cyclic [W$(RW)_4$]−Dox was incubated with phosphate-buffered saline (PBS) and fetal bovine serum (FBS) solution at 37 °C at different time intervals. The results indicated that cyclic [W$(RW)_4$]−Dox is relatively

stable in both systems with half-life values of 10.77 and 26.20 h in PBS and FBS, respectively. No interaction between serum proteins and cyclic $[W(RW)_4]$−Dox was observed since the mixture was clear and no precipitation or turbidity was found during the assay. Cyclic $[W(RW)_4]$−Dox was found to be stable in PBS (97%) and FBS (84%) after 1 h. For cellular uptake studies using FACS, the cells were incubated by cyclic $[W(RW)_4]$−Dox for 1 h followed by 24 h incubation with drug-free media. During the 1 h period, the compound showed minimal hydrolysis in serum, suggesting that most of the compound is hydrolyzed intracellularly (Figures S5 and S6 in the Supporting Information).

Intracellular Hydrolysis. Intracellular hydrolysis results for cyclic $[W(RW)_4]$−Dox were monitored in CCRF-CEM cells. CCRF-CEM cells (1.37×10^7) were incubated with the conjugate (1 μM) for 4 h followed by drug-free medium to determine the possibility of the intracellular hydrolysis to Dox. Drug-free medium was used to rule out the continuous cellular uptake of the conjugate, while the compound is hydrolyzed intracellularly. HPLC analysis with detection at 490 nm and at specific time intervals after cellular lysis was used to measure the ratio of the cyclic $[W(RW)_4]$−Dox and released Dox. The cellular hydrolysis data exhibited that the cyclic peptide−Dox conjugate was hydrolyzed intracellularly and released Dox in a time-dependent manner. More than 46% of cyclic $[W(RW)_4]$−Dox was hydrolyzed intracellularly within 12 h. Approximately 86% of cyclic $[W(RW)_4]$−Dox was hydrolyzed intracellularly within 48 h (Figure 5). These data suggest that the enhanced uptake,

retention, and sustained intracellular hydrolysis of cyclic [W(RW)$_4$]−Dox to Dox contribute to overall activity of the conjugate as a potential prodrug

Cell Cycle Distribution Analysis. In addition to apoptosis,[35,36] Dox treatment causes cell cycle arrest in cancer cells.[37] The impact of cyclic [W(RW)$_4$]−Dox on cell cycle distribution was investigated in colorectal carcinoma cells (HCT-116) compared to Dox. All experiments were performed under similar conditions, and appropriate controls were used to confirm the results. An hour incubation was selected followed by 24 h incubation in drug-free medium, due to the significant difference in the cellular uptake of cyclic [W(RW)$_4$]−Dox and Dox. Control cells were found in G0/G1 phase (46.8 ± 1.0%), S phase (36.5 ± 0.7%), and G2/M phase (16.5 ± 0.2%). The percentage of the pre-G0/G1 population indicates the apoptosis rate of cells. There was no significant pre-G0-G1 population as shown in the histograms because the cells were incubated with Dox and the prodrug only for 1 h. Cells treated with compounds (Dox and cyclic [W(RW)$_4$]−Dox) showed different patterns than control cells for G0/G1 phase (53.0 ± 1.0% and 42.2 ± 1.4%), S phase (21.8 ± 3.0% and 23.5 ± 0.2%), and G2/M phase (25.1 ± 2.0% and 34.1 ± 1.2%), respectively (Figure 6). The data showed that, in cells treated with cyclic [W(RW)$_4$]−Dox, the proportion of cells in G0/G1 phase was decreased nearly 10% compared to values for Dox. On the other hand, the proportion of cells in G2/M phase increased nearly 10% compared to values for Dox. These data suggest that cyclic [W(RW)$_4$]−Dox led to a significant reduction of cells in G0/G1 phase, and caused more accumulation in G2/M phase in HCT-116 cells. This pattern is slightly different when compared to Dox. This could be due to the

requirement for cyclic [W(RW)$_4$]−Dox to get hydrolyzed to Dox. Based on the population of cells at different phases, prodrug follows a different pattern when compared with Dox. Some of the antiproliferative activity by cyclic [W(RW)$_4$]−Dox could be due to the differential pattern of cell cycle distribution by the conjugate, in addition to intracellular hydrolysis to Dox. The histograms were also provided in the Supporting Information (Figure S4).

Topo II Inhibitory Activity. One of the major anticancer mechanisms of Dox is the inhibition of topoisomerase II.[2] Thus, a comparative study was performed between cyclic [W(RW)$_4$]−Dox and Dox to determine whether the conjugate has Topo II inhibitory activity similar to that of the parent drug. Topo II is responsible for catalyzing the DNA double-stranded cleavage process by isolating catenated DNA duplexes. Kinetoplast DNA (kDNA) is used as a DNA substrate in the in vitro decatenation assay. The potency of Dox and cyclic [W(RW)$_4$]−Dox to inhibit Topo II enzyme for the decatenation of kDNA was used to analyze the comparative inhibitory activity of the compounds. Topo II decatenation assay exhibited that Dox inhibited Topo II at concentrations between 10 and 20 μM; however cyclic [W(RW)$_4$]−Dox inhibited the Topo II activity at concentrations between 20 and 30 μM (Figure 7) under similar reaction conditions. As expected, the conjugate acts at higher concentration compared to Dox since the conjugate is required to get hydrolyzed to Dox to be able to inhibit Topo II more efficiently. Under the in vitro conditions used here, the conjugate is not hydrolyzed and the reduced Topo II inhibitory activity is possibly due to the conjugation to the peptide and associated steric hindrance.

Hydrolysis to Dox is required to generate maximum Topo II inhibitory activity associated with Dox. The conjugate does not undergo hydrolysis under in vitro conditions in this assay.

CONCLUSIONS

In summary, linear and cyclic peptide−Dox conjugates were synthesized as prodrugs, were evaluated for their activities against various cancer cell lines, and were compared with the corresponding physical mixtures. The conjugation of Dox with a specific cyclic peptide, cyclic [W$(RW)_4$]−Dox, improved the antiproliferative activity compared to the corresponding physical mixtures in all tested cell lines. Cyclic peptide−Dox conjugate showed comparable antiproliferative activity against CCRF-CEM and MDA-MB-468 when compared to Dox. However, the antiproliferative activities of cyclic [W$(RW)_4$]− Dox conjugate in SK-OV-3 and HCT-116 cells were higher than those of Dox and linear $(RW)_4$−Dox at a concentration of 1 μM after 96 and 120 h incubation. Dox has short retention time in some cancer cells (e.g., ovarian adenocarcinoma SKOV-3) due to the efficient efflux effect. Thus, the differential cytotoxicity of cyclic [W$(RW)_4$]−Dox with Dox in SK-OV-3 could be due to the retention of Dox in the presence of the cyclic peptide. Since the system was designed as a prodrug, we did not expect to detect a huge difference between Dox and cyclic [W$(RW)_4$]−Dox in cytotoxicity. Furthermore, we demonstrated that the prodrug approach for Dox using a cyclic peptide conjugate significantly improved the cellular uptake and retention time of Dox in SK-OV-3 cancer cells. Flow cytometry analysis showed 3.3−3.6-fold higher cellular uptake of cyclic [W$(RW)_4$]−Dox than Dox alone

and the physical mixtures, cyclic $[W(RW)_4]$ + Dox and linear $(RW)_4$ + Dox, in SK-OV-3 cells after 24 h incubation. The conjugate exhibited nuclear localization and retention after 24 h, and underwent intracellular hydrolysis to Dox in CCRF-CEM cells, suggesting to be a potential prodrug for delivery of the drug. The cellular hydrolysis study showed that 99% of cyclic $[W(RW)_4]$−Dox was hydrolyzed intracellularly within 72 h and released Dox. These data suggest that cyclic $[W(RW)_4]$−Dox can be used as a potential prodrug for improving the biological profile, cellular delivery, and retention of Dox.

ASSOCIATED CONTENT

Supporting Information

Materials and methods, general chemistry, mass spectra, and additional supporting data and figures for stability and cell cycle arrest. This material is available free of charge via the Internet at: http://pubs.acs.org.

Notes

The authors declare no competing financial interest.

ACKNOWLEDGMENTS

We acknowledge the American Cancer Society, Grant No. RSG-07-290-01-CDD, and the US National Science Foundation, Grant No. CHE 0748555, for the financial support. We thank National Center for Research Resources, NIH, and Grant No. 1 P20 RR16457 for sponsoring the core facility.

ABBREVIATIONS USED

CCRF-CEM, human leukemia carcinoma cell line; CPPs, cellpenetrating peptides; DCM, dichloromethane; Dox, doxorubicin; DIPEA, *N*,*N*-diisopropylethylamine; HBTU, DDS, drug delivery systems; FACS, fluorescence activated cell sorter; FBS, fetal bovine serum; DCM, dichloromethane; HCT-116, human colorectal carcinoma; HOBt, hydroxybenzotriazole; HBTU, 1,1,3,3-tetramethyluronium hexafluorophosphate; MDA-MB- 468, human breast adenocarcinoma; MRPs, multidrug resistance proteins; NMM (*N*-methylmorpholine); P-gp, P-glycoprotein; PBS, phosphate buffered saline solution; PyBOP, benzotriazol-1-yloxytripyrrolidinophosphonium hexafluorophosphate; SK-OV-3, human ovarian adenocarcinoma, 1,1,3,3-tetramethyluronium hexafluorophosphate; TOPO II, topoisomerase II

REFERENCES

(1) Vincenzi, B.; Frezza, A. M.; Santini, D.; Tonini, G. New therapies in soft tissue sarcoma. Expert Opin. Emerging Drugs 2010, 15, 237−248.

(2) (a) Quigley, G. J.; Wang, A. H.; Ughetto, G.; van der Marel, G.; van Boom, J. H.; Rich, A. Molecular structure of an anticancer drug-DNA complex: daunomycin plus d(CpGpTpApCpG). Proc. Natl. Acad. Sci. U.S.A. 1980, 77, 7204−7208. (b) Patel, D. J.; Kozlowski, S. A.; Rice, J. A. Hydrogen bonding, overlap geometry, and sequence specificity in anthracycline antitumor antibiotic.DNA complexes in solution. Proc. Natl. Acad. Sci. U.S.A 1981, 78, 3333−3337.

(3) Gottesman, M. M. Mechanisms of drug resistance. Annu. Rev. Med. 2002, 53, 615−627.

(4) Longely, D. B.; Johnston, P. G. Molecular mechanisms of drug resistance. J. Pathol. 2005, 205, 275−292.

(5) Stavrovskaya, A. A. Cellular mechanisms of multidrug resistance of tumor cells. Biochemistry 2000, 65, 95−106.

(6) Kratz, F. DOXO-EMCH (INNO-206): The first albumin binding prodrug of doxorubicin to enter clinical trials. Expert Opin. Invest. Drugs 2007, 16, 855−866.

(7) Tang, Y.; McGoron, A. J. Combined effects of laser-ICG photothermotherapy and doxorubicin chemotherapy on ovarian cancer cells. J. Photochem. Photobiol., B 2009, 97, 138−144.

(8) Raoul, J. L.; Heresbach, D.; Bretagne, J. F.; Ferrer, D. B.; Duvauferrier, R.; Bourguet, P.; Messner, M.; Gosselin, M. Chemoembolization of hepatocellular

carcinomas a study of the biodistribution and pharmacokinetics of doxorubicin. Cancer 1992, 70, 585−590.

(9) Rahman, A.; Carmichael, D.; Harris, M.; Roh, J. K. Comparative pharmacokinetics of free doxorubicin and doxorubicin entrapped in cardiolipin liposomes. Cancer. Res. 1986, 46, 2295−2299.

(10) (a) Chhikara, B. S.; St. Jean, N.; Mandal, D.; Kumar, A.; Parang, K. Fatty acyl amide derivatives of doxorubicin: Synthesis and in vitro anticancer activities. Eur. J. Med. Chem. 2011, 46, 2037−2042. (b) Chhikara, B.S.; Mandal, D.; Parang, K. Synthesis, anticancer activities, and cellular uptake studies of lipophilic derivatives of doxorubicin succinate. J. Med. Chem. 2012, 55, 1500−1510.

(11) Takemura, G.; Fujiwara, H. Doxorubicin-induced cardiomyopathy from the cardiotoxic mechanisms to management. Prog. Cardiovasc. Dis. 2007, 49, 330−352.

(12) Ayla, S.; Seckin, I.; Tanriverdi, G.; Cengiz, M.; Eser, M.; Soner, B. C.; Oktem, G. Doxorubicin induced nephrotoxicity: protective effect of nicotinamide. Int. J. Cell Biol. 2011, 390238.

(13) Seelig, A.; Gatlik-Landwojtowicz, E. Inhibitors of multidrug efflux transporters: their membrane and protein interactions. Mini-Rev. Med. Chem. 2005, 5, 135−151.

(14) Yang, X.; Deng, W.; Fu, L.; Blanco, E.; Gao, J.; Quan, D.; Shuai, X. Folate functionalized polymeric micelles for tumor targeted delivery of a potent multidrug-resistance modulator FG020326. J. Biomed. Mater. Res., Part A 2008, 86, 48−60.

(15) Chavanpatil, M. D.; Khdair, A.; Gerard, B.; Bachmeier, C.; Miller, D. W.; Shekhar, M. P. V.; Panvam, J. Surfactant-polymer nanoparticles overcome P-glycoprotein-mediated drug efflux. Mol. Pharmaceutics 2007, 4, 730−738.

(16) Sadava, D.; Coleman, A.; Kane, S. E. Liposomal daunorubicin overcomes drug resistance in human breast, ovarian and lung carcinoma cells. J. Liposome Res. 2002, 12, 301−309.

(17) Ibsen, S.; Zahavy, E.; Wrasdilo, W.; Berns, M.; Chan, M.; Esener, S. A novel doxorubicin prodrug with controllable photolysis activation for cancer chemotherapy. Pharm. Res. 2010, 27, 1848−1860.

(18) Chhikara, B. S.; Parang, K. Development of cytarabine prodrugs and delivery systems for leukemia treatment. Expert Opin. Drug Delivery 2010, 7, 1399−1414.

(19) Wang, Y.; Li, L.; Jiang, W.; Yang, Z.; Zhang, Z. Synthesis and preliminary antitumor activity evaluation of a DHA and doxorubicin conjugate. Bioorg. Med. Chem. Lett. 2006, 16, 2974−2977.

(20) Kumar, S. A.; Peter, Y. A.; Nadeau, J. L. Facile biosynthesis, separation and conjugation of gold nanoparticles to doxorubicin. Nanotechnology 2008, 19, 495101.

(21) You, J.; Zhang, G.; Li, C. Exceptionally high payload of doxorubicin in hollow gold nanosphere for near-infrared light triggered drug release. ACS Nano 2010, 4, 1033−1041.

(22) Massing, U.; Fuxius, S. Liposomal formulations of anticancer agents: selectivity and effectiveness. Drug Resist. Updates 2000, 3, 171−177.

(23) Derossi, D.; Joliot, A. H.; Chassaing, G.; Prochiantz, A. The third helix of the Antennapedia homeodomain translocates through biological membranes. J. Biol. Chem. 1994, 269, 10444−10450.

(24) Derossi, D.; Chassaing, G.; Prochiantz, A. Trojan peptides: the penetratin system for intracellular delivery. Trends Cell Biol. 1998, 8, 84−87.

(25) Meyer-Losic, F.; Quinonero, J.; Dubois, V.; Alluis, B.; Dechambre, M.; Michel, M.; Cailler, F.; Fernandez, A. M.; Trouet, A.; Kearsey, J. Improved therapeutic efficacy of doxorubicin through conjugation with a novel peptide drug delivery technology (Vectocell). J. Med. Chem. 2006, 49, 6908−6916.

(26) Ché, C.; Yang, G.; Thiot, C.; Lacoste, M.-C.; Currie, J.-C.; Demeule, M.; Régina, A.; Béliveau, R.; Castaigne, J.-P. New angiopep modified doxorubicin (ANG1007) and etoposide (ANG1009) chemotherapeutics with increased brain penetration. J. Med. Chem. 2010, 53, 2814−2824.

(27) Lindgren, M.; Rosenthal-Aizman, K.; Saar, K.; Eiriksdottir, E.; Jiang, Y.; Sassian, M.; Ostlund, P.; Hallbrink, M.; Langel, U. Overcoming methotrexate resistance in breast cancer tumour cells by the use of a new cell-penetrating peptide. Biochem. Pharmacol. 2006, 71, 416−425.

(28) Zhu, S.; Hong, M.; Zhang, L.; Tang, G.; Jiang, Y.; Pei, Y. PEGylated PAMAM dendrimer-doxorubicin conjugates: In vitro evaluation and in vivo tumor accumulation. Pharm. Res. 2010, 27, 161−174.

(29) Lee, J.-Y.; Choi, Y.-S.; Suh, J.-S.; Kwon, Y.-M.; Yang, V. C.; Lee, S.-J.; Chung, C.-P.; Park, Y.-J. Cell-penetrating chitosan/doxorubicin/ TAT conjugates for efficient cancer therapy. Int. J. Cancer 2011, 128, 2470−2480.

(30) Shi, N.-Q.; Gao, W.; Xiang, B.; Qi, X.-R. Enhancing cellular uptake of activable cell-penetrating peptide−doxorubicin conjugate by enzymatic cleavage. Int. J. Nanomed. 2012, 7, 1613−1621.

(31) Aroui, S.; Ram, N.; Appaix, F.; Ronjat, M.; Kenani, A.; Pirollet, F.; De, Waard, M. Maurocalcine as a non toxic drug carrier overcomes doxorubicin resistance in the cancer cell line MDA-MB 231. Pharm. Res. 2009, 28, 836−845.

(32) Mandal, D.; Nasrolahi Shirazi, A.; Parang, K. Cell-penetrating homochiral cyclic peptides as nuclear-targeting molecular transporters. Angew. Chem., Int. Ed. 2011, 50, 9633−9637.

(33) Nagy, A.; Schally, A. V.; Armatis, P.; Szepeshazi, K.; Halmos, G.; Miyazaki, M.; Jungwirth, A.; Horvath, J. Cytotoxic analogs of luteinizing hormone-releasing hormone containing doxorubicin or 2-pyrrolinodoxorubicin, a derivative 500−1000 times more potent. Proc. Nat. Acad. Sci. U.S.A. 1996, 93, 7269−7273.

(34) Nasrolahi Shirazi, A.; Mandal, D.; Tiwari, R. K.; Guo, L.; Lu, W.; Parang, K. Cyclic peptide-capped gold nanoparticles as drug delivery systems. Mol. Pharmaceutics 2012, 10, 488-499.

(35) Swift, L. P.; Rephaeli, A.; Nudelman, A.; Philips, D. R.; Cutts, S. M. Doxorubicin-DNA adducts induce a non-topoisomerase II mediated form of cell death. Cancer 2006, 66, 4893−4871.

(36) Tsang, W. P.; Chau, S. P. Y.; Kong, S. K.; Fung, K. P.; Kwok, T. T. Reactive oxygen species mediate doxorubicin induced p53-independent apoptosis. Life Sci. 2003, 73, 2047−2058.

(37) Kim, H. S.; Lee, Y. S.; Kim, D. K. Doxorubicin exerts cytotoxic effects through cell cycle arrest and fas-mediated cell death. Pharmacology 2009, 84, 300−309.

Figure Legends:

Figure 1: Cytotoxicity assay of cyclic $[WR]_4$ and cyclic $[W(RW)_4K]$-(β-Ala) in MDA-MB-468, HCT-116, CCRF-CEM, and SK-OV-3

Figure 2: Inhibition of (a) CCRF-CEM, (b) SK-OV-3, (c) HCT-116, and (d) MDA-MB-468 cells by compounds (1 μM) after 24−120 h incubation. The results are shown as the percentage of the control DMSO that has no compound (set at 100%). All the experiments were performed in triplicate (±SD)

Figure 3: FACS analysis of cellular uptake assays of cyclic $[W(RW)_4]$−Dox (5 μM) in SK-OV-3 cells compared with linear $(RW)_4$−Dox (5 μM) and the physical mixtures, cyclic $[RW)_4]$ (5 μM) + Dox (5 μM) and linear $(RW)_4$ (5 μM) + Dox (5 μM)

Figure 4: (a) Confocal microscopy images of Dox and cyclic $[W(RW)_4]$−Dox (5 μM) uptake in SK-OV-03 cells after 1 h. Red represents the fluorescence of Dox. (b) Confocal microscopy images of Dox and cyclic $[W(RW)_4]$−Dox (5 μM) uptake in SK-OV-03 cells. SK-OV-3 cells were treated with the compound for 1 h. The compound was removed, and the cells were incubated with complete media for 24 h. Red represents the fluorescence of Dox)

Figure 5: HPLC chromatograms for the cellular uptake studies of cyclic $[W(RW)_4]$−Dox using CCRF-CEM cells after incubation for 1−72 h

Figure 6: Comparison of cell cycle arrest by Dox and cyclic $[W(RW)_4]$-Dox

Figure 7: Topo II assay for Dox (middle) and cyclic $[W(RW)_4]$−Dox (right). The lines A1 and A2 were linear markers and decatenated DNA markers, respectively. Line A3

represents the blank kDNA in the absence of any compound. kDNA was incubated with compound Dox (10−50 μM, lanes B1−B5) and cyclic [W(RW)$_4$]−Dox (10−50 μM, lanes C1−C5) and decatenated using topoisomerase II for 30 min at 37 °C. The decatenation was monitored by gel electrophoresis and imaged by ethidium bromide fluorescence

Scheme Legends:

Scheme 1: Synthesis of Linear (RW)$_4$ Peptide

Scheme 2: Synthesis of Cyclic [W(RW)$_4$K](β-Ala) Peptide

Scheme 3: Synthesis of Dox−Peptide (Linear or Cyclic) Conjugates

Figure 1

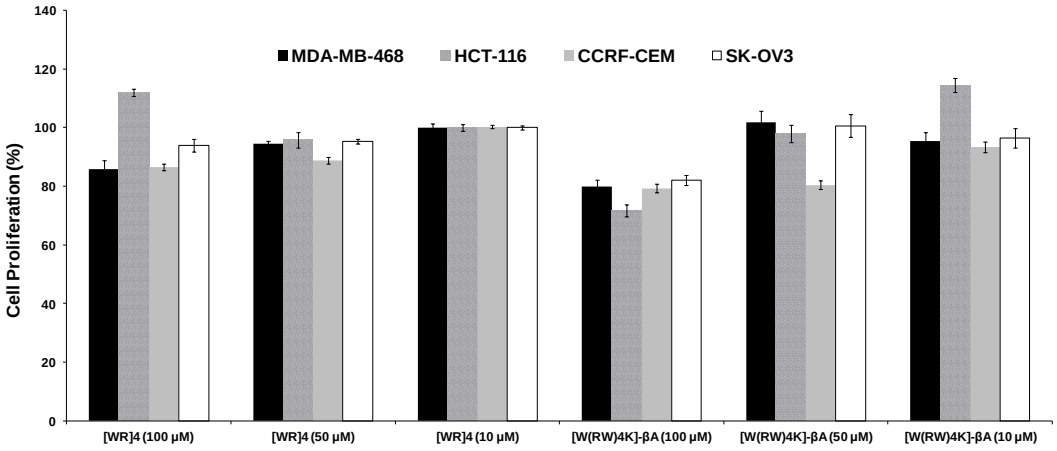

Figure 2

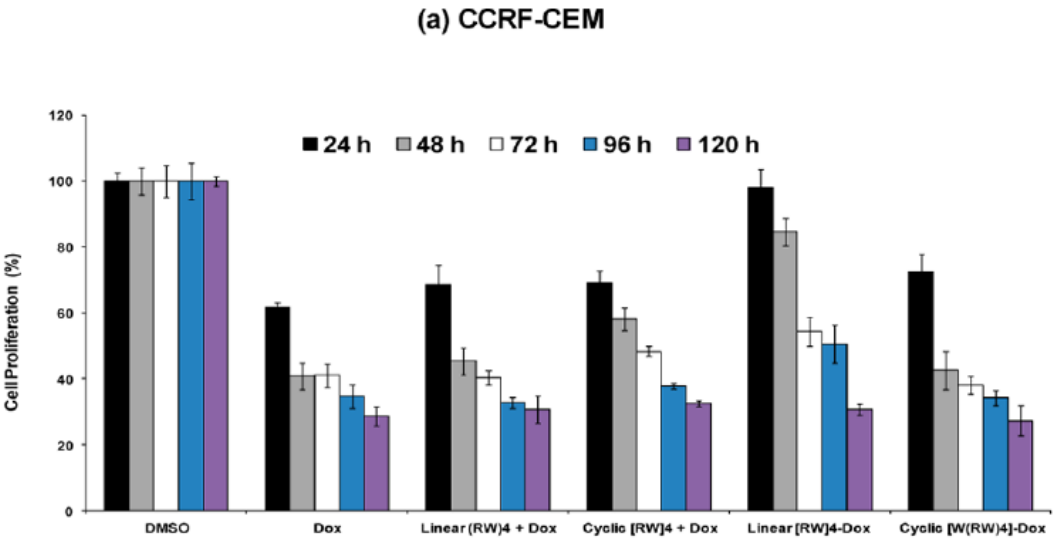

(b) SK-OV-3

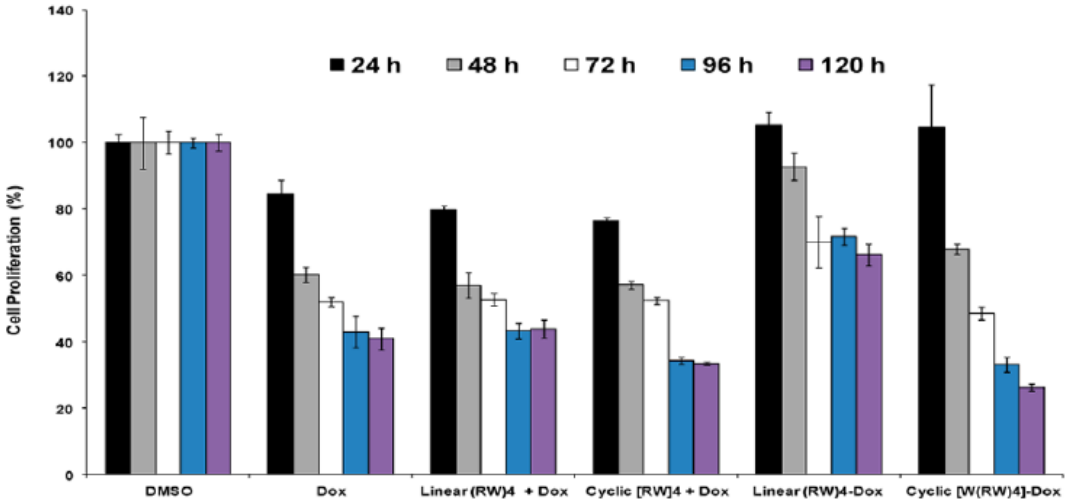

(c) HCT-116

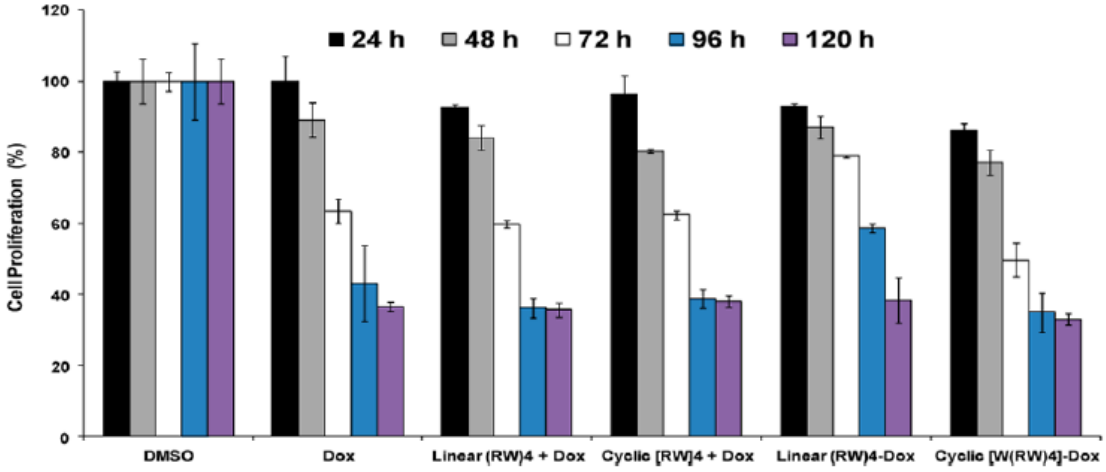

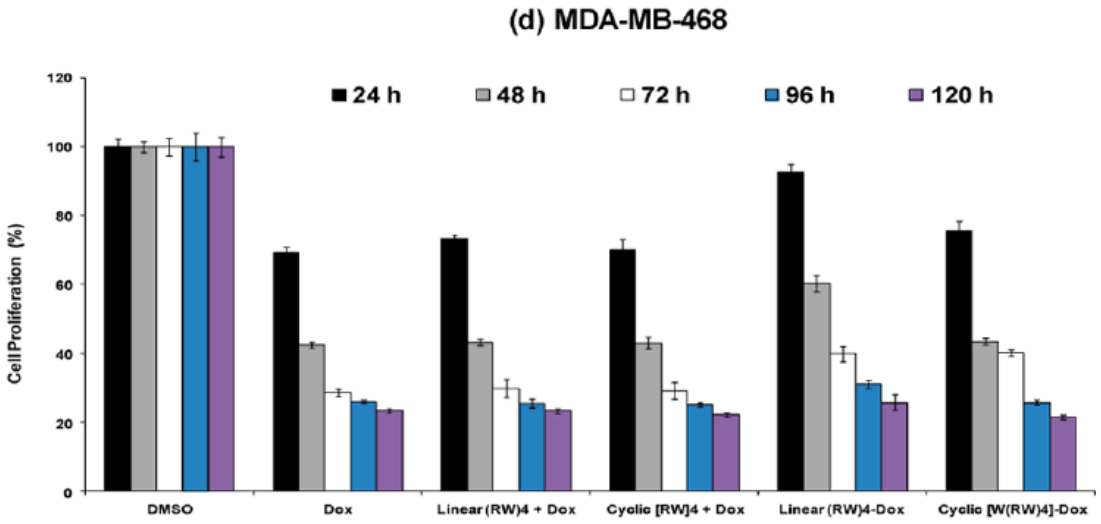
(d) MDA-MB-468
24 h
48 h
72 h
96 h
120 h
Cell Proliferation (%)
120
100
80
60
40
20
0
DMSO
Dox
Linear (RW)4 + Dox
Cyclic [RW]4 + Dox
Linear (RW)4-Dox
Cyclic [W(RW)4]-Dox

Figure 3

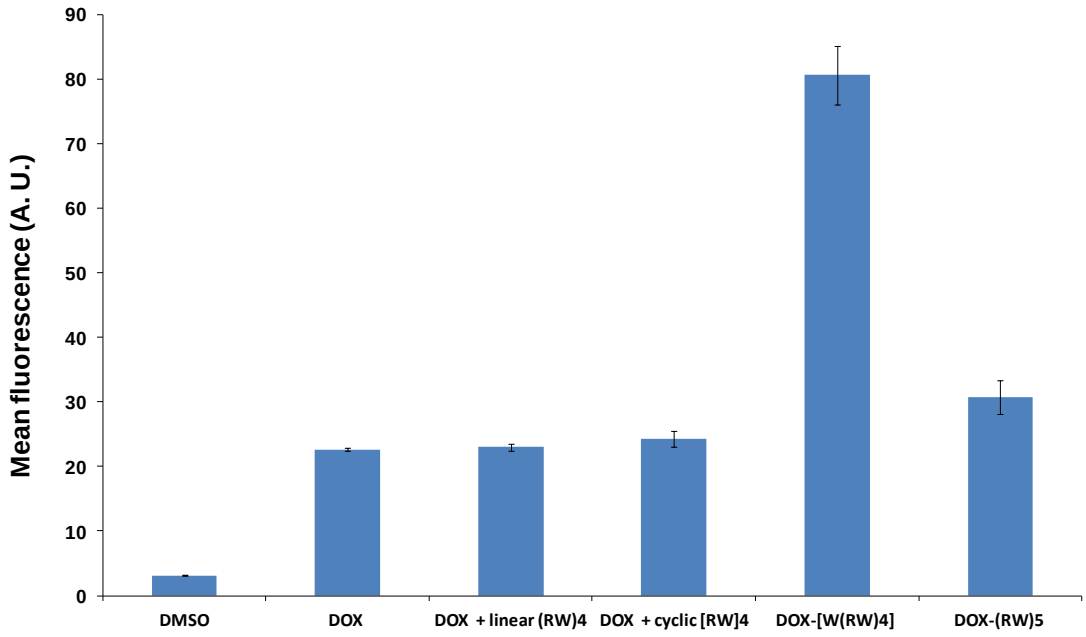
Mean fluorescence (A. U.)
90
80
70
60
50
40
30
20
10
0
DMSO
DOX
DOX + linear (RW)4
DOX + cyclic [RW]4
DOX-[W(RW)4]
DOX-(RW)5

Figure 4

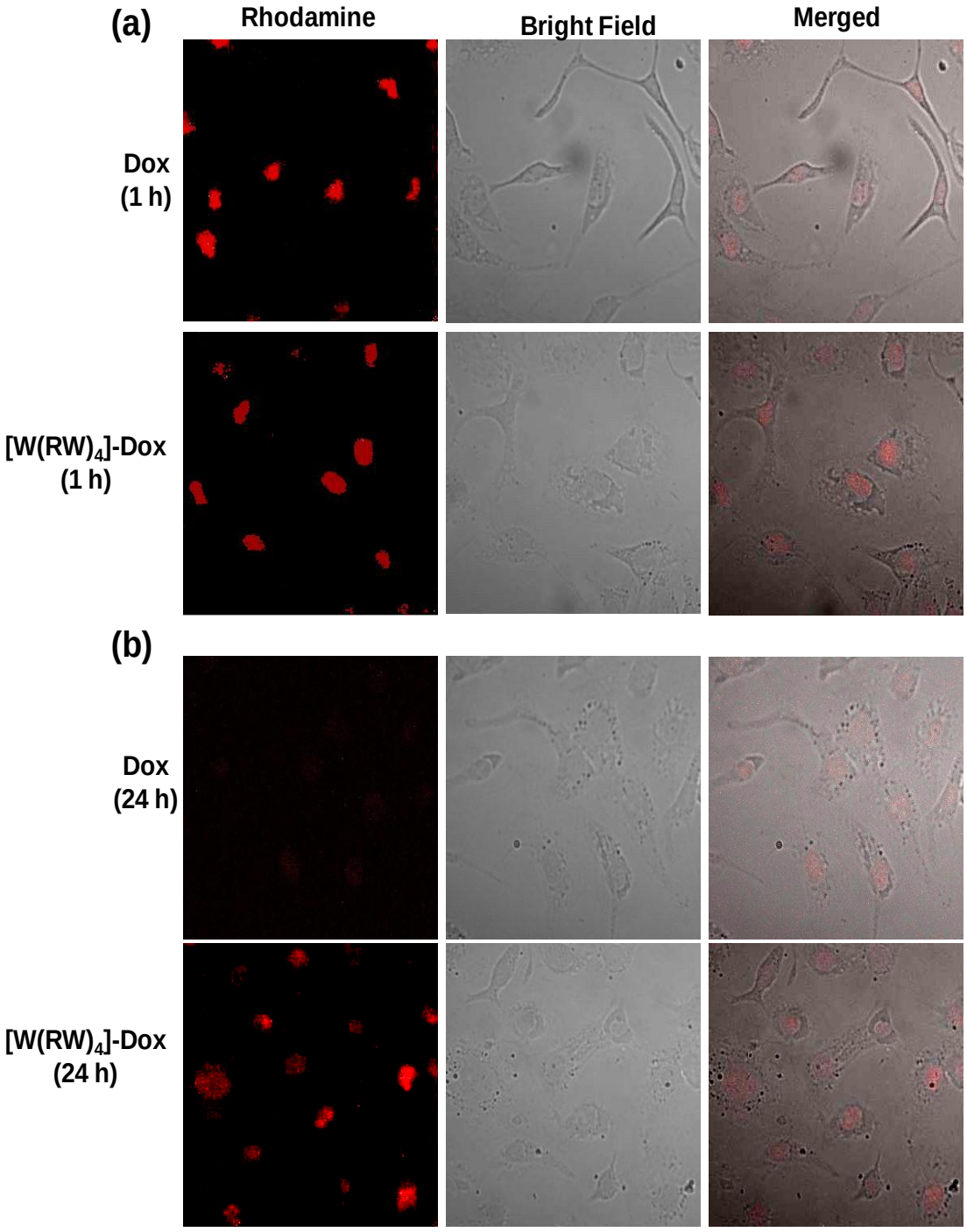
(a)
Rhodamine
Bright Field
Merged
Dox
(1 h)
[W(RW)4]-Dox
(1 h)
(b)
Dox
(24 h)
[W(RW)4]-Dox
(24 h)

Figure 5

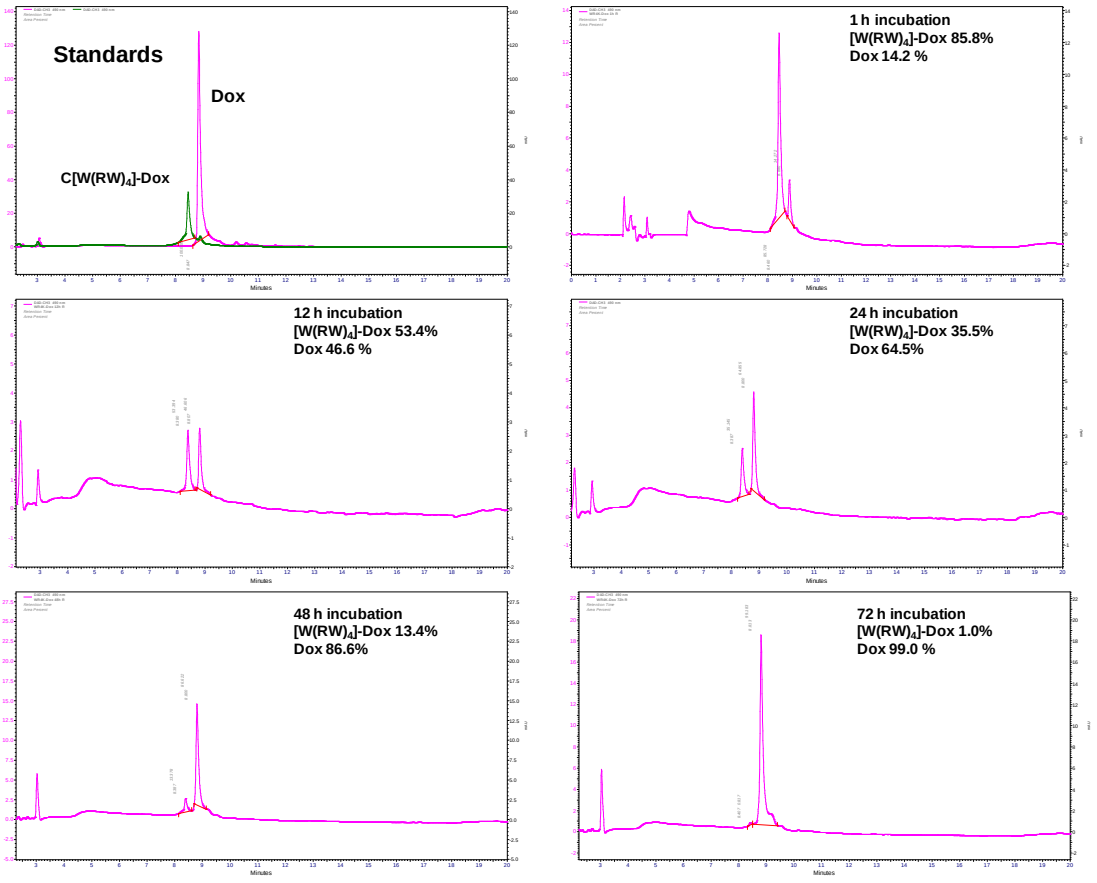
Standards
Dox
C[W(RW)4]-Dox
1 h incubation
[W(RW)4]-Dox 85.8%
Dox 14.2 %
12 h incubation
[W(RW)4]-Dox 53.4%
Dox 46.6 %
24 h incubation
[W(RW)4]-Dox 35.5%
Dox 64.5%
48 h incubation
[W(RW)4]-Dox 13.4%
Dox 86.6%
72 h incubation
[W(RW)4]-Dox 1.0%
Dox 99.0 %
Minutes

Figure 6

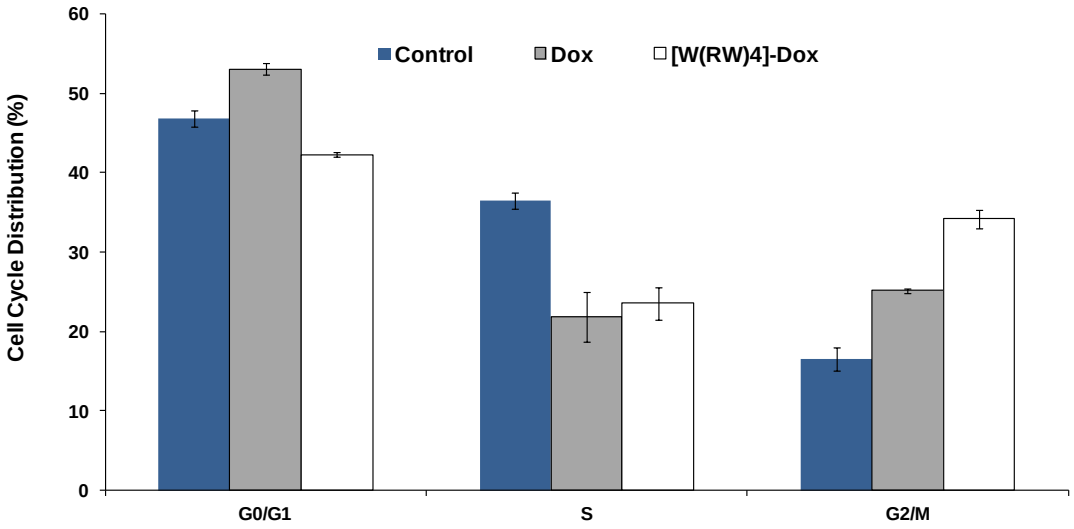

Figure 7

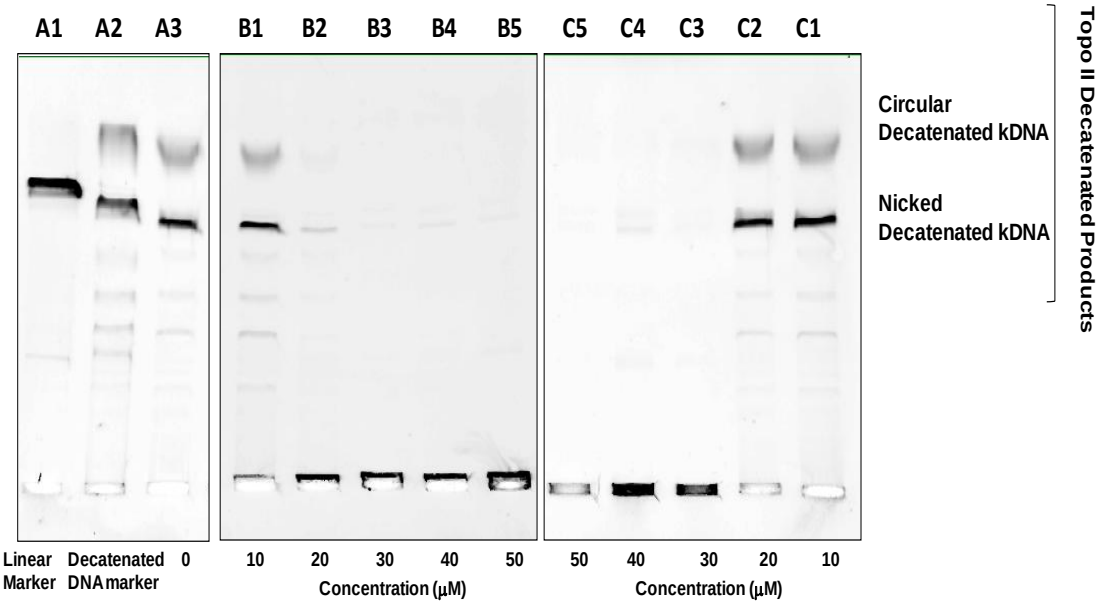

Scheme 1

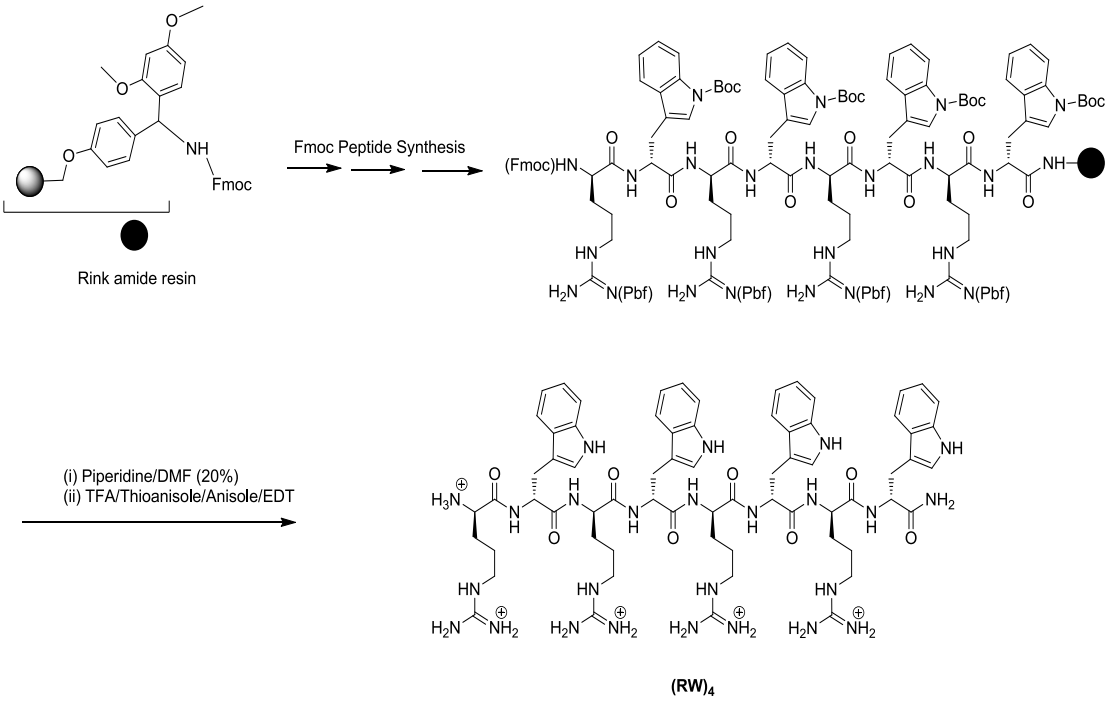
Rink amide resin
Fmoc Peptide Synthesis
(i) Piperidine/DMF (20%)
(ii) TFA/Thioanisole/Anisole/EDT
(RW)4

Scheme 2

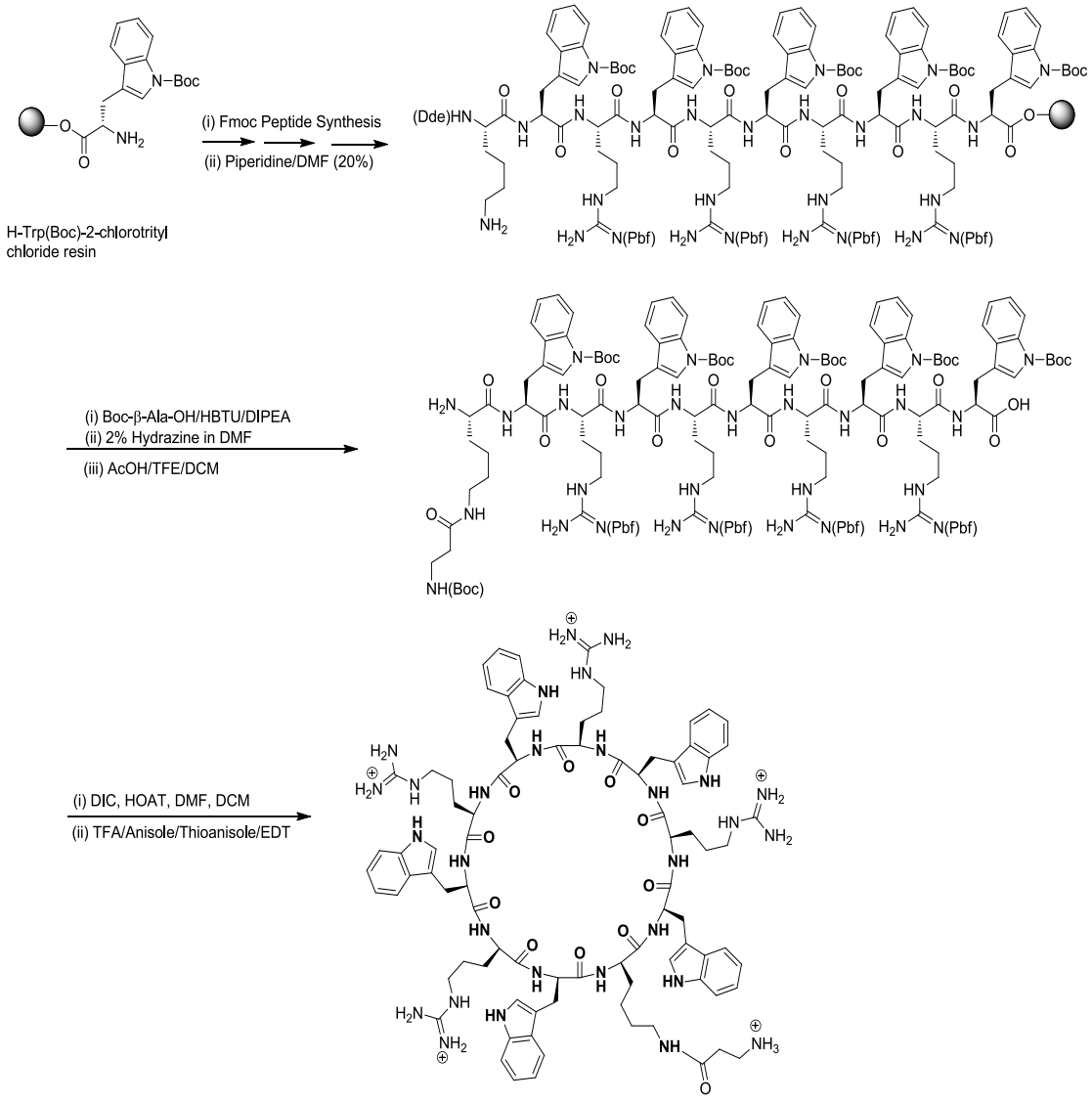
(i) Fmoc Peptide Synthesis
(ii) Piperidine/DMF (20%)
H-Trp(Boc)-2-chlorotrityl chloride resin
(i) Boc-β-Ala-OH/HBTU/DIPEA
(ii) 2% Hydrazine in DMF
(iii) AcOH/TFE/DCM
(i) DIC, HOAT, DMF, DCM
(ii) TFA/Anisole/Thioanisole/EDT

Scheme 3

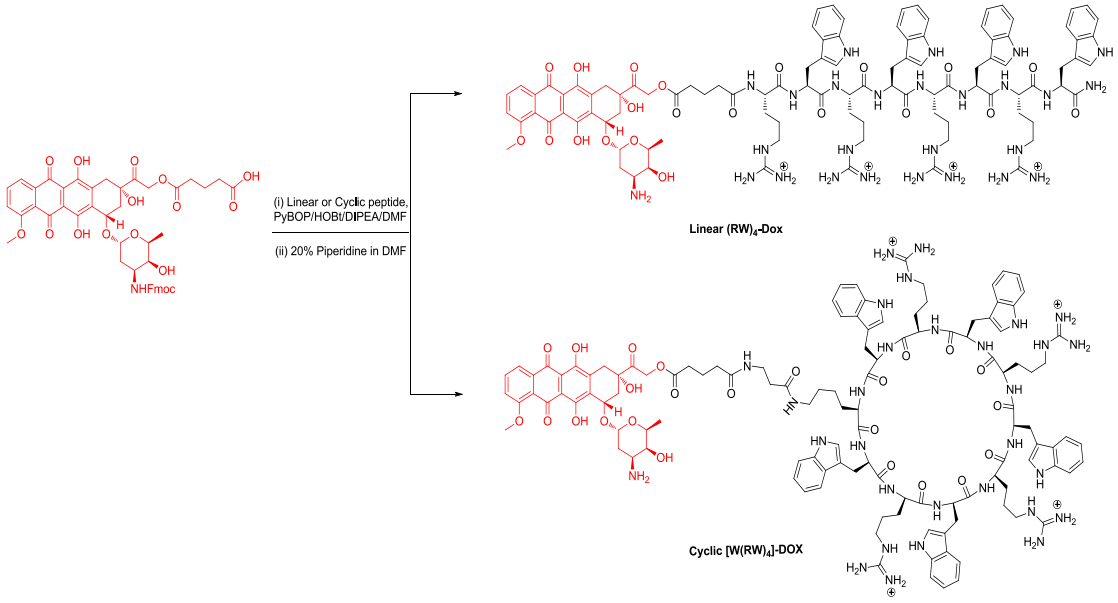
(i) Linear or Cyclic peptide, PyBOP/HOBt/DIPEA/DMF
(ii) 20% Piperidine in DMF
NHFmoc
Linear (RW)4-Dox
Cyclic [W(RW)4]-DOX

Manuscript III

Published in ***Molecular Pharmaceutics***, 2013, 10, 500-511

Cyclic peptide-capped gold nanoparticles as drug delivery systems

Amir Nasrolahi Shirazi, Dindyal Mandal, Rakesh K. Tiwari, Liangran Guo, Wei Lu, and Keykavous Parang*

Department of Biomedical and Pharmaceutical Sciences, College of Pharmacy, University of Rhode Island, Kingston, Rhode Island 02881, United States

Corresponding Author

*7 Greenhouse Road, Department of Biomedical and Pharmaceutical Sciences, College of Pharmacy, University of Rhode Island, Kingston, RI 02881, USA. Tel: +1-401-874-4471. Fax: +1-401-874-5787. E-mail: kparang@uri.edu.

ABSTRACT

A number of cyclic peptides were synthesized and evaluated as simultaneous reducing and capping agents for generation of cyclic peptide-capped gold nanoparticles (CPAuNPs). Among them, direct dissolution of cyclic peptides containing alternate arginine and tryptophan $[WR]_n$ (n = 3−5) into an aqueous solution of $AuCl_4^-$ led to the formation of CPAuNPs, through the reducing activity of tryptophan residues and attraction of positively charged arginine residues toward chloroaurate anions in the reaction environment. Differential interference contrast microscopy of fluorescence-labeled lamivudine in the presence of $[WR]_4$-capped AuNPs showed significantly higher cellular delivery of antiviral drug versus that of parent drug alone. Flow cytometry studies also showed that the cellular uptake of fluorescence-labeled lamivudine, emtricitabine, and stavudine was significantly enhanced in human ovarian adenocarcinoma (SK-OV-3) cells in the presence of $[WR]_4$-AuNPs. For example, fluorescence labeled lamivudine loaded $[WR]_4$-AuNPs exhibited approximately 12- and 15-times higher cellular uptake than that of fluorescence labeled lamivudine alone in CCRF-CEM cells and SK-OV-3 cells, respectively. Confocal microscopy revealed that the presence of the $[WR]_4$-AuNPs enhanced the retention and nuclear localization of doxorubicin in SK-OV-3 cells after 24 h. These data suggest that these complexes can be used as potential noncovalent prodrugs for delivery of antiviral and anticancer agents.

KEYWORDS: arginine, cellular delivery, cyclic peptide, gold nanoparticle, tryptophan

INTRODUCTION

Gold nanoparticles (AuNPs) have become subjects of major interest because of their broad applications in biosensing,[1] imaging,[2] drug delivery,[3] and cancer therapy.[4−6] AuNP-based drug delivery systems (DDS) have become attractive due to their low toxicity, nonimmunogenicity, and biocompatibility.[7] To date, most current prodrug strategies for cellular delivery of compounds with limited cell permeability have taken advantage of covalent conjugation with carriers. These strategies require cleavage and release of the cargo compounds from the conjugate. The covalent conjugation of gold and drugs through functionalization of AuNPs by −SH and −NH moieties has been also investigated as an efficient strategy for drug delivery.[8]

We have previously reported the application of a number of cyclic peptides as nuclear targeting molecular transporters.[9] Herein, we report evaluation of L-cyclic peptides as simultaneous reducing and capping agents for generation of cyclic peptide-capped gold nanoparticles (CP AuNPs). We used cellpenetrating properties of both cyclic peptides and capped AuNPs for in situ generation of a DDS. To the best of our knowledge, this is the first report of using cyclic peptides in generation of cell-penetrating CP-AuNPs and as drug delivery tools.

Multifunctional CP-AuNPs with Au^{3+} reducing, capping, and cell-penetrating properties are distinct from the previously reported AuNPs for the following reasons: (1) Cell-penetrating properties of both cyclic peptides and capped AuNPs are used for cellular drug delivery applications. Positively charged and hydrophobic residues in the peptides can be designed to perturb and/or permeate membranes by interacting with the corresponding negatively charged and hydrophobic residues, respectively, in the

phospholipid bilayer and to promote a higher uptake of molecular cargo than conventional delivery routes. (2) No chemical modification or functionalization is required on the surface of the generated AuNPs by the cyclic peptides. Furthermore, no covalent conjugation is needed between biologically active compounds and CP-AuNPs. Hydrophobic amino acids of the peptide generate a pocket for noncovalent entrapment of drugs. (3) Amino acid residues in the structure of the cyclic peptide work as simultaneous reducing and capping agents. Amino acids and linear peptides have been studied as reducing agents.[10−13] Linear peptides incorporating amino acids containing nitrogen heteroaromatics are strong metal binders. Tryptophan (W) has been shown as the most efficient reducing agent among 20 amino acids.[13] Furthermore, positively charged linear peptides found to enhance the reduction because of the favorable charge interactions can bring the chloroaurate anions in proximity for reaction.[13] The application of cell-penetrating cyclic peptides as simultaneous reducing and capping agents in AuNP formation remains unexplored. (4) The enhancement of intracellular delivery of biologically active cargos by employing linear cationic cell-penetrating peptides (CPPs) has been previously reported.[14,15] Compared to linear peptides that are susceptible to hydrolysis by endogenous peptidases, cyclic peptide counterparts are chemically and enzymatically more stable.[16] (5) CP-AuNPs in combination with antiviral and anticancer drugs can be used as potential scaffold for generation of noncovalent prodrugs.

EXPERIMENTAL SECTION

Materials and Methods. The synthesis of cyclic peptides was carried out according to the previously reported procedure.[7] All reactions were carried out in Bio-Rad polypropylene columns by shaking and mixing using a Glass-Col small tube rotator in dry conditions at room temperature unless otherwise stated. Chlorotrityl chloride resin, trityl chloride resins, coupling reagents, and Fmoc-amino acid building blocks were purchased from Chempep (Miami, FL).

Other chemicals and reagents were purchased from Sigma-Aldrich Chemical Co. (Milwaukee, WI). All peptides were synthesized using a solid-phase synthesis method employing *N*-(9-fluorenyl)methoxycarbonyl (Fmoc)-based chemistry and Fmoc-L-amino acid building blocks. In the solid-phase synthesis 2-(1H-benzotriazol-1-yl)-1,1,3,3-tetramethyluronium hexafluoro phosphate (HBTU) and *N*,*N*-diisopropylethylamine (DIPEA) in *N*,*N*-dimethylformamide (DMF) were used as coupling and activating reagents, respectively. Piperidine in DMF (20% v/v) was used for Fmoc deprotection at each step. Side chain protected peptides were cleaved from the resins by shaking the resins with a mixture of trifluoroethanol (TFE)/acetic acid/ dichloromethane (DCM) (2:2:6, v/v/v, 15 mL) for 2 h. The resins were filtered off, and the liquid was evaporated to dryness to obtain side-chain protected linear peptide. In general, the cyclization of the peptides was carried out in the presence of a mixture of 1-hydroxy-7-azabenzotriazole (HOAt, 163.3 mg, 1.2 mmol) and *N*,*N*′-diisopropylcarbodiimide (DIC, 187.0 μL, 1.2 mmol) in dry DMF (100 mL) and dry DCM (40 mL) for 24 h. DMF and DCM were evaporated. The side chain deprotection was carried with trifluoroacetic acid (TFA)/thioanisole/anisole/1,2-ethanedithiol

(EDT) (90:5:2:3 v/v/v/v) for 2 h. The crude peptides were precipitated by the addition of cold diethyl ether (Et_2O) and purified by reversed-phase Hitachi HPLC (L-2455) on a Phenomenex Prodigy 10 μm ODS reversed-phase column (2.1 cm × 25 cm) with using a gradient system on a Phenomenex Prodigy 10 μm ODS reversed-phase column (2.1 cm × 25 cm). The peptides were purified by eluting the crude peptides at 10.0 mL/min using a gradient of 0−100% acetonitrile (0.1% TFA) and water (0.1% TFA) over 60 min, and then, they were lyophilized to yield cyclic. The chemical structure of $[WR]_4$ was characterized by nuclear magnetic resonance spectra (^1H NMR) determined on a Varian NMR spectrometer (500 MHz). The chemical structures of all final products were confirmed by a high-resolution Biosystems QStar Elite time-of-flight electrospray mass spectrometer as described previously[7] or MALDI AXIMA Performance TOF/ TOF mass spectrometer (Shimadzu Biotech.). The purity of final products (>95%) was confirmed by analytical HPLC. The analytical HPLC was performed on the Hitachi analytical HPLC system on a C18 Shimadzu Premier 3 μm column (150 cm × 4.6 mm). As representative examples, the synthesis of cyclic $[WE]_4$ and linear $(WR)_4$ is outlined in Scheme S1 in the Supporting Information. A similar procedure was employed for the synthesis of other cyclic peptides by using appropriate resins and protected amino acids as described previously.[7]

Linear $(WR)_4$. H-Trp(Boc)-2-chlorotrityl chloride resin (385 mg, 0.30 mmol, 0.78 mmol/g) was swelled in anhydrous DMF for about 15 min under dry nitrogen. The excess of the solvent was filtered off. The swelling and filtration steps were repeated for 2 more times before the coupling reactions. Fmoc-Arg(Pbf)-OH (584 mg, 0.9

mmol) was coupled to the *N*-terminal of tryptophan trityl resin in the presence of HBTU (340 mg, 0.894 mmol) and DIPEA (313.4 μL, 1.8 mmol) in DMF (6 mL) by mixing for 1.5 h. After the coupling was completed (confirmed by Kaiser test), the reaction solution was filtered off, and the resin was collected by filtration and washed with DMF (7 × 15 mL), followed by *N*-terminal Fmoc deprotection using piperidine in DMF (20% v/v, 10 mL, 2 times, 5 and 10 min). The resin was washed with DMF (7 × 15 mL). The subsequent amino acids, Fmoc-Trp(Boc)-OH (474 mg, 0.9 mmol) and Fmoc-Arg(Pbf)-OH (584 mg, 0.9 mmol), were coupled alternatively three times, respectively, in a similar manner. Fmoc-deprotection at the *N*-terminal was carried out in the presence of piperidine in DMF (20% v/v, 10 mL, 2 × 10 min) to afford the linear peptide on solid phase. The resin was washed with DMF, DCM, DMF-MeOH, and MeOH, respectively (each 2 × 25 mL). The resins were dried in vacuum for 24 h. Freshly prepared cleavage cocktail, reagent R, TFA/thioanisole/EDT/anisole (90:5:3:2 v/v/v/v, 10 mL), was added to the resins. The mixture was shaken at room temperature for 2 h. The resin was collected by filtration and washed with another 2 mL of cleavage cocktail. Combined filtrates were evaporated to a minimum volume under dry nitrogen. The crude peptide was precipitated by the addition of cold diethyl ether (75 mL, Et_2O), lyophilized, and purified by reversed-phase Hitachi HPLC (L-2455) on a Phenomenex Prodigy 10 μm ODS reversed-phase column (2.1 cm × 25 cm) using a gradient system to yield linear $(WR)_4$. MALDI-TOF (*m/z*) [$C_{68}H_{90}N_{24}O_9$]: calcd, 1386.7323; found, 1387.5351 $[M + H]^+$, 1409.5862 $[M + Na]^+$.

Synthesis of Cyclic Peptides. The synthesis of cyclic peptides was carried out according to the previously reported procedure.[9] As a representative example, the synthesis of $[WE]_4$ is described here.

Cyclic $[WE]_4$. The linear peptide was assembled on the H-Trp(Boc)-2-chlorotrityl chloride resin (513 mg, 0.40 mmol, 0.78 mmol/g) in 0.40 mmol scale as described above except with the use of Fmoc-Glu(OtBu)-OH in place of arginine. After the final deprotection of the *N*-terminal Fmoc group by piperidine in DMF (20% v/v), the side chain protected peptide was cleaved from trityl resin in the presence of the cleavage cocktail acetic acid/TFE/DCM (1:2:7 v/v/v, 50 mL) by shaking for 1 h at room temperature to yield the side chain protected linear peptide. The resin was collected by filtration and washed with TFE/DCM (2:8 v/v, 2 × 10 mL). The combined filtrates were evaporated to dryness under reduced pressure. To the residue were added hexane (2 × 25 mL) and DCM (1 × 25 mL) to remove the acetic acid from the mixture and to solidify the crude material as white solid. The crude protected peptide was dried in vacuum overnight. Examining a small portion of the crude showed a main peak by HPLC analysis. Thus, the crude was used directly for the cyclization reaction. The dried crude linear protected peptide was dissolved in DMF/DCM (5:1 v/v, 250 mL). HOAt (223 mg, 1.64 mmol, 4 equiv) and DIC (290 μL, 1.86 mmol, 4.5 equiv) were added to the mixture, and the solution was stirred for 4 h. After completion of the cyclization, as shown by the MALDI-TOF, the solvents were removed under reduced pressure on a rotary evaporator. The crude product was dried overnight in vacuum before the final cleavage. Freshly prepared cleavage cocktail, reagent R,

TFA/thioanisole/EDT/ anisole (90:5:3:2 v/v/v/v, 20 mL) was added to the crude product. The mixture was stirred at room temperature for 2 h. The cleavage cocktail was concentrated to a minimum volume under reduced pressure by a rotary evaporator. After precipitation of crude peptide in cold diethyl ether (75 mL, Et_2O) and centrifugation, the crude peptide was lyophilized and purified by reversed-phase Hitachi HPLC (L-2455) on a Phenomenex Prodigy 10 μm ODS reversed-phase column (2.1 cm × 25 cm) using a gradient system to yield $[WE]_4$. MALDI-TOF (*m/z*) $[C_{64}H_{68}N_{12}O_{16}]$: calcd, 1260.4876; found, 1261.3163 $[M]^+$, 1283.3769 $[M + Na]^+$, 1299.3489 $[M + K]^+$.

Synthesis of AuNPs. The formation of AuNPs was studied in the presence of the peptides. In general, a peptide stock solution (1−2 mM) was mixed with an aqueous solution of $HAuCl_4$ (1−2 mM) at room temperature, and the absorbance was read using SpectraMax M2 spectrophotometer (Molecular Devices, CA). The color of the solution turned red after 4−8 h due to the formation of peptide capped AuNPs. Furthermore, UV−vis spectroscopy study was carried out using $HAuCl_4$ (1 mM) and $[WR]_4$ (100 μM to 2 mM) on a 96-well plate, and the absorbance was read after 4 h incubation using a SpectraMax M2 spectrophotometer to determine the optimized concentration ratio for the reduction. The visible range was chosen because of the characteristic surface plasmon peak of AuNPs appearing around 520−550 nm. All experiments were performed in triplicate.

Fluorescence Study of $[WR]_5$ in the Presence of $HAuCl_4$. A fluorescence study was carried out in the presence of $HAuCl_4$ (1 mM) solution in deionized water and various concentrations of $[WR]_5$ (1 μM to 2 mM) in deionized water. After mixing, the solutions were transferred into a 96-well plate and fluorescence intensity was read using a SpectraMax M2 fluorescence spectrophotometer (Molecular Devices, CA). At lower concentrations of the peptide, the fluorescent intensity remained constant. At peptide concentrations of 250 μM and higher the intensity proportionally increased, demonstrating maximum binding at 1 mM concentration of the peptide. These data were consistent with visible spectroscopy data described above. Thus, 1:1 equivalent ($[WR]_5/HAuCl_4$) and 1 mM optimal concentration were selected for further studies.

Transmission Electron Microscopy (TEM), Selected Area Electron Diffraction (SAED), Energy Dispersive Xray Spectroscopy (TEM-EDS), and Scanning Electron Microscopy (SEM). To prepare a sample for TEM or SEM microscopy, $[WR]_4$-AuNPs (5 μL of 0.5 mM solution in H_2O) solution was spotted onto a carbon-coated copper grid (300 mesh). The liquid drop was then allowed to stay on the carbon film for 10 min. The excess of the solution was removed from the surface of the grid, and the sample was kept overnight to get dried. TEM analyses were conducted in a JEOL transmission electron microscope (Tokyo, Japan) at an accelerating voltage 80 keV as described in the Supporting Information. SEM analyses of $[WR]_5$-AuNPs were conducted in an FEI Nova NanoSEM using the directional backscatter (DBS) electron detector.

Cell Culture. Human ovarian adenocarcinoma cell line (SKOV-3, ATCC No. HTB-77), human leukemia cell line (CCRFCEM, ATCC No. CCL-119), and normal human colon myofibroblast (CCD-18Co, ATCC No. CRL-1459) cell lines were obtained from American Type Culture Collection. The cells were grown on 75 cm^2 cell culture flasks with RPMI-16 medium for CCRF-CEM cells and with EMEM (Eagle's minimum essential medium) for SK-OV-3 and CCD-18Co cells, supplemented with 10% fetal bovine serum (FBS), and 1% penicillin−streptomycin solution (10,000 units of penicillin and 10 mg of streptomycin in 0.9% NaCl) in a humidified atmosphere of 5% CO_2, 95% air at 37 °C. Cytotoxicity Assay of $[WR]_4$ and $[WR]_4$-AuNP Complexes. SK-OV-3 (5,000 cells), CCRF-CEM (40,000 cells), and CCD 18Co (3,000 cells) were seeded in 0.1 mL per well in 96-well plates 24 h prior to the experiment. The old medium (EMEM containing FBS (10%) for SK-OV-3 and CCD-18Co) was replaced by different concentrations of $[WR]_4$ or $[WR]_4$-AuNPs (100 μM) in serum containing medium and incubated for 24 or 72 h at 37 °C in a humidified atmosphere of 5% CO_2. For CCRF-CEM the concentration was calculated after addition of the compounds. Cell viability was then determined by measuring the fluorescence intensity of the formazan product at 490 nm using a SpectraMax M2 microplate spectrophotometer. The percentage of cell survival was calculated as [(OD value of cells treated with the test mixture of compounds) − (OD value of culture medium)]/[(OD value of control cells) − (OD value of culture medium)] × 100%. Other cell-penetrating peptides polyArg CR_7, TAT (YGRKKRRQRRRC) (100 μM), and oligofectamine 2000 (Invitrogen, a cationic lipid formulation) were used as controls.

Cytotoxicity of Dox in the Presence or Absence of $[WR]_4$**-AuNPs.** The cell viability in the presence of Dox and $[WR]_4$-AuNPs and Dox alone against ovarian carcinoma cells SK-OV-3 was determined by MTT assay. All cells were plated overnight in 96-well plates with a density of 5000 cells per well in 0.1 mL of appropriate growth medium at 37 °C. Dox alone (5 μM) or a combination of Dox (5 μM) and $[WR]_4$-AuNPs (25 μM) were incubated with the cells for 8 h. Excess of compounds were removed and washed by fresh media. The cells were kept in an incubator for 24−120 h. The cells without compounds were included in each experiment as controls. After 24 h, 48 h, 72 h, 96 h, and 120 h incubation, 20 μL of MTT was added and incubated for 2 h. The absorbance of the formazan product was measured at 490 nm using microplate reader. The percentage of cell viability was calculated as (OD value of untreated cells - OD value of treated cells)/OD value of untreated cells × 100%.

Loading of Doxorubicin. Aqueous Dox solution (10 μL, 10−3 M) was mixed with aqueous $[WR]_4$-AuNP solution (100 μL, 10−4 M) to obtain 1:1 molar ratio. Dox in H_2O was mixed with water as a negative control. Mixed solution was incubated in a 96-well plate at room temperature for 2 h. Fluorescence of the solution was measured using SpectraMax M2 fluorescence spectrophotometer (Molecular Devices, CA) with excitation at 480 nm and emission at 550 nm.

Fluorescence Microscopy. Fluorescence-Labeled Peptide-AuNP Uptake. The cellular uptake studies of carboxyfluorescein- labeled peptide-AuNP were imaged using a

ZEISS Axioplan 2 light microscope equipped with transmitted light microscopy with a differential-interference contrast method and an Achroplan 40X objective. Human leukemia cells (CCRF-CEM) were taken in 6-well plates (2×10^6 cells/well) in serum-free media. Then F′-[W_5R_4K]-AuNPs (10 μM) was added. After 1 h incubation at 37 °C, the media containing peptide were removed. The cells were digested with 0.25% trypsin/EDTA (0.53 mM) for 5 min to remove any artificial cell surface association and to detect only intracellular uptake. Then the cells were washed twice with PBS, resuspended in media, and were observed under a fluorescent microscope under bright field and FITC channels (480/520 nm).

Differential Interference Contrast Microscopy. The cellular uptake studies of fluorescence labeled beta alanine-3TC (F′-3TC) were imaged using a ZEISS Axioplan 2 light microscope equipped with transmitted light microscopy with a differential interference contrast method and an Achroplan 40X objective. In the case of SK-OV-3 cell line, ovarian carcinoma cells (SKOV- 3) were grown on a coverslip in a 6-well plate. The cells were incubated with F′-3TC (5 μM) and $[WR]_4$-AuNPs (25 μM), F′-3TC alone (5 μM), and $[WR]_4$-AuNPs alone (25 μM, SK-OV-3 and CCRF-CEM cells) in opti-MEM for 1 h at 37 °C. Then the cells were washed with PBS three times, fixed with 3.5% paraformaldehyde followed by washing with PBS three times, and observed under a fluorescence microscope as described above.

Flow Cytometry. Human leukemia cells (CCRF-CEM) were taken in 6-well plates (1 × 107 cells/well) in serum-free medium. Then F′-3TC, F′-GpYEEI, fluorescence-

labeled FTC (F′-FTC), or fluorescence-labeled d4T (F′-d4T) (5 μM) was added to the different wells containing $[WR]_4$ (25 μM) or $[WR]_4$-AuNPs (25 μM) in serum-free medium. $[WR]_4$-AuNPs (25 μM) were used as a control. The plates were incubated for 1 h at 37 °C. DMSO and 5(6)-carboxyfluorescein (FAM) were used as negative controls. After 1 h incubation at 37 °C, the medium containing the peptide was removed. The cells were digested with 0.25% trypsin/EDTA (0.53 mM) for 5 min to remove any artificial surface association and to detect only intracellular uptake. Then the cells were washed twice with PBS. Finally, the cells were resuspended in flow cytometry buffer and analyzed by flow cytometry (FACSCalibur:Becton Dickinson) using FITC channel and CellQuest software. The data presented were based on the mean fluorescence signal for 10,000 cells collected. All assays were performed in triplicate. In the case of Dox, SK-OV-3 cells were seeded in 6-well plates (3 × 105 cells/well) in opti-MEM. The drugs (Dox, F′- 3TC, F′-GpYEEI, F′-FTC, and F′-d4T) (5 μM) were added to the various wells containing $[WR]_4$ (25 μM) or $[WR]_4$-AuNPs (25 μM) in opti-MEM. The plates were incubated for 1 h at 37 °C. A well containing cells and drug alone was used as negative control. After 1 h incubation, the medium was removed. The cells were digested with 0.25% trypsin/EDTA (0.53 mM) for 5 min to remove any artificial surface association and to detect only intracellular uptake. Then the cells were washed twice with PBS. Finally, the cells were resuspended in flow cytometry buffer and analyzed by flow cytometry (FACSCalibur: Becton Dickinson) using FL2 channel and CellQuest software. The data presented are based on the mean fluorescence signal for 10,000 cells collected. All assays were performed in triplicate. Doxorubicin Retention Assay. Human ovarian cancer cells (SK-OV-3)

were seeded in 6-well plates (3 × 105 cells/ well) in EMEM including 10% FBS. The cells were incubated overnight. The medium was removed, and Dox (5 μM) was added to the various wells containing $[WR]_4$ (25 μM) or $[WR]_4$-AuNPs (25 μM) in opti-MEM (reduced serum). The plates were incubated for 1 h at 37 °C. Two wells containing cells and Dox and cells and $[WR]_4$-AuNPs alone were used as negative controls. The medium was removed after 1 h incubation, and complete medium including 10% FBS (EMEM) was added to the cells and incubated for 48 h. The medium was removed after 48 h, and the cells were digested with 0.25% trypsin/0.53 mM EDTA for 5 min to remove any artificial surface association and to detect only intracellular uptake. Then the cells were washed twice with PBS. Finally, the cells were resuspended in flow cytometry buffer and analyzed by flow cytometry (FACSCalibur: Becton Dickinson) using FL2 channel and CellQuest software. The data presented are based on the mean fluorescence signal for 10,000 cells collected. All assays were performed in triplicate.

Confocal Microscopy of $[WR]_4$**-AuNPs and Dox or F′- d4T in Live Cells.** Adherent SK-OV-3 cells were seeded with EMEM media overnight on coverslips in 6-well plates. Then the medium was removed and washed with opti-MEM (reduced serum). The cells were treated with Dox or F′-d4T (5 μM), the mixture of Dox (5 μM) and $[WR]_4$ (25 μM), and the mixture of Dox or d4T (5 μM) and $[WR]_4$-AuNPs (25 μM) in opti-MEM for 1 h at 37 °C. After 1 h incubation, the medium containing the peptide was removed followed by washing with PBS three times, and treated with complete EMEM including 10% of FBS. Then, the coverslips were mounted on a microscope

slide with mounting medium with cell-attached side facing down. Laser scanning confocal microscopy was carried out using Carl Zeiss LSM 510 system. The cells were imaged using rhodamine and phase contrast channels. In the case of drug efflux studies, after a 1 h incubation period, the medium containing drugs was removed and washed with opti-MEM. Then fresh medium with serum was added into the cells. After 24 h, the medium was removed and washed with PBS three times, and then the cells were visualized under confocal microscopy.

RESULTS

Chemistry. *Synthesis of Cyclic Peptides*. Cyclic octapeptides, $[WR]_4$, $[FK]_4$, $[AK]_4$, $[EL]_4$, $[RFEF]_2$, $[EK]_4$, and $[FR]_4$, containing hydrophobic residues (W, F, L) and charged residues (K, R, E) (Figure 1) were synthesized by using 9-fluorenylmethyoxycarbonyl (Fmoc)-based chemistry.[9]

Evaluation of Cyclic Peptides for Generation of CP-AuNPs. The generation of AuNPs was studied in the presence of the synthesized cyclic peptides. The formation of AuNPs using peptides includes two key steps: reduction reaction of Au3+ solution ($HAuCl_4$) and capping the newly nanosized gold particles. The surface plasmon maximum band for generated AuNPs was observed in the range of 520−550 nm by using UV−vis spectroscopy. Among all cyclic peptides, direct dissolution of $[WR]_4$ into an aqueous solution of $AuCl4^-$ led to the formation of AuNPs showing maximum absorption at 539 nm (Figure 1B) and change in the color of the solution to red. The

broad absorption peak at >954 nm represents the surface plasmon resonance (SPR) peak associated with the excitation of surface plasmons in AuNPs. $[WR]_4$-AuNP formation is a controlled process by the balance between reduction, nucleation, and growth steps. In general, anisotropy in the nanoparticle product is caused by the asymmetric adsorption of capping peptides on different crystallographic planes of the nuclei.

Because peptides were also used here as the reducing agent, the reduction kinetics affected both the size and the shape of the nanoparticles. The presence of extremely smaller particles indicated that the growth of the AuNP nanoparticles to spherical forms occurs via an initial nucleation step. Triangular and hexagonal shapes exhibit SPR bands in the near-infrared region 800−1100 nm,[16] suggesting the formation of anisotropic Au particles. Generally, synthesis of AuNPs is a kinetically controlled process where a slow growth environment favors the selective adsorption of the capping molecules on the nuclei and the development of anisotropy.[13] Cyclic peptides were used as the reducing agent. Thus, the reduction process affected both the size and the shape of the nanoparticles. $[WR]_4$-AuNP formation is a controlled process by the balance between reduction, nucleation, and growth steps. The presence of spherical AuNPs is consistent with a single localized surface plasmon resonance (LSPR) in visible spectroscopy around 539 nm. UV−vis spectroscopy demonstrated that the formation of $[WR]_4$-AuNPs from $[WR]_4$ and $HAuCl_4$ was concentration dependent. The main experiment was performed by mixing a fixed concentration of an aqueous solution of $HAuCl_4$ with the same volume of different concentrations of

aqueous solutions of peptides. The intensity of the SPR band was altered as the concentration of peptides changed (Figure S3, Supporting Information).

Because of the capability of $[WR]_4$ in generating AuNPs, other cyclic peptides with similar amino acids, $[WR]_3$ and $[WR]_5$ (Figure 1A), were investigated under similar conditions to determine whether the ring size has any effect in the AuNP formation. UV−vis spectroscopy suggested that all the peptides in the $[WR]_n$ (n = 3−5) series were able to generate AuNPs from Au^{3+}, but $[WR]_5$ and $[WR]_4$ generated higher intensity of SPR band at 537−539 nm (Figure 1B). These data suggest that the number of tryptophan residues has an impact on the SPR band intensity. The intensity of the SPR band of $[WR]_4$-AuNPs is less than that of $[WR]_5$-AuNPs. The intensity difference in the SPR band showed more efficient generation of AuNPs in the presence of $[WR]_5$ compared to $[WR]_4$. Tryptophan works as reducing agent for generating AuNPs. Thus, the number of tryptophan residues is critical in reducing efficiency of the peptide.

$[WMeR]_4$, a cyclic peptide containing *N*-methyl-L-tryptophan showed no color change in the presence of $HAuCl_4$ even after 1 week. These data suggest that the presence of a free amino group in the indole of tryptophan for reduction is critical in generating AuNPs. Furthermore, $[WE]_4$ as a cyclic peptide containing tryptophan and glutamic acid was synthesized to determine whether the presence of arginine residues was required for AuNP formation. This peptide was not capable of generating AuNPs. The presence of glutamic acid was detrimental (Figure 1B), possibly because the negatively charged amino acid has unfavorable electrostatic interaction with negatively charge $AuCl_4^-$, reducing the accessibility of reducing tryptophan residue with Au^{3+}. The $[WR]_n$ series (n =3−5) generated AuNPs with higher intensity in SPR

band at 537−539 nm, possibly because tryptophan acted as a reducing agent and positively charged arginine residues attracted and absorbed $AuCl_4^-$ anions.

$[WR]_4$-AuNPs were characterized using transmission electron microscopy (TEM), selected area electron diffraction (SAED), scanning electron microscopy (SEM), and energy dispersive X-ray spectroscopy (TEM-EDS) (Supporting Information). As described in the Supporting Information, TEM images (Figures S3−S5 in the Supporting Information) exhibited nanosized structures with approximate size of 5−50 nm after 4 days incubation. AuNPs were obtained in a mixture of spherical and triangular shapes (Figures S3−S5 in the Supporting Information). $[WR]_4$-AuNP formation is a controlled process by the balance between reduction, nucleation, and growth steps. In general, anisotropy in nanoparticle product is caused by the asymmetric adsorption of capping peptides on different crystallographic planes of the nuclei. AuNP formation includes nucleation from spherical forms to triangular. Hexagonal shapes, growth, and aggregation were obtained at higher concentration and incubation times. Because peptides were also used here as the reducing agent, the reduction kinetics affected both the size and the shape of the nanoparticles. Some of the $[WR]_4$-AuNPs form aggregates as seen in some parts of the TEM grid perhaps because of hydrophobic interactions between oxidized tryptophan residues in CP-AuNPs. In summary, these data showed, there is a formation of spherical and trigonal platelets and particles with diameters of 5−50 nm. Longer incubation times and higher concentrations led to the hexagonal shapes (100−200 nm) and aggregation of the particles.

Two methods were used for preparing the samples for TEM analysis. The samples (1 mM of peptide and $HAuCl_4$ each) were prepared by depositing a droplet of a mixture of gold and peptide on a carbon-coated Cu support grid of mesh size 300 and drying at room temperature overnight. Alternatively, another method for the preparation of peptide-capped AuNPs was the direct addition of peptide powder to the aqueous Au solution. When the peptide was added to $HAuCl_4$ as a powder, TEM showed a layer of peptide surrounding AuNPs, suggesting the capping of the formed AuNPs by the peptide (Figure S4C in the Supporting Information). Some of the CP-AuNPs form aggregates as seen in some parts of TEM grid perhaps because of hydrophobic interactions between oxidized tryptophan residues in CP-AuNPs. This observation is consistent with earlier investigation with tryptophan-reduced AuNPs that showed a membrane surrounding the synthesized AuNPs.[11]

Cyclic $[WR]_4$ and linear $(WR)_4$, which have the same number and sequence of amino acids, were compared using visible spectroscopy under similar conditions. Both peptides generated AuNPs (Figure 1B), but a weaker SPR band was observed for linear $(WR)_4$ in the region higher than 600 nm. We have previously reported significantly higher cellular uptake of a cyclic peptide compared to that of the corresponding linear peptide.[9] Thus, $[WR]_4$-AuNPs were selected for further cellular studies.

It is important to emphasize that UV−vis and TEM studies were carried out at high concentration peptides (500 μM to 2 mM) and long incubation times that may not correlate with significantly lower concentrations (10−25 μM) of peptides prepared in short incubation time and used for the cell-based and cellular delivery studies. At this

low concentration, only spherical AuNPs were observed for cyclic peptides because of nucleation steps and the number of AuNPs decreased dramatically. Herein, we have provided some details about the characterization of $[WR]_4$-AuNPs under high concentration that is beyond the scope of this work for cellular studies. We focused on using generated cyclic peptide-capped nanoparticles formed under mild conditions as molecular transporters. In all comparative experiments, $[WR]_4$ and $[WR]_4$-AuNPs were used under similar conditions. In general, the stock solution of $[WR]_4$-AuNPs was generated by mixing the same volume of aqueous solution of $[WR]_4$ and $HAuCl_4$. The concentration of $[WR]_4$-AuNPs was based on the concentration of peptide solutions. All the particles are in the form of $[WR]_4$-AuNPs instead of AuNPs + $[WR]_4$. The solution was filtered by using 0.2 μm and diluted with water for further cell-based assays. The inductively coupled plasma mass spectrometry (ICP-MS) data for the $[WR]_4$-AuNPs showed that the conversion of $[WR]_4$ and HAuCl4 to $[WR]_4$-AuNPs was in high yield.

Cytotoxicity of $[WR]_4$**-AuNPs.** $[WR]_4$-AuNPs did not show any significant toxicity in human ovarian adenocarcinoma (SK-OV-3) and human leukemia (CCRF-CEM) cancer cells and normal human colon myofibroblast (CCD-18Co) cells at a concentration of ≤25 μM (Figure S5 in the Supporting Information) while other cell-penetrating peptides polyArg CR_7, TAT (YGRKKRRQRRRC), and oligofectamine 2000 (Invitrogen, a cationic lipid formulation) reduced the viability by 21−55% (Figure S6 in the Supporting Information). After formation of $[WR]_4$-AuNPs at higher

concentrations (>1 mM), the solution was diluted and a noncytotoxic concentration of ≤25 μM was selected for cell-based studies.

Cellular Uptake of CP-AuNPs. A 5(6)-carboxyfluorescein (FAM)-labeled conjugate of $[WR]_5$ as F′-[K-W-R-W-R-W-RW-R-W] (F′-[W_5R_4K]) was synthesized as described previously, where F′ = fluorescein.[9] F′-[W_5R_4K] was reacted with $HAuCl_4$ solution to generate CP-AuNPs. Incubation of F′-[W_5R_4K]-capped AuNPs with CCRF-CEM cells showed significantly higher cellular uptake when compared with that of FAM (Figure 2A). Flow cytometry studies exhibited the cellular uptake of F′-[W_5R_4K]-capped AuNPs to be rapid even after 10 min (Figure 2B). The cellular uptake of cyclic F′-[W_5R_4K]-capped AuNP was approximately 1.5-, 1.7-, and 3.2- fold higher than that of linear F′-(W_5R_4K)-capped AuNP, cyclic F′-[W_5R_4K], and linear F′-(W_5R_4K), respectively, after 1 h incubation (Figure S7 in the Supporting Information).

Further evidence of the accumulation of AuNPs in SK-OV-3 cells was obtained by inductively coupled plasma mass spectrometry (ICP-MS) for quantifying the cellular uptake of gold. $[WR]_4$-AuNPs (25 μM) were incubated with SK-OV-3 cells for 3 and 24 h. The cell lysate was subjected to digestion and analysis by ICP-MS. The data showed the 163 ng (3 h) and 233 ng (24 h) corresponding to 33−47% cellular uptake (Figure S8 in the Supporting Information), suggesting the intracellular accumulation of AuNPs in cells.

The cellular membrane integrity in SK-OV-3 cells was examined in the presence of $[WR]_4$-AuNPs and using propidium iodide and showed no significant modification (Figure S9 in the Supporting Information), ruling out the damage of the

plasma membrane by $[WR]_4$-AuNPs (50 μM) and confirming that the highly efficient transport of the complex was not a result of decreased cellular membrane integrity.

Entrapment of Drugs by CP-AuNPs. To study the potential of $[WR]_4$-AuNPs as molecular transporters, doxorubicin (Dox) were selected as a model drug for loading studies using fluorescence spectroscopy. Incubation of Dox with $[WR]_4$-AuNPs demonstrated significant decreased in emission intensity (Figure S10 in the Supporting Information), possibly due to the self-quenching of bound drug and/or the result of the partitioning and entrapment in the hydrophobic pocket generated by the CP-AuNPs.

Evaluation of CP-AuNPs as Molecular Transporters. Cellular Delivery of Lamivudine. To evaluate $[WR]_4$-AuNPs as DDS, lamivudine ((−)-2′,3′ dideoxy-3′-thiacytidine, 3TC), an anti-HIV and anti-HBV nucleoside reverse transcriptase inhibitor,[17] was selected as a cargo drug. To monitor the molecular transport ability of the CP AuNPs, a carboxyfluorescein derivative of 3TC (F′-3TC, Figure 3A) was synthesized. 18 SK-OV-3 cells were incubated with F′-3TC in the presence or absence of carrier $[WR]_4$-AuNPs for 1 h at 37 °C and then treated with trypsin to remove cell surface-bound drugs. F′-3TC uptake was monitored by fluorescence microscopy, showing significantly higher fluorescence signals in cells treated with F′-3TC-loaded $[WR]_4$-AuNPs (Figure 3A) as compared to those treated with controls F′-3TC alone (Figure S11 in the Supporting Information). Furthermore, nuclear localization of F′-3TC was observed as shown by overlapping of green (FITC) and blue (4′,6 diamidino-2-phenylindole, DAPI) colors as the result of fluorescence of F′-3TC and stained

nuclei, respectively (Figure 3A). In a control experiment, the incubation of $[WR]_4$-AuNPs alone with CCRFCEM cells and SK-OV-3 cells showed no fluorescence or the cellular autofluorescence (Figure S12 in the Supporting Information), suggesting that the enhanced fluorescence signal in the presence of F′-3TC is related to the increased cellular drug uptake.

Cellular uptake of F′-3TC (5 μM) was examined in CCRF-CEM cells using fluorescence activated cell sorter (FACS) in the presence or absence of $[WR]_4$ and $[WR]_4$-AuNPs (25 μM) with trypsin treatment (Figure 3B). FACS showed significantly higher fluorescence signals in cells treated with F′-3TC-loaded $[WR]_4$-AuNPs compared to those treated with F′-3TC alone and F′-3TC-loaded with $[WR]_4$, suggesting that the uptake of F′-3TC is facilitated by $[WR]_4$ AuNPs. F′-3TC-loaded $[WR]_4$-AuNPs exhibited approximately 12- and 15-times higher cellular uptake than that of F′-3TC alone in CCRF-CEM cells (Figure 3B) and SK-OV-3 cells (Figure S13 in the Supporting Information), respectively. F′-3TC-loaded $[WR]_4$-AuNPs (25 μM) exhibited approximately 2.0-, 2.50-, and 7.5-fold higher cellular uptake than F-3TC-loaded linear (WR)4-AuNPs, cyclic $[WR]_5$, and linear $(WR)_5$, respectively (Figure S14 in the Supporting Information). $[WR]_4$-AuNPs showed minimal fluorescence intensity in the absence of the fluorescence-labeled compounds as shown with FACS, suggesting that the increased fluorescence is due to the cellular drug uptake.

Cellular Delivery of Emtricitabine and Stavudine. Furthermore, anti-HIV drugs 2′,3′-dideoxy-5-fluoro-3′-thiacytidine (emtricitabine, FTC) and 2′,3′-didehydro-2′,3′-dideoxythymidine (stavudine, d4T) were attached to 5(6)-carboxyfluorescein (FAM)

through β-alanine to afford fluorescently labeled conjugates F′-FTC and F′-d4T, respectively.[18,19] F′- FTC and F′-d4T showed 12- and 15-times higher cellular uptake in CCRF-CEM cells, respectively, in the presence of $[WR]_4$-AuNPs, while control peptide-capped AuNPs did not show significant fluorescence intensity (Figure 4A). Significantly higher cellular uptake for F′-FTC and F′-d4T in the presence of $[WR]_4$-AuNPs than the parent analogs alone was also observed in SK-OV-3 cells (Figure 4B). Confocal microscopy of F′-d4T in the presence of $[WR]_4$-AuNPs in SK-OV-3 live cells demonstrated significant cellular delivery, while F′-d4T alone showed minimal uptake (Figure 4C).

Cellular Delivery of Doxorubicin. Cellular uptake studies of Dox in the presence of $[WR]_4$ and $[WR]_4$-AuNPs also exhibited slightly higher cellular uptake than Dox after 1 h, but the enhancement was modest since Dox itself has a high inherent cellular uptake (Figure S15 in the Supporting Information). Confocal microscopy was employed in order to study the application of $[WR]_4$-AuNPs on the intracellular retention of Dox in SK-OV-3 cells. Dox is effluxed efficiently within 1 h in ovarian cancer SK-OV-3 cells. The cells were treated with free Dox (5 μM) and Dox-loaded $[WR]_4$-AuNPs alone (Figure 6A). The data showed higher Dox retention in the presence of CP-AuNPs.

These data show that more Dox is retained in cells even after 48 h. Cellular viability studies showed that when Dox is used in the presence of $[WR]_4$-AuNPs, cyctoxicity increases in a time-dependent manner. The cytotoxicity of Dox in the presence of $[WR]_4$-AuNPs is approximately 13% and 15% more than Dox alone after 96 and 120

h, respectively (Figure 6B). Time-dependent cell proliferation data showed that there is a time-dependent inhibitory effect on the cell proliferation of SK-OV-3 cells, suggesting sustained release of Dox. Binding between $[WR]_4$-AuNPs and Dox has a noncovalent nature, and the release will not be in the same nature of the conversion of prodrug to the parent drug. These data indicate that $[WR]_4$-AuNPs may have a prolonged effect possibly due to the sustained intracellular release of Dox. Dox is possibly trapped between AuNPs and the cyclic peptide and is released in a sustained pattern. We have been previously shown the binding affinity of Dox with $[WR]_4$ using isothermal calorimetry.[9] Dox (free or encapsulated with $[WR]_4$) was placed inside a dialysis membrane (molecular weight cut off 250) immersed in PBS (pH 7.4) or HCl (0.02 N). The dialysis membrane was sampled at predetermined time increments, and the amount of Dox was determined by UV. Monitoring of in vitro drug release revealed sustained release for over 10 days. These data indicate that [WR]4 may have a prolonged effect possibly due to the sustained intracellular release of Dox.

Thus, acute cytotoxicity is not observed immediately even when higher concentration of Dox is retained intracellularly. $[WR]_4$-AuNPs are composed of charged (R) and hydrophobic (W) residues and are able to noncovalently entrap or bind therapeutic molecules for delivery. The peptide portion of the $[WR]_4$-AuNPs is responsible for binding with the drug.

DISCUSSION

AuNPs are usually synthesized under sometimes harsh conditions in the presence of Au(III) ions and inorganic (e.g., sodium borohydride, hydrazine) or

organic (e.g., sodium citrate, ascorbic acid) reducing agents to control the size and shape of particles. It has been previously reported that AuNPs generated by peptides exhibited less toxicity compared to chemical methods.[13] As described above, $[WR]_4$-AuNPs did not show any significant toxicity in SK-OV-3 and CCRF-CEM cancer cells, and normal human colon myofibroblast (CCD-18Co) cells at a concentration of ≤25 μM. Formed AuNPs are usually stabilized by peptides, proteins, DNA, surfactants, or carbohydrates.[20−23] Traces of remaining reagents are unsuitable for use in biomedical and cellular uptake studies.[24−26] CPAuNPs were generated under mild reaction conditions using cyclic peptides as reducing and capping agents. The formation of capped structures was confirmed by TEM showing tryptophan-reduced AuNPs with a membrane surrounding the synthesized nanostructures.

$[WR]_4$-AuNPs did not exhibit any significant toxicity against normal human colon myofibroblast (CCD-18Co) cells, human ovarian adenocarcinoma (SK-OV-3), and human leukemia (CCRF-CEM) cancer cells at a concentration of of ≤25 μM. Thus, the $[WR]_n$ series (n = 3−5) could provide alternative potential noncytotoxic simultaneous reducing and capping reagents.

Flow cytometry studies showed the cellular uptake of the corresponding fluorescence-labeled CP-AuNPs to be rapid even after 10 min in CCRF-CEM cells. Inductively coupled plasma mass spectrometry further confirmed the intracellular presence of gold after incubation of $[WR]_4$-AuNPs in SK-OV-3 cells. The mechanism of cellular uptake is under investigation, but it is presumably through cellular uptake of AuNPs and the interactions of positively charged and hydrophobic residues of the cell-penetrating peptide[9] with the corresponding negatively charged and hydrophobic

moieties in the phospholipid bilayer. Both the peptide and AuNPs have cell-penetrating properties. We previously reported that the cyclic peptides can act as nuclear targeting molecular transporters.[9] Cyclic peptide-capped AuNPs presented a new complex system including both AuNPs and the cyclic peptide.

$[WR]_4$-capped AuNPs showed significantly higher cellular delivery of antiviral drugs versus that of parent drug alone. Flow cytometry studies showed that the cellular uptake of fluorescence-labeled 3TC, FTC, and d4T was significantly enhanced in CCRF-CEM and SK-OV-3 cells in the presence of $[WR]_4$-AuNPs. F′-3TC-loaded $[WR]_4$-AuNPs exhibited approximately 12- and 15-times higher cellular uptake than that of F′-3TC alone in CCRF-CEM cells and SK-OV-3 cells, respectively. Similarly F′-FTC and F′-d4T showed 12- and 15-times higher cellular uptake in CCRF-CEM cells, respectively, in the presence of $[WR]_4$-AuNPs. Thus, biologically active compounds can be loaded onto AuNPs through noncovalent interactions without any structural modification to the drug for release. The presence of tryptophan makes an appropriate hydrophobic cavity for loading different drugs. The interactions between drugs and $[WR]_4$ and AuNPs containing hydrophobic pockets have been previously reported.[9,27,28]

Confocal microscopy revealed that the presence of the $[WR]_4$-AuNPs enhances the retention of Dox in SK-OV-3 cells after 24 h. Our previous report showed that there are intermolecular interactions between the cyclic peptide and drugs, including Dox as shown by isothermal titration calorimetry.[9] The peptide portion of the $[WR]_4$-AuNPs is responsible for binding with the drug. UV titration analysis of $[WR]_4$ and Dox also confirmed the complex formation. The cyclic peptide forms a complex with

Dox possibly through intermolecular noncovalent interactions. We assume that there is interaction through entrapment of the drug in the hydrophobic pocket part of this complex due to the available tryptophan.

CONCLUSIONS

In summary, CP-AuNPs containing tryptophan and arginine residues were generated under a mild reaction condition without any surface functionalization of gold. To the best of our knowledge this is the first study for designing AuNPs using cyclic peptides as both reducing and capping agents. CP-AuNPs offered several advantages including low cytotoxicity, hydrophobic drug entrapment through noncovalent interactions, and improving cellular uptake by both cell-penetrating cyclic peptide and AuNPs. CP-AuNPs were able to act as molecular transporters of fluorescence-labeled lamivudine, emtricitabine, and stavudine intracellularly and to improve the Dox intracellular retention. High cellular internalization of the labeled drugs and retention of Dox by $[WR]_4$-AuNP suggest the potential application of CP-AuNPs as molecular transporters and for generation of noncovalent prodrugs. The peptide nature of CP-AuNPs should make this system highly amenable to targeting strategies.

ASSOCIATED CONTENT

Supporting Information

Synthesis of peptides, nanoparticle characterization, additional supporting data, and Figures for cytotoxicity and control cellular uptake studies. This material is available free of charge via the Internet at http://pubs.acs.org.

Notes

The authors declare no competing financial interest.

ACKNOWLEDGMENTS

We acknowledge the financial support from the American Cancer Society, Grant No. RSG-07-290-01-CDD, and from the US National Science Foundation, Grant No. CHE 0748555.

REFERENCES

(1) Sepúlveda, B.; Angelomé, P. C.; Lechuga, L. M.; Liz-Marzán, L. M. LSPR-based nanobiosensors. Nano Today 2009, 4, 244−251.

(2) Hu, M.; Chen, J.; Zhi-Yuan, L.; Leslie, A.; Hartland, G. V.; Li, X.; Marquez, M.; Xia, Y. Gold nanostructures: engineering their plasmonic properties for biomedical applications. Chem. Soc. Rev. 2006, 35, 1084−1094.

(3) Ghosha, P.; Hana, G.; Dea, M.; Kima, C. K.; Rotello, V. M. Gold nanoparticles in delivery applications. Adv. Drug Delivery Rev. 2008, 60, 1307−1315.

(4) Huang, X. H.; Jain, P. K.; El-Sayed, I. H.; El-Sayed, M. A. Gold nanoparticles: interesting optical properties and recent applications in cancer diagnostics and therapy. Nanomedicine 2007, 2, 681−693.

(5) Jain, P. K.; El-Sayed, I. H.; El-Sayed, M. A. Au nanoparticles target cancer. Nano Today 2007, 2, 18−29.

(6) Dykman, L.; Khlebtsov, N. Gold nanoparticles in biomedical applications: recent advances and perspectives. Chem. Soc. Rev. 2012, 41, 2256−2282.

(7) De, M.; Ghosh, P. S.; Rotello, V. M. Applications of nanoparticles in biology. Adv. Mater. 2008, 20, 4225−4241.

(8) Lévy, R. Peptide-capped gold nanoparticles: towards artificial proteins. ChemBioChem 2006, 7, 1141−1145.

(9) Mandal, D.; Nasrolahi Shirazi, A.; Parang, K. Cell-penetrating homochiral cyclic peptides as nuclear-targeting molecular transporters. Angew. Chem., Int. Ed. 2011, 50, 9633−9637.

(10) Satyabrata, S.; Mandal, T. K. Tryptophan-based peptides to synthesize gold and silver nanoparticles: a mechanistic and kinetic study. Chem. Eur. J. 2007, 13, 3160−3168.

(11) Selvakannan, P. R.; Mandal, S.; Phadtare, S.; Gole, A.; Pasricha, R.; Adyanthaya, S. D.; Sastry, M. Water-dispersible tryptophanprotected gold nanoparticles prepared by the spontaneous reduction of aqueous chloroaurate ions by the amino acid. J. Colloid Interface Sci. 2004, 269, 97−102.

(12) Bhargava, S. K.; Booth, J. M.; Agrawal, S.; Coloe, P.; Kar, G. Gold nanoparticle formation during bromoaurate reduction by amino acids. Langmuir 2005, 21, 5949−5956.

(13) Tan, Y. N.; Lee, J. Y.; Wang, D. I. C. Uncovering the design rules for peptide synthesis of metal nanoparticles. J. Am. Chem. Soc. 2010, 132, 5677−5686.

(14) Ye, G.; Nam, N. H.; Saleh, A.; Kumar, A.; Sun, G.; Shenoy, D. B.; Amiji, M. M.; Lin, X.; Sun, G.; Parang, K. Synthesis and evaluation of tripodal peptide analogs for cellular delivery of phosphopeptides. J. Med. Chem. 2007, 50, 3604−3617.

(15) Ye, G.; Gupta, A.; DeLuca, R.; Parang, K.; Bothun, G. D. Bilayer disruption and liposome restructuring by a homologous series of small Arg-rich synthetic peptides. Colloids Surf., B 2010, 76, 76−81.

(16) Katsara, M.; Tselios, T.; Deraos, S.; Deraos, G.; Matsoukas, M. T.; Lazoura, E.; Matsoukas, J.; Apostolopoulos, V. Round and round we go: cyclic peptides in disease. Curr. Med. Chem. 2006, 13, 2221−2232.

(17) Massard, J.; Benhamou, Y. Treatment of chronic hepatitis B in HIV co-infected patients. Gastroenterol. Clin. Biol. 2008, 32, 20−24.

(18) Agarwal, H. K.; Chhikara, B. S.; Hanley, M. J.; Ye, G.; Doncel, G. F.; Parang, K. Synthesis and biological evaluation of fatty acyl ester derivatives of (−)-2′,3′-dideoxy-3′-thiacytidine. J. Med. Chem. 2012, 55, 4861−4871.

(19) Agarwal, H. K.; Loethan, K.; Mandal, D.; Doncel, G. F.; Parang, K. Synthesis and biological evaluation of fatty acyl ester derivatives of 2′,3′-didehydro-2′,3′-dideoxythymidine. Bioorg. Med. Chem. Lett. 2011, 21, 1917−1921.

(20) Alivisatos, A. P.; Johnsson, K. P.; Peng, X. G.; Wilson, T. E.; Loweth, C. J.; Bruchez, M. P. Organization of 'nanocrystal molecules' using DNA. Nature 1996, 382, 609−611.

(21) Mirkin, C. A.; Letsinger, R. L.; Mucic, R. C.; Storhoff, J. J. A DNA-based method for rationally assembling nanoparticles into macroscopic materials. Nature 1996, 382, 607−609.

(22) Levy, R.; Thanh, N. T. K.; Doty, R. C.; Hussain, I.; Nichols, R. J.; Schiffrin, D. J. Rational and combinatorial design of peptide capping ligands for gold nanoparticles. J. Am. Chem. Soc. 2004, 126, 10076−10084.

(23) Skidmore, M. A.; Patey, S. J.; Thanh, N. T. K.; Fernig, D. G.; Turnbull, J. E.; Yates, E. A. Attachment of glycosaminoglycan oligosaccharides to thiol-derivatised gold surfaces. Chem. Commun. 2004, 23, 2700−2701.

(24) Wang, S.; Lu, W.; Tovmachenko, O.; Rai, U. S.; Yu, H.; Ray, P. C. Challenge in understanding size and shape dependent toxicity of gold nanomaterials in human skin keratinocytes. Chem. Phys. Lett. 2008, 463, 145−149.

(25) Alkilany, A. M.; Nagaria, P.; Hexel, C. R.; Shaw, T. J.; Murphy, C. J. Cellular uptake and cytotoxicity of gold nanorods: molecular origin of cytotoxicity and surface effects. Small 2009, 5, 701−708.

(26) Murphy, C. J.; Gole, A. M.; Stone, J. W.; Sisco, P. N.; Alkilany, A. M.; Goldsmith, E. C.; Baxter, S. C. Gold nanoparticles in biology: beyond toxicity to cellular imaging. Acc. Chem. Res. 2008, 41, 1721−1730.

(27) Kim, C. K.; Ghosh, P.; Pagliuca, C.; Zhu, Z. J.; Menichetti, S.; Rotello, V. M. Entrapment of hydrophobic drugs in nanoparticles monolayers with efficient release into cancer cells. J. Am. Chem. Soc. 2009, 131, 1360−1361.

(28) Duncan, B.; Kim, C.; Rotello, V. M. Gold nanoparticle platforms as drug and biomacromolecule delivery systems. J. Controlled Release 2010, 148, 122−127.

Figure Legends:

Figure 1: (A) Chemical structures of synthesized peptides. A = alanine, E = glutamic acid, F = phenylalanine, K = lysine, L = leucine, R = arginine, W = tryptophan. (B) UV– Vis absorption spectra of HAuCl4 and/or AuNP formation in the presence of cyclic peptides (1 mM), $[WR]_n$ (n = 3−5), linear $(WR)_4$, and $[WE]_4$ (1 mM)

Figure 2: (A) Cellular uptake of F′-$[W_5R_4K]$-capped AuNP compared with FAM (10 μM) in CCRF-CEM cells. (B) Rapid uptake of F′-$[W_5R_4K]$-AuNPs versus FAM (10 μM) in CCRF-CEM cells (FACS) (mean ± SD)

Figure 3: (A) Differential interference contrast microscopy of fluorescence-labeled lamivudine (F′-3TC) (5 μM) in the presence of $[WR]_4$-AuNP (25 μM) in SK-OV-3 cells. (B) Flow cytometry studies for F′-3TC (5 μM) in the presence or absence of $[WR]_4$ or $[WR]_4$-AuNPs (25 μM) in CCRF-CEM cells (mean ± SD, n = 3)

Figure 4: Flow cytometry studies in (A) CCRF-CEM and (B) SK-OV-3 cells for fluorescence-labeled FTC and fluorescence-labeled d4T alone (5 μM) and in the presence or absence of $[WR]_4$ (25 μM) or $[WR]_4$-AuNPs (25 μM) after 1 h (mean ± SD). (C) Confocal microscopy of F′-d4T (5 μM) uptake in the presence of $[WR]_4$-AuNPs (25 μM) in SK-OV-3 cells (live cells)

Figure 5: Confocal microscopy images of Dox (5 μM) and $[WR]_4$-AuNPs (25 μM) uptake in SK-OV-3 cells. SK-OV-3 cells treated with drug for 1 h. The compound was removed, and the cells were incubated with complete medium for 24 h. Red represents fluorescence of Dox

Figure 6: (A) Flow cytometry studies in SK-OV-3 cells for Dox alone (5 μM) and in the presence of $[WR]_4$ (25 μM) or $[WR]_4$-AuNPs (25 μM) for 1 h (mean ± SD). The compound was removed, and the cells were incubated with complete medium for 48 h. (B) Cytotoxicity assay of Dox (5 μM) in the absence and presence of $[WR]_4$-AuNP (25 μM) in SK-OV-3 cells (24−120 h) (mean ± SD)

Figure 1

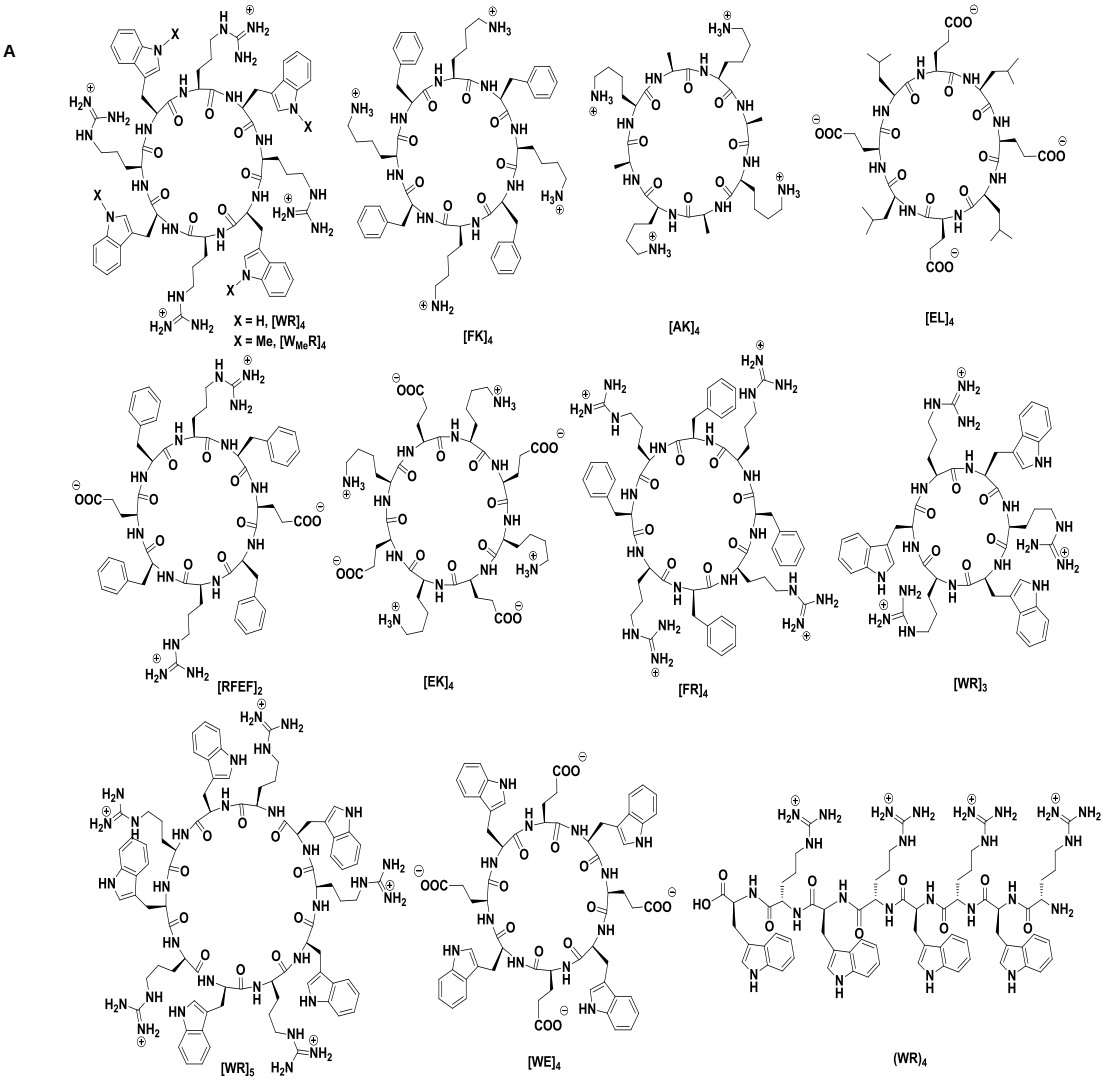
A
X = H, [WR]4
X = Me, [WMeR]4
[FK]4
[AK]4
[EL]4
[RFEF]2
[EK]4
[FR]4
[WR]3
[WR]5
[WE]4
(WR)4

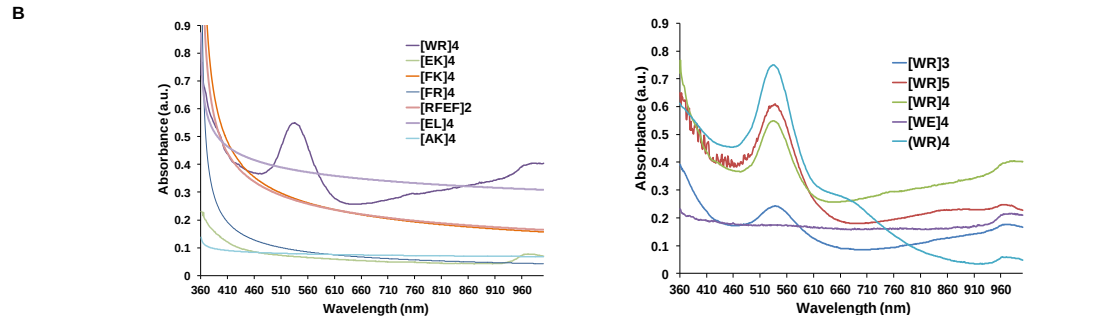
B
Absorbance (a.u.)
Wavelength (nm)
[WR]4
[EK]4
[FK]4
[FR]4
[RFEF]2
[EL]4
[AK]4
[WR]3
[WR]5
[WR]4
[WE]4
(WR)4

Figure 2

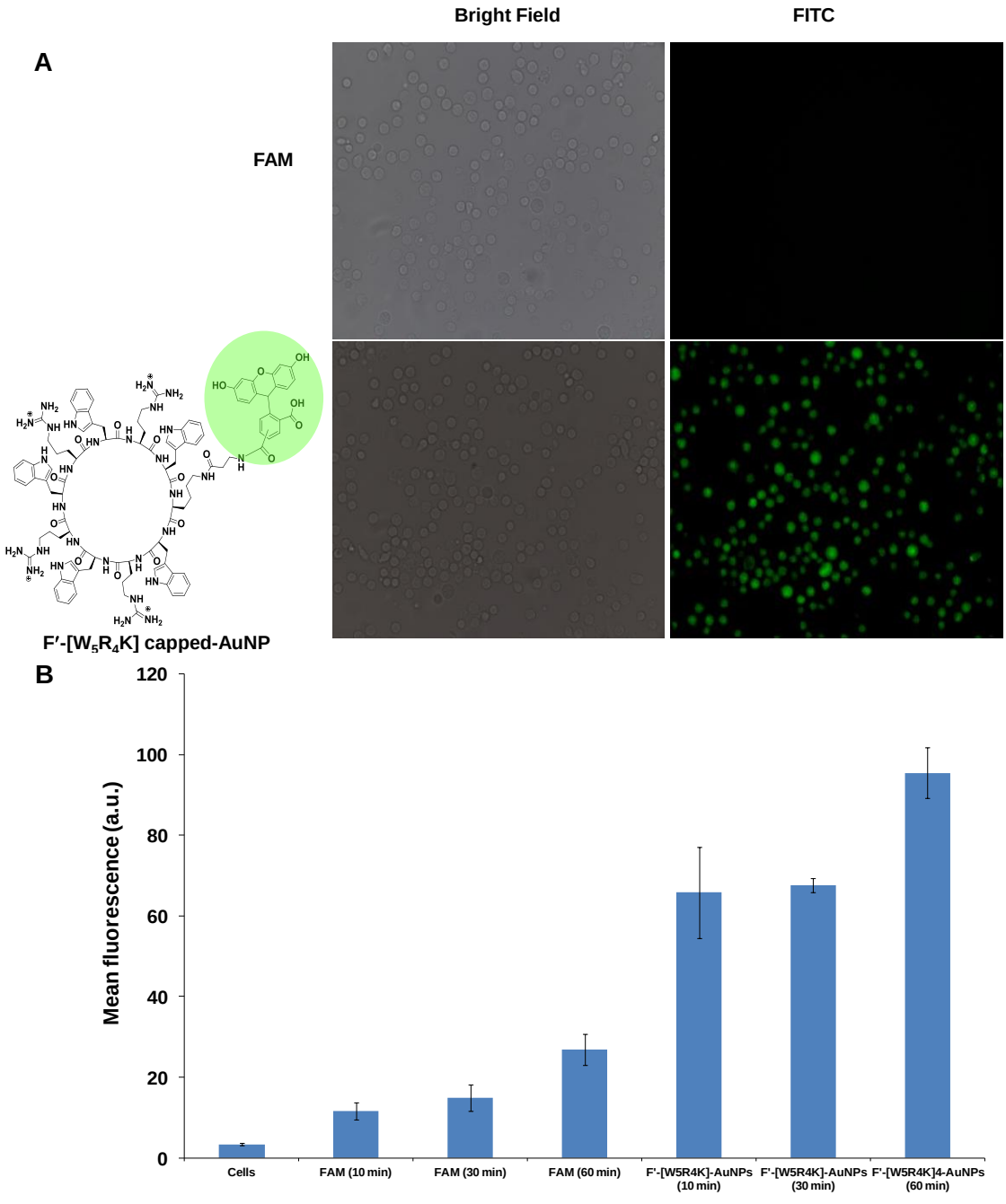
A
Bright Field
FITC
FAM
F′-[W5R4K] capped-AuNP
B
Mean fluorescence (a.u.)
120
100
80
60
40
20
0
Cells
FAM (10 min)
FAM (30 min)
FAM (60 min)
F'-[W5R4K]-AuNPs (10 min)
F'-[W5R4K]-AuNPs (30 min)
F'-[W5R4K]4-AuNPs (60 min)

Figure 3

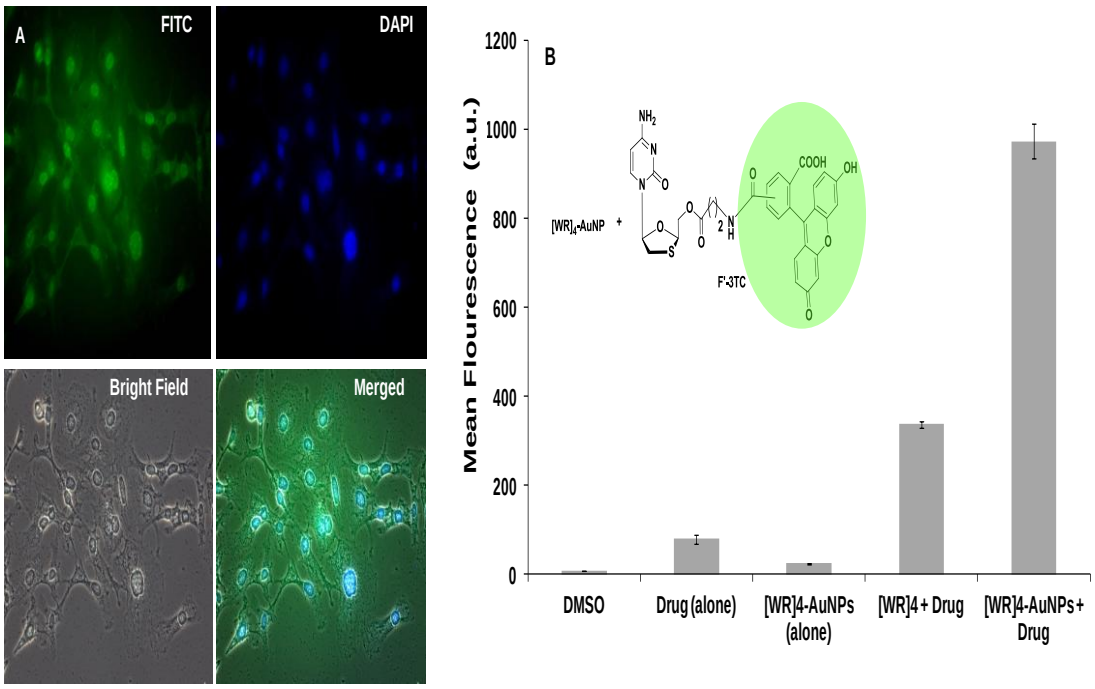
A
FITC
DAPI
Bright Field
Merged
B
Mean Flourescence (a.u.)
1200
1000
800
600
400
200
0
[WR]4-AuNP
F'-3TC
COOH
OH
DMSO
Drug (alone)
[WR]4-AuNPs (alone)
[WR]4 + Drug
[WR]4-AuNPs + Drug

Figure 4

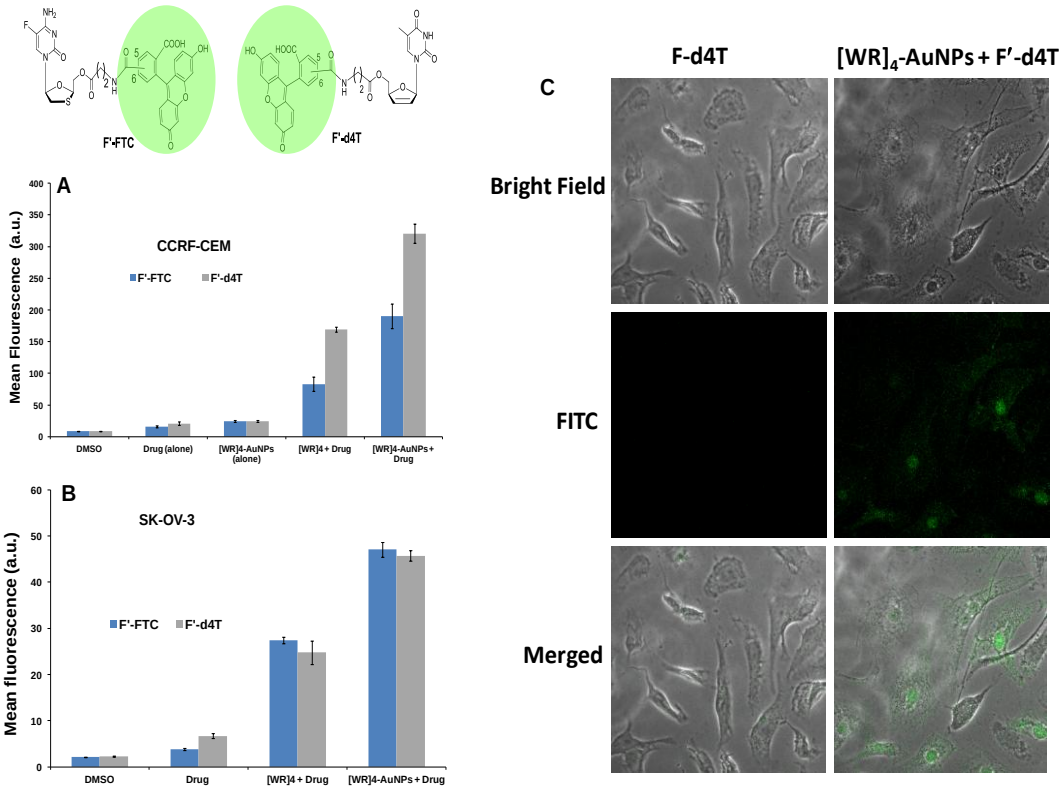
F'-FTC
F'-d4T
A
CCRF-CEM
F'-FTC
F'-d4T
Mean Flourescence (a.u.)
DMSO
Drug (alone)
[WR]4-AuNPs (alone)
[WR]4 + Drug
[WR]4-AuNPs + Drug
B
SK-OV-3
F'-FTC
F'-d4T
Mean fluorescence (a.u.)
DMSO
Drug
[WR]4 + Drug
[WR]4-AuNPs + Drug
C
F-d4T
[WR]4-AuNPs + F'-d4T
Bright Field
FITC
Merged

Figure 5

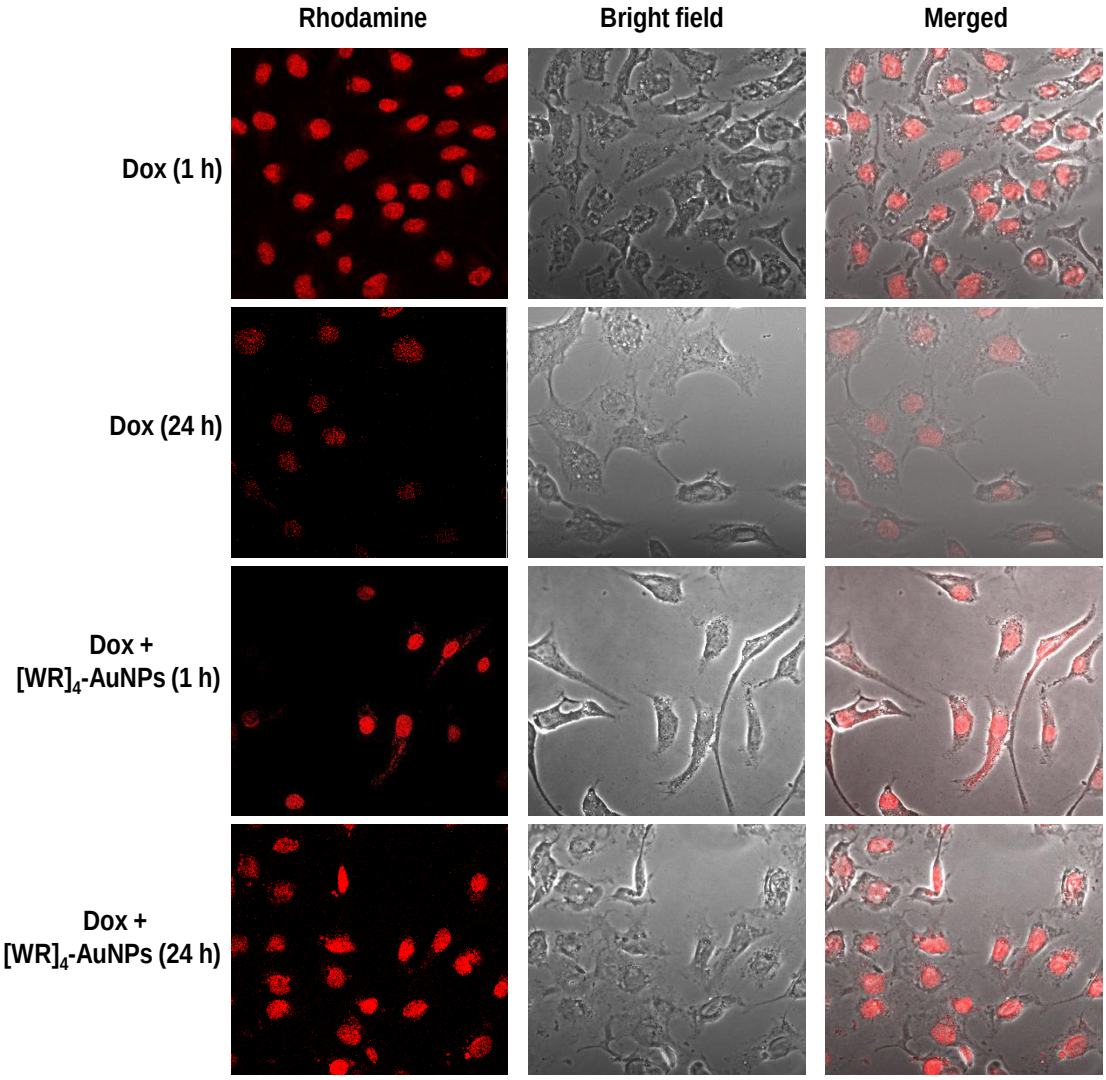
Rhodamine
Bright field
Merged
Dox (1 h)
Dox (24 h)
Dox + [WR]4-AuNPs (1 h)
Dox + [WR]4-AuNPs (24 h)

Figure 6

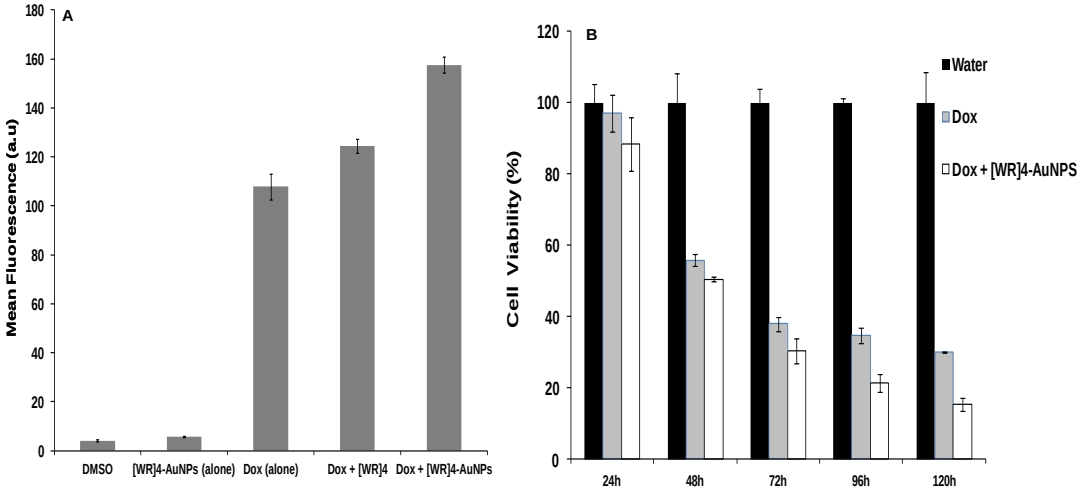
A
Mean Fluorescence (a.u)
180
160
140
120
100
80
60
40
20
0
DMSO
[WR]4-AuNPs (alone)
Dox (alone)
Dox + [WR]4
Dox + [WR]4-AuNPs
B
Cell Viability (%)
120
100
80
60
40
20
0
24h
48h
72h
96h
120h
Water
Dox
Dox + [WR]4-AuNPS

Manuscript IV

Published in "***Molecular Pharmaceutics***", ***DOI:*** *10.1021/mp400199e*

Surface decorated gold nanoparticles by linear and cyclic peptides as molecular transporters

Amir Nasrolahi Shirazi, Rakesh Kumar Tiwari, Donghoon Oh, Brian Sullivan, Kellen McCaffrey, Dindyal Mandal, and Keykavous Parang*

Department of Biomedical and Pharmaceutical Sciences, College of Pharmacy, University of Rhode Island, Kingston, Rhode Island 02881, United States

Corresponding Author

*7 Greenhouse Road, Department of Biomedical and Pharmaceutical Sciences, College of Pharmacy, University of Rhode Island, Kingston, RI 02881, USA. Tel: +1-401-874-4471. Fax: +1-401-874-5787. E-mail: kparang@uri.edu.

ABSTRACT

Gold nanoparticles (AuNPs) were synthesized *in situ* in a green and rapid method from the reaction of reducing linear and cyclic peptides containing tryptophan and lysine residues, $(KW)_5$ and cyclic $[KW]_5$, with an aqueous solution of $HAuCl_4$ and were evaluated as cellular nanodrug delivery systems. The cyclic or linear nature of the peptide was found to determine the morphology and size of the formed peptide-AuNPs and their *in vitro* molecular transporting efficiency. While cyclic $[KW]_5$-AuNPs formed sponge-like agglomerates, linear $(KW)_5$-AuNPs demonstrated ball-shaped structures. A comparative flow cytometry study showed that the cellular uptake of fluorescence-labeled anti-HIV drugs (emtricitabine (FTC) and lamivudine (3TC)) in human Leukemia (CCRF-CEM) cells, and a negatively charged cell-impermeable phosphopeptide (GpYEEI) in human ovarian adecarcinoma (SK-OV-3) cells was significantly higher in the presence of cyclic $[KW]_5$-AuNPs than that of linear $(KW)_5$-AuNPs, parent cyclic $[KW]_5$, and linear $(KW)_5$ peptides. For example, the cellular uptake of F′-GpYEEI was enhanced 12.8-fold by c$[KW]_5$-AuNPs. Confocal microscopy revealed the localization of fluorescence-labeled-3TC in the presence of c$[KW]_5$-AuNPs mostly in nucleus in SK-OV-3 cells after 1 h. On the other hand, l$(KW)_5$-AuNPs delivered fluorescence-labeled-3TC in cytoplasm. These data suggest that non-cell penetrating peptides can be converted to efficient molecular transporters through peptide-capped AuNPs formation.

Keywords: cellular uptake, cyclic peptide, drug delivery, gold nanoparticles, lysine, nuclear targeting, tryptophan

INTRODUCTION

The cellular delivery of hydrophobic and poorly water-soluble compounds to enhance the efficacy using Drug delivery systems (DDS) is a subject of major interest.[1] Among all delivery systems, nuclear targeting nanodrug delivery systems (nano-DDS) have attracted significant attention. Common approaches in gene therapy involve using DNA as a pharmaceutical agent to replace or correct a mutated gene.[2] Moreover, the nucleus is a target for a diverse number of anticancer and antiviral drugs,[3] due to the presence of the genetic information and transcription systems.

The nuclear membrane (envelope) is composed of a double lipid bilayer that works as a physical barrier between cell nucleus content and the cytoplasm. The nuclear membrane contains many nuclear pore complexes (NPCs) that facilitate and regulate the exchange of proteins and RNA between the cell nucleus and the cytoplasm. Depending on the cell line, NPCs have different sizes from 20 to 60 nm.[4] Although NPCs operate as available passages for all exchange between the nucleoplasm and cytoplasm, they can be exploited as pathways for nanoparticle delivery.[5,6] Therefore, the delivery of the therapeutic agents to the nucleus by using nano-DDS offers several advantages compared to other systems.

The application of prodrug strategy among researchers is now well established. Prodrugs are chemically modified analogs of the active metabolite that can improve pharmacokinetics and pharmacodynamic (PK/PD) properties of the active drug. However, intracellular chemical transformation needed to be occurred in the presence of different enzymes to convert prodrugs to their corresponding pharmacologically potent compounds in *in vivo* systems. Prodrug approach offers several advantageous,

such as enhancing water solubility, improved chemical stability, decreased toxicity, and insufficient brain penetration.[7]

Gold nanoparticles (AuNPs) have received an increased attention due to their unique potential use as nano-DDS.[8] Most of the known AuNPs as nano-DDS lead to the intracellular localization of nanoparticles mainly in the cytoplasm.[9] However, appropriate functionalization of AuNPs with other compounds can be used for their optimization as nano-DDS for a specific application.

Peptide-mediated drug delivery has been widely used for a broad range of cargo molecules including drugs, siRNA, and genes due to their versatility and the presence of a wide range of amino acids.[10] Thus, the peptides have the potential to be used for decoration of the surface of metal nanoparticles. Recently, AuNPs functionalized by peptides have been used as biocompatible systems in drug delivery.[11] For example, AuNPs capped by linear Tat was reported to be able to get internalized into the cytoplasm of 3T3 and HepG2 cells.[11c]

After the localization of DDS in the destination, it should release the cargo. Thus, drug loading and release issues are critical for optimized DDS function. Two major strategies for drug loading include covalent and non-covalent binding between AuNPs and drugs.[12] Non-covalent loading offers two main advantages, including ease of the drug loading and facilitating drug release in intact form over covalent loading.[13] Thus, the entrapment of unmodified drugs into functionalized AuNPs through non-covalent interaction is introduced as one of the prodrug strategies for the delivery of a broad range of drugs. Employing appropriate surface functionalization provides a hydrophobic pocket for the loading of drugs.

We have previously reported cyclic peptides containing alternative arginine (R) and tryptophan (W) as efficient molecular transporters that showed improving the cellular uptake of different cargos.[14] Subsequently, it was found that a physical mixture of the cell-penetrating cyclic peptide $[WR]_4$ and $HAuCl_4$ led to the formation of peptide-capped gold nanoparticles (P-AuNPs) and enhanced the cellular uptake of drugs significantly.[15] It remains to be determined whether non-cell penetrating peptides can be converted to a nuclear targeting DDS through generation of peptide-AuNPs.

Herein, we report the generation of a novel nuclear-targeting nano-DDS containing AuNPs and a non-cell penetrating peptide containing alternative lysine and tryptophan residues. The presence of these amino acids was found to be appropriate to generate *in situ* biocompatible AuNPs. To the best of our knowledge, this is the first report of converting a non-cell penetrating peptide to an efficient nuclear targeting nano-DDS through cyclic peptide-capped AuNPs formation.

EXPERIMENTAL SECTION

General

All reactions were carried out in Bio-Rad polypropylene columns by shaking and mixing using either a Glass-Col small tube rotator or PS3 automated peptide synthesizer in dry conditions at room temperature unless otherwise stated. In general, all cyclic and linear peptides were synthesized by the solid-phase synthesis strategy employing *N*-(9-fluorenyl)methoxycarbonyl (Fmoc)-based chemistry and Fmoc-L-amino acid building blocks. 2-(1*H*–Benzotriazole-1-yl)-1,1,3,3-tetramethyluronium

hexafluorophosphate (HBTU) and *N*,*N*-diisopropylethylamine (DIPEA) in *N*,*N*-dimethylformamide (DMF) were used as coupling and activating reagents, respectively. 2-Chlorotrityl chloride resin, Fmoc-amino acid trityl chloride resins, coupling reagents, and Fmoc-amino acid building blocks were purchased from Chempep (Miami, FL). Other chemicals and reagents were purchased from Sigma-Aldrich Chemical Co. (Milwaukee, WI). Fmoc deprotection at each step was carried out using piperidine in DMF (20%). Side chain protected peptides were cleaved from the resins by shaking the resins with a mixture of trifluoroethanol (TFE)/acetic acid/dichloromethane (DCM) (1:2:7 v/v/v, 15 ml) for 2 h. The resins were filtered off, and the liquid was evaporated to dryness to get side-chain protected linear peptide. Generally, the cyclization of the peptides was carried out in the presence of a mixture of 1-hydroxy-7-azabenzotriazole (HOAt) and *N*,*N'*-diisopropylcarbodiimide (DIC) in dry DMF and dry dichloromethane (DCM) for 24 h. DMF and DCM were evaporated. The side chain deprotection was carried with TFA/thioanisole/anisole/1,2-ethanedithiol (EDT) (90:5:2:3 v/v/v/v) for 2 h. The crude peptides were precipitated by the addition of cold diethyl ether (Et_2O) and were purified by using a reversed-phase Hitachi HPLC (L-2455) on a Phenomenex Prodigy 10 μm ODS reversed-phase column (2.1 cm × 25 cm) and a gradient system. The peptides were separated by eluting the crude peptides at 10.0 mL/min using a gradient of 0-100% acetonitrile (0.1% TFA) and water (0.1% TFA) over 60 min, and then were lyophilized to yield cyclic peptides (Figure 1). The purity of final products (≥95%) was confirmed by analytical HPLC. The analytical HPLC was performed on a Hitachi analytical HPLC system using a C18 Shimadzu Premier 3 μm column (150 cm × 4.6 mm) and a

gradient system (water/CH_3CN), and a flow rate of 1 mL/min with detection at 220 nm. The chemical structures of final products were confirmed by high-resolution MALDI AXIMA performance TOF/TOF mass spectrometer (Shimadzu Biotech) or a high-resolution Biosystems QStar Elite time-of-flight electrospray mass spectrometer**.** As a representative example, the synthesis of linear $(KW)_4$ is outlined here.

Synthesis of Linear $(KW)_4$ and **Linear $(KW)_5$.** Fmoc-Trp(Boc)-Wang resin (555 mg, 0.54 mmol/g, 0.3 mmol) was swelled in anhydrous DMF for about 15 min under dry nitrogen. The excess of the solvent was filtered off. The swelling and filtration steps were repeated for 2 more times before the coupling reactions. Fmoc-Lys(Boc)-OH (325 mg, 0.75 mmol) was coupled to the *N*-terminal of tryptophan Wang resin in the presence of HBTU (285 mg, 0.75 mmol) and DIPEA (262 μL, 1.50 mmol) in DMF (7 mL) by mixing for 1.5 h. After the coupling was completed, the reaction solution was filtered off, and the resin was collected by filtration and washed with DMF (7 × 15 mL), followed by *N*-terminal Fmoc deprotection using piperidine in DMF (20% v/v, 10 mL, 2 times, 5 and 10 min). The resin was washed with DMF (7 × 15 mL). The subsequent amino acids, Fmoc-Trp(Boc)-OH (395 mg, 0.75 mmol) and Fmoc-Lys(Boc)-OH (325 mg, 0.75 mmol), were coupled alternatively three times, respectively, in a similar manner (Scheme S2). Fmoc-deprotection at the *N*-terminal was carried out in the presence of piperidine in DMF (20% v/v, 10 mL, 2 × 10 min) to afford the linear peptide on solid phase. The resin was washed with DMF and DCM respectively (each 2 × 25 mL). The resins were dried under vacuum for 24 h. Fresh cleavage cocktail, reagent R, TFA/thioanisole/ EDT/anisole (90:5:3:2 v/v/v/v, 10 mL),

was added to the resins. The mixture was shaken at room temperature for 2 h. The resin was collected by filtration and washed with another 2 mL of cleavage cocktail. Combined filtrates were evaporated to a minimum volume under dry nitrogen. The crude peptide was precipitated by the addition of cold diethyl ether (75 mL, Et_2O), lyophilized, and purified by reversed-phase Hitachi HPLC (L-2455) on a Phenomenex Prodigy 10 μm ODS reversed-phase column (2.1 cm × 25 cm) using a gradient system as described above to yield linear $(KW)_4$. MALDI-TOF (*m/z*) $[C_{68}H_{90}N_{16}O_9]$: calcd, 1274.7077; found, 1275.1780 $[M + H]^+$, 1297.1747 $[M + Na]^+$. A simliar procedure was performed for the synthesis of the linear $(KW)_5$. **l(KW)$_5$**: MALDI-TOF (*m/z*) $[C_{85}H_{112}N_{20}O_{11}]$: calcd, 1588.8819; found, 1589.7442 $[M + H]^+$, 1611.7890 $[M + Na]^+$, 1627.7601 $[M + K]^+$.

Synthesis of Cyclic Peptides. The synthesis of cyclic peptides was carried out according to the previously reported procedure.[14,16] As a representative example, the synthesis of cyclic $[KW]_4$ is described here.

Cyclic [KW]$_4$. The linear protected peptide (KWKWKWKW) was assembled on the H-Trp(Boc)-2-chlorotrityl chloride resin (975 mg, 0.41 mmol/g) in 0.40 mmol scale as described above. After the final deprotection of the *N*-terminal Fmoc group by piperidine in DMF (20% v/v, 15 mL, 2 times, 5 and 10 min), the side chain protected peptide was cleaved from assembled trityl resin in the presence of the cleavage cocktail TFE/acetic acid/DCM (1:2:7 v/v/v, 50 mL) by shaking for 1 h at room temperature to yield the side chain protected linear peptide. The filtrates were

evaporated to dryness under reduced pressure. To the residue was added hexane (2 × 25 mL) and DCM (1 × 25 mL) to remove the acetic acid from the mixture and to solidify the crude material as white solid. The crude protected peptide was dried under vacuum overnight. Examining a small portion of the crude by MALDI analysis confirmed the formation of the linear protected peptide. Thus, the crude was used directly for the cyclization reaction. The dried crude linear protected peptide was dissolved in DMF/DCM (2:1 v/v, 150 mL). HOAt (135 mg, 1 mmol) and DIC (137 μL, 0.88 mmol) were added to the mixture, and the solution was stirred for 12 h under the nitrogen atmosphere. After completion of the cyclization as confirmed by the MALDI-TOF, the solvents were removed under reduced pressure on a rotary evaporator. The crude product was dried overnight in vacuum before the final cleavage. Freshly prepared cleavage cocktail, reagent R, TFA/thioanisole/EDT/anisole (90:5:3:2 v/v/v/v, 15 mL) was added to the crude product. The mixture was stirred at room temperature for 2 h. The cleavage cocktail was concentrated to a minimum volume under reduced pressure by a rotary evaporator. After precipitation of crude peptide in cold diethyl ether (75 mL, Et_2O) and centrifugation, the crude peptide was lyophilized and purified by reversed-phase Hitachi HPLC (L-2455) on a Phenomenex Prodigy 10 μm ODS reversed-phase column (2.1 cm × 25 cm) using a gradient system to yield cyclic $[KW]_4$. A similar procedure was employed for the synthesis of other cyclic peptides by using appropriate resins and protected amino acids. The mass spectra data for c$[KW]_5$, c$[KF]_4$, c$[KA]_4$, c$[RFEF]_2$, and c$[KE]_4$ have been previously reported by us.[16]

c[KW]$_4$: MALDI-TOF (*m/z*) [$C_{68}H_{88}N_{16}O_8$]: calcd, 1256.6971; found, 1257.2083 [M + H]$^+$, 1281.2555 [M + H + Na]$^+$, 1295.2420 [M + K]$^+$; **C[EL]$_4$:** HR-MS (ESI-TOF) (*m/z*): $C_{44}H_{72}N_8O_{16}$ calcd, 968.5066 ; found, 969.4220 [M + H]$^+$, 485.2551 [M + 2H]$^{2+}$; **C[RF]$_4$:** HR-MS (ESI-TOF) (*m/z*): $C_{60}H_{84}N_{20}O_8$: calcd, 1212.6781; found, 1212.6052 [M + H]$^+$, 607.3026 [M + 2H]$^{2+}$, 405.5428 [M+ 3H]$^{3+}$, 304.1588 [M + 4H]$^{4+}$; **C[RC]$_4$:** HR-MS (ESI-TOF) (*m/z*): $C_{36}H_{68}N_{20}O_8S_4$ calcd, 1036.4412; found, 1037.4096 [M + H]$^+$, 345.1323 [M + 3H]$^{3+}$, 259.1024 [M + 4H]$^{4+}$.

Synthesis of Fluorescence Labeled-βA-Cyclic[KWKWKWKWKW] (F′-[KW]$_5$). The linear peptide (Dde-K(Fmoc)-WKWKWKWKW) was assembled on solid phase using Fmoc/tBu solid phase methodology. Appropriately protected amino acids were assembled on H-Trp(Boc)-2 chlorotrityl resin (513 mg, 0.40 mmol, 0.78 mmol/g) according to the solid-phase synthesis strategy described above. Dde-Lys(Fmoc)-OH was used at the *N*-terminal of the peptide. The Fmoc protecting group was removed from the side chain of lysine using piperidine in DMF (20%, 10 mL, 2 times, 5 and 10 min) and a short linker Fmoc-β-alanine (312 mg, 1 mmol) was coupled with the unprotected side chain amine group of lysine using HBTU/DIPEA (380 mg, 1 mmol/349 uL, 2 mmol) in DMF (8 mL). Fmoc of β-alanine was removed in the presence of piperidine in DMF (20%, 10 mL, 2 times, 5 and 10 min) to attach carboxyfluorescein. 5(6)-Carboxyfluorescein diisobutyrate (CFDI, US Biological) (516 mg, 1 mmol) was used for labeling the peptide. This was achieved by adding resin-bound linear peptide (0.4 mmol) into a solution of CFDI (516 mg, 1 mmol), azabenzotriazol-1-yloxy)tripyrrolidinophosphonium hexafluorophosphate (PyBOP,

520 mg, 1 mmol), HOAT (135 mg, 1 mmol), and DIPEA (350 μL, 2 mmol) in dry DMF (12.0 mL). The mixture was shaken for 3 h at room temperature and then the solvents were filtered off. The resin was washed with DMF (3 × 10 mL). The ester group of carboxyfluorescein was deprotected with 20% piperidine (20 mL) for 30 min. The *N*-terminal Dde protection was deprotected by treating the resin-bound peptide with hydrazine hydrate in DMF (2% v/v, 20 mL, 2 × 5 min). Finally, the side chain protected peptide was cleaved from the resin by shaking the resins with a mixture of TFE/acetic acid/DCM (15 mL, 1:2:7 v/v/v) for 1 h. The resin was filtered off, and the solution was evaporated to dryness under reduced pressure to yield side-chain protected linear peptide. The cyclization and purification was carried out according the described general method above used for other cyclic peptides to yield fluorescence-labeled cyclic $[KW]_5$. MALDI-TOF (*m/z*) $[C_{109}H_{127}N_{21}O_{17}]$: calcd, 2001.9719; found, 2000.9316 $[M]^+$, 2023.0032 $[M + Na]^+$, 2038.9458$[M + K]^+$.

Synthesis of Fluorescence Labeled-βA-Linear(KWKWKWKWKW) (F′-$(KW)_5$). The labeled linear sequence was assembled on H-Trp(Boc)-2 chlorotrityl resin (513 mg, 0.40 mmol, 0.78 mmol/g). The synthesis of the fluorescence-labeled side chain-protected linear peptide was carried out according to the similar procedure that described above. The peptide was assembled on resin using Dde-Lys(Fmoc)-OH at *N*-terminal. The Fmoc was removed in the presence of piperidine (20%, DMF). After the coupling of β-alanine and carboxyfluorscein in the side chain, the Dde protection at the *N*-terminal was removed by reacting with 2% hydrazine hydrate in DMF followed by washing with DMF. Then, the linear peptide was removed from the resin by using

TFA/thioanisole/anisole/EDT (15 mL, 90:5:2:3 v/v/v/v) for 2 h to obtain the crude product. The crude peptide was precipitated by the addition of cold diethyl ether (75 mL, Et_2O). Reversed-phase Hitachi HPLC (L-2455) and the gradient system described above were used for the purification of the peptide. MALDI-TOF (m/z) [$C_{109}H_{129}N_{21}O_{18}$]: calcd, 2019.9824; found, 2019.8717 $[M]^+$, 2042.8717 $[M + Na]^+$, 2058.8717 $[M + K]^+$.

$HAuCl_4$ Reduction by Peptides Dissolved in DMSO/Water Mixtures. The peptides were dissolved in 1 mL of deionized water in order to prepare a stock solution of 1 mM. The stock solution (1 mL, 1 mM) was physically mixed with $HAuCl_4$ solution (1 mL, 1 mM) in deionized water to obtain AuNPs. The final concentrations of gold and peptides were 500 μM. The formation of purple AuNPs was observed by the apparent change in the color of solution and confirmed by UV-Vis spectroscopy.

UV-Vis Spectroscopy Studies. The formation of P-AuNPs was studied in the presence of different peptides. In general, a peptide stock solution (1 mM) was mixed with an aqueous solution of $HAuCl_4$ (1 mM) at room temperature. The color of solution turned red after 1 h due to the formation of peptide capped-AuNPs. UV-Vis spectroscopy study was carried out using $HAuCl_4$ (1 mM) and different cyclic peptides (1 mM) using 96-well plate, and the absorbance was read using SpectraMax M2 spectrophotometer (Molecular Devices, CA) (Figure S16). The visible range was chosen because of the characteristic maxima peak of AuNPs appeared around 520-560 nm. All experiments were performed in triplicate.

Encapsulation of Camptothecin (CPT). CPT was dissolved in DMSO, and 10 μL of 10^{-3} M camptothecin solution was mixed with 100 μL of 10^{-4} M aqueous peptide solution in a 1:1 molar ratio. CPT in DMSO was mixed with water as a negative control. Mixed solution was incubated in a 96 well plate at room temperature for 4 h. Fluorescence of the solution was measured using SpectraMax M2 fluorescence spectrophotometer (Molecular Devices, CA) with excitation at 290 nm and emission at 360 nm.

Drug Loading. Doxorubicin (Dox) aqueous solution (100 μL, 100 μM) was added into $[KW]_5$-AuNPs solution (900 μL, 500 μM) with the concentration ratio of 1:5 for Dox to peptide-capped AuNPs. The mixture was transferred into a 1 mL dialysis membrane (with the cutoff molecular weight 1000 D; Float-A-Lyzer G2, Spectrum Labs). The membrane was sealed and submerged into water (500 mL) as a medium. After stirring in dark for 24 h, unloaded Dox in the mixture was collected and evaporated to reduce the volume. The concentration of Dox was measured using a reverse phase HPLC system installed with Hitachi premier C18 column (3 μm, 4.6 x 150 mm) at UV/Vis 490 nm wavelength. Mobile phases were water (0.1% trifluoroacetic acid) and acetronitrile (0.1% trifluoroacetic acid). The gradient of 10% to 90% acetonitrile was applied to separate the Dox peak from other impurities. The calibration standard solutions were injected to quantify Dox in the sample solution.

The loading efficiency was calculated using the following equation:

$$\text{Loading efficiency (wt/wt, \%)} = \frac{\text{Dox in feed} - \text{free Dox}}{\text{Dox in feed}} \times 100$$

To measure the loading capacity, the amount of the AuNPs in the dialysis membrane was measured after 24 h by using ICP-MS. The ICP-MS results showed the amount of AuNPs were responsible for the encapsulation of Dox. Thus, the loading capacity was calculated based on the following equation.

$$\text{Loading capacity (wt/wt, \%)} = \frac{\text{Dox in feed} - \text{free Dox}}{\text{Peptide} - \text{AuNPs in feed}} \times 100$$

Transmission Electron Microscopy (TEM). TEM analyses were conducted in JEOL Transmission Electron Microscope (Tokyo, Japan) at an accelerating voltage 80 keV. The stock solution (1 mL, 1 mM) was physically mixed with $HAuCl_4$ solution (1 mL, 1 mM) in deionized water to obtain AuNPs. The final concentrations of gold and peptides were 500 μM. The mixture was incubated for 12 days. TEM samples of c$[KW]_5$-AuNPs and l$(KW)_5$-AuNPs were prepared by depositing a droplet of 5 μL of 0.5 mM solution in H_2O on a carbon-coated Cu support grid of mesh size 300 that were dried in air overnight.

Cell Culture. Human leukemia cell line CCRF-CEM (ATCC no. CCL-119), ovarian carcinoma SK-OV-3 (ATCC no HTB-77), and colon myofibroblasts CCD-18Co (ATCC no. CRL-1459) were obtained from American Type Culture Collection. Cells were grown on 75 cm^2 cell culture flasks with RPMI-16 medium (for leukemia cells) and EMEM medium (for SK-OV-3 and CCD-18Co cells), supplemented with 10% fetal bovine serum (FBS), and 1% penicillin-streptomycin solution (10,000 units of penicillin and 10 mg of streptomycin in 0.9 % NaCl) in a humidified atmosphere of 5% CO_2, 95% air at 37 ºC.

Cytotoxicity Assay. SK-OV-3, CCRF-CEM, and CCD-18Co cells were seeded at 5,000 cells, 30,000 cells, and 3,000 cells, respectively, in 0.1 ml per well in 96-well plates 24 h prior to the experiment. The old medium (EMEM containing FBS (10%)) was replaced (not in case of CCRF-CEM) by different concentrations of c[KW]$_5$, l(KW)$_5$, c[KW]$_5$-AuNPs or l(KW)$_5$-AuNPs in serum containing medium and incubated for 24 h (or 72 h) at 37 °C in a humidified atmosphere of 5% CO_2. Cell viability was then determined by measuring the fluorescence intensity at 490 nm using a SpectraMax M2 microplate spectrophotometer. The percentage of cell survival was calculated as [(OD value of cells treated with the test mixture of compounds) − (OD value of culture medium)]/[(OD value of control cells) − (OD value of culture medium)] × 100% (Figure S17).

Flow Cytometry Studies. Human leukemia and ovarian carcinoma cells (CCRF-CEM and SK-OV-3) were taken in 6-well plates (1×10^7 cells/well (CCERF-CEM) and 3×10^5 cells/well (SK-OV-3)) in opti-MEM. Then the fluorescence-labeled compound (F′-3TC, F′-FTC, or F′-GpYEEI) (5 μM) was added to the different wells containing c[KW]$_5$-AuNPs (25 μM), l(KW)$_5$-AuNPs (25 μM), l(KW)$_5$ (25 μM), or c[KW]$_5$ (25 μM) in serum-free media. The plates were incubated for 1 h at 37 °C. Cells, P-AuNPs, and the fluorescence-labeled compound alone were used as negative controls. After 1 h incubation, the media containing the peptide was removed. The cells were digested with 0.25% trypsin/EDTA (0.53 mM) for 5 min to remove any artificial surface binding. Then the cells were washed twice with PBS. Finally, the

cells were resuspended in flow cytometry buffer and analyzed by flow cytometry (FACSCalibur™:Becton Dickinson) using FITC channel and CellQuest software. The data presented were based on the mean fluorescence signal for 10,000 cells collected. All assays were performed in triplicate.

In the case of fluorescence-labeled peptide gold nanoparticles (F′-Peptide-AuNPs) and their corresponding peptides (F′-Peptide), SK-OV-3 cells were seeded in 6-well plates (3×10^5 cells/well) in opti-MEM. The F′-labeled compound (F′-c$[KW]_5$, F′-l$(KW)_5$, F′-c$[KW]_5$-AuNPs, or F′-l$(KW)_5$-AuNPs (5 μM) was added to the various wells. The plates were incubated for 1 h at 37 °C. Wells containing no treatment and 5-(6) carboxyfluorescein (FAM) were used as negative controls. After 1 h incubation, the medium was removed. The cells were digested with 0.25% trypsin/EDTA (0.53 mM) for 5 min to remove any artificial surface association and to detect only intracellular uptake. Then the cells were washed twice with PBS. Finally, the cells were resuspended in flow cytometry buffer and analyzed by flow cytometry (FACSCalibur: Becton Dickinson) using FL2 channel and CellQuest software. The data presented are based on the mean fluorescence signal for 10,000 cells collected. All assays were performed in triplicate.

Cellular Uptake Studies in the Presence of Inhibitors. Human ovarian adenocarcinoma cells (SK-OV-3) were seeded in six well plates (3×10^5 cells/well) in opti-MEM. The cells were pre-incubated by various inhibitors including, nystatin (50 μg/ml), chloroquine (100 μM), chlorpromazine (30 μM), methyl-β-cyclodextrin (2.5 mM), and 5-(*N*-ethyl-*N*-isopropyl)amiloride (EIA, 50 μM) for 30 min. The treatment

was removed, and the cells were incubated with F′-l$(KW)_5$-AuNPs or F′-c$[KW]_5$-AuNPs (5 μM) a similar concentration of inhibitors for 1 h. Consequently, similar FACS protocol was performed as described above.

Membrane Integrity Test. Ovarian carcinoma cells SK-OV-3 were grown in six well plates (1×10^5 cells/ well). Cells were treated with $[KW]_5$-AuNPs (50 μM) and $(KW)_5$-AuNPs (50 μM) in serum-free media for 1 h at 37 ^{0}C. After 1 h incubation, the cells were detached with trypsinization for 5 min followed by washing twice with PBS. Then they were resuspended in serum-free media. Trypan blue (2 μL) was added into the cell suspension (18 μL) and incubated for 5 min. Finally, trypan blue-stained cells were counted using cellometer vision (Nexcelom Bioscience, Lawrence, MA, USA) (Figure S18).

Confocal Microscopy on Live Cells. Adherent SK-OV-3 cells were seeded with EMEM media overnight on coverslips in six well plates (1×10^5 cells per well). Then, the media were removed and washed with opti-MEM. The cells were treated with the mixture of F′-3TC (5 μM) and c$[KW]_5$-AuNPs (25 μM), and the mixture of F′-3TC (5 μM) and l$(KW)_5$-AuNPs (25 μM) in opti-MEM for 1 h at 37 ºC. After 1 h incubation, the media containing the treatments were removed followed by washing with PBS three times. To stain the nuclei, cells were incubated with 4,6-diamidino-2-phenylindole (DAPI, 0.5 mL) solution in PBS for 5 min. After the incubation, the cells were softly washed twice with PBS to remove the excessive DAPI. The coverslips were mounted on a microscope slide with mounting media with cells-attached side

facing down. Laser scanning confocal microscopy was carried out using Carl Zeiss LSM 700 system. The cells were imaged using FITC and phase contrast channels. The fluorescence images were taken under 20 × objective. Blue and green luminescent emissions from DAPI and FITC were excited at the wavelength of 405 nm and 488 nm, respectively. The emission wavelengths were ranged from 425 nm to 475 nm for DAPI and 500 nm to 550 nm for FITC. There was no interference between these two channels. The scanning mode was in sequential frame.

Time-Dependent Antiproliferative Assay. The antiproliferative activity of CPT alone and in the presence of c[KW]$_5$-AuNPs against SK-OV-3 cells was determined by MTS assay. All cells were plated overnight in 96-well plates with a density of 5000 cells per well in 0.1 mL of appropriate growth medium at 37 °C. CPT alone (5 μM) or a combination of CPT (5 μM) and c[KW]$_5$-AuNPs (25 μM) were incubated with the cells for 4 h. Excess of compounds was removed and washed by fresh media. The cells were kept in an incubator for 24−72 h. The cells without compounds were included in each experiment as controls. After 24 h, 48 h, and 72 h incubation, 20 μL of MTS solution was added and incubated for 2 h. The absorbance of the formazan product was measured at 490 nm using microplate reader. The percentage of cell viability was calculated as (OD value of untreated cells - OD value of treated cells)/OD value of untreated cells × 100%.

Intracellular Release of Dox. Intracellular release and accumulation of Dox were determined in CCRF-CEM cells by HPLC analysis. CCRF-CEM cells were grown in

75 cm^2 culture flasks with RPMI medium (containing 10% FBS and 1% penicillin-streptomycin) to achieve ~70−80% confluence (1.2×10^7 cells/mL). The cells were partitioned/transferred to culture plates (six well) having 1.2×10^7 cells per well in 2 mL of medium. The treatment in fresh RPMI medium containing Dox-loaded $c[KW]_5$-AuNPs (7.5/37.5 μM) was added to cells, and they were incubated at 37 °C for different incubation times including 2, 12, 24, and 48 h. After the incubation time, the cells were collected by centrifugation. The medium was removed and cell pellets were washed with ice-cold PBS (5 mL) twice to remove any medium. The cell pellets were thoroughly extracted with an equal volume of methanol, chloroform, and isopropanol mixture (4:3:1 v/v/v) and filtered through 0.2 μm filters. The solvents were evaporated under N_2 gas. The released Dox was quantified by reverse phase HPLC system with UV/Vis detector (490 nm) (Figures S4-S9, Supporting Information). The HPLC condition was using mobile phase water (0.1% trifluoroacetic acid) and acetronitrile (0.1% trifluoroacetic acid) and the gradient of 10% to 90% acetonitrile as described above in drug loading section.

RESULTS AND DISCUSSION

Chemistry

A number of cyclic octapeptides containing diverse combination of amino acids including $c[KW]_4$, $c[KF]_4$, $c[KA]_4$, $c[EL]_4$, $c[RFEF]_2$, $c[EK]_4$, $c[RF]_4$, and $c[RC]_4$ (Figure S16) were synthesized by employing 9-fluorenylmethyoxycarbonyl (Fmoc)-based chemistry according to the previously reported procedure.[14,16] Synthesis of $c[KW]_4$ and $l[KW]_4$ is described in Supporting Information (Schemes S1 and S2).

Fluorescently-labeled conjugates of linear $(KW)_5$ and cyclic $[KW]_5$ were synthesized as described previously.[14] For example, F′-l$(KW)_5$ was synthesized by the Fmoc protection group at the *N*-terminal was removed. Subsequent conjugation reaction with 5(6)-carboxyfluorescein isobutyrate was performed in the presence of HOAt, PyAOP, and *N*,*N*-diisopropylethylamine (DIPEA) in DMF:DCM followed by deprotection and cleavage from the resin in the presence of reagent R afforded the crude product that was purified by preparative reversed-phase HPLC (Scheme S2). The structures of all the final compounds were confirmed by high-resolution MALDI TOF/TOF and/or high-resolution electrospray mass spectrometry.

Evaluation of Cyclic and Linear Peptides for Generation of Peptide-AuNPs and Characterization

All peptides were examined for their ability to generate AuNPs by direct addition of the peptide solution (1 mM) into an aqueous solution of $HAuCl_4$ (1 mM) at room temperature. UV-Vis spectra and monitoring of surface plasmon resonance peak at ~550 nm showed that among all peptides, c$[KW]_4$ and the corresponding linear peptide l$(KW)_4$ were able to produce peptide capped AuNPs (P-AuNPs) (Figure S16). Mechanistically, c$[KW]_4$ acts as reducing and capping agent, making this method a one-step (one-pot) reaction without any need for chemical modification on the surface of AuNPs. Amino acids have been used as reducing agents. Among them, tryptophan (W) has been shown to be the most efficient reducing agents among 20 amino acids.[17] Addition of positively charged residues, such as lysine (K) in the structure of the

peptide enhances the reduction through the favorable charge interactions with the chloroaurate anions.[18]

To optimize the yield of P-AuNPs by increasing the reducing and capping efficiency of the peptide, cyclic $c[KW]_5$ containing ten alternative tryptophan and lysine (Figure 1) was synthesized. The corresponding linear peptide $l(KW)_5$ (Figure 1) was also designed and synthesized to determine the effect of the peptide cyclic nature of the peptide on the shape and size of P-AuNPs. UV-Vis spectra of both $c[KW]_5$-AuNPs and $l(KW)_5$-AuNPs showed also a SPR peak at approximately 550 nm.

Further studies were conducted by Transmission electron microscopy (TEM) to characterize the size and shape of P-AuNPs. TEM images of $c[KW]_5$-AuNPs and $l(KW)_5$-AuNPs showed that these two systems formed entirely different nanosized structure. $c[KW]_5$-AuNPs formed sponge-like agglomerates containing peptide and AuNPs containing peptide and AuNPs with an approximate diameter size of 250-450 nm (Figure 2) along with some isolated AuNPs in mostly spherical and triangular shapes (6-60 nm). Compared to cyclic peptide-capped AuNPs, TEM images of $l(KW)_5$-AuNPs demonstrated ball-shaped structures with the approximate diameter size of 900-1000 nm composed of a large number of AuNPs (Figure 3). The majority of individual $l(KW)_5$-AuNPs were found to be spherical and approximately in the size range of 4-35 nm. The distribution pattern of AuNPs in the ball-shape structure of $l(KW)_5$-AuNPs showed an organized arrangement (Figure 3). No visible peptide agglomerates were observed. Cavities between AuNPs were found to be tailored in a similar range size (approximately 45 ± 2 nm). The presence of the tryptophan in the structure of the linear peptide induces presumably hydrophobic interactions that could

be an efficient driving force for the formation of this specific structure. c[KW]$_5$ and l(KW)$_5$ alone did not form any specific nanostructures under similar conditions, suggesting that the binding between AuNPs and peptides contributes to different morphology in P-AuNPs.

cyclic nature and rigidity of the peptide in c[KW]$_5$-AuNPs and different orientation of amino acids in the skeleton of peptide generated a different environment surrounding the complex that led to aggregation or agglomeration of the peptides. This orientation altered the number of available tryptophan and/or lysine residues in reduction of Au^{3+} reaction.[18] However, l(KW)$_5$ has more flexible conformation compared to the corresponding conformationally constrained cyclic counterpart c[KW]$_5$ during the AuNPs formation. The presence of additional positively charge amino group and negatively charge carboxylate at *N*-terminal lysine and *C*-terminal tryptophan, respectively, could also contribute in intermolecular interactions of the peptide. Thus, the cyclic and linear nature of the peptide and the orientation of amino acids were found to be responsible for the different morphology and size of formed P-AuNPs.

Circular dichroism (CD) was used to obtain a better understanding about the effect of AuNPs formation on the secondary structure of these peptides. CD experiment of aqueous solution of peptides and their corresponding P-AuNPs (100 μM) was performed at room temperature. CD spectra of c[KW]$_5$ (Figure 4) revealed a negative band at approximately 216 nm and a positive band around 230 nm. Compared to c[KW]$_5$, the linear counterpart l(KW)$_5$ showed a different CD spectra pattern with a negative band at 201 nm and a positive band at 227 nm. However, the

CD spectra of both c[KW]$_5$-AuNPs and l(KW)$_5$-AuNPs exhibited relatively similar pattern with a minima at 204 ± 2 nm and a maxima at maxima at 229 ± 1 nm. Although two P-AuNPs showed approximately similar pattern and intensity, l(KW)$_5$-AuNPs (206 nm) minima was shifted compared to that of c[KW]$_5$-AuNPs (203 nm). The CD spectra demonstrated a significant decrease in spectral elipticity of both P-AuNPs compared to their corresponding parent peptides, suggesting significant modification of secondary structures upon reducing Au^{3+} and/or binding to AuNPs. These data show the binding between peptides and AuNPs leads to the formation of c[KW]$_5$-AuNPs and l(KW)$_5$-AuNPs with differential CD spectra pattern compared to the parent peptides.

Encapsulation of Camptothecin by Peptide-AuNPs

To evaluate the potential of c[KW]$_5$-AuNPs and l(KW)$_5$-AuNPs to encapsulate drugs, camptothecin (CPT), a hydrophobic potent anticancer drug targeting topoisomerase I[19] was selected as a model drug for evaluation of loading using fluorescence spectroscopy. Incubation of CPT with c[KW]$_5$-AuNPs and l(KW)$_5$-AuNPs demonstrated significant shift in emission maxima of CPT. A characteristic maxima band of CPT alone at 458 nm was shifted to 433 nm and 430 nm in the presence of c[KW]$_5$-AuNPs and l(KW)$_5$-AuNPs, respectively (Figure S19). The spectral blue shift in the presence of c[KW]$_5$-AuNPs and l(KW)$_5$-AuNPs was possibly due to partitioning of CPT into a hydrophobic core and hydrophobic interactions. Moreover, the intensity of the maxima band was decreased that could be due to the

self-quenching of bound-drug and/or the result of the partitioning and entrapment in the hydrophobic pocket generated by the P-AuNPs.[20] These data exhibited that the P-AuNPs were able to encapsulate CPT due to the generated hydrophobic pocket possibly by tryptophan in the structure of the peptide.

Drug Loading. To get a better understanding of the quantitative drug loading efficiency of the system, Dox was selected as a model drug because of its stability and fluorescence property. The loading measurement was performed based on the previously reported method.[27] Aqueous Dox solution (100 μL, 100 μM) was mixed with aqueous c$[KW]_5$-AuNPs solution (900 μL, 500 μM) to obtain 1:5 molar ratio. The unloaded Dox was separated by using dialysis to analyze the Dox loading efficiency and loading capacity in the c$[KW]_5$-AuNPs. After 24 h stirring, the loading efficiency was found to be 72 ± 1% when the weight ratio of Dox to c$[KW]_5$-AuNPs in feed is 1:5. The loading capacity was calculated to be 16 ± 1 % based on the weight ratio of Dox to c$[WK]_5$-AuNPs (1:5) when the amount of AuNPs was determined using inductively coupled plasma mass spectrometry (ICP-MS).

Cytotoxicity of Peptide-AuNPs. Generated c$[KW]_5$-AuNPs and l$(KW)_5$-AuNPs did not show any significant toxicity in human ovarian adecarcinoma (SK-OV-3), human leukemia (CCRF-CEM) cancer cells, and normal human colon myofibroblast (CCD-18Co) cells at a concentration of 100 μM after 24 and 72 h incubation times (Figure S17). Thus, concentration of <100 μM was selected for further cell-based studies. It is important to emphasize that the cytotoxicity of c$[KW]_5$ and l$(KW)_5$ (100 μM) was

decreased through P-AuNPs formation dramatically. For example, c[KW]$_5$ was found to be toxic in normal colon CCD-18Co cells (61.3% cell viability) compared to c[KW]$_5$-AuNPs (99.3% cell viability) after 24 h at a concentration of 100 μM. These data indicate that the cytotoxicity of the parent peptide significantly reduces upon generation of P-AuNPs.

Cellular Uptake of Peptide-AuNPs. To confirm the internalization of P-AuNPs alone, F′-l(KW)$_5$-AuNPs and F′-c[KW]$_5$-AuNPs were prepared as described above by incubating of fluorescently-labeled conjugates of linear (KW)$_5$ and cyclic [KW]$_5$, F′-l(KW)$_5$ and F′-c[KW]$_5$, with $HAuCl_4$ solution according to the previously reported procedure.[15] Incubation of F′-l(KW)$_5$-AuNPs and F′-c[KW]$_5$-AuNPs with SK-OV-3 cells showed 3.3- and 4.3-fold higher cellular uptake compared to the corresponding fluorescently-labeled peptides F′-l(KW)$_5$ and F′-c[KW]$_5$, respectively, thus suggesting the formation of P-AuNPs is crucial for the enhanced cellular permeability (Figure 5). FACS results confirmed that F′-c[KW]$_5$-AuNPs showed approximately 1.6-fold higher cellular uptake than F′-l(KW)$_5$-AuNPs, suggesting that the cyclic nature of the peptide in P-AuNPs contributes to improving the cellular uptake.

To investigate whether c[KW]$_5$-AuNPs and l(KW)$_5$-AuNPs localize in different locations in the cell, F′-l(KW)$_5$-AuNPs (5 μM) and F′-c[KW]$_5$-AuNPs (5 μM) were incubated with SK-OV-3 for 1 h. 4',6-Diamidino-2-phenylindole (DAPI) was employed as a marker of nucleus. Confocal microscopy showed significantly higher nuclear localization of the cyclic peptide-capped AuNPs (F′-c[KW]$_5$-AuNPs)

versus the corresponding linear system (F′-l$(KW)_5$-AuNPs) as shown by overlayed picture with DAPI (Figure 6).

Cells use different mechanisms to internalize macromolecules and particles, such as phagocytosis, micropinocytosis, and receptor-mediated endocytosis (RME) pathways including clathrin-mediated, caveolae-mediated, and caveolae/clathrin independent endocytosis.[21] To get a better understanding of the mechanism of peptide-capped gold nanoparticles uptake by cells, the cellular uptake of fluorescein-labeled peptide capped gold nanoparticles, F′-l$(KW)_5$-AuNPs and F′-c$[KW]_5$-AuNPs (5 μM), were tested quantitatively in the presence of several inhibitors by using FACS including, nystatin, chloroquine, chlorpromazine, methyl-β-cyclodextrin, and 5-(*N*-ethyl-*N*-isopropyl)- amiloride (EIA).

As it is shown in Figure 7, the intracellular uptake of F′-l$(KW)_5$-AuNPs and F′-c$[KW]_5$-AuNPs did not significantly change in SK-OV-3 cells in the presence of different endocytic inhibitors after 1 h incubation, suggesting that the mechanism of cellular uptake is not exclusively clathrin-mediated or caveolae-mediated endocytosis, and macropinocytosis. These peptide-AuNPs provide an advantage to known gold nanoparticles and cell-penetrating peptides that their uptake is dependent mainly on endocytotic entry.[22]

The surface decoration of AuNPs by amphipathic c$[KW]_5$ and l$(KW)_5$ peptides could improve the interactions of lysine and tryptophan residues with the corresponding negatively charged phospholipids and hydrophobic residues in lipid bilayer. This interaction could be a strong driving force for the initial entry into the cell membrane. Hydrophobic interactions generated by tryptophan residues and the

lipids can potentially distort the outer phospholipid monolayer. This process will be followed by peptide internalization and enhanced cellular uptake of the cargo. The nature of the peptide in surface of AuNPs is an important parameter that can alter the mechanism of nanoparticle uptake by cells. Further investigation is required to pinpoint the detailed mechanism of cell entry by these P-AuNPs.

The cellular membrane integrity in SK-OV-3 cells was examined in the presence of c$[KW]_5$-AuNPs and l$(KW)_5$-AuNPs and using trypan blue and showed no significant difference to the control cells (Figure S18), ruling out the damage of the plasma membrane by P-AuNPs at 50 μM and confirming that the highly efficient transport of the complex was not a result of decreased cellular membrane integrity.

Evaluation of Peptide-AuNPs as Molecular Transporters. To evaluate P-AuNPs as molecular transporters, model experiments with anti-HIV drugs 2',3'-dideoxy-5-fluoro-3'-thiacytidine (emtricitabine, FTC) and 2',3'-didehydro-2',3'-dideoxythymidine (lamivudine, 3TC) as cargo drugs were performed. FTC and 3TC are nucleoside reverse transcriptase inhibitors those blocks HIV-1 and hepatitis B virus replication.[22] The efficient cellular uptake of FTC and 3TC are critical for anti-HIV activity. To monitor the molecular transporter ability of P-AuNPs, carboxyfluorescein derivatives of FTC (F′-FTC) and 3TC (F′-3TC) were synthesized as described previously, where F′= fluorescein.[24,25]

CCRF-CEM cells were incubated with F′-FTC and F′-3TC (5 μM) in the presence or absence of diluted carriers c$[KW]_5$-AuNPs and l$(KW)_5$-AuNPs (25 μM) and their parent peptides for 1 h at 37 ºC and then treated with trypsin to remove cell

surface-bound drugs. Intracellular uptake of F′-FTC and F′-3TC (5 μM) was measured in cells using fluorescence activated cell sorter (FACS). FACS showed significantly higher fluorescence signals in cells treated with F′-Drug-loaded P-AuNPs compared to those with drug alone. The cellular uptake of F′-drug-loaded c[KW]$_5$-AuNPs and F′-drug–loaded l(KW)$_5$-AuNPs were found to be 5.2–5.3- and 2.5–2.9-fold higher for F′-FTC and F′-3TC, respectively, than those of drug alone respectively (Figure 8), suggesting that the uptake of drugs is facilitated by P-AuNPs. The results showed that parent cyclic or linear parent peptides did not improve the cellular uptake of drugs. However, after the formation of P-AuNPs, the cellular uptake of drugs was increased significantly. c[KW]$_5$-AuNPs were found to be more efficient transporter than l(KW)$_5$-AuNPs, while c[KW]$_5$ and l(KW)$_5$ exhibited similar results. These data suggest that a non-cell penetrating cyclic peptide can be converted to cell-penetrating P-AuNPs, presumably due to the new orientation of amino acids and the secondary structure in peptides as shown with CD in the presence of generated AuNPs for drug entrapment.

To visualize the enhancement of the cellular uptake of drugs, F′-3TC was used as a model for confocal microscopy in SK-OV-3 cells. Confocal microscopy showed nuclear localization of F′-3TC–loaded c[KW]$_5$-AuNPs compared to the corresponding linear system and drug alone. F′-3TC-loaded l(KW)$_5$-AuNPs exhibited a modest fluorescence mostly in the cytoplasm of the cells. However, incubation of cells with F′-3TC alone did not show any fluorescence intensity in cells. These data confirm that the cyclic nature of the peptide is critical for the enhanced cellular permeability (Figure 9) and the nuclear targeting delivery of cargos.

Thus, differential application of linear and cyclic $[KW]_5$-AuNPs was discovered for localization of fluorescence-labeled-3TC. Confocal microscopy revealed the localization of fluorescence-labeled-3TC in the presence of $c[KW]_5$-AuNPs mostly in nucleus in SK-OV-3 cells after 1 h. On the other hand, $l(KW)_5$-AuNPs delivered fluorescence-labeled-3TC in cytoplasm. Furthermore, $c[KW]_4$-AuNPs offered two major advantages over $c[RW]_4$-AuNPs that we previously reported.[15] First, the reaction time for the formation of $c[KW]_4$-AuNPs (1 h) was significantly shorter compared to that of $c[RW]_4$-AuNPs (4-8 h). The Surface Plasmon Resonance peak for both $c[KW]_4$-AuNPs and $c[RW]_4$-AuNPs[15] was compared by using UV-Vis spectroscopy (Figure S20) after 1 h. The results showed that $c[KW]_4$-AuNPs formed faster than $c[RW]_4$-AuNPs. Second, the size and morphology of nanoparticles can be used to control the amount of intracellular uptake of AuNPs by cells. Intracellular accumulation of 233 ng and 288 ng of $c[RW]_4$-AuNPs and $c[KW]_4$-AuNPs was detected, respectively, in SK-OV-3 cells after 24 h incubation[15] as measured by ICP-MS.

The molecular transporting efficiency of P-AuNPs for cell-impermeable negatively charges phosphopeptides was also evaluated using flow cytometry. The phosphopeptide do not cross the cell-membrane readily because of the presence of the negatively charged phosphate group. The pTyr-Glu-Glu-Ile (GpYEEI) peptide template has been reported to be an optimal binding sequence for the Src SH2 domain of Src kinase.[25] The cellular uptake of F′-GpYEEI was monitored in the presence of P-AuNPs in SK-OV-3 cells. FACS analysis showed that the cellular uptake of F′-GpYEEI was enhanced 3.5- and 12.8-fold by $l(KW)_5$-AuNPs and $c[KW]_5$-AuNPs,

respectively (Figure 10), suggesting that these systems may function as a delivery tools for F′-GpYEEI. c[KW]$_5$-AuNPs improved the cellular uptake of F′-GpYEEI 4.2-fold higher when compared to l(KW)$_5$-AuNPs, suggesting the critical role of the cyclic peptide in improving the cellular uptake. These results are consistent with cellular uptake studies of lamivudine and emtricitabine.

Considering the significant enhancement of F′-GpYEEI in the presence of P-AuNPs (Figure 10), confocal microscopy was used to confirm the cellular uptake of this negatively charged phosphopeptide in the presence and absence of P-AuNPs. Thus, confocal microscopy was conducted by measuring the fluorescence intensity of F′-GpYEEI-loaded P-AuNPs compared to F′-GpYEEI alone in SK-OV-3 cells. 4',6-Diamidino-2-phenylindole (DAPI) was employed as a marker of nucleus. The cells were incubated with F′-GpYEEI-loaded c[KW]$_5$-AuNPs, F′-GpYEEI-loaded L[KW]$_5$-AuNPs, and F′-GpYEEI alone. No green fluorescence was observed for the parent fluorescence-labeled phosphopeptide, suggesting that F′-GpYEEI alone did not cross the membrane because of the presence of negative charge phosphate. As shown in Figure 11, the cell nuclei stained by DAPI (blue) were circumvented by the green fluorescence showing the fluorescent-labeled phosphopeptide localized in the cytoplasm in the presence of L[KW]$_5$-AuNPs (Figure 11b). However, the presence of c[KW]$_5$-AuNPs led an overlay of green and blue fluorescence signals revealing the localization of the phosphopeptide mostly in the nuclei of SK-OV-3 cells (Figure 11c). These results indicated that the presence of P-AuNPs is critical to improve the cellular uptake of cell-impermeable phosphopeptide. Furthermore, the linear or cyclic nature of the peptide determines the final destination of the cargo.

Time-Dependent Antiproliferative Assay. To determine whether c[KW]$_5$-AuNPs can be exploited for the delivery of biologically relevant doses of CPT to cells, the antiproliferative activity of CPT was evaluated in SK-OV-3 cells in the presence and absence of peptide-capped AuNPs in a time-dependent manner. The antiproliferative activity of CPT (5 μM) in the presence of the c[KW]$_5$-AuNPs was improved by approximately 9%, 32%, and 33% compared to that of CPT alone after 24, 48, and 72 h incubation, respectively (Figure 12). Time-dependent inhibitory effect on the cell proliferation of SK-OV-3 cells suggests that the sustained intracellular release of CPT and improved efficacy of the compound. c[KW]$_5$-AuNPs alone did not show any toxicity in SK-OV-3 cells under similar condition, suggesting that the higher antiproliferative is possibly related to the enhanced uptake of the drug in the presence of the peptide-capped AuNPs and intracellular release of CPT.

Intracellular Release of Dox. To investigate the kinetics of drug release in cells, Dox was selected as a model drug. The intracellular release of Dox in the presence of the c[KW]$_5$-AuNPs in CCRF-CEM cells was monitored by HPLC. The CCRF-CEM cells (1.2×10^7) were incubated with Dox (7.5 μM)-loaded c[KW]$_5$-AuNPs (37.5 μM) for different times including 2, 12, 24, and 48 h. HPLC analysis at 490 nm and a specific time intervals after cellular lysis was used to measure the quantity of the released Dox. The data exhibited that the intracellular release of Dox occurred in a time-dependent manner. Dox was observed at 15.8-15.9 min in the HPLC profile (Figures S4-S9, Supporting Information). HPLC data showed that approximately 30, 35, 55, and 88%

of Dox was released intracellularly within 2, 12, 24, and 48 h, respectively. These data suggest the sustained release of Dox contributes to overall activity of the Dox–loaded c$[KW]_5$-AuNPs as a potential prodrug.

Conclusions

In conclusion, a new class of DDS containing AuNPs and peptides with tryptophan and lysine residues were generated under a mild reaction condition. Cyclic and linear peptide capped-AuNPs (l$(KW)_5$-AuNPs and c$[KW]_5$-AuNPs) exhibited entirely different morphology and sizes. Both l$(KW)_5$-AuNPs and c$[KW]_5$-AuNPs showed minimal cytotoxicity at 100 μM. P-AuNPs were able to entrap hydrophobic CPT through non-covalent interactions, and act as molecular transporters of fluorescence-labeled lamivudine, emtricitabine, and a phosphopeptide (GpYEEI) intracellularly. High cellular internalization of the labeled drugs by P-AuNPs suggests the potential application of P-AuNPs as molecular transporters. Confocal microscopy showed that l$(KW)_5$-AuNPs and c$[KW]_5$-AuNPs delivered cargos to different destinations in cells e.g. cytoplasm and nucleus, respectively. The present results provide insights for generation of a new class of peptide-capped metal nanoparticles as cellular delivery transporters.

ASSOCIATED CONTENT

Supporting Information

Additional synthetic Scheme and Figures, UV-VIS spectroscopy, cytotoxicity, and encapsulation with CPT. This information is available free of charge via the Internet at http://pubs.acs.org/.

Notes

The authors declare no competing financial interest.

ACKNOWLEDGMENTS

We acknowledge the financial support from the American Cancer Society, Grant No. RSG-07-290-01-CDD, and from the US National Science Foundation, Grant No. CHE 0748555. We thank National Center for Research Resources, NIH, and Grant Number 1 P20 RR16457 for sponsoring the core facility.

REFERENCES

(1) Allen, T. M.; Cullis, P.R. Drug delivery systems: entering the mainstream. *Science.* **2004**, 303, 1818–1823.

(2) Van der Aa, M. A. E. M.; Mastrobattista, E.; Oosting, R. S.; Hennink, W. E.; Koning, G. A.; Crommelin, D. J. A. The nuclear pore complex: the gateway to successful nonviral gene delivery. *Pharm. Res.* **2006**, 23, 447–459.

(3) (a) Liu, J-n.; Bu, W.; Pan, L-m.; Zhang, S.; Chen, F.; Zhou, L. Zhao, K.; Peng, W.; Shi, J. Simultaneous nuclear imaging and intranuclear drug delivery by nuclear-targeted multifunctional upconversion nanoprobes. *Biomaterials* **2012**, 33, 7282–7290.

(b) Shiraishi, T.; Hamzavi, R.; Nielsen, P. E. Targeted delivery of plasmid DNA into

the nucleus of cells via nuclear localization signal peptide conjugated to DNA intercalating bis- and trisacridines. *Bioconjugate Chemistry* **2005**, 16, 1112–1116. (c) Hodoniczky, J.; Sims, C. G.; Best, W. M.; Bentel, J. M.; Wilce, J. A. The intracellular and nuclear-targeted delivery of an antiandrogen drug by carrier peptides. *Biopolymers* **2008**, 90, 595–603.

(4) Kubitscheck, U. Grnwald, D.; Hoekstra, A.; Rohleder, D.; Kues, T.; Siebrasse, J. P.; Peters, R. J. Nuclear transport of single molecules: dwell times at the nuclear pore complex. *Cell. Biol*. **2005**, 168, 233–243.

(5) Meinema, A. C.; Laba, J. K.; Hapsari, R. A.; Otten, R.; Mulder, F. A.; Kralt, A.; Van den Bogaart, G.; Lusk, C. P.; Poolman, B.; Veenhoff, L. M. Long unfolded linkers facilitate membrane protein import through the nuclear pore complex. *Science*, **2011**, 333, 90–93.

(6) Kang, B.; Megan, A. M.; Mostafa, A. E. Nuclear targeting of gold nanoparticles in cancer cells induces DNA damage, causing cytokinesis arrest and apoptosis. *J. Am. Chem. Soc*, **2010**, 132, 1517–1519.

(7) Raurio, J.; Kumpulainen, H.; Heimbach, T.; Oliyai, R.; Oh, D.; Jarvinen, T.; S, J. Prodrugs: design and clinical applications, *Nature Rev.* **2008**, 7, 255-270.

(8) (a) De, M.; Ghosh, P. S.; Rotello, V. M. Applications of nanoparticles in biology. *Adv. Mater*. **2008**, 20, 4225–4241. (b) Subramani, C.; Yu, X.; Agasti, S. S.; Duncan, B.; Eymur, S.; Tonga, M.; Rotello, V. M. Direct photopatterning of light-activated gold nanoparticles. *J. Mater. Chem.*, **2011**, 21, 14156–14158.

(9) (a) Dekiwadia, C. D.; Lawrie, A. C.; Fecondo, J. V. Peptide-mediated cell penetration and targeted delivery of gold nanoparticles into lysosomes. *J. Peptide Sci*.

2012, 18, 527–534. (b) Kim, C. K.; Ghosh, P.; Pagliuca, C.; Zhu, Z. J.; Menichetti, S.; Rotello, V. M. Entrapment of hydrophobic drugs in nanoparticle monolayers with efficient release into cancer cells. *J. Am. Chem. Soc*. **2009**, 131, 1360–1361.

(10) (a) Langel, U. Cell-penetrating peptides: processes and applications, **2002** CRC Press, Boca Rotan; (b) Torchilin, V. P.; Rammohan, R.; Weissig, V.; Levchenko, T. S. TAT peptide on the surface of liposomes affords their efficient intracellular delivery even at low temperature and in the presence of metabolic inhibitors**.** *Proc. Nat. Acad. Sci. U.S.A.* **2001**, 98, 8786–8791. (c) Silhol, M.; Tyagi, M.; Giacca, M.; Lebleu, B; Vives, E. Different mechanisms for cellular internalization of the HIV-1 Tat-derived cell penetrating peptide and recombinant proteins fused to Tat. *Eur. J. Biochem.* **2002**, 269, 494–501. (d) Thorén, P. E.; Persson, D.; Isakson, P.; Goksör, M.; Onfelt, A.; Nordén, B. Uptake of analogs of penetratin, Tat(48–60) and oligoarginine in live cells. *Biochem. Biophys. Res. Commun.* **2003**, 307, 100–107.

(11) (a) Rana, S.; Bajaj, A.; Mout, R.; Rotello, V. M. Monolayer coated gold nanoparticles for delivery applications, *Advanced Drug Delivery Reviews*, **2012**, 64, 200–216. (b) Saha, K.; Bajaj, A.; Duncan, B.; Rotello, N.M. Beauty is skin deep: a surface monolayer perspective on nanoparticle interactions with cells and bio-macromolecules. *Small* **2011**, 7, 1903–1918. (c) Yuan, H.; Fales, A. M.; Vo-Dinh, T. TAT Peptide-functionalized gold nanostars: enhanced intracellular delivery and efficient NIR photothermal therapy using ultralow irradiance. *J. Am. Chem. Soc*. **2012**, 134, 11358–11361.

(12) (a) Torchilin, V. P. Structure and design of polymeric surfactant-based drug delivery systems**.** *J. Controlled Release*, **2001**, 73, 137–172. (b) Lee, C. C.; MacKay,

J. A.; Frechet, J. M. J.; Szoka, F. C. Designing dendrimers for biological applications. *Nat. Biotechnol*. **2005**, 23, 1517–1526.

(13) (a) Morgan, M. T.; Nakanishi, Y.; Kroll, D. J.; Griset, A. P.; Carnahan, M. A.; Wathier, M.; Oberlies, N. H.; Manikumar, G.; Wani, M. C.; Grinstaff, M. W. Dendrimer-encapsulated camptothecins: increased solubility, cellular uptake, and cellular retention affords enhanced anticancer activity *in vitro*. *Cancer Res*. **2006**, 66, 11913–11921. (b) Duncan, B.; Kim, C.; Rotello, V. M. Gold nanoparticles platforms as drug and biomolecule delivery systems, *J. Controlled Release.* **2010**, 148, 122-127.

(14) (a) Mandal, D.; Nasrolahi Shirazi, A.; Parang, K. Cell-penetrating homochiral cyclic peptides as nuclear-targeting molecular transporters**.** *Angew. Chem. Int. Ed*., **2011**, 50, 9633–9637. (b) Nasrolahi Shirazi, A.; Tiwari, R. K.; Oh, D.; Banerjee, A.; Yadav, A.; Parang, K. Efficient delivery of cell impermeable phosphopeptides by a cyclic peptide amphiphile containing tryptophan and arginine. *Mol Pharm.* **2013,** DOI: 10.1021/mp400046u.

(15) Nasrolahi Shirazi, A.; Mandal, D.; Tiwari, R. K.; Guo, L.; Lu, W.; Parang. K. cyclic peptide-capped gold nanoparticles as drug delivery systems, *Molecular Pharmaceutics.* **2013**, 10, 500–511.

(16) Nasrolahi Shirazi, A.; Tiwari, R. K.; Brown, A.; Mandal, D.; Sun, G.; Parang, K. cyclic peptides containing tryptophan and arginine as Src kinase inhibitors. *Bioorg. Med. Chem. Lett.* **2013**, 23, 3230–3234.

(17) Tan, Y. N.; Lee, J. Y.; Wang, D. I. C. Uncovering the design rules for peptide synthesis of metal nanoparticles. *J. Am. Chem. Soc.* **2010**, 132, 5677–5686.

(18) Iosin, M.; Baldeck, P.; Astilean. S. Study of tryptophan assisted synthesis of gold nanoparticles by combining UV-Vis, fluorescence, and SERS spectroscopy *J. Nanoparticle. Res*, **2010**, 12, 2843–2849.

(19) Garcia-Carbonero, R.; Supko, J.G. Current perspectives on the clinical experience, pharmacology, and continued development of the camptothecins**.** *Cancer Res.* **2002**, 8, 641–661.

(20) Kailasan, A.; Yuan, Q.; Yang, H. Synthesis and characterization of thermoresponsive polyamidoamine-polyethylene glycol-poly(D,L-lactide) core-shell nanoparticles**,** *Acta Biomater.* **2009**, 6, 1131–1139.

(21) Conner, S. D.; Schmid. S. L. Regulated portals of entry into the cell, *Nature*, **2003**, 422, 37–44.

(22) Alkilany, A. M.; Murphy, C. J. Toxicity and cellular uptake of gold nanoparticles: what we have learned so far. *J Nanopart Res*, **2010**, 12, 2313–2333.

(23) (a) Massard, J.; Benhamou, Y. Treatment of chronic hepatitis B in HIV co-infected patients. *Gastroenterol. Clin. Biol.* **2008**, 32, S20–S24. (b) Saag, M. S. Emtricitabine, a new antiretroviral agent with activity against HIV and hepatitis B virus. *Clin. Infect. Dis.* **2006**, 42, 126–131. (c) Nelson, M.; Schiavone, M. Emtricitabine (FTC) for the treatment of HIV infection. *Int. J. Clin. Pract.* **2004**, 58, 504–510.

(24) Agarwal, H. K.; Chhikara, B. S.; Hanley, M. J.; Ye, G.; Doncel, G. F.; Parang, K. Synthesis and biological evaluation of fatty acyl ester derivatives of (-)-2',3'-Dideoxy-3'-thiacytidine. *J. Med. Chem.* **2012**, 55, 4861–4871.

(25) Agarwal, H. K.: Chhikara, B. S.: Bhavaraju, S.: Mandal, D.: Doncel, G. F.: Parang, K. Emtricitabine prodrugs with improved anti-HIV activity and cellular uptake. *Molecular Pharmaceutics* **2013**, 10, 467–476.

(26) (a) Songyang, Z.; Shoelson, S. E.; Chaudhuri, M. Gish, G. Pawson, T.; Haser, W. G.; King, F.; Roberts, T.; Ratnofsky, S.; Lechleider, R. J.; Neel, B. G.; Birge, R. B.; Fajardo, J. E.; Chou, M. M.; Hanafusa, H.; Schaffhausen, B.; Cantley, L. C. SH2 domains recognize specific phosphopeptide sequences. *Cell* **1993**, 72, 767–778. (b) Waksman, G.; Kominos, D.; Robertson, S. C.; Pant, N.; Baltimore, D.; Birge, R. B.; Cowburn, D.; Hanafusa, H.; Mayer, B. J.; Overduin, M. Resh, M. D.; Rios, C. B.; Silverman, L.; Kuriyan, J. Crystal structure of the phosphotyrosine recognition domain SH2 of v-src complexed with tyrosine-phosphorylated peptides. *Nature* **1992**, 358, 646–653.

(27) Cai, H.; Yao, P. *In-Situ* preparation of gold nanoparticle-loaded lysozyme-dextran nanogels and applications for cell imaging and drug delivery. *Nano Scale* **2013**, 5, 2892-2900.

Figure Legends:

Figure 1: Chemical structures of synthesized cyclic peptides

Figure 2: TEM images of c[KW]$_5$-AuNPs

Figure 3: TEM images of l(KW)$_5$-AuNPs

Figure 4: Comparative CD of cyclic c[KW]$_5$, linear l(KW)$_5$, and compared to c[KW]$_5$-AuNPs and l(KW)$_5$-AuNPs

Figure 5: Cellular uptake of F′-l(KW)$_5$-AuNPs and F′-c[KW]$_5$-AuNPs (5 μM) versus the corresponding fluorescently-labeled peptides F′-l(KW)$_5$ and F′-c[KW]$_5$ (5 μM) after 1 h incubation

Figure 6: Confocal microscope images of F′-l$(KW)_5$-AuNPs (5 μM) and F′-c$[KW]_5$-AuNPs (5 μM) uptake by SK-OV-3 cells after 1 h incubation

Figure 7: Cellular uptake of (a) F′-l$(KW)_5$-AuNPs (5 μM) and (b) F′-c$[KW]_5$-AuNPs (5 μM) in the absence or presence of different endocytic inhibitors in SK-OV-3 cells after 1 h

Figure 8: Cellular uptake studies for F′-FTC and F′-3TC alone (5 μM) in the presence of cyclic and linear peptides and their corresponding P-AuNPs (25 μM) after 1 h incubation

Figure 9: Confocal microscope images of F′-3TC (5 μM) uptake by SK-OV-3 cells in the presence of l$(KW)_5$-AuNPs and c$[KW]_5$-AuNPs (25 μM) after 1 h incubation

Figure 10: Cellular uptake of F′-GpYEEI (5 μM) in the presence of l$(KW)_5$-AuNPs, c$[KW]_5$-AuNPs, l$(KW)_5$ and c$[KW]_5$ (25 μM) after 1 h incubation

Figure 11: Confocal microscope images of F′-GpYEEI (5 μM) uptake by SK-OV-3 cells in the presence of l$(KW)_5$-AuNPs and c$[KW]_5$-AuNPs (25 μM) after 1 h incubation

Figure 12. Time-dependent antiproliferative assay of CPT in the absence and presence of c$[KW]_5$-AuNPs.

Figure 1

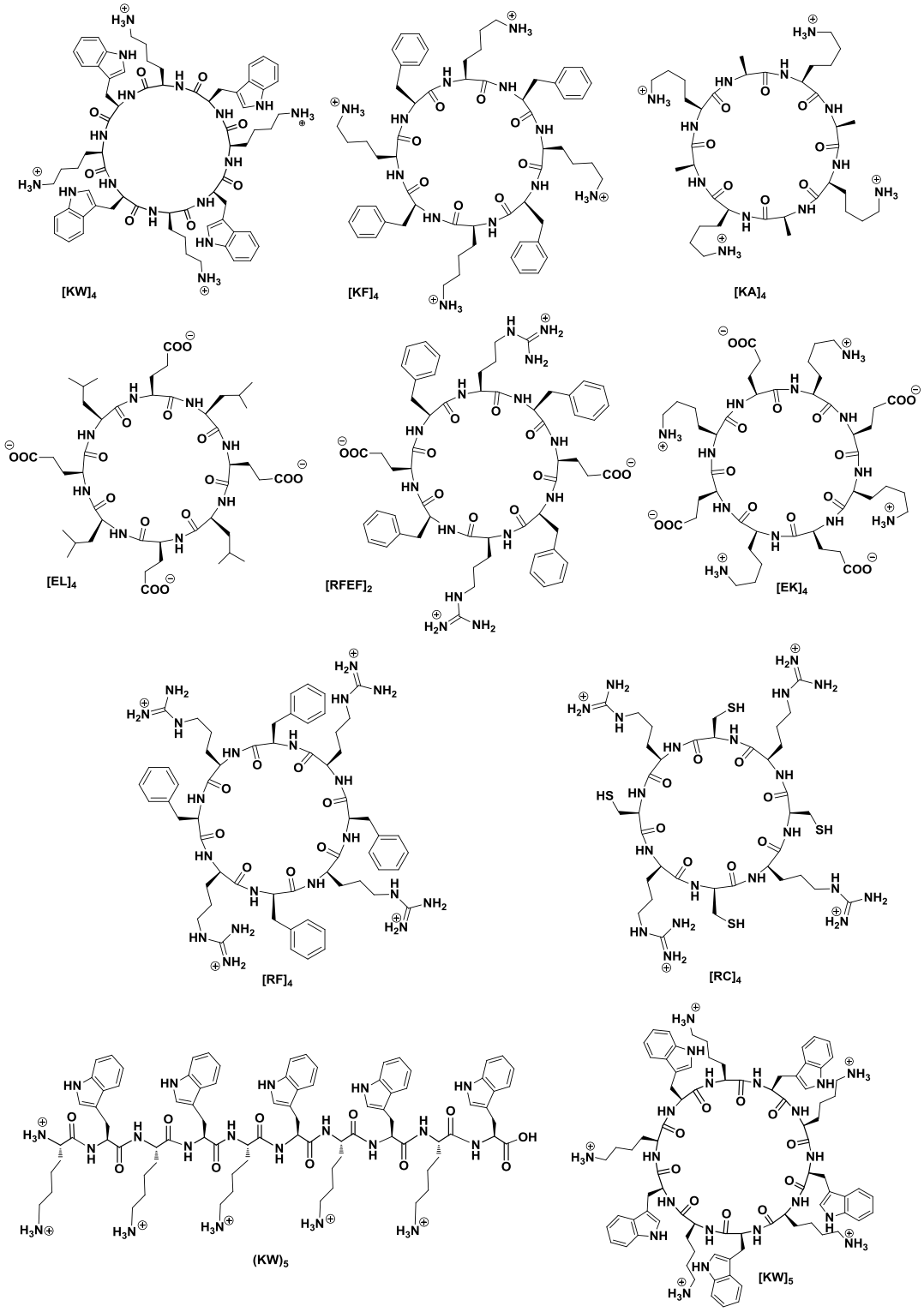

Figure 2

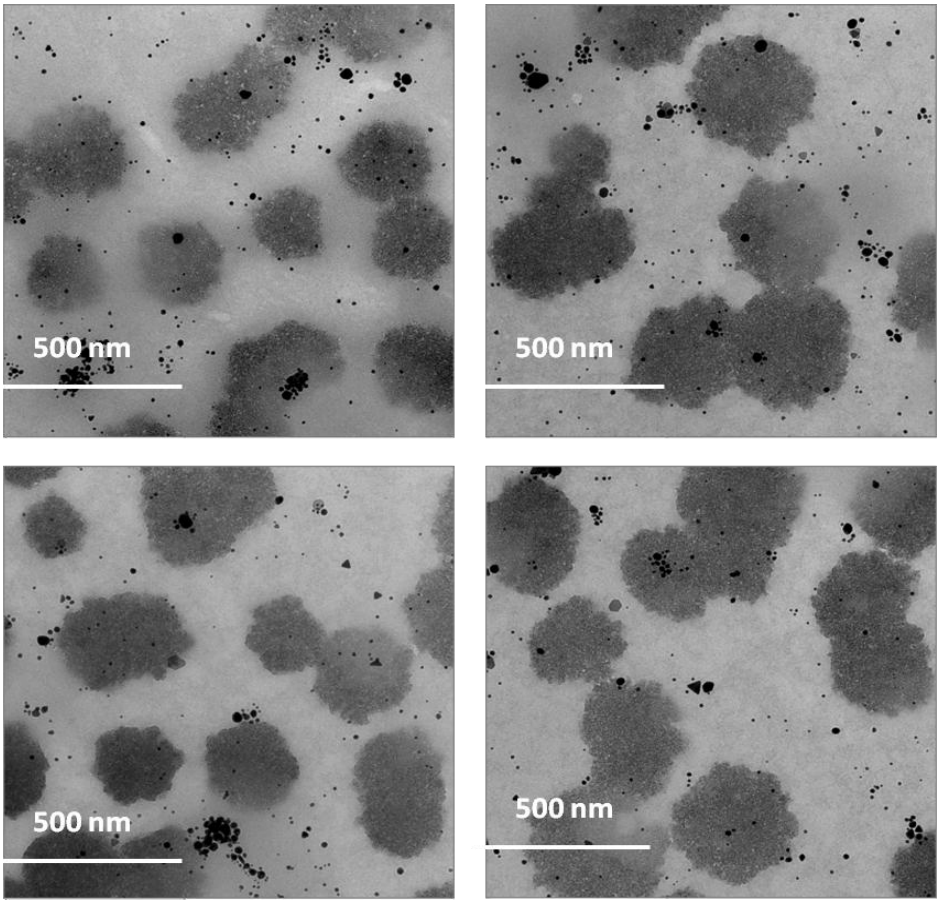

Figure 3

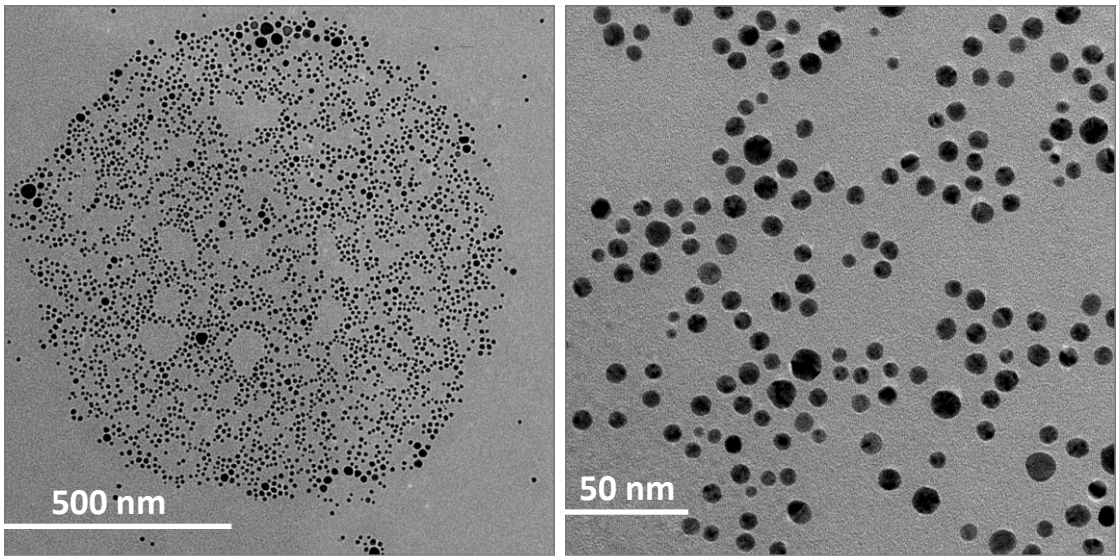

Figure 4

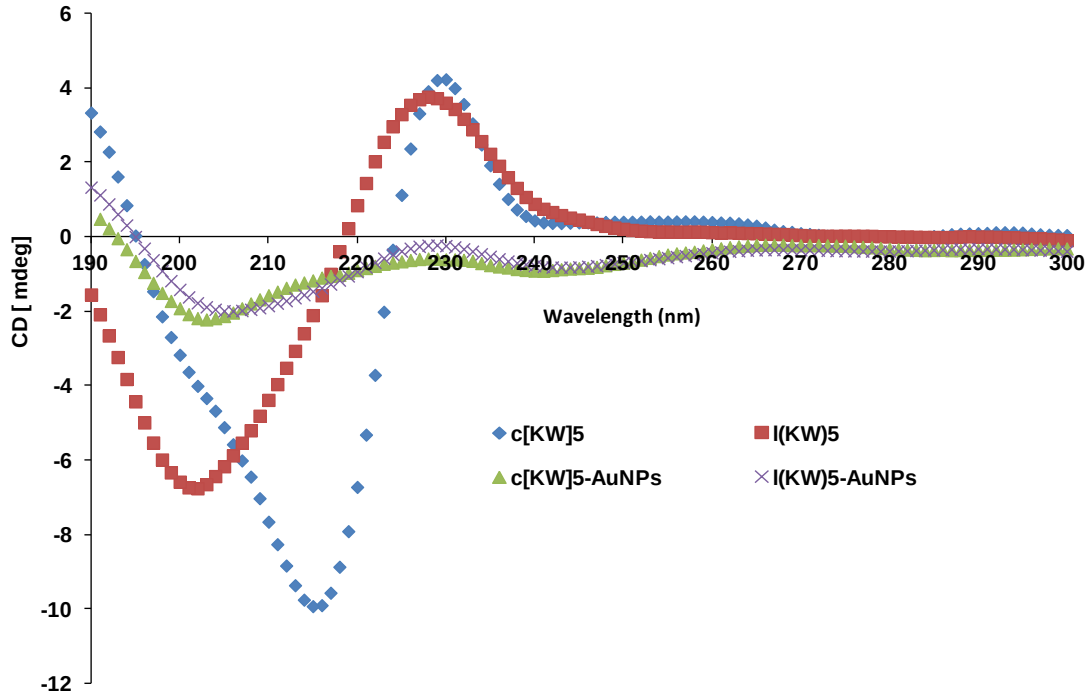

Figure 5

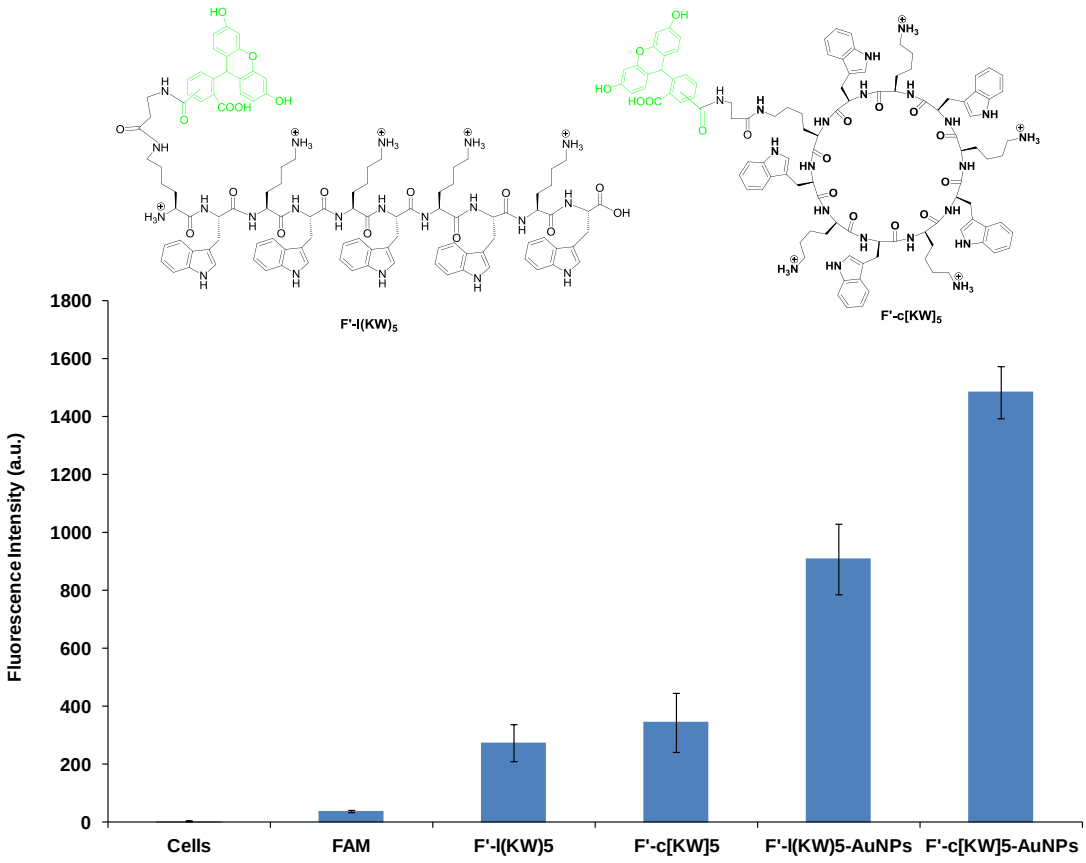
F'-l(KW)5
F'-c[KW]5
Fluorescence Intensity (a.u.)
1800
1600
1400
1200
1000
800
600
400
200
0
Cells
FAM
F'-l(KW)5
F'-c[KW]5
F'-l(KW)5-AuNPs
F'-c[KW]5-AuNPs

Figure 6

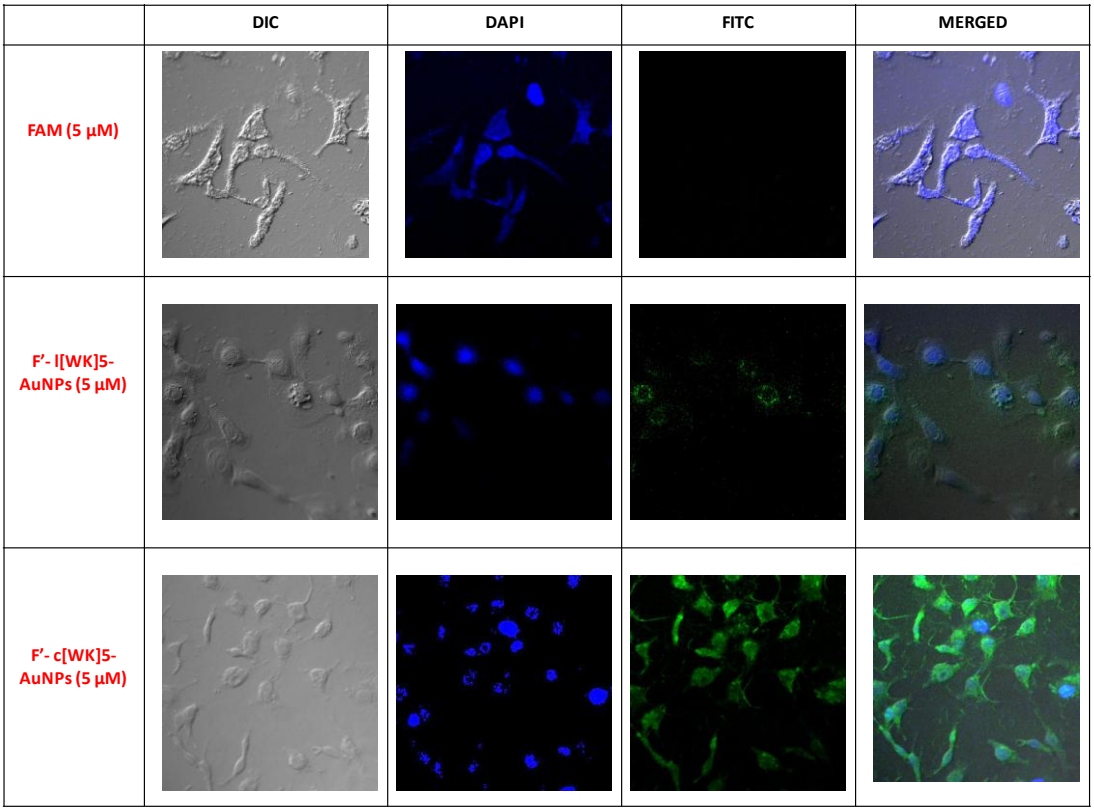

Figure 7

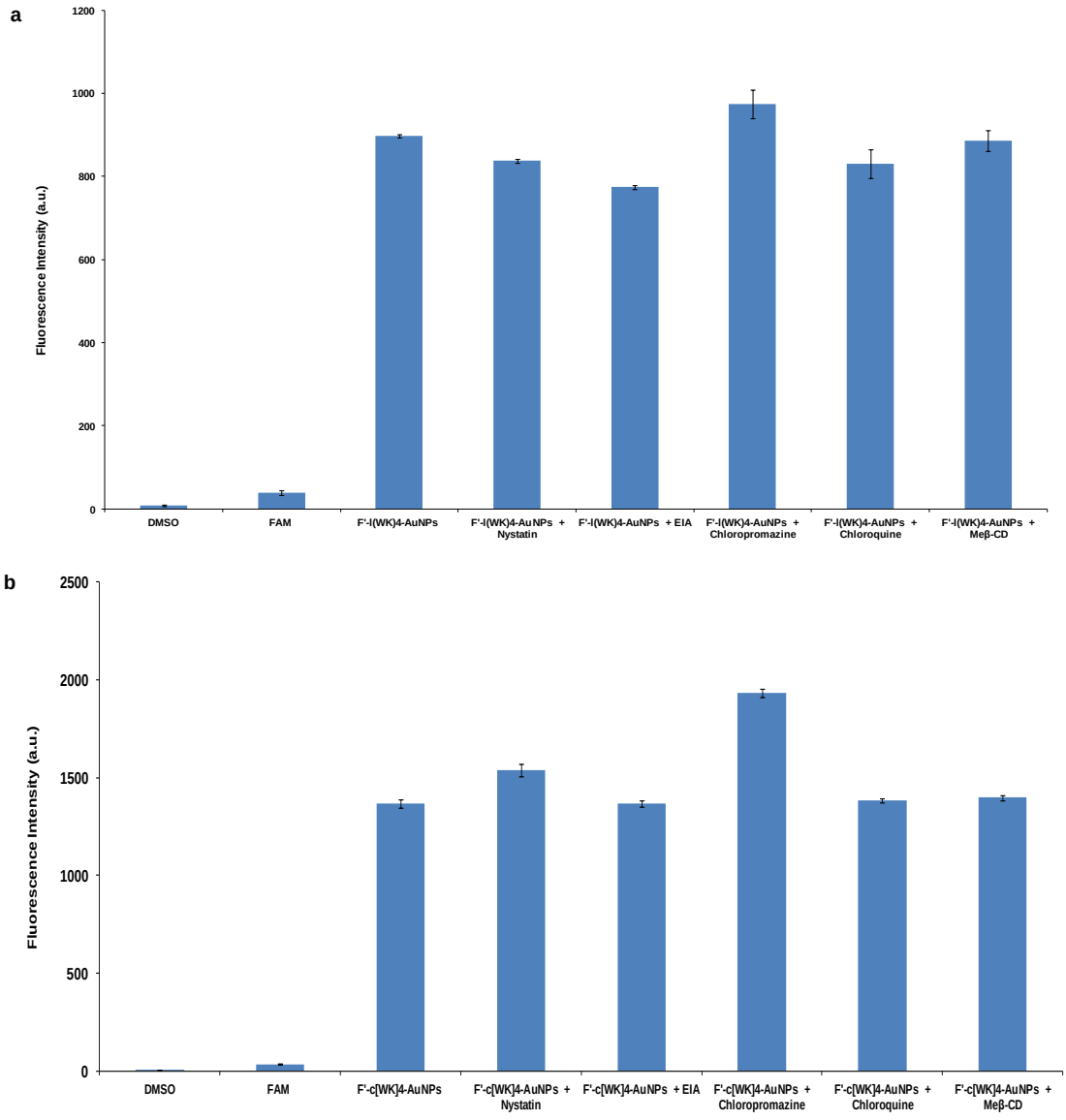
a
Fluorescence Intensity (a.u.)
1200
1000
800
600
400
200
0
DMSO
FAM
F'-l(WK)4-AuNPs
F'-l(WK)4-AuNPs + Nystatin
F'-l(WK)4-AuNPs + EIA
F'-l(WK)4-AuNPs + Chloropromazine
F'-l(WK)4-AuNPs + Chloroquine
F'-l(WK)4-AuNPs + Meβ-CD
b
Fluorescence Intensity (a.u.)
2500
2000
1500
1000
500
0
DMSO
FAM
F'-c[WK]4-AuNPs
F'-c[WK]4-AuNPs + Nystatin
F'-c[WK]4-AuNPs + EIA
F'-c[WK]4-AuNPs + Chloropromazine
F'-c[WK]4-AuNPs + Chloroquine
F'-c[WK]4-AuNPs + Meβ-CD

Figure 8

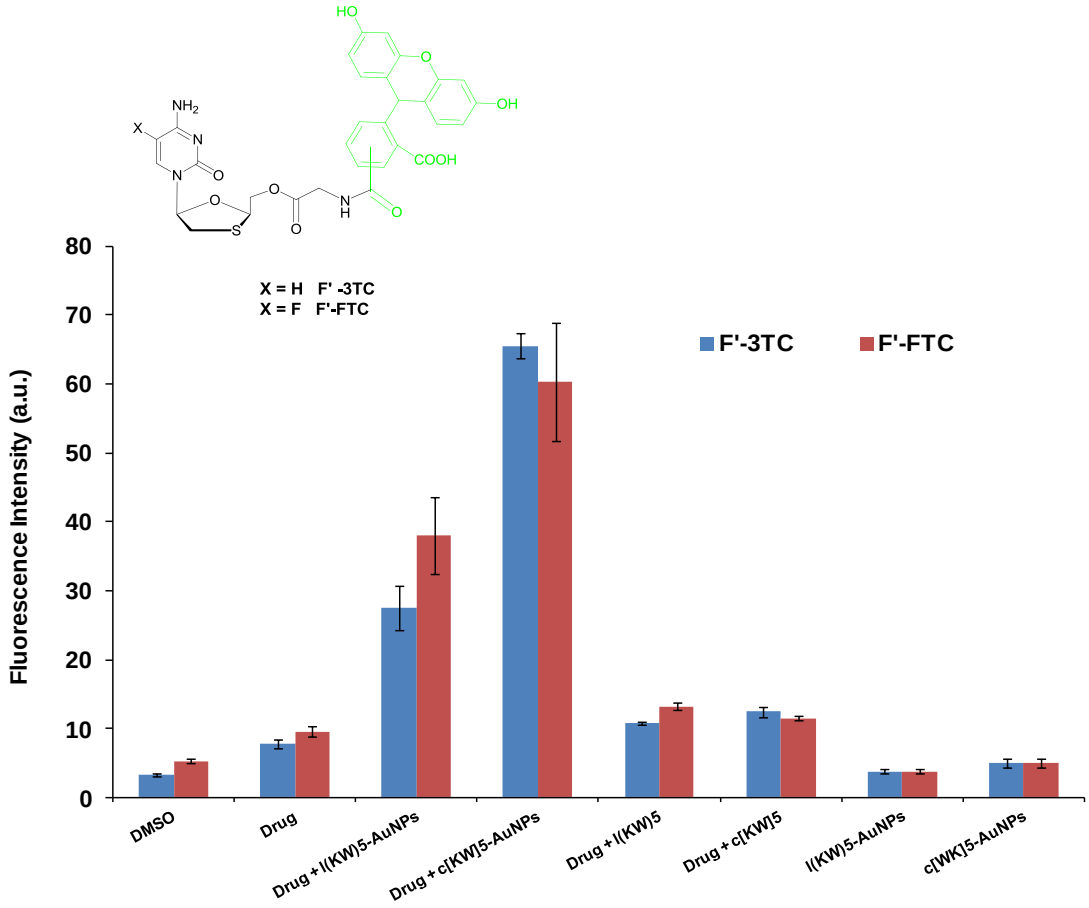
HO
O
OH
COOH
NH2
X
N
N
O
O
O
O
N
H
O
S
X = H F' -3TC
X = F F'-FTC
F'-3TC
F'-FTC
Fluorescence Intensity (a.u.)
0
10
20
30
40
50
60
70
80
DMSO
Drug
Drug + l(KW)5-AuNPs
Drug + c[KW]5-AuNPs
Drug + l(KW)5
Drug + c[KW]5
l(KW)5-AuNPs
c[WK]5-AuNPs

Figure 9

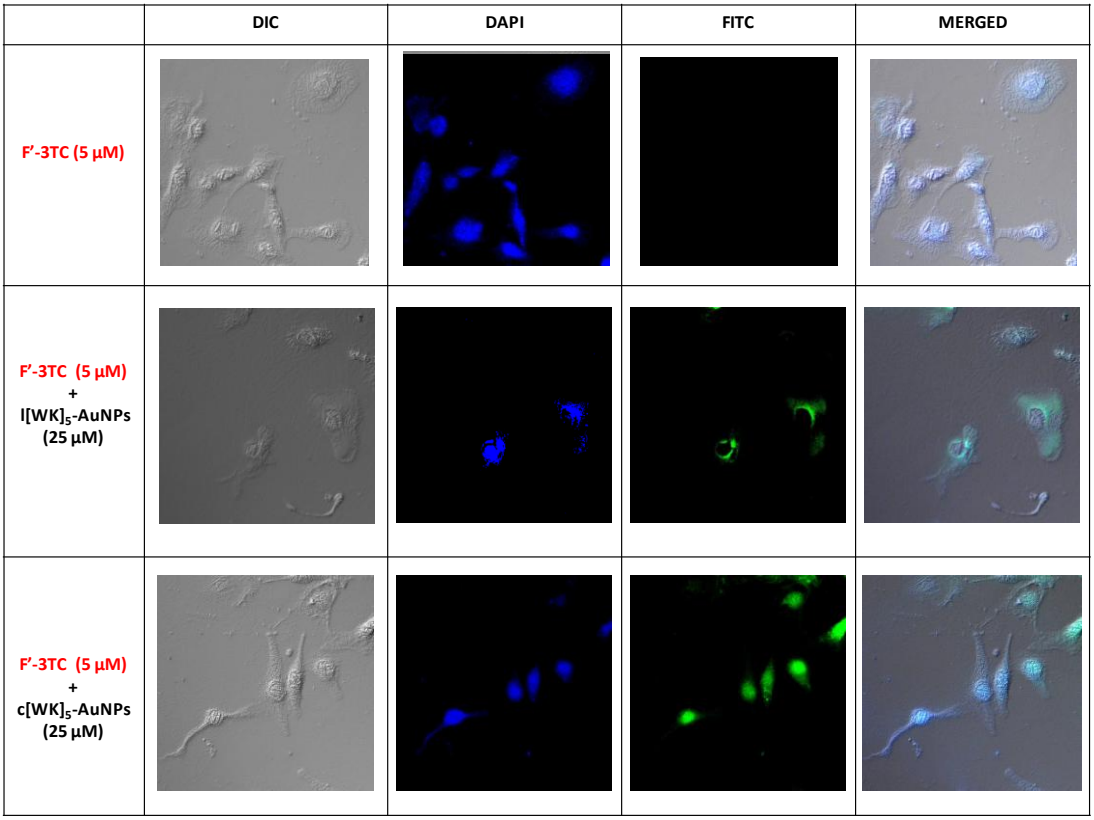
DIC
DAPI
FITC
MERGED
F'-3TC (5 µM)
F'-3TC (5 µM) + l[WK]5-AuNPs (25 µM)
F'-3TC (5 µM) + c[WK]5-AuNPs (25 µM)

Figure 10

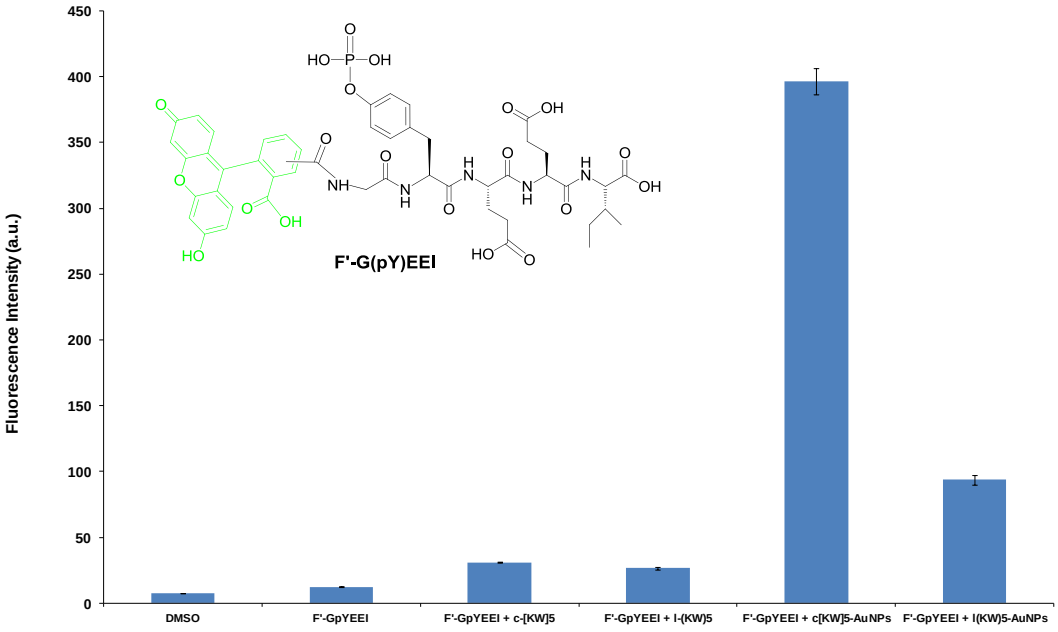
Fluorescence Intensity (a.u.)
450
400
350
300
250
200
150
100
50
0
F'-G(pY)EEI
DMSO
F'-GpYEEI
F'-GpYEEI + c-[KW]5
F'-GpYEEI + l-(KW)5
F'-GpYEEI + c[KW]5-AuNPs
F'-GpYEEI + l(KW)5-AuNPs

Figure 11

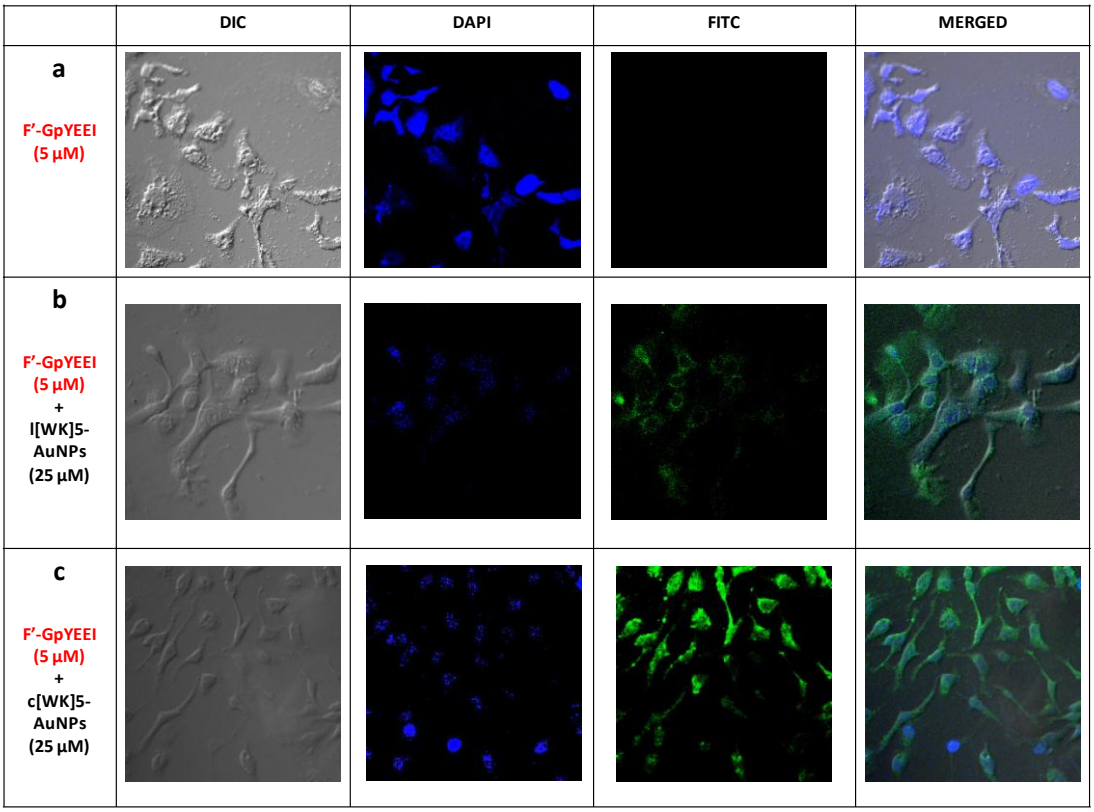

Figure 12

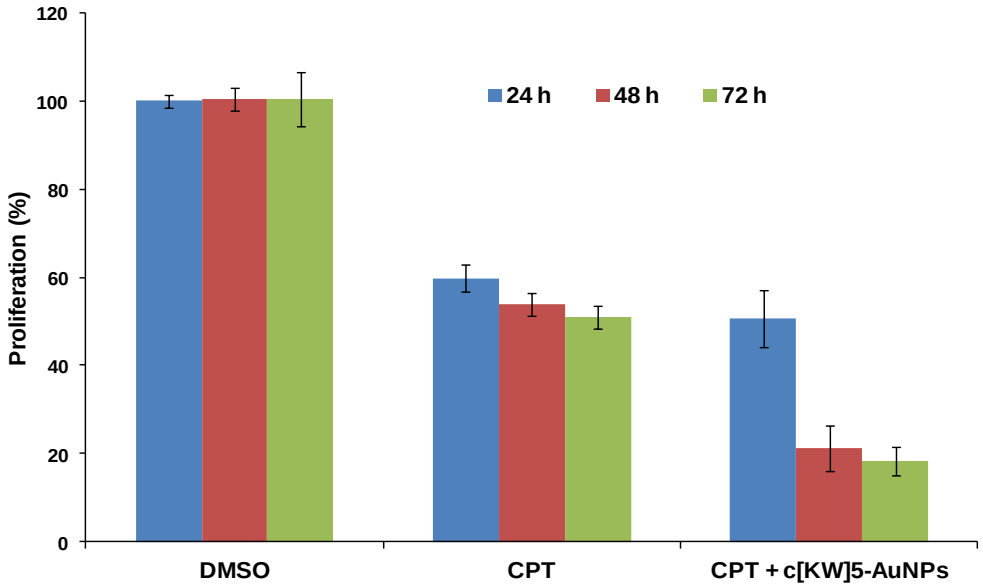

SUPPORTING FIGURES AND SCHEMES

Figure S1. Stability of cyclic [W(RW)$_4$]-Dox after incubation with (a) PBS and (b) FBS.

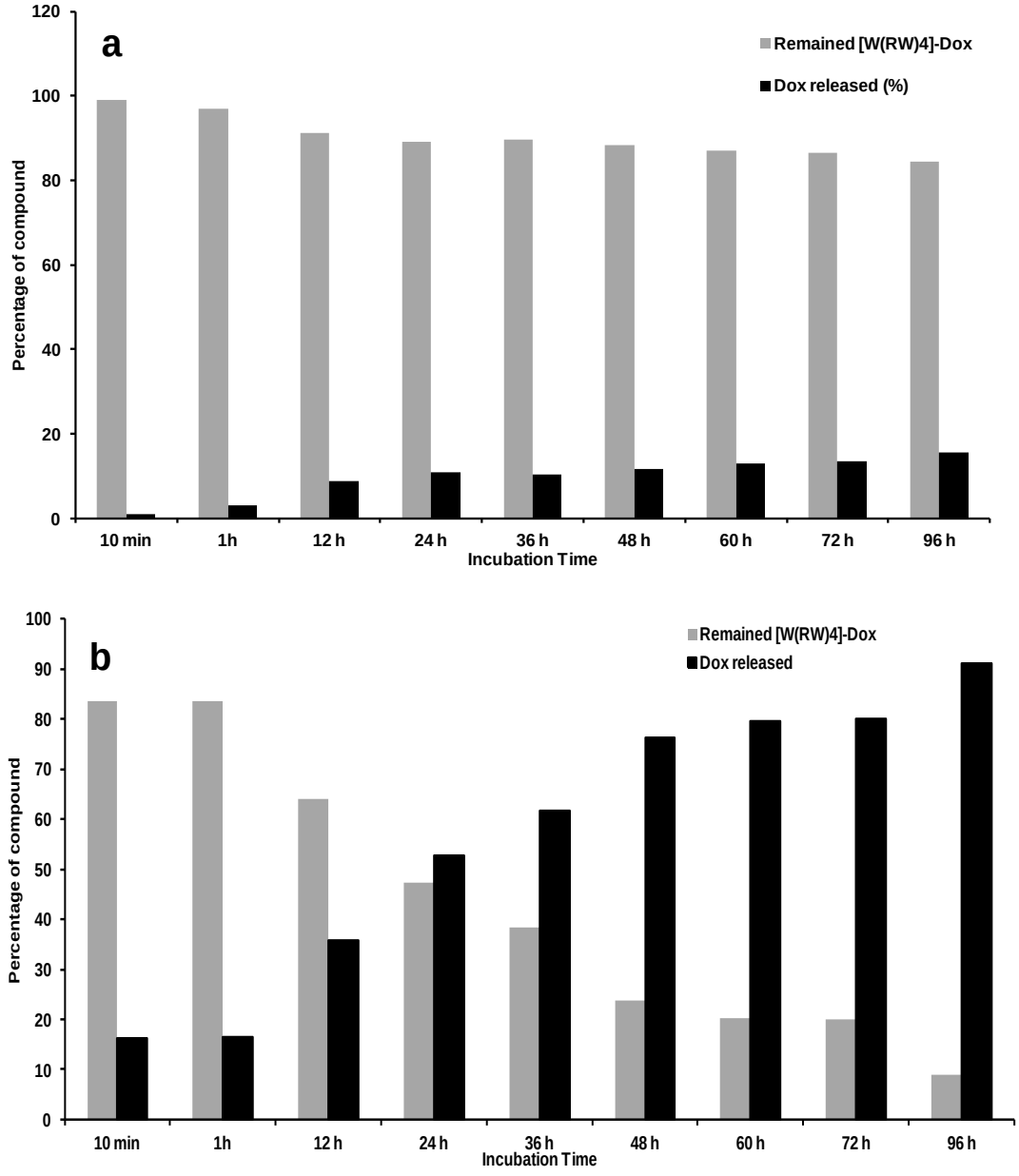

Figure S2. Comparison of cell cycle arrest by Dox and cyclic [W(RW)$_4$]-Dox.

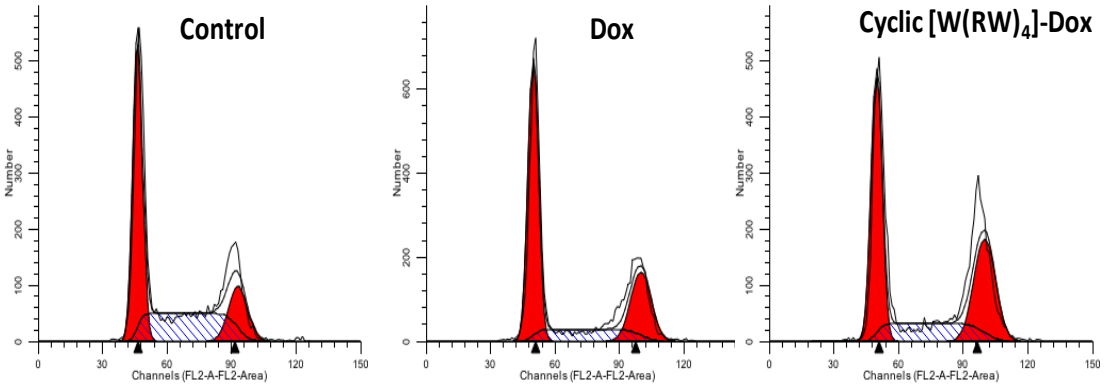

Figure S3. Detection of AuNP formation by UV-Vis absorption spectroscopy by HAuCl$_4$ (1 mM) with different concentrations of [WR]$_4$ (100 μM-2 mM).

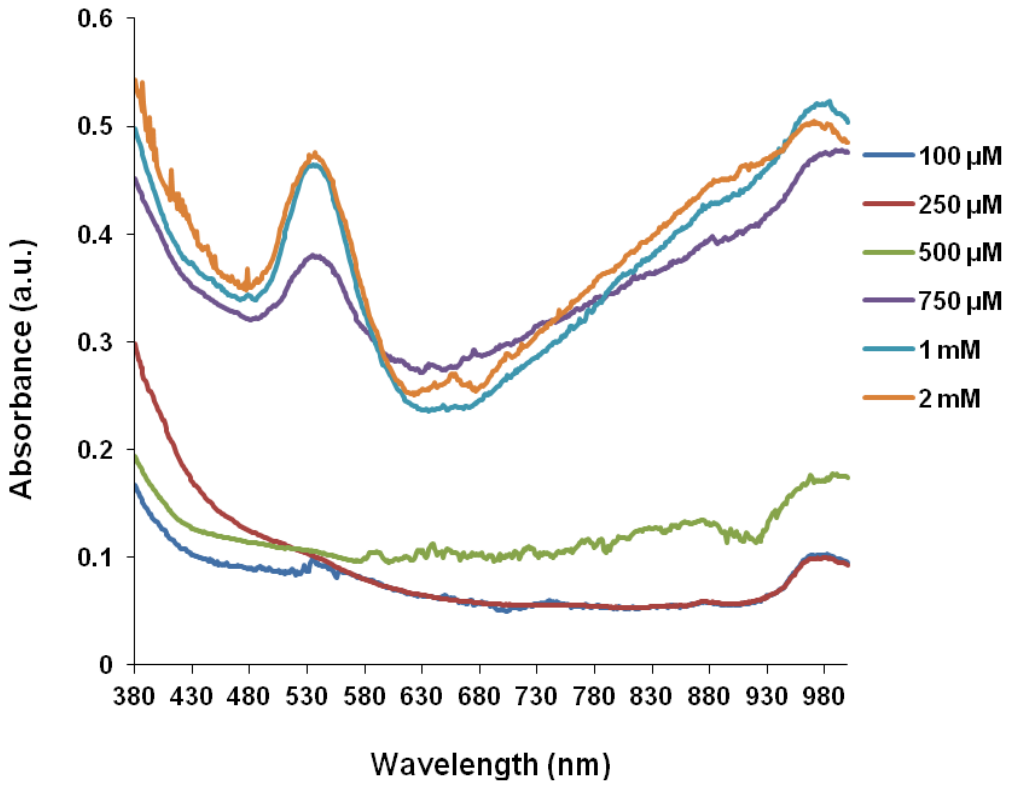

Figure S4. TEM images of $[WR]_4$-AuNPs generated from incubation of $[WR]_4$ with $HAuCL_4$.

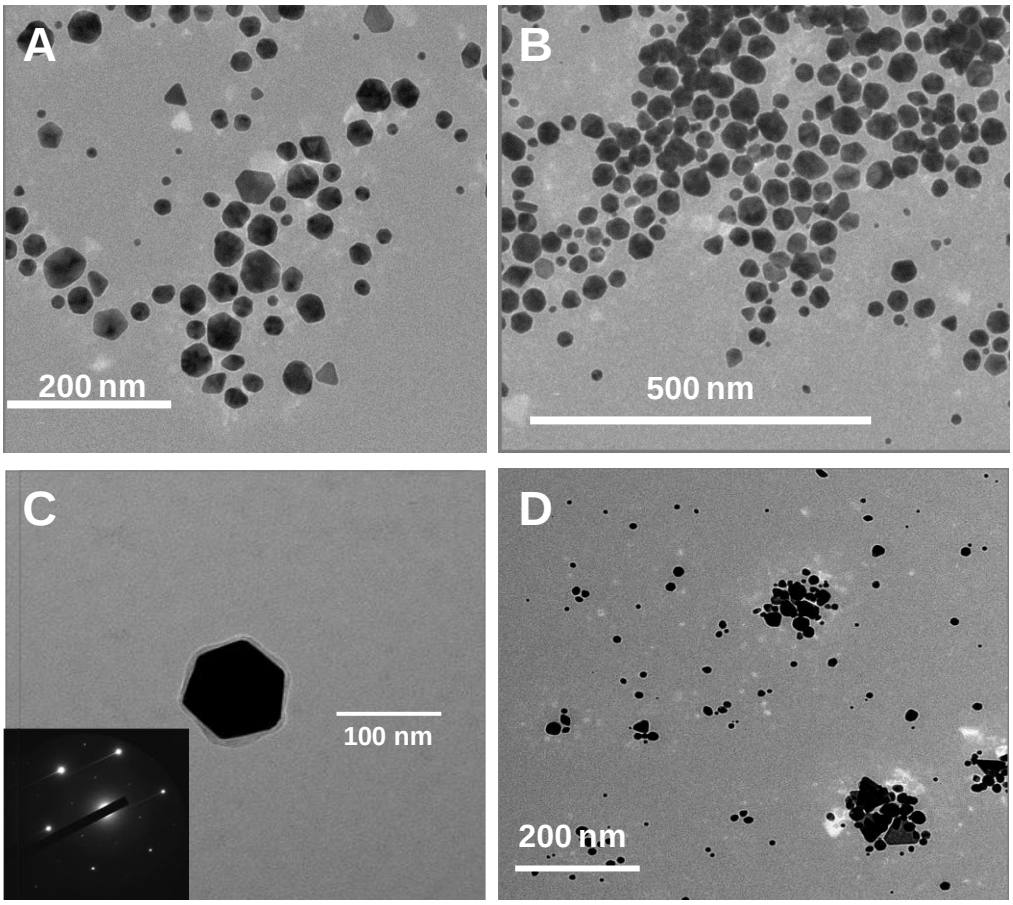

Figure S5. Cytotoxicity assay of $[WR]_4$-AuNP and $[WR]_4$ in SK-OV-3 cells (24 h and 72 h), CCRF-CEM (24 h), and CCD-18Co (24 h) (mean ± SD).

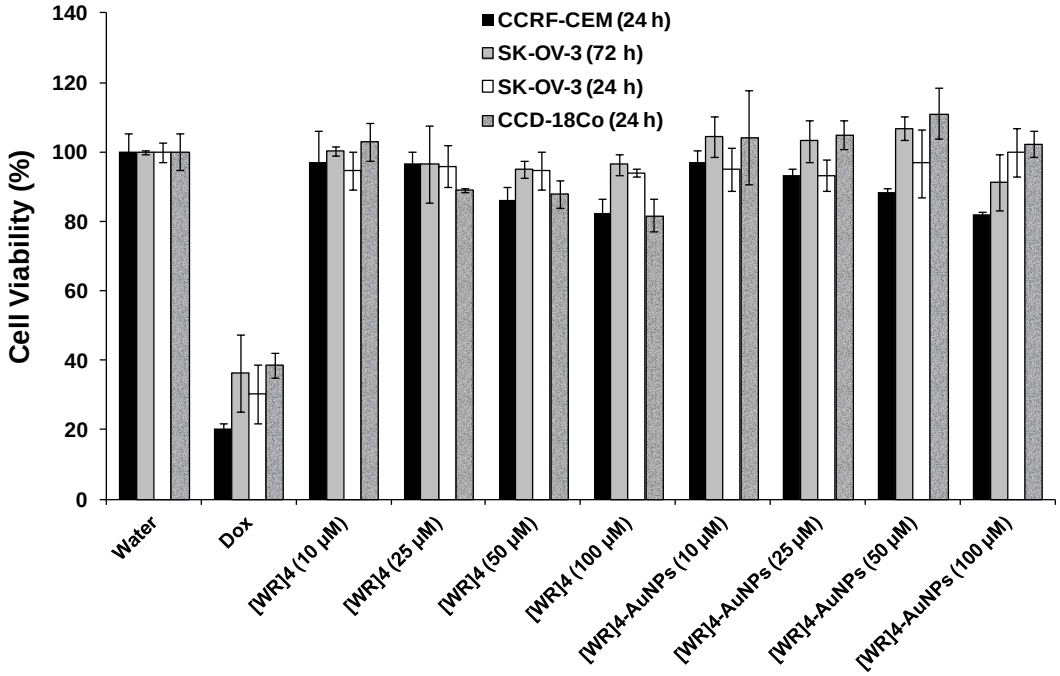

Figure S6. Cytotoxicity assay of $[WR]_4$-AuNP and $[WR]_4$ compared with polyArg CR_7, TAT (YGRKKRRQRRRC) (100 µM), and oligofectamine 2000 in CCD-18Co (48 h) (mean ± SD, n = 3).

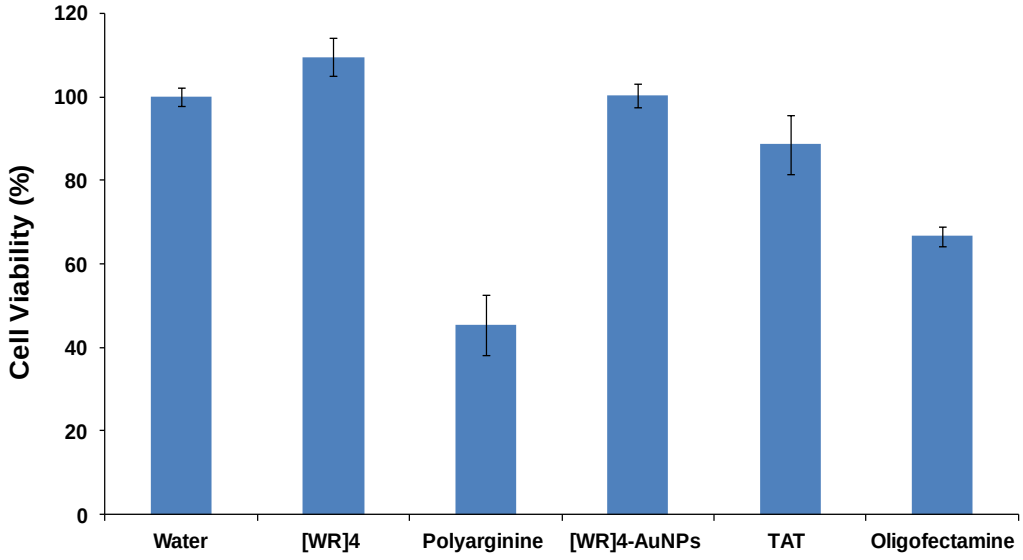

Figure S7. Cellular uptake of cyclic F′-[W_5R_4K] capped-AuNP compared with FAM (10 μM) and linear F′-(W_5R_4K) capped-AuNP in CCRF-CEM cells.

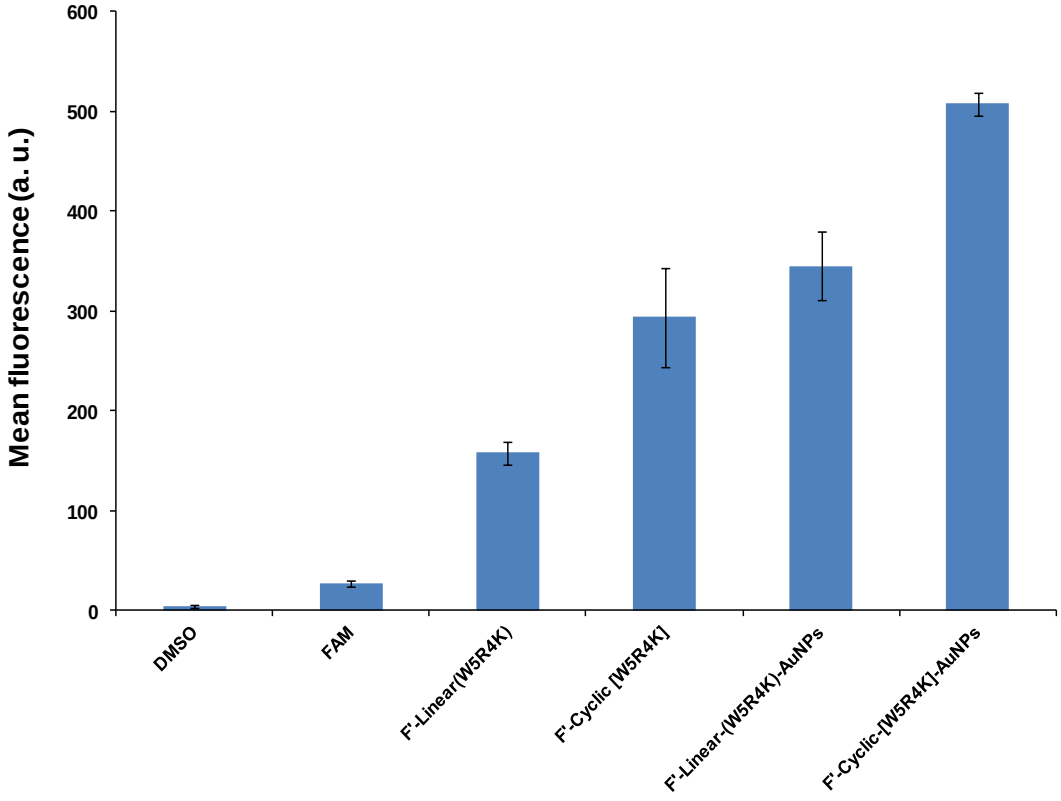

Figure S8. ICP-MS of $[WR]_4$-AuNPs (50 μM) in SK-OV-3 cells after 3 h and 24 h incubation (mean ± SD, n = 3).

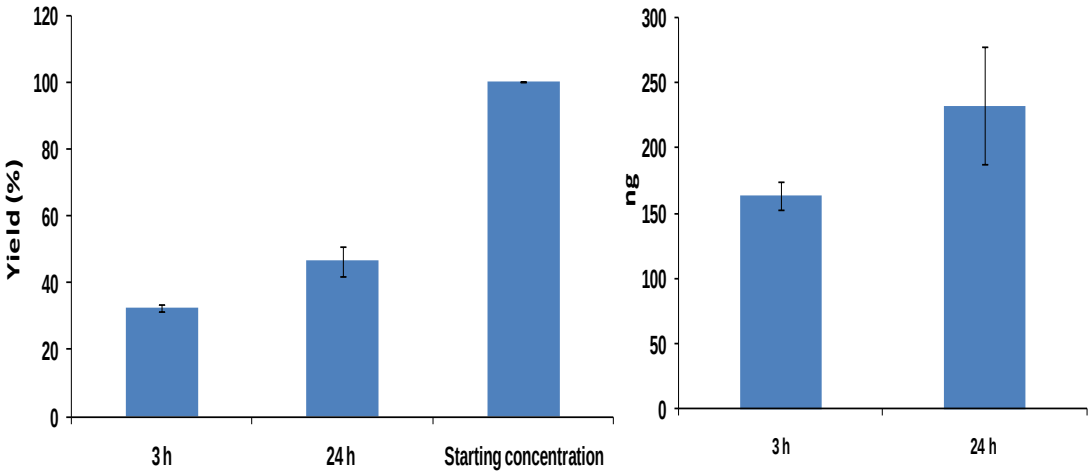

Figure S9. Membrane integrity of SK-OV-3 cells in the presence of (50 μM) and control (cells with serum-free media without any treatment with AuNPs) (mean ± SD, n = 3).

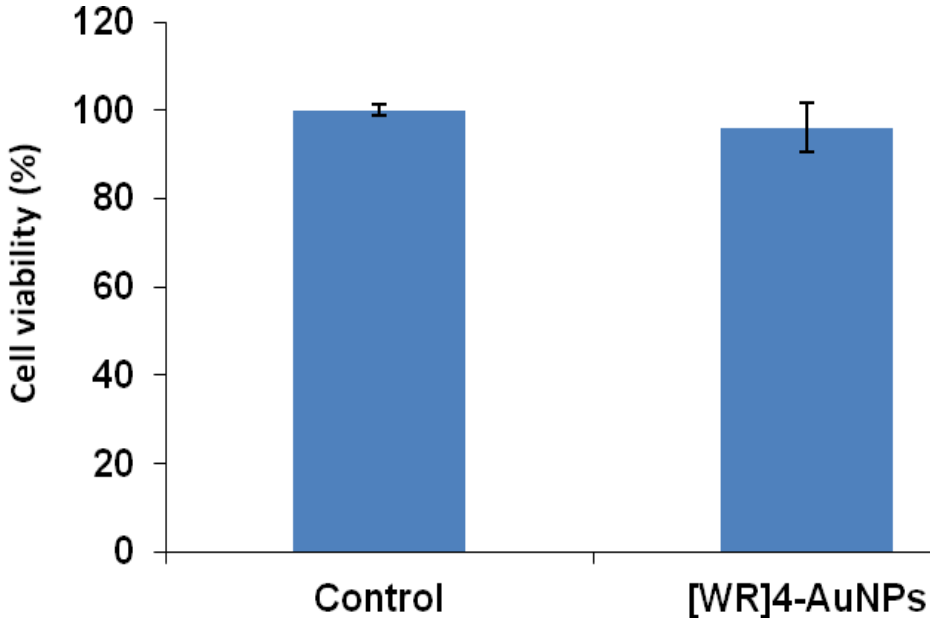

Figure S10. Fluorescence of Dox in the presence of $[WR]_4$-AuNPs (1:1 molar ratio) after 2 h incubation.

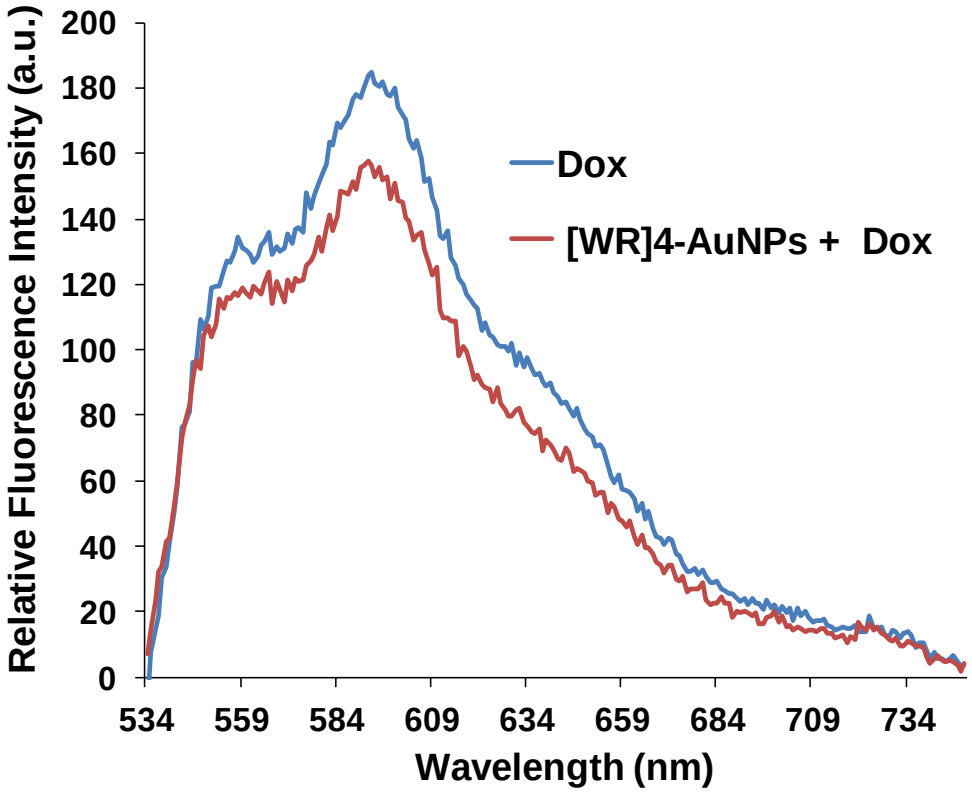

Figure S11. Differential interference contrast microscopy of fluorescence-labeled lamivudine (F-3TC) (5 μM) in the absence of $[WR]_4$-AuNP in SK-OV-3 cells.

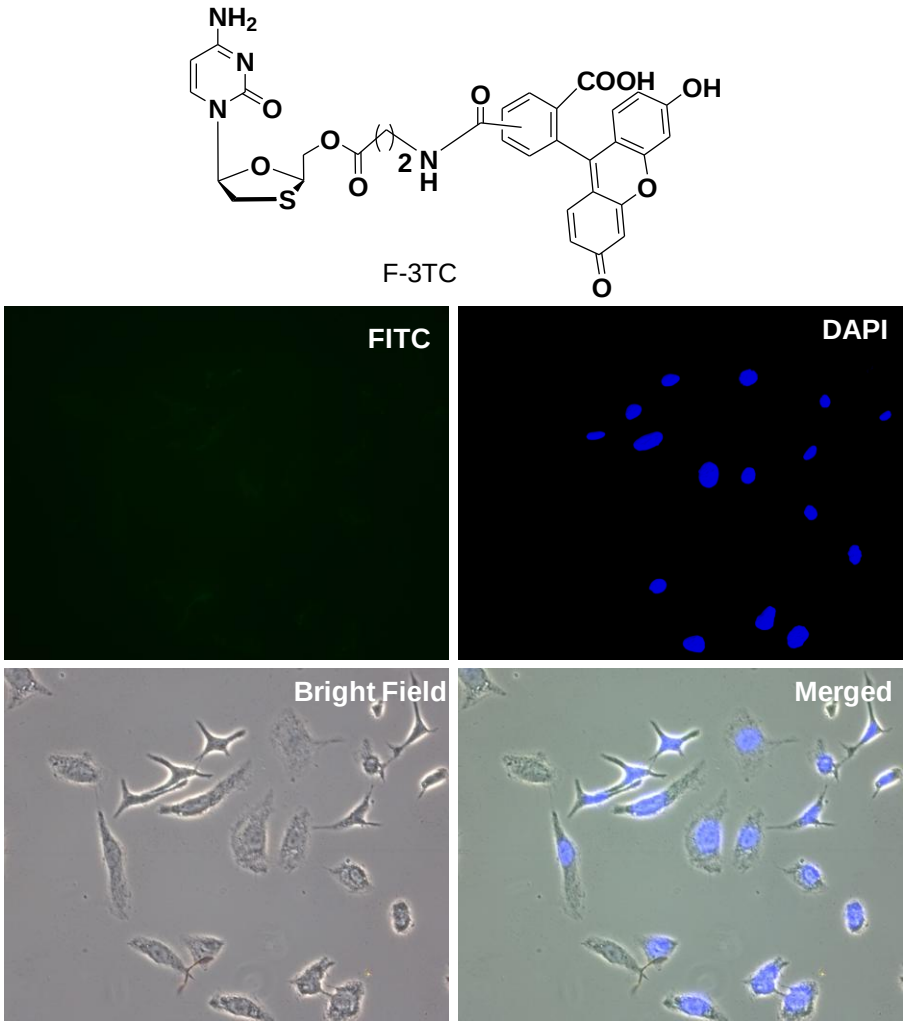

Figure S12. Cellular uptake of $[WR]_4$ capped-AuNP without a fluorescent label (10 μM) in CCRF-CEM and $[WR]_4$ capped-AuNP (25 μM) in SK-OV-3 cells.

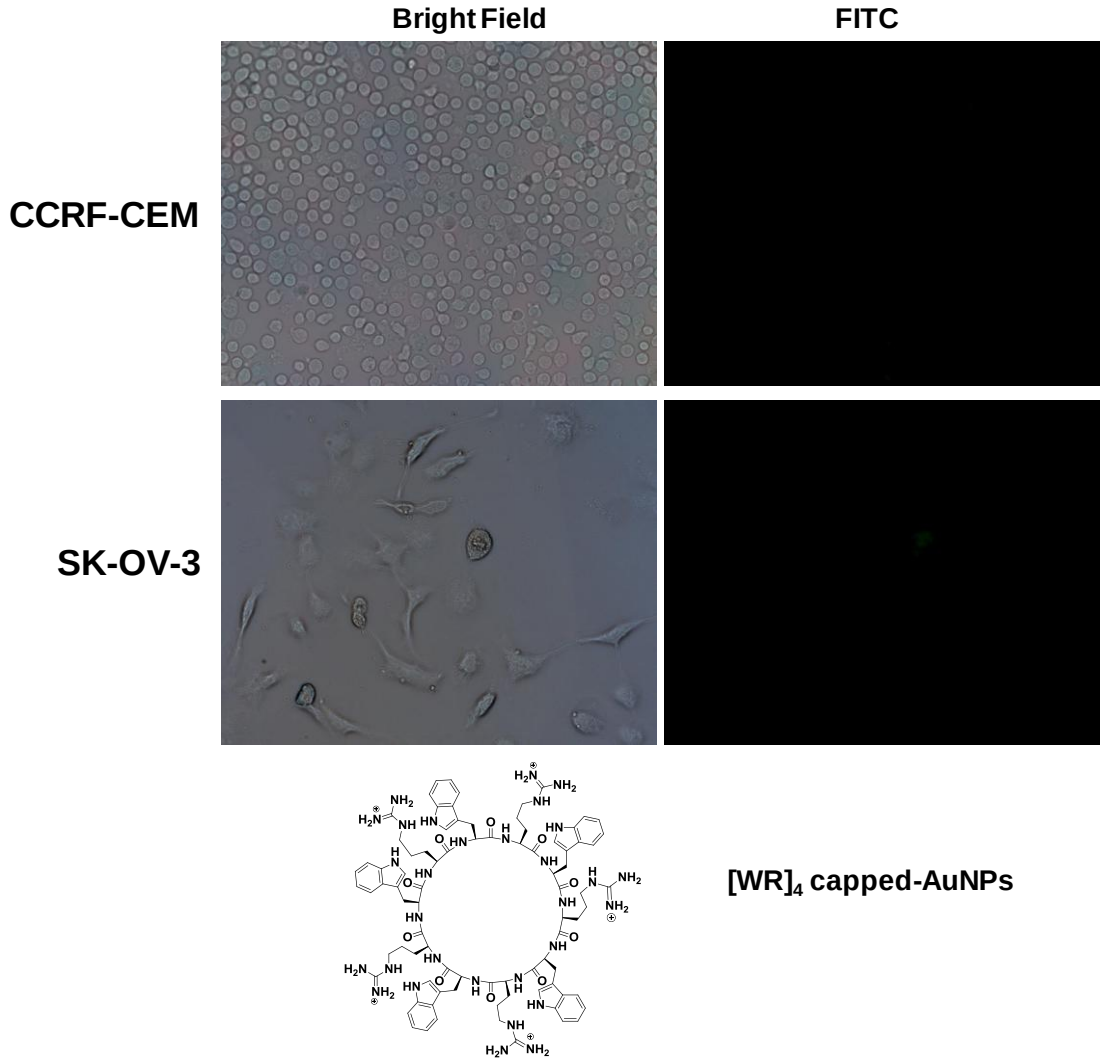

Figure S13. Flow cytometry studies for F′-3TC (5 μM) in the presence or absence of $[WR]_4$ or $[WR]_4$-AuNPs (25 μM) in SK-OV-3 cells, (mean ± SD, n = 3).

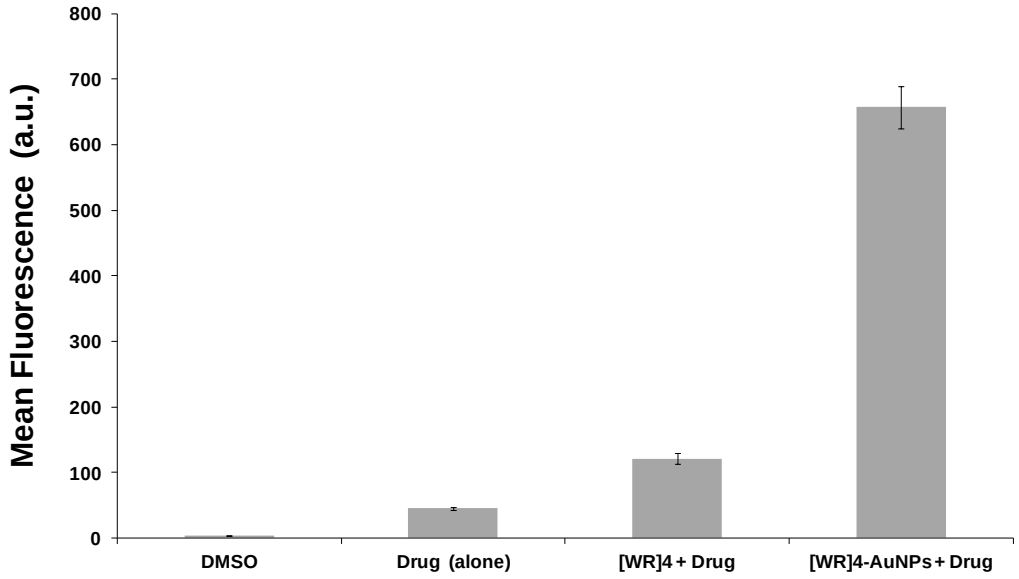

Figure S14. Flow cytometry studies for F′-3TC (5 μM) in the presence of linear $(WR)_4$, cyclic $[WR]_4$, linear $[WR]_4$-AuNPs, and cyclic $[WR]_4$-AuNPs (25 μM) in CCRF-CEM cells, respectively (mean ± SD, n = 3).

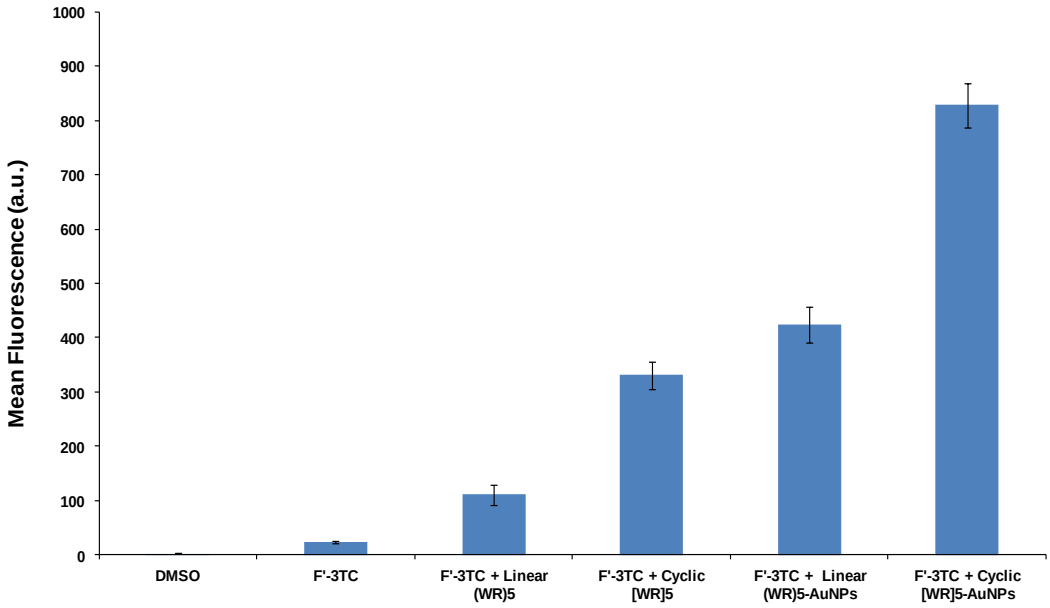

Figure S15. Flow cytometry studies in SK-OV-3 cells for Dox alone (5 μM) and in the presence of $[WR]_4$ (25 μM) or $[WR]_4$-AuNPs (25 μM) after 1 h (mean ± SD, n = 3).

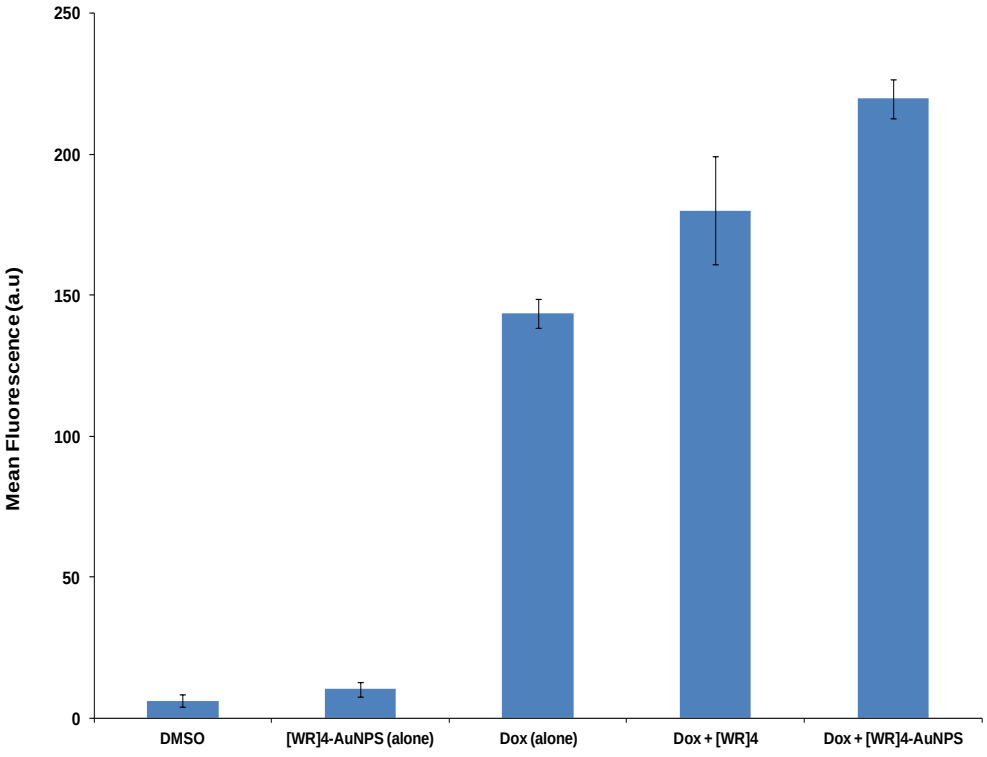

Figure S16. UV-Vis spectroscopy of peptide-capped gold nanoparticles.

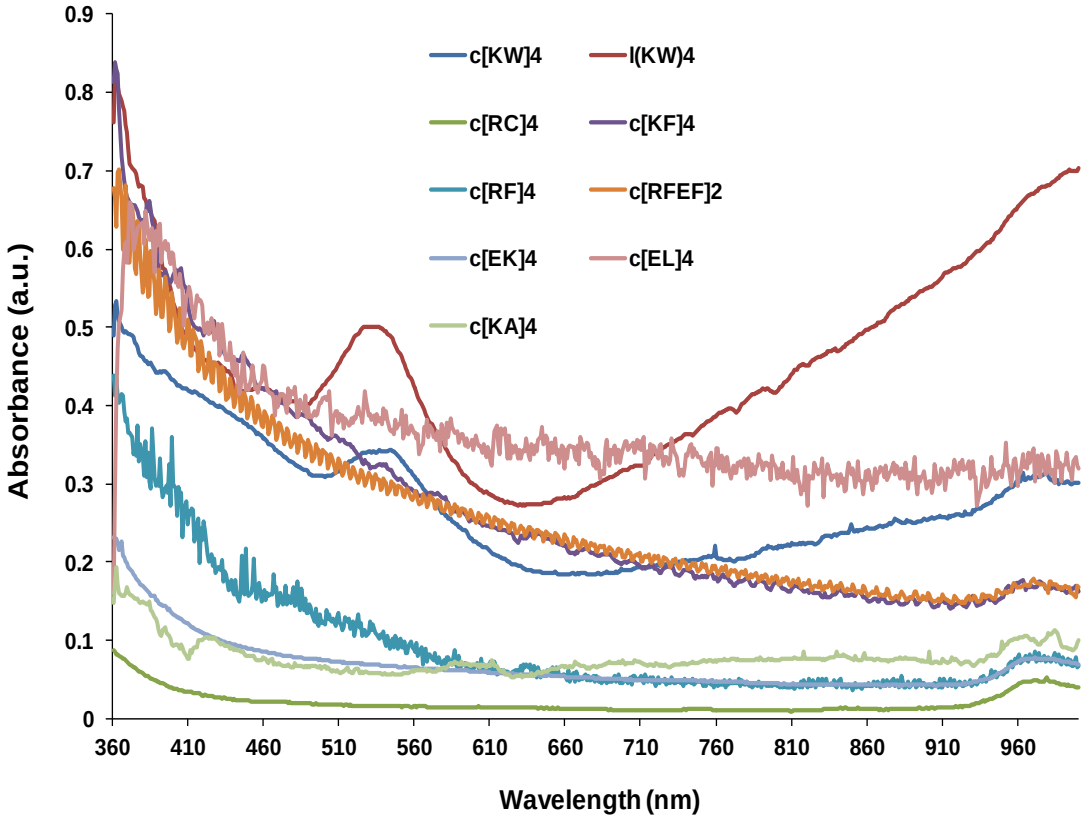

Figure S17. Cytotoxicity of peptides and corresponding P-AuNPs.

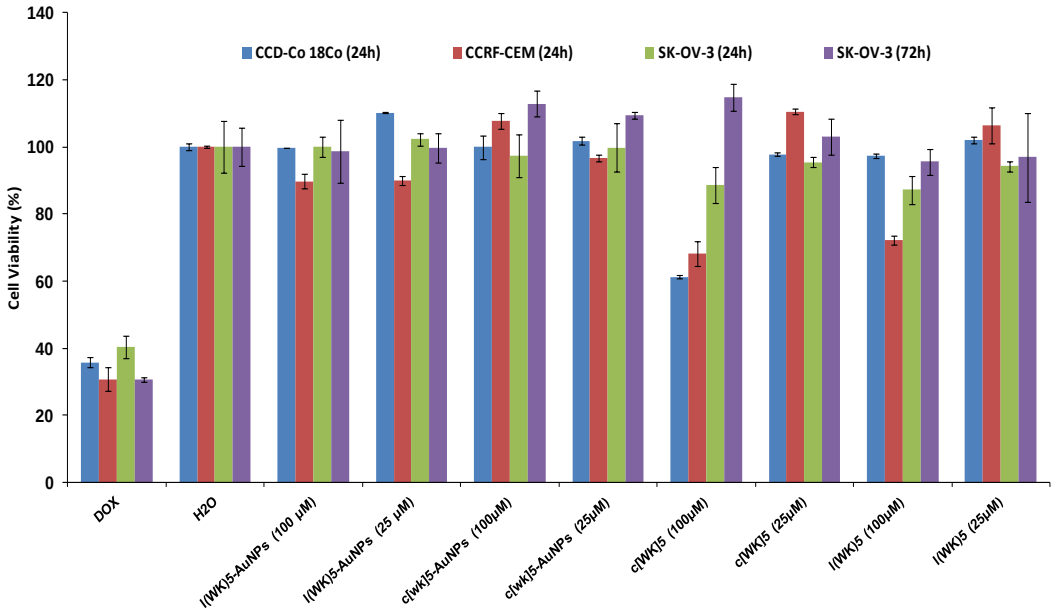

Figure S18. Membrane integrity of SK-OV-3 cells in the presence of P-AuNPs (50 µM) (mean ± SD, n =3).

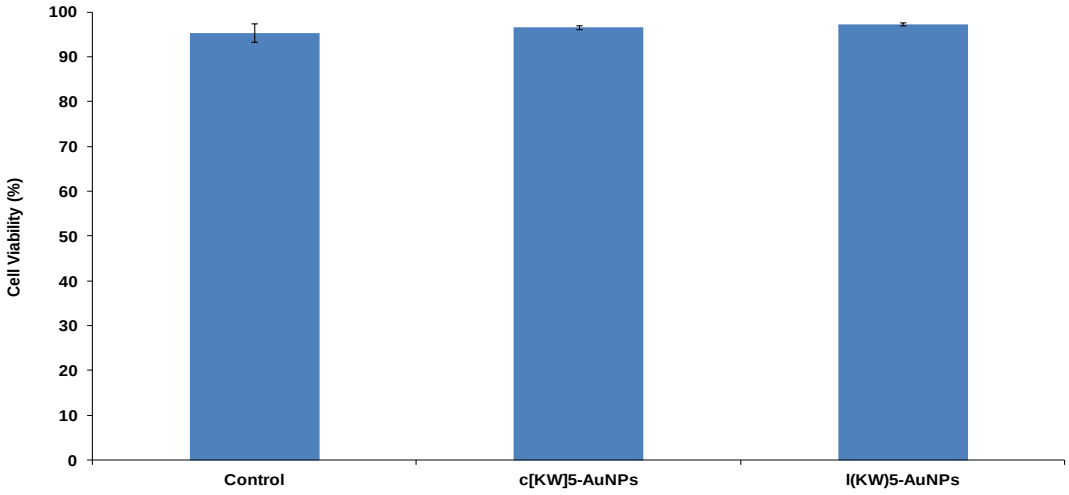

Figure S19. Fluorescence of CPT in the presence of c[KW]$_5$-AuNPs and l[(KW)$_5$-AuNPs (1:1 molar ratio) after 4 h incubation.

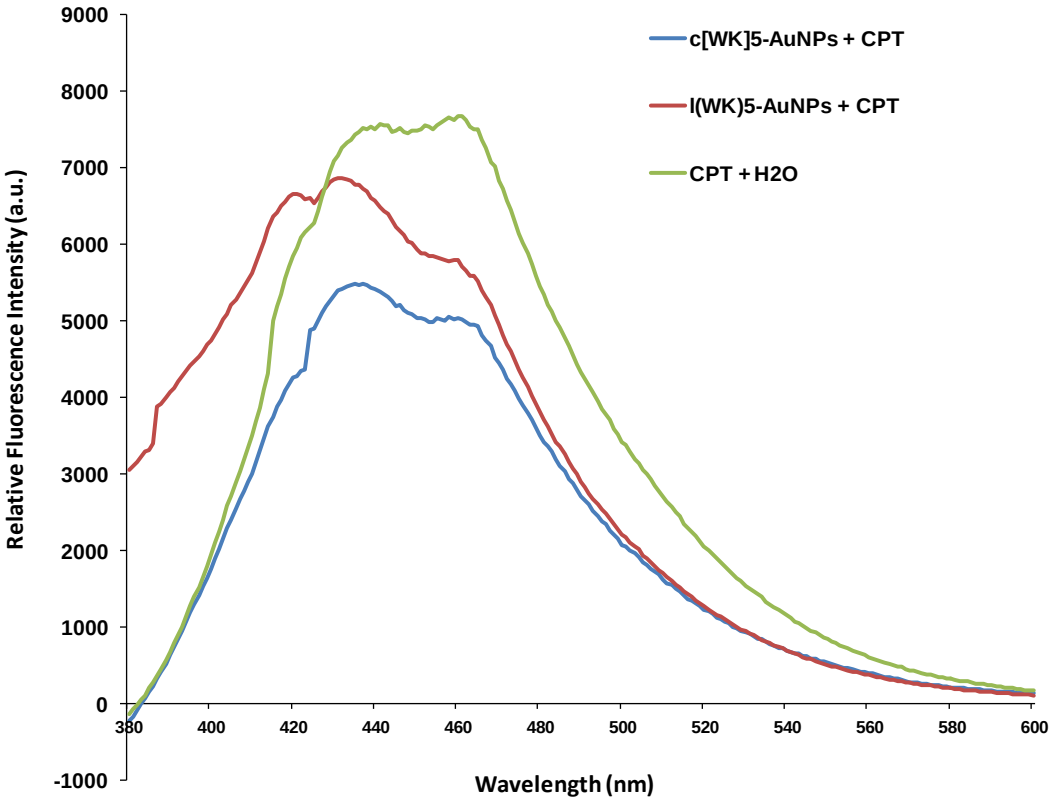

Figure S20. UV-Vis spectroscopy of c[KW]$_4$-AuNPs and c[RW]$_4$-AuNPs.

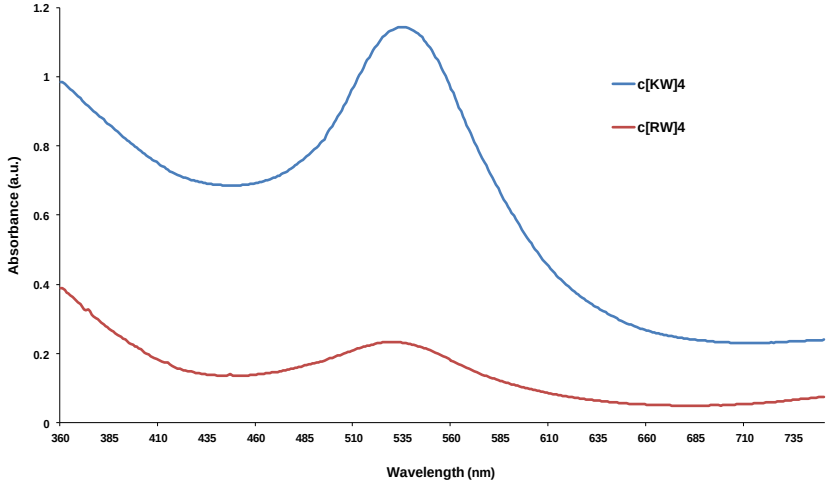

Scheme S1. Solid-phase synthesis of $[WE]_4$ and linear $(WR)_4$.

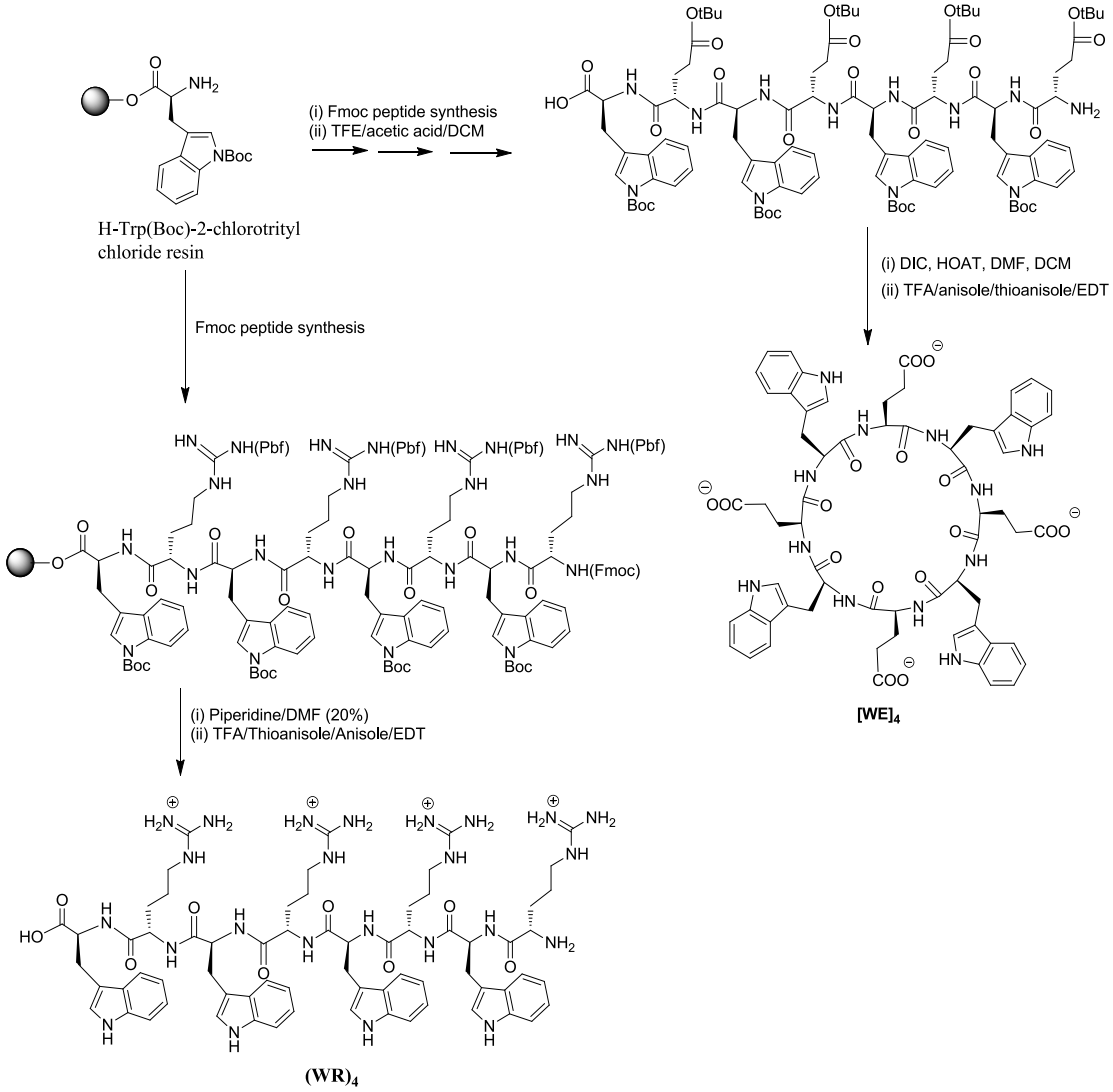

Scheme S2. Solid-phase synthesis of l(KW)$_4$, c[KW]$_4$, and F′-l(KW)$_5$.